Short-term Innovative and Exploratory Research Project

ALPHA FOUNDATION FOR THE IMPROVMENT OF MINE SAFETY AND HEALTH

Final Technical Report

1.0 Cover page

Title: Early-Warning Safety Hazard Predictor for Preventive Ventilation Management

Organization: The Board of Regents, Nevada System of Higher Education, on behalf of the University of Nevada, Reno

Grant number: ASTI14-3

Principal Investigator: George Danko, Ph.D., D.Sc.
Contact Information:

1664 N. Virginia St., Mailstop 173, Reno, NV 89557
Phone: (775)784-4284; Fax: (775)784-1833
E-Mail: danko@unr.edu

Full Period of Performance: 5/1/14 – 07/31/15

ACKNOWLEDGEMENTS/DISCLAIMERS:

This study was sponsored by the Alpha Foundation for the Improvement of Mine Safety and Health, Inc. (ALPHA FOUNDATION). The views, opinions and recommendations expressed herein are solely those of the authors and do not imply any endorsement by the ALPHA FOUNDATION, its Directors and staff.

Table of Contents

1.0 Cover page 1
List of Figures 3
List of Tables 7
List of Acronyms 8
2.0 Executive summary 9
3.0 Problem Statement and Innovation Objective 11
3.1 Problem statement 11
3.2 Innovation objective 12
4.0. Research Approach 12
4.1 Link the native VAM of a mine to APPS used in EWP 13
4.2 Link the MPD, RSM and AMS to EWP for BC and test the APPS as corrector 15
4. 3. Develop forward prediction with APPS and make an EWP warning display 16
4.4 Test for flagging safety criticality conditions at critical location 17
5.0 Summary of Accomplishments and Innovation Highlights 18
5.1 Methane in-burst from encountering a pocket at the face 22
5.1.1 Two methane sources (Scenario 1A, coal mine example 1) 24
5.1.2 Three methane sources (Scenario 1B, coal mine example 1) 25
5.1.3 Three methane sources (Scenario 1C, coal mine example 2) 32
5.2 Airway blockage as a result of partial collapse of a hazardous roof section in the mine (Scenario 2, mine example 1) 38
5.3 Atmospheric barometric pressure variations causing methane inflow from the gob (Scenario 3, mine example 1) 44
5.4. Fan malfunctioning (Scenario 4, mine example 2) 45
5.5. Fire heat load (Scenario 5, mine example 2) 54
5.6 Prepare reports, publications and plan for follow-up phase 58
6.0 Conclusions and Innovation Assessment 59
7.0 References 60
8.0 Appendices 62
APPENDIX 1. Declaration of interest in MULTIFLUX 62
APPENDIX 2. Testing of direct connection between Ventsim and MULTIFLUX 63
APPENDIX 3. Software macro to configure the APPS model from the native VAM data files 65
APPENDIX 4. Gob model and analysis of expected gas inflow 70
APPENDIX 5. Emergency Rescue Chambers (ERC) in the APPS model 75
APPENDIX 6. Model comparison and validation of the APPS model 78
APPENDIX 7. Definition of measurement locations in Ventsim Live GUI 88
APPENDIX 8. Testing and evaluation of the EWP system with random and perturbed data 90
APPENDIX 9. Forward-prediction algorithms 93
APPENDIX 10. Signal-based trend analysis for EWP evaluation 100
APPENDIX 11. Signal analysis for flagging threshold crossing 111
APPENDIX 12. Atmospheric barometric pressure variations effects on methane inflow 114
APPENDIX 13. Fan characteristics in fan malfunctioning scenario 118

APPENDIX 14. Fan power comparison 119
9.0 Acknowledgement/Disclaimer 120

List of Figures

Figure 2.1. The structure of the EWS embedded in Ventsim Premium with MULTIFLUX. 10
Figure 4.1. Schematic components of a mine ventilation and climate control system (After Danko, 2012). 14
Figure 5.1. EWS in accident-preventive, real-time mining application. 19
Figure 5.2. Schematic of the EWP "forecast in space and time" concept for methane concentration early warning at the workplace (critical location), based on a trigger from the AMS signal at monitored location (in real-time) and APPS model prediction (in simulation-time scale). Sequence of events are numbered from (1) to (8). 21
Figure 5.3. Monitored (M), modeled (m), and critical (C) locations at a mine. Note that a critical location may not be monitored at the mine but will always be predicted with the EWP system. 22
Figure 5.4. Continuous mine-wide APPS with root-cause source terms. 22
Figure 5.5. Gas inflow from strata. 23
Figure 5.6. Schematic of modeled section showing areas of gas inflow with source locations for coal mine example 1 (Jong et al, 2013). 24
Figure 5.7. Layout of coal mine example 1 with methane sources and assumed monitored sensor locations in Ventsim. 26
Figure 5.8a. Results of methane concentration at selected observed locations from native VAM simulation in Scenario 1A. Selected locations with significant changes only are plotted. 27
Figure 5.8b. Emulated sensor signals used as assumed monitored data input to trigger the APPS forward predictor in the EWS system in Scenario 1A (shown in thick lines with confidence bounds). Assumed sensor 15 (and 17 if installed) trip(s) threshold for EWP forward prediction. The curves show real-time changes in CH_4 concentration. Selected locations with significant changes only are plotted. Note that the sensor signals are also used for the APPS predictor continuously (shown in dashed lines). 28
Figure 5.8c. APPS model forward prediction at selected observed locations in real-time and in fast simulation time scales for Scenario 1A. Only two selected locations are shown. 29
Figure 5.9a. Results of methane concentration at selected observed locations from native VAM simulation in Scenario 1B. Selected locations with significant changes only are plotted. 30
Figure 5.9b. Emulated sensor signals used as assumed monitored data input to trigger the EWS system in Scenario 1B (shown in thick lines with confidence bounds). Assumed sensors 15, 12, 16 (and 17 if installed) trip threshold for EWP forward prediction (sensor 16 is too close to threshold to trip). The curves show real-time changes in CH_4 concentration. Selected locations (with significant changes only) are plotted. Note that the sensor signals are also used for the APPS corrector continuously (shown in dashed lines) 31
Figure 5.9c. APPS model forward prediction at selected observed locations in real-time and in fast simulation time scales for Scenario 1B. Only two selected locations are shown. 32
Figure 5.10. Schematic of modeled section showing areas of perturbation with source locations for coal mine example 2. 33
Figure 5.11. Layout of coal mine example 2 with methane sources and assumed monitored sensor locations in Ventsim. 34

Figure 5.13. Schematic of area of perturbation for airway blockage for coal mine example 1. 39
Figure 5.14a. Results of methane concentration at selected observed locations from native VAM simulation in Scenario 2. Selected locations with significant changes only are plotted. 40
Figure 5.14b. Emulated sensor signal used as assumed monitored data input to trigger the EWS system in Scenario 2 (shown in thick lines with confidence bounds). Assumed sensors 15 (and 17 if installed) trip threshold for EWP forward prediction. The curves show real-time changes in CH_4 concentration. Selected locations with significant changes only are plotted. Note that the sensor signals are also used for the APPS predictor continuously (shown in dashed lines). 41
Figure 5.15. Results of airflow at assumed monitored locations due to airway blockage in coal mine example 1. 42
Figure 5.16. Results of velocity at assumed monitored locations due to airway blockage in coal mine example 1. 43
Figure 5.17. Results of absolute pressure at assumed monitored locations due to airway blockage in coal mine example 1. 43
Figure 5.18: Barometric pressure drop inducing CH_4 flow. 45
Figure 5.19a. Results of methane concentration at selected observed locations from native VAM simulation in Scenario 3. Selected locations with significant changes only are plotted. 46
Figure 5.19b. Emulated sensor signal used as assumed monitored data input to trigger the EWS system Scenario 3 (shown in thick lines with confidence bounds). Assumed sensors 15 (and 17 if installed) trip threshold for EWP forward prediction. The curves show real-time changes in CH_4 concentration. Selected locations with significant changes only are plotted. Note that the sensor signals are also used for the APPS corrector continuously (shown in dashed lines). 47
Figure 5.19c. APPS model forward prediction at selected observed locations in real-time and in fast simulation time scales for Scenario 3. Only two selected locations are shown. 48
Figure 5.20. Results of absolute pressure at assumed monitored locations due to barometric pressure drop in coal mine example 1. 48
Figure 5.21. Schematic of modeled section showing areas of perturbation with source locations and fan RPM drop location for coal mine example 2. 49
Figure 5.22a. Results of methane concentration at selected observed locations from native VAM simulation in Scenario 4. Selected locations with significant changes only are plotted. 50
Figure 5.22b. Emulated sensor signal used as assumed monitored data input to trigger the EWS system in Scenario 4 (shown in thick lines with confidence bounds). Assumed sensors 13, 17 (and 18 if installed) trip(s) threshold for EWP forward prediction. The curves show real-time changes in CH_4 concentration. Selected locations with significant changes only are plotted. Note that the sensor signals are also used for the APPS predictor continuously (shown in dashed lines). 51
Figure 5.22c. APPS model forward prediction at selected observed locations in real-time and in fast simulation time scales for Scenario 4. Only two selected locations are shown. 52
Figure 5.23. Results of airflow at assumed monitored locations due to fan malfunction in coal mine example 2. 52
Figure 5.24. Results of velocity at assumed monitored locations due to fan malfunction in coal mine example 2. 53
Figure 5.25. Results of absolute pressure at assumed monitored locations due to fan malfunction in coal mine example 2. 53

Figure 5.26. Schematic of modeled section illustrating areas of perturbation with source locations and belt fire location for coal mine example 2. 54
Figure 5.27a. Results of methane concentration at selected observed locations from native VAM simulation in Scenario 5. Selected locations with significant changes only are plotted. 55
Figure 5.27b. Emulated sensor signal used as assumed monitored data input to trigger the EWS system in Scenario 5 (shown in thick lines with confidence bounds). Assumed sensors 13, 17 (and 18 if installed) trip(s) threshold for EWP forward prediction. The curves show real-time changes in CH_4 concentration. Selected locations with significant changes only are plotted. Note that the sensor signals are also used for the APPS predictor continuously (shown in dashed lines). 56
Figure 5.27c. APPS model forward prediction at selected observed locations in real-time and in fast simulation time scales for Scenario 5. Only two selected locations are shown. 57
Figure 5.28. Results of airflow at assumed monitored locations due to belt fire in coal mine example 2. 57
Figure 5.29. Results of velocity at assumed monitored locations due to belt fire in coal mine example 2. 58
Figure A2.1. MULTIFLUX (MF) button in Ventsim Visual's toolbar. 63
Figure A2.2. Comparison between the native VAM model in Ventsim and the results from APPS in MULTIFLUX. 63
Figure A2.3. Comparison between the native VAM model in Ventsim and the results from APPS in MULTIFLUX at another mine section. 64
Figure A3.1. Activity chart for running MULTIFLUX. 66
Figure A3.2. APPS model example 1in MULTIFLUX (coal mine) converted from VnetPC. 67
Figure A3.3. APPS model example 2 in MULTIFLUX (metal mine) converted from VnetPC 68
Figure A3.4. APPS model example 5 (metal mine) in MULTIFLUX converted from Ventsim. 69
Figure A3.5. APPS model example of the Bingham Canyon Coal Mine in MULTIFLUX converted from MineVent. 70
Figure A4.1. Schematic diagram of the longwall panel ventilation system (Jong et al, 2013). 71
Figure A4.2. Ventilation schematic demonstrating the gob in MULTIFLUX. 72
Figure A4.3. Flux increase (b) due to pressure drop (a) per 1000 m airway section (Danko et al, 2013). . 72
Figure A4.4. Typical Barometric Pressure, Pb, variation in Nevada (Danko et al, 2013). 73
Figure A4.5. Methane concentration change from gob with time due to airway blockage. 75
Figure A4.6. Methane inflow rate from gob due to barometric pressure change. 75
Figure A5.1. MULTIFLUX import/export module added to the Ventsim GUI. 76
Figure A5.2. MULTIFLUX model of the example RA imported into the Ventsim GUI. 77
Figure A6.1. Airflow % difference between VnetPC and MULTIFLUX models for mine example 1 (coal mine). 78
Figure A6.2. Fan working points comparison between VnetPC and MULTIFLUX models for mine example 1 (coal mine). 79
Figure A6.3. Difference for fan working points between VnetPC and MULTIFLUX models for mine example 1 (coal mine). 79
Figure A6.4. Airflow % difference between VnetPC and MULTIFLUX models for mine example 2 (metal mine). 80
Figure A6.5. Fan pressure comparison between VnetPC and MULTIFLUX. 81
Figure A6.6. Fan airflow rate comparison between VnetPC and MULTIFLUX. 81

Figure A6.7. Fan pressure difference between VnetPC and MULTIFLUX. 82
Figure A6.8. Fan airflow rate difference between VnetPC and MULTIFLUX. 82
Figure A6.9. Fan curve comparison difference between VnetPC and MULTIFLUX for fan number 61. . 83
Figure A6.10. Fan curve comparison difference between VnetPC and MULTIFLUX for fan number 62. 83
Figure A6.11. Airflow difference comparison between VnetPC and MULTIFLUX models for mine example 3 (metal mine example from VnetPC). 84
Figure A6.12. Fan working points comparison between VnetPC and MULTIFLUX models for mine example 3 (metal mine example from VnetPC). 84
Figure A6.13. Difference in fan working points between VnetPC and MULTIFLUX models for mine example 3 (metal mine example from VnetPC). 85
Figure A6.14. Airflow % difference comparison between VnetPC and MULTIFLUX models for mine example 4 (coal mine example from VnetPC). 85
Figure A6.15. Fan working points comparison between VnetPC and MULTIFLUX for mine example 4 (coal mine example from VnetPC). 86
Figure A6.16. Difference for fan working points between VnetPC and MULTIFLUX for mine example 4 (coal mine example from VnetPC). 86
Figure A6.17. Airflow % difference comparison between Ventsim and MULTIFLUX models for mine example 5 (metal mine). 87
Figure A6.18. Fan working points comparison between Ventsim and MULTIFLUX models for mine example 5 (metal mine). 87
Figure A6.19. Difference for fan working points between Ventsim and MULTIFLUX models for mine example 5 (metal mine). 88
Figure A7.1. Ventsim LiveView feature to connect to real-time monitoring data. 88
Figure A7.2. Example of monitoring station mapping using dynamic monitor icon in Ventsim. 89
Figure A7.3. Example of plotted data from a monitoring station, M1 in Ventsim. 90
Figure A8.1. Comparison between measured velocities and the results from the MULTIFLUX model with confidence bound. 91
Figure A8.2. Comparison between measured barometric pressure and the results from the MULTIFLUX model with confidence bound. 91
Figure A8.3. Weather data, Elko, NV. April 9-10, 2014 http://www.wunderground.com/history). 92
Figure A8.4. Branch 253 monitored location for mine temperature. 92
Figure A8.5. Model results for wet bulb and dry bulb temperatures for branch 253 with error. 93
Figure A9.1. Methane flow rate from gob model for 2000 Pa pressure drop. 94
Figure A9.2. NTCF surrogate model compared with the CFD gob model for -2000 Pa drop. 95
Figure A9.3. Airway pressure variation for the +/-2000 Pa variable pressure 95
Figure A9.4. NTCF surrogate model comparison with the CFD gob model for the +/-2000 Pa variable pressure. 96
Figure A9.5. Airway pressure variation including a sudden change. 96
Figure A9.6. NTCF surrogate model comparison with the CFD gob model. 97
Figure A9.7. Pressure sensor data together with the filtered data. 98
Figure A9.8. Pressure first derivative. 99
Figure A9.9. Pressure second derivative. 100

Figure A10.1. (a) Primary signal (b) first derivative (c) second derivative and (d) trend of system constants.....100
Figure A10.2. Schematic of an airflow blockage and its effect on pressure and airflow.....102
Figure A10.3.Continuous mine-wide APPS Simulator with root-cause source terms, (a); detail of CDC with NTCF, (b).....103
Figure A10.4. Signal data together with the filtered data. 105
Figure A10.5. Signal data first derivative. 105
Figure A10.6. Signal data second derivative. 106
Figure A10.7. Signal system properties, A_0 constant.....106
Figure A10.8. Signal system properties, A_1 constant.....107
Figure A10.9. Signal system properties, A_2 constant.....107
Figure A10.10. Signal data together with the filtered data. 108
Figure A10.11. Signal data first derivative. 108
Figure A10.12. Signal data second derivative. 109
Figure A10.13. Signal system properties, A_0 constant.....109
Figure A3. A10.14. Signal system properties, A_1 constant.....110
Figure A10.15. Signal system properties, A_2 constant.....110
Figure A11.1. Flow chart for signal analysis problem identification.....112
Figure A11.2. “Moving window” evaluation of the signal flow.....113
Figure A11.3: “Moving window” filter processing schematic. 113
Figure A11.4. Signal processing and trend analysis chart. 114
Figure A12.1. Layout of the longwall.....115
Figure A12.2. 3D section of the Gob. 115
Figure A12.3. Layout of flow of Air-CH_4 mixture in and out of the airway due to barometric pressure drop. 115
Figure A12.4. 3D Flow of Air- CH_4 mixture in and out of the airway. 116
Figure A12.5. 2D Flow profile of Air- CH_4 mixture in and out of the airway for selected time divisions. 116
Figure A12.6. Methane concentration profile from Air-CH_4 mixing in the gob. 117
Figure A12.7. Results of airflow at monitored locations due to barometric pressure drop. 117
Figure A12.8. Results of velocity at monitored locations due to barometric pressure drop. 118
Figure A13.1. Fan curves for original (a) and reduced (b) fan points.....119

List of Tables

Table 5.1. Modeled scenarios used in demonstrational examples. 21
Table A4.1. Development mining parameters and their range of values used for modeling purposes (Schatzel et al, 2008).....71
The base points of the fan characteristics used in the scenario are given in table A13.1. 118
Table A13.1 Fan points.....118
Table A14.1. Fan power for various scenarios modeled in mine example 1. 119
Table A14.2. Fan power for various scenarios modeled in mine example 2. 120
Table A14.3. Signal type and the model type for each scenario.....120

List of Acronyms

AMS:	Atmospheric Monitoring System
APPS:	Air Parameter Predictor Simulator
BC:	Boundary Condition
CDC:	Continuous Dynamic Correlator
CFD:	Computational Fluid Dynamics
ERC:	Emergency Refuge Chamber
EWP:	Early Warning Predictor
EWS:	Early Warning System
GUI:	Graphical User Interface
MCD:	Model Configuration Data
MF:	MULTIFLUX
MPD:	Mine Production Data
NIOSH:	National Institute for Occupational Safety and Health
NTCF:	Numeral Transport Code Functionalization
RMS:	Root Mean Square
RSM:	Roof Stability Monitoring
SME:	Society of Mining and Metallurgical Engineers
UNR:	University of Nevada, Reno
US:	United States
VAM:	Ventilation Air Model
VOD:	Ventilation On Demand

2.0 Executive summary

The focus area of the research project is mine safety. A new technology is developed to recognize hazardous atmospheric conditions in a mine ventilation system based on analyzing continuous mine monitoring signals from sensors and information systems. Methods are developed to recognize safety hazards during their development real-time caused by heat, combustible gases, or the accumulation of poisonous gases in a mine.

Five representative, potentially hazardous cases are studied in detail by numerical simulation to prove the concept of early warning of dangerous conditions in their evolution toward an accident. The Early Warning System (EWS) model has the ability of recognizing threat to safety at a significantly earlier time, well before the actual event would lead to an accident at a future time. The demonstrational exercises of the EWS apply future-in-time as well as spatial forward predictions by computer simulations, expanding the ability of human supervision in the evaluation of monitored data.

The design of the EWS is based on the assumption that the mine has a calibrated ventilation model; a fast-response monitoring system for atmospheric properties and operating parameters; all feeding signals to the EWS real-time. While all partner mines in past and current research projects have used validated ventilation models, few run continuous monitoring systems with central data acquisition. The project, therefore, uses emulated sensor signals for the EWS study by design from its inception.

For the applicability to a mine, a converter macro is developed between a native Ventilation Atmosphere Model (VAM) of a mine and the Air Properties Predictor Simulator (APPS). The APPS model runs in MULTIFLUX. In addition to completion of the converter, a development partnership with the Chasm Consulting, the owner and software distributor of Ventsim has been reached. The development is conducted under a tryout software license agreement signed by Chasm Consulting and the University of Nevada, Reno, the owner of MULTIFLUX. Appendix 1 is a declaration of intent of this joint agreement. The new Version 4 of Ventsim introduced in 2015 includes the MULTIFLUX solver engine under an “MF icon”. This is a major achievement regarding the commercialization potential and industrial accessibility of our new technology. The Ventsim Ventilation Software package can import the mine ventilation model from other ventilation packages such as VnetPC. A native VAM model can be linked to the new Early Warning System (EWS) running MULTIFLUX through the Ventsim Visual Premium V4. Therefore, our stated goal for wide dissemination will be achievable once the project completes the commercialization phase.

The EWS software uses real-time data from the Atmospheric Monitoring System (AMS); the variable Mine Production Data (MPD); and the signals from the Roof Stability Monitors (RSM). It must be addressed that not all signals are available for the EWS at any operating mine. Nevertheless, these signals are achievable by installing commercial data acquisition and mine information systems. One of the outcomes of the study is the recognition of the needs of the input signals for the applicability of the new EWS to a mine. The data from the AMS must be processed

to filter out the disturbances caused by the normal mining operations to avoid a false Early Warning Predictor (EWP) alarm. The signals from the RSM are real-time safety hazard indicators by their own, in addition to indicators to potential gas in-burst that must be checked by the signal analyzers of the gas concentration sensors with a lowered acceptance tolerance than for as-usual variations.

The configuration of the sensor system of an operating mine and access to sensors' output data is available for the EWS through the Ventsim Visual Premium V4 with the embedded MULTIFLUX solver. Instead of working on a low-level software macro to import the sensor system of an operating mine, the MULTIFLUX solver is imported into the Ventsim Visual Graphical User Interface (GUI) framework. Figure 2.1 shows the structure of the EWS embedded in the Ventsim Visual Premium V4 with MULTIFLUX. As shown, the sensor system configuration in Ventsim is user defined. The direct connection between Ventsim and MULTIFLUX has been tested as shown in the screen shot figures in Appendix 2.

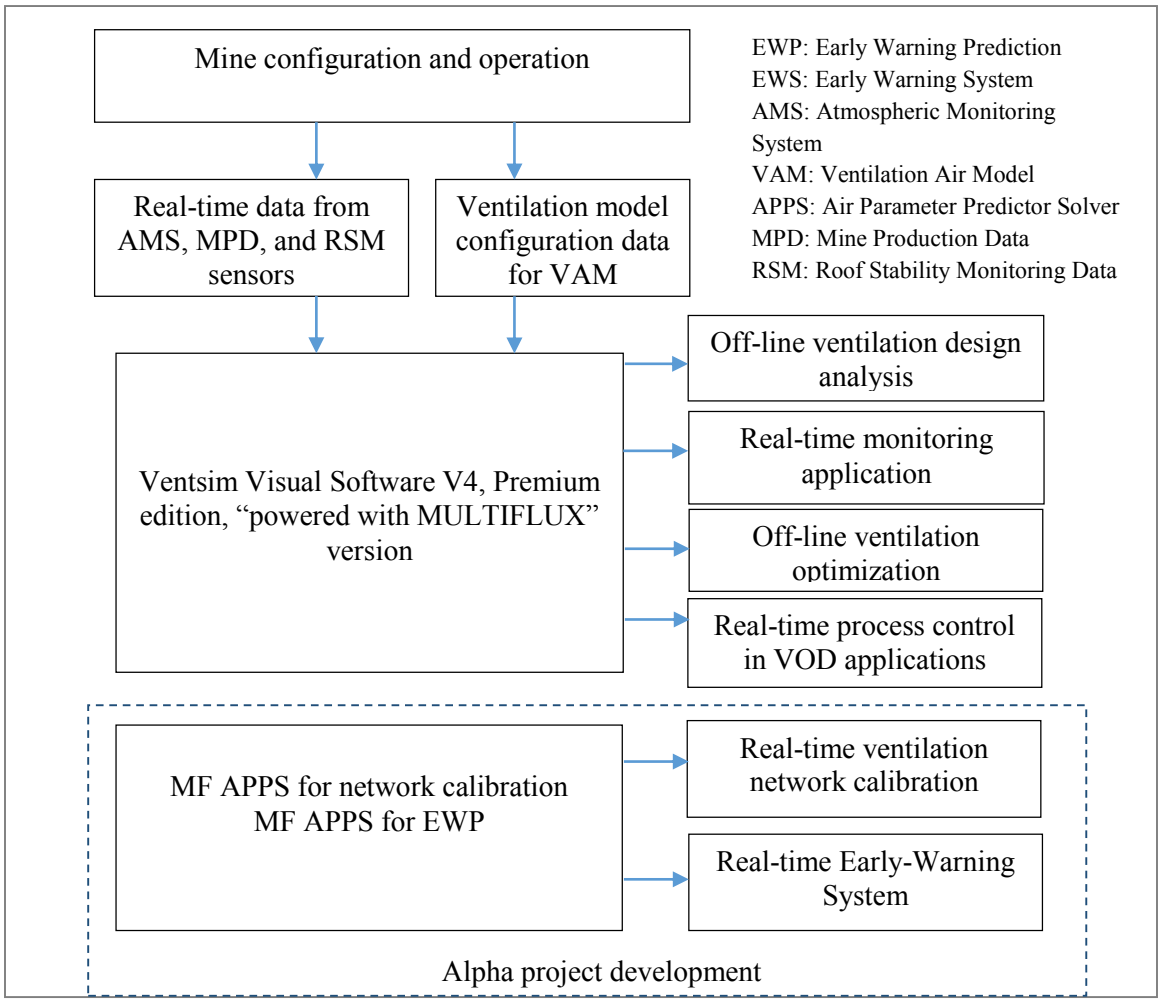

Figure 2.1. The structure of the EWS embedded in Ventsim Premium with MULTIFLUX.

The main, innovative component of the EWS is the EWP forward predictor of emerging hazards with APPS. Synthetic data from model simulations are used for the development of EWP. Hazardous scenarios are defined, modeled, and recorded as AMS, RSM and MPD data. First, gas in-burst is modeled as AMS data with increased gas concentration, such as methane. Second, airflow blockage is studied as it may be caused by roof collapse that may or may not be detected by the RMS sensors. Third, the effect of pressure drop in barometric pressure, causing increased gas inflow from the strata into the ventilating air is simulated. A highly innovative component in the EWP is a simulation method for the forward prediction of gas concentrations due to time and pressure-dependent gas inflow variations. The new simulation method is programed as a Continuous Dynamic Correlator (CDC). Fourth, fan malfunction or the effect of fan stoppage, indicated by the MPD data, is analyzed for hazardous effects on contaminant gas dilution. Fifth, mine belt fire is modeled, which may be detected from the typical signal trends observable from the continuous processing of the AMS sensors data for concentration, temperature, and relative humidity.

The forward-predicting APPS algorithm is programed as a fast-running direct calculation starting from the deteriorated input data. The APPS can be executed as a stand-alone real-time simulator or run under Ventsim as a result of a cooperative agreement between UNR and Chasm. This agreement is outside of the current Alpha project, but it has a great potential for commercialization of the EWP system in the future. The cooperative work with the Ventsim developers is beneficial to the project in reaching the stated goals in time but at a higher level than it was originally proposed. Current test results show excellent numerical performance of the APPS results under the Ventsim GUI environment. Flagging critical conditions at critical locations can be momentarily posted in the GUI of Ventsim Visual Premium V4 with the MF as a special application package.

The results of this exploratory, innovative project are published in two interim reports and a presentation at the 2015 SME Annual Meeting & Exhibit in Denver. Another presentation is accepted for publication at the upcoming 2016 SME Annual Meeting & Exhibit to be held in Arizona. A Ph.D. dissertation is in development in the topic of root-cause analysis of atmospheric sensor data, an important element of EWS. A manuscript is being prepared for submission to an international journal.

3.0 Problem Statement and Innovation Objective

3.1 Problem statement

The recognition of safety hazard by manual evaluation is difficult because of the complex nature of information and the large amount of monitored data from measurement by atmospheric sensors such as air velocity, pressure, hazardous gas contaminants and temperature. In order to recognize problem-causing trends, it is necessary to evaluate continuously individual measurement data from the AMS of the mine during their time-dependent variations. In addition, the combined effects of various signal trends need to be simultaneously interpreted in their cross-effects.

It is difficult to evaluate the possible meaning of intertwined monitoring signals, from various sensors all changing with time. For example, a steady, continuous methane concentration measurement together with a sharp drop in barometric pressure from the AMS sensors may be a case for worry in future time due to pressure-induced methane increase from the coal seam or the gob (Danko and Bahrami, 2014a). Future increase in concentration can be predicted by a time-dependent VAM and its surrogate APPS model. A VAM or APPS model can indeed predict a likely methane concentration variation in future time as a function of historical and real-time concentrations, air pressure as well as air velocity. Such a future trend, however, cannot be seen from the raw measurement data. The innovation is a new type of application of the ventilation and contaminant transport models running at a fast-forward simulation speed to support mine management in recognizing warning trends in a timely manner. Continuous, automatic evaluation of the data stream of ventilation parameters is developed to pick up the warning signals and make a predictive forecast. The EWP provides (1) effective recognition of a hazardous condition during its evolution; and (2) warning signal for preventive actions without delay for effective resolution of the hazardous scenario.

A major breakthrough in safety improvement can be achieved by the recognition of early trends that indicate potential safety hazards. Measures must be taken in time to counteract the interplay of many reasons leading to an accident. The study of past mine accident scenarios related to mine ventilation, e.g., published by (Page, et.al, 2012), show that the accidents were preventable. However, early-warning events must be recognized during their evolution before the chain reaction of many events may trigger a catastrophic accident. For such a complex analysis, a breakthrough is needed using computational model prediction such as the one used in the innovative EWP.

3.2 Innovation objective

The general research objective is to develop a software-based EWS that can recognize accident scenarios during the evolution of the hazardous conditions and warn mine management for preventive measures before the "would-be" accident happened in order to avoid it.

Specific objectives are to develop and test the EWP real-time predictor for atmospheric monitoring and ventilation parameters, incorporating a fast simulator model, called APPS. The APPS model runs in corrector-predictor mode real-time using the inputs from the mine's AMS, MPD, and RSM data, and forward-predicts critical mine conditions regarding ventilation air parameters at an early time before the condition actually develops in real time. If the safety threshold is crossed in the simulated atmospheric conditions at a future time, the EWP generates a warning alarm for the management to act for resolving the hazardous condition before the actual safety hazard will have developed.

4.0. Research Approach

The EWS is developed for use by operating mines which already have (a) monitoring system of atmospheric conditions real-time;(b) a mine information system that transfers real-time data from the monitoring system to the EWS and from the ventilation operation parameters as well

as ground control sensors; and (c) a mine ventilation model running in either VnetPC (VnetPC, 2007), Ventsim (Ventsim, 2009), or MULTIFLUX (Danko, 2008, Danko and Bahrami, 2008). All modern mines have advanced, monitoring and mine information systems and adopted at least one or sometimes more ventilation models of their choice. The focus of the research project is the development of the EWS as it is embedded into the infrastructure of a modern mine with a mine ventilation and control system. The architecture of such a system is shown in Figure 4.1. The main components necessary for an EWS to function are a number of atmospheric sensors such as air parameter sensors for velocity, airflow rate, relative humidity, pressure and temperature, and gas concentration sensors in the order of at least a few dozen for a mine with a few hundred airways. Atmospheric sensors in strategic locations must be monitored real-time. Roof stability and operating parameters in the mine should as well be recorded continuously.

The EWS requires real-time data to be passed from the mine monitoring system for evaluation and forward prediction. Bits and pieces of the components for the EWS are available at any modern mine. However, they are not connected and often are left out of calibration or maintenance, lacking their direct real-time applicability to safety. The innovative approach of the EWS is that it links together the mine ventilation model, the data stream from the real-time sensors, and an expert system with a forecasting evaluation program that provides a warning message, flagging imminent or near-future safety hazards.

The research approach includes four components 4.1 through 4.4. The development of the EWS is defined in components 4.1 through 4.3 for the required capacity. Test for flagging safety criticality conditions at critical location is described in section 4.4.

4.1 Link the native VAM of a mine to APPS used in EWP

An input data transfer macro program is developed to read the input data files of the native ventilation model (such as VnetPC, Ventsim) and to translate the model configuration of the surrogate APPS model in the EWP. Best conversion is provided in Ventsim as it is the most convenient with a user friendly GUI. Conversion from Ventsim to the surrogate APPS source-code model is automatic. Ventsim can import a VnetPC or MULTIFLUX VAM automatically therefore, it can connect to the APPS source-code model directly.

The APPS is used first as a past time simulator in corrector mode for identification of the changing BC of the ventilation model against real-time mine measurement data. The APPS model is run by a macro and uses data files for input, a very different application style from using the native the native VAM of the mines directly.

The surrogate APPS is configured in MULTIFLUX, a ventilation, heat, moisture, and contaminant transport model and software which is owned by the University of Nevada, Reno. MULTIFLUX has been tested and qualified under US Governmental Standards for software qualification according to 10 CFR Part 830 (Danko, 2008).

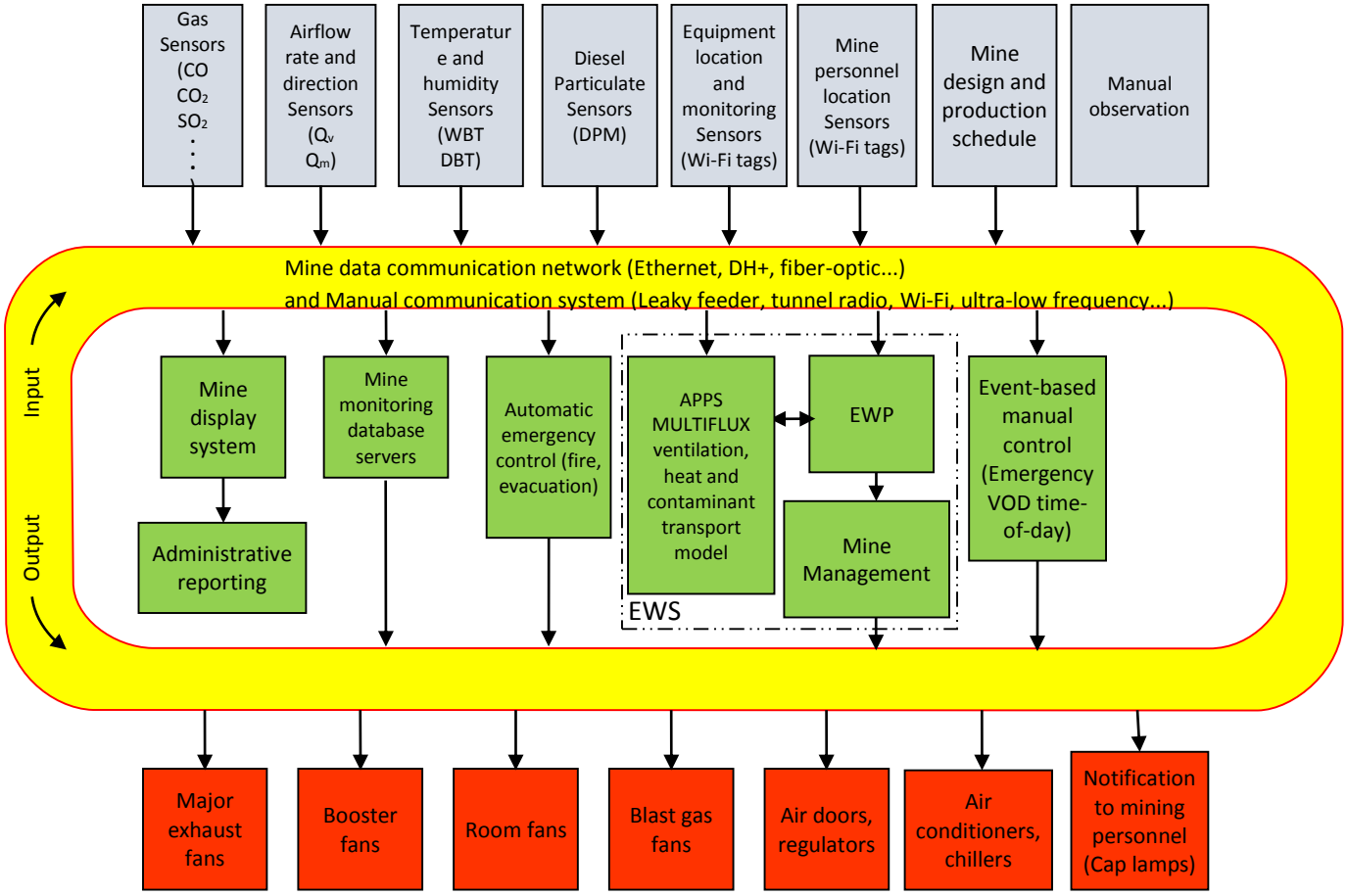

Figure 4.1. Schematic components of a mine ventilation and climate control system (After Danko, 2012).

The native VAM of a mine is assumed to be calibrated, providing correct data for relevant air parameters for the mine. The task of setting up a ventilation and contaminant transport model and verifying such a model is not part of the current work.

In addition to importing the air flow model, further steps are needed to convert the thermal and concentration model-elements and to add the model of the gob or leaky-sealed mine areas to the APPS predictor model. The additional elements are:

- A software macro, written to read any of the three native VAM's data files to configure the APPS model in MULTIFLUX. The Model Configuration Data (MCD) does not change with mining operations hourly, daily or even weekly or perhaps monthly. The APPS model uses other input data specifying mine production, MPD, and associated ventilation parameters from underground operations. The additional data are passed as BC of the APPS model real-time by the EWS software. Appendix 3 shows the details of the software macro.

- The model of the gob and/or any sealed-off part of a coal or other mine, added directly in MULTIFLUX if such mine area is to be considered in the EWP. Gob and gas inflow model is adopted from NIOSH recommendations (Schatzel, et al, 2008) and configured in MULTIFLUX for a complete APPS. Appendix 4 describes the gob model and a simplified analysis of expected gas flow into the airway.
- The ventilation and thermal environment of the ERC, added to the APPS. ERC of adequate capacity is mandated by every metal and coal mine in the US. The capacity of an ERC is dependent of the actual mine environment. The APPS model predicts derating of an ERC for capacity for an emergency rescue operation to be available at the time of issuing a EWP. Derating of thermal limit (max. 95^{o}F equivalent temperature inside the ERC after 98 hours of occupation without ventilation) follows the requirement specified by 30 CFR §7.504 (2012). The ERC element is demonstrated in Appendix 5.

The software macro is tested for three examples from the partner mines for acceptable match between the APPS model and the native VAM model in air parameter predictions. Appendix 6 illustrates the detailed comparisons qualifying the APPS as a validated, surrogate model to replace the native VAM in operating the EWP.

4.2 Link the MPD, RSM and AMS to EWP for BC and test the APPS as corrector

A data interface is developed to define the mapping of data stream from MPD, RSM, and AMS to EWP using (a) the physical locations of the sensors relative to the VAM coordinates; (b) the nature of the signal (e.g., power use of the faces, roof stability rating, air velocity, pressure, gas species concentration, temperature, humidity; and (c) the expected data uncertainty and measurement noise. Appendix 7 shows the definition of measurement locations in Ventsim Live, a GUI that can be used if the current EWS is linked to Ventsim.

In the current exploratory development work, synthetic output data are generated from validated mine ventilation and contaminant flow as well as mine fire models at the real or planned sensor layout locations in our partner mines. Likewise, synthetic change at the BC are used, with added error to emulate measurement error. Roof collapse is modeled by increasing the resistance of the air branch at the hazardous locations manually and generating the air parameter changes accordingly.

The EWP system is tested with synthetic MDP, RSM, and AMS data in which all possible problems can be superimposed or emulated. For example, sudden contaminant in-bursts, airway collapse, fan malfunction and other hazardous conditions are introduced to the APPS model. The EWP is programmed for correct and timely alarm warning in response to any of the synthetic, induced hazard scenario. This way, the EWP is tested under controlled conditions in the simulated, computational environment, whereas the mines in the real world are not disturbed in any scenario to create hazardous conditions.

The EWP system is tested for a suit of disturbances in the computer laboratory at UNR. Five VAM models are imported for the studies to create the APPS internal simulation model for the perturbations in the EWP. The AMS system layout and the measurement accuracy as well as

uncertainty range are acquired from the partner mines for the development and test phase of the EWP. The test data with random error are documented in Appendix 8.

For an informed APPS model, MPD from mine operations are needed, such as electrical power of longwall shearer, conveyor belt, operation of machinery, power centers, and ventilation fans. AMS monitored data are matched with the APPS model according to the continuous self-calibration concept illustrated in Figure 2.1 during normal operations. Such a continuous model calibration is necessary to reduce the large and typical matching confidence bounds shown in the Figures in Appendix 8.

Mine data from an industrial partner are used to set up realistic measurement error ranges in the emulator of their AMS system. The measurement uncertainty ranges are discussed and given in Appendix 7. The development of the EWS system is completed using real mine VAM examples from two different mines (to be realistic) and synthetic and controlled for creating any disturbances for the numerical tests (to be safe and productive), but not disruptive to the mines. Therefore, while the test cases are defined with hazard-causing disturbances for the EWP, no interference is caused with the mining production activities at the partner mines.

The EWP system is tested in its ability to forecast hazardous scenarios during their evolution but before the thresholds for accidents have been crossed. Several scenarios are checked in forward-predicting mode, including: (1) methane in-burst from encountering a pocket at the face; (2) airway blockage as a result of partial collapse of a hazardous roof section in a mine; (3) atmospheric barometric pressure variations causing methane inflow from the gob (4) booster fans malfunction; fan starts or stops can cause barometric pressure variation that may trigger pressure unbalances and methane inflow from sealed areas, seams, or gob; and (5) Fire heat load. The test results are discussed in section 5.

4. 3. Develop forward prediction with APPS and make an EWP warning display

A parallel APPS predictor model is developed to predict all air parameters at all locations independently from the APPS corrector model. The two models share the same BC and the airway flow and transport properties. The APPS predictor model is controlled by a set of BC, carrying the signals of changing conditions. The BCs are identified by the APPS corrector using the MDP, RSM, and AMS data. A detailed explanation of the forward predictor algorithms are discussed in Appendix 9. The trend analysis based on signal processing is explained in Appendix 10.

The forward-prediction algorithm is developed, using APPS in predictor mode. Two methods are available: (1) fast direct simulation and (2) an innovative, differential forward prediction algorithm based on the use of the Jacobian matrices between differential BC parameters and differential responses for air flows, concentrations of critical mine gas components and heat. Direct simulation deals with the solution of the entire mine model whereas the Jacobian model run is a matrix-vector calculation. The forward prediction time with the Jacobian model is minimal, requiring only matrix-vector multiplications. However, the direct simulation method is used due to the high computational efficiency of the MULTIFLUX solver engine (for example, the CPU

solution time of a 27,000-branch mine flow network model is 1.6 second in a laptop computer with a single Intel i7 core).

The system is tested using emulated, synthetic MDP, RSM, and AMS data. Debugging and testing the EWP system with synthetic data are necessary due to the lack of actual mine monitoring data as well as advantageous for performing the test cases under controlled conditions.

The synthetic data are emulated using the native mine ventilation model, which is matched with the APPS model in the EWP. Therefore, no systematic error is suspected in this study simplifying the need for the performance validation in the current exploratory work phase. The results of the validation of model matches are discussed in Appendix 5.

4.4 Test for flagging safety criticality conditions at critical location

Data from the sensors are collected at regular time intervals in real application. In the current, exploratory project phase, emulated, synthetic data are used in lieu of real sensor data from VAM simulations of planned accident scenario. The necessary activities for recognizing safety hazard are: (1) data collection; (2) primary data processing; (3) root-cause analysis; (4) forward prediction; and (5) flagging for criticality. The test comprises of using the "blind" emulated data sensor data; analyzing the trends of the signals for the root-cause of the changes; and forward predict from that point the possible outcome of the perceived scenario. If threshold crossing for criticality is found from the APPS predictor model (which is a fast running, separate simulator from VAM), the test is considered successful for hazard prediction. The critical elements for success are (a) the accuracy of recognizing the root cause of an unexpected signal change, crossing the tolerance limit of normal regime; and (b) the timely forward prediction, much faster than real-time of future outcome of the disturbance riding toward an accident in real-time.

It is necessary to use time series analysis and other methods to smoothen and also characterize variations in the primary data in order to distinguish critical changes from the normal signal trends. Time series analysis comprises methods for analyzing time series data in order to extract meaningful statistics and other characteristics of the data. Time series forecasting is the use of a model to predict future values based on previously observed values. Two techniques are used for time series analysis, namely, parametric and non-parametric. The parametric approaches assume that the underlying stationary stochastic process has a certain structure which can be described using a small number of parameters (for example in autoregressive or moving average models). In these approaches, the task is to estimate the parameters of the model that describes the stochastic process. Non-parametric approaches explicitly estimate the covariance or the spectrum of the process without assuming that the process has any particular structure (Jianqing and Qiwei, 2003).

Different time series statistical models represent different stochastic processes which are applicable in filtering the primary data such as auto regression, integral, and moving average models (Shumway and Stoffer, 2010). These models are used to filter the noise and analyze the trends. Figures A11.2 and A11.3 in Appendix 11 demonstrate the "moving average window"

evaluation chart for usage of time series analysis in filtering and evaluating the primary data for identifying the root cause of the change which is used to forward predict future outcomes.

An internal expert system is developed in the form of a look-up table to make warning decisions. For a safety margin, stochastic perturbation is added to the forecasted parameters by the APPS predictor model with assumed, probabilistic changes in ΔCH_4, ΔCO, ΔCO_2, ΔSO_2, etc., for methane, coal dust, carbon monoxide, carbon dioxide, sulfite dioxide, or any other, injury-causing gas component at specific locations related to mining operations. The perturbation is kept in the same range as those for the measurement uncertainty in Appendix 8.

Tests are carried out for flagging safety criticality conditions at critical, working face location. Threshold crossing for criticality are demonstrated in future-time predictions from the APPS model in forecasting mode, the methods detailed in Appendix 11.

5.0 Summary of Accomplishments and Innovation Highlights

The exploratory phase of the development of a new EWS is completed, ready to be continued for prototype development to assist in mine disaster prevention. The new and innovative components are:

(1) The EWS uses real-time monitoring signals for forecasting in accelerated, simulation-time from the data to predict any likely event in the near future that may compromise safety; and
(2) The EWS uses the mine layout to forecasts in space, in order to evaluate safety at any critical working area, even at a place where no monitoring station is installed.

Figure 5.1 depicts the main components of the EWS in accident-preventive, real time applications. Figure 5.2 illustrates the concept of the EWP for a methane concentration example at an assumed critical location, critical workplace that is different from the AMS location.

The air parameters and their changes are simulated by the EWP model in forward predicting mode calculating gas concentrations at critical (forecasted) locations and critical (forecasted) time in the near future. The simulation time is much shorter (shown in dashed lines), by orders of magnitude less than the mine's assumed signal at critical location in real-time, giving an advantage in time for warning message for accident prevention. The air parameters and the changes are "sensed" by the EWP model all over the mine including places where there are no sensors.

Figure 5.3 depicts the schematic layout of monitored and critical locations for the explanation of the 'forecast in space' concept. The criteria used to determine a critical location is based on the areas that may have high concentration of gases that could lead to threshold crossing. Note that all nodes are modeled, but only a few are monitored; the critical location (C,m) may not have a monitor and a hazardous concentration may not be 'sensed' without a model. This is a new and innovative element in using the EWP system, improving a serious limitation in current monitoring systems that hamper their direct usefulness in disaster avoidance. A question must be asked: how can a sparsely monitored system sense e.g., sudden gas in-bursts and concentration spikes at the critical location close to the source if no sensors are installed near that location? The innovative EWP provides the answer and solution to this question by evaluating the critical

concentrations, temperatures, velocities, pressures, etc. at all locations and matching the spatial distribution of the solution with those from measurements at the available, monitored locations.

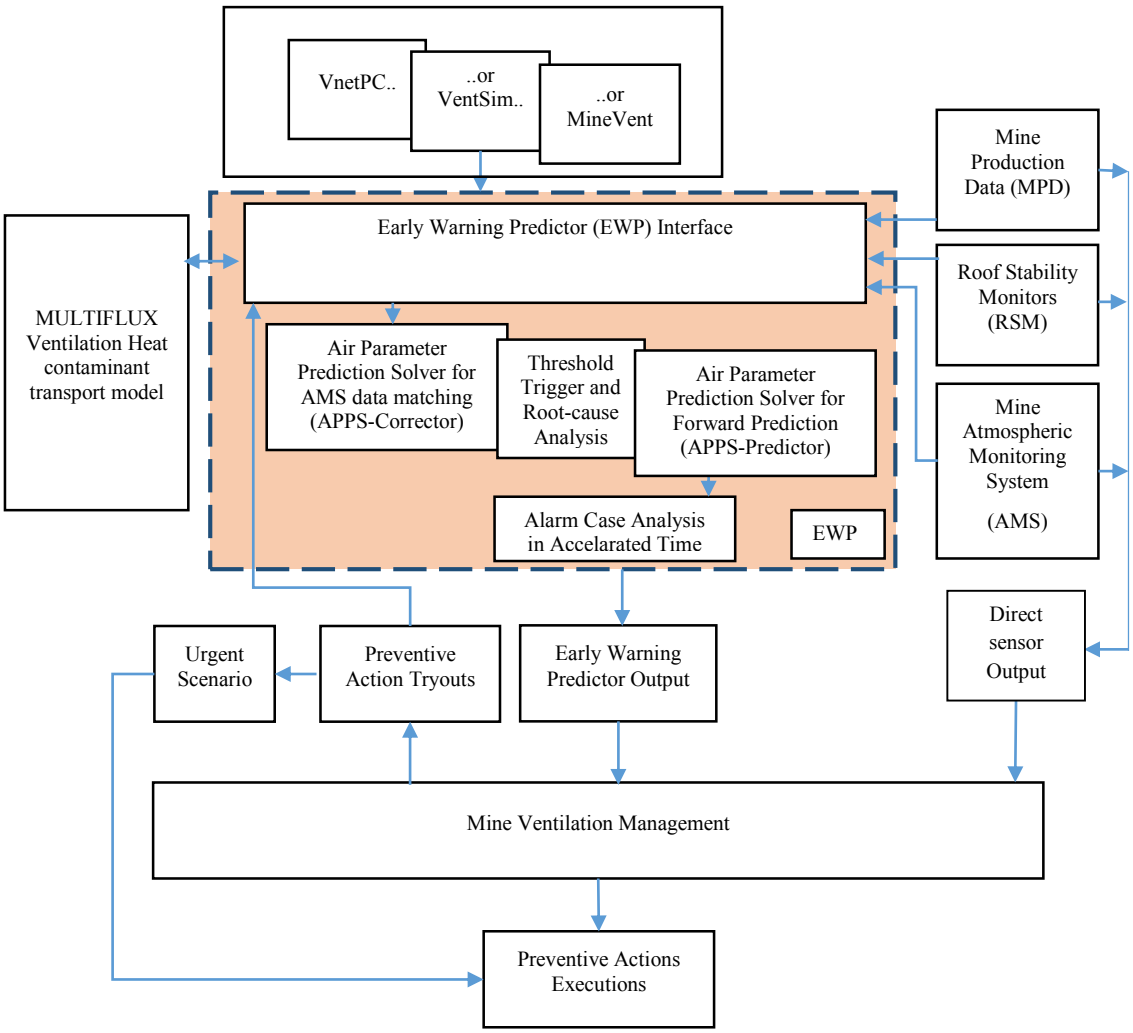

Figure 5.1. EWS in accident-preventive, real-time mining application.

The innovative EWP system runs five real-time processes simultaneously, performing

(1) Interpretation of the AMS signals in comparison with the APPS model;
(2) Validation of both the model and the sensor readings in their relationship to each other;
(3) Identification of plausible source changes as reasons for differences other than model error or sensor malfunction as unexpected changes at the BC (boundary conditions);
(4) Evaluation of the hazard conditions at critical locations; and
(5) Extrapolation of the trend with time and flagging crossing points with maximum threshold values for issuing an EWP alarm.

A special, most innovative form of the forward prediction algorithm that does not require a separate root-cause source identification is the CDC model discussed in detail in Appendix 10. The CDC model, depicted in Figure 5.4, represents an APPS model with root-cause source term built using the NTCF model-element.

Five scenarios are used to demonstrate the capability of the EWS system in two different coal mine examples:

(1) Methane in-burst from encountering a pocket at the face;
(2) Airway blockage as a result of partial collapse of a hazardous roof section in a mine;
(3) Atmospheric barometric pressure variations causing methane inflow from the gob;
(4) Booster fans malfunction; fan starts or stops can cause barometric pressure variation that may trigger pressure unbalances and methane inflow from sealed areas, seams, or gob; and
(5) Fire heat load.

The modeled scenarios of the five examples are summarized in Table 5.1.

The five scenarios are modeled in two coal mine examples depicted in Figures 5.7 and 5.11. Eighteen selected observed locations are marked in the model. These locations are represented in the model using markers called “dynamic monitors” in Ventsim. The observed locations include assumed monitoring sensor locations and critical location (not necessarily monitored) determined by knowing the dangerous spots in the mine.

The modeling process is performed in two parts. First, the VAM model is used and data are generated from it emulating sensors’ output. Second, the emulated sensor signals from some observed locations from the VAM results are used as assumed monitored data input to trigger the EWS system at 0.5% methane. Note that the sensor signals are also used for the APPS predictor continuously. Once the 0.5% methane concentration threshold limit value is crossed at any sensor, the EWP is triggered, which starts with a root-cause analysis and an APPS forward prediction at locations that may not be necessarily monitored. If the forward-predicted values lead to a threshold crossing of 1% methane, an EWS alarm is triggered. The delay time, which is the time required for the methane concentration to cross the threshold limit value of 1% for a particular critical location is determined from the time the sensor trips the EWP forward prediction at 0.5% methane as a reference time. The delay time minus the computational time of the APPS predictor is available as advance time for warning. This approach is used in all five EWS capacity demonstration examples. The APPS prediction simulation takes approximately 2 minutes from the time a sensor crosses the 0.5% methane threshold to the time of finishing the forward prediction at the (1% methane) threshold limit value crossing at a critical location, which might not be necessarily monitored. The simulation time of approximately 2 minutes has to be deducted from the delay time to determine the actual time gain for management to take action.

The time-dependent methane concentration results for each of the five scenarios are presented in three parts: (a) the native VAM model simulation results; (b) the emulated sensor

signals used as monitored data input to trigger the EWS system; and (c) the APPS model forward prediction signals starting from an early threshold crossing of monitored signals to check and issue EWS alarm if needed.

Table 5.1. Modeled scenarios used in demonstrational examples.

Scenario 1A (Base case for scenarios 2 and 3)	Methane in-burst (2 sources)	Mine example 1
Scenario 1B	Methane in-burst (3 sources)	Mine example 1
Scenario 1C(Base case for scenarios 4 and 5)	Methane in-burst (3 sources)	Mine example 2
Scenario 2	Airway blockage	Mine example 1
Scenario 3	Atmospheric barometric pressure variations	Mine example 1
Scenario 4	Fans malfunction	Mine example 2
Scenario 5	Fire heat load	Mine example 2

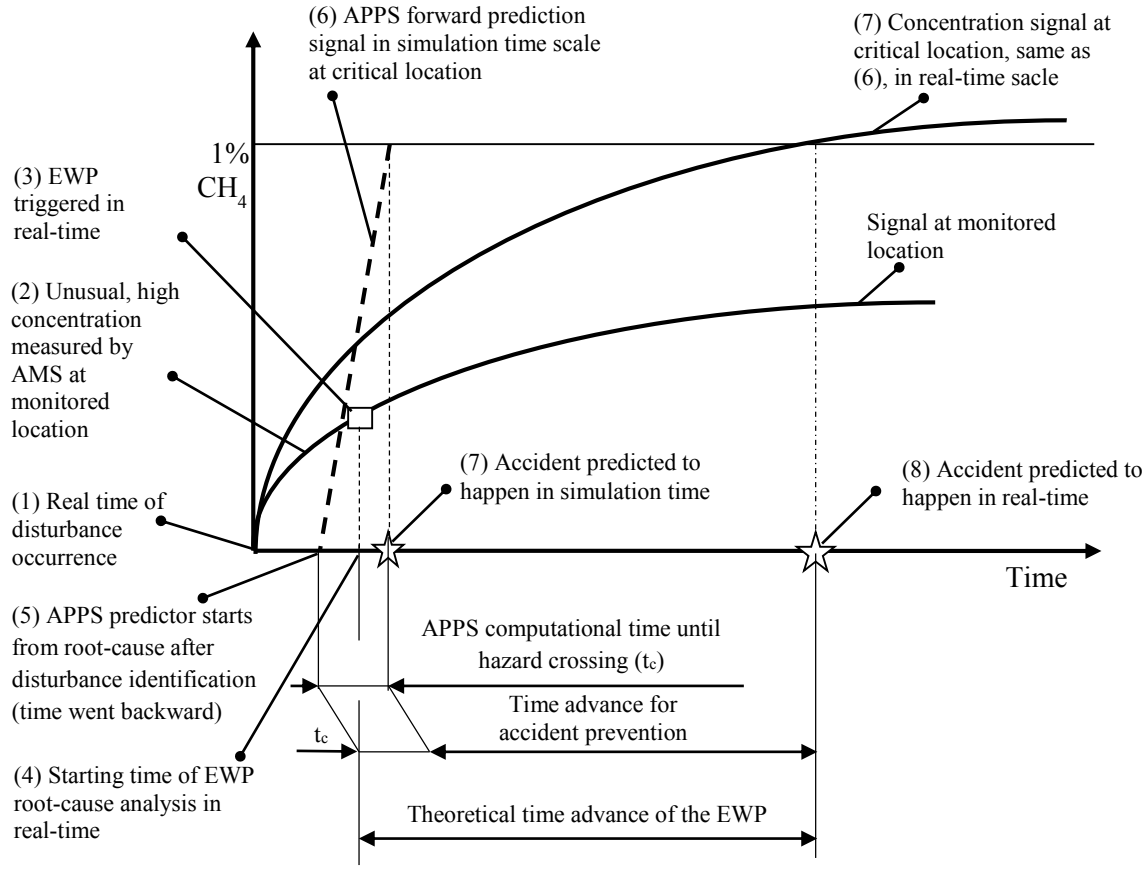

Figure 5.2. Schematic of the EWP "forecast in space and time" concept for methane concentration early warning at the workplace (critical location), based on a trigger from the AMS signal at monitored location (in real-time) and APPS model prediction (in simulation-time scale). Sequence of events are numbered from (1) to (8).

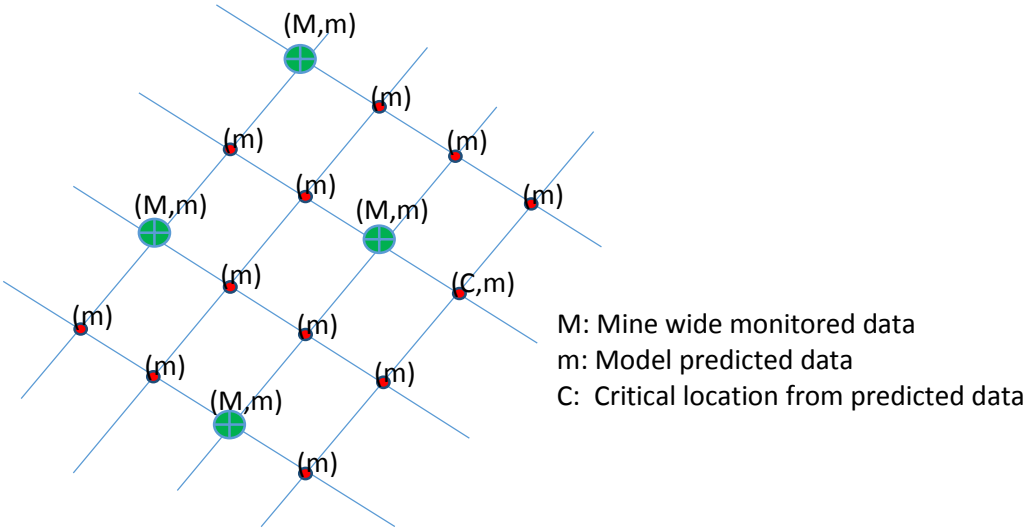

Figure 5.3. Monitored (M), modeled (m), and critical (C) locations at a mine. Note that a critical location may not be monitored at the mine but will always be predicted with the EWP system.

5.1 Methane in-burst from encountering a pocket at the face

Gas in-burst is considered when inflow of methane gas from the strata enters the mine airway due to e.g., face collapse, roof collapse, leakage from a gas pocket due to cracks in the strata, or water inflow that may be accompanied by methane. The gas inflow is caused by opening of a pathway to ventilating air. Methane in-burst is a hazardous event and is more likely to occur in coal mines, illustrated in Figure 5.5.

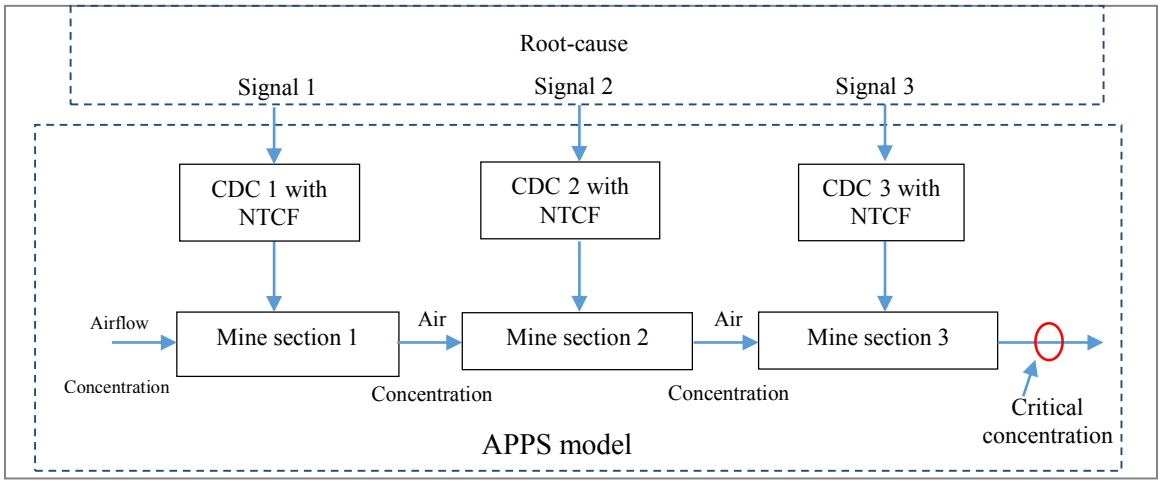

Figure 5.4. Continuous mine-wide APPS with root-cause source terms.

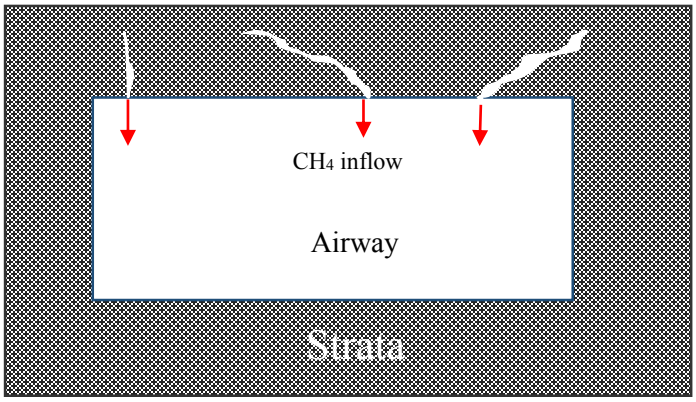

Figure 5.5. Gas inflow from strata.

Two examples are demonstrated in a longwall coal mine assuming two different methane source arrangements. This coal mine has 766 branches and 3 surface fans. The ventilation around the panel is facilitated using a three entry headgate, a single entry tailgate, a three entry bleeder, and a fringe ventilation path, which utilizes a small amount of intake air provided to the outside edges of the gob to ventilate any accumulation of gases. Three potential methane gas sources S1, S2, and S3 are assumed in the mine at three different locations, shown in Figure 5.6 with S1 in one of the longwall intake airways (branch 758), S2 at the working face (branch 761), and S3 in the longwall return airway (branch 760). S1, S2, and S3 only serve as methane gas input locations. Figure 5.7 illustrates the layout of the mine model with 18 observed locations of interest. All or only some of the marked-up locations may be used as monitored locations from which, the signals are used in real-time to trigger the EWP for forward predictions. The roles of the monitored signals, always in real-time, are (a) to trigger the EWP and start, if needed, a forward prediction by the fast APPS predictor; and (b) to serve for supporting the APPS corrector. Some or all of the same "observed" locations (or any other locations included in the mine ventilation network) are used in the hazard analysis by the APPS predicator in the accelerated, simulation time. The APPS predictor uses the same model as the APPS corrector, but the two processes run in parallel and on two very different time scales. If the two time scales are the same, no advance warning is possible. This is the reason for using high-performance simulation technique such as provided by MULTIFLUX. The area of investigation for methane in-burst in the two mines is the working face.

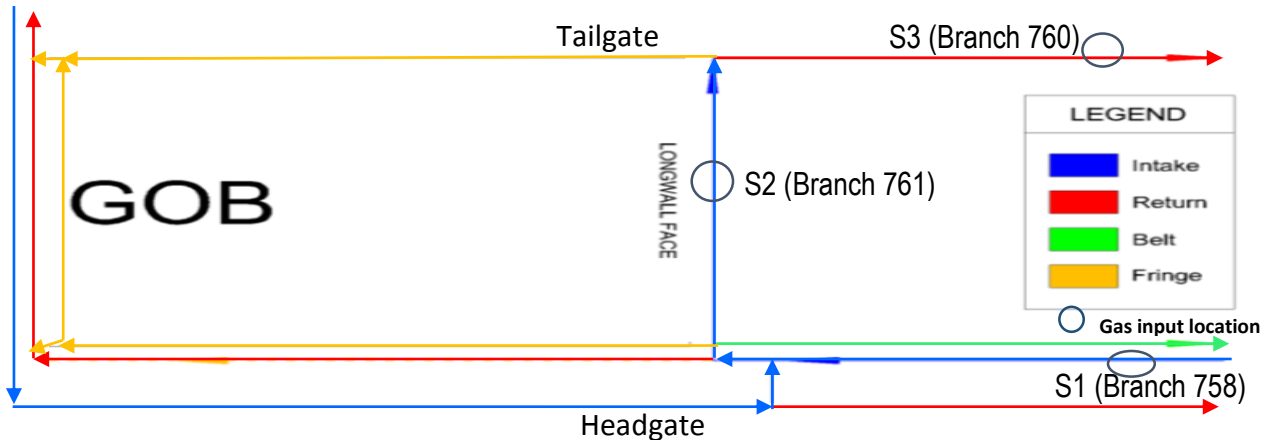

Figure 5.6. Schematic of modeled section showing areas of gas inflow with source locations for coal mine example 1 (Jong et al, 2013).

5.1.1 Two methane sources (Scenario 1A, coal mine example 1)

Gas in-burst is modeled first by injecting only two methane sources at S2 (line load, across the entire longwall face, 55 liters/second/100m of CH_4) and S3 (point source, 50% CH_4 at 0.1m^3/s). The simulation results for selected locations with significant changes only are plotted. The time-dependent VAM results for methane concentration are demonstrated in Figure 5.8a. The emulated sensor signals used as monitored data input to trigger the EWS system is shown in Figure 5.8b. Figure 5.8c depicts the APPS model forward prediction results for observed locations 15 and 17 based on the 0.5% methane crossing at assumed sensor 15. The results for airflow, velocity, and absolute pressure do not show any changes at the observed locations. A threshold limit value of 1% methane for stopping work is used in this analysis. Using 0.5% methane for a safety assumption to start a forward prediction and using branch 742 (monitoring sensor 15), which is a sensor location just at the end of the active face as a reference, the delay time in methane front arrival can be estimated. Branch 742 reaches 0.5% in 21 minutes and branch 760 reaches 0.8% in 33 minutes and remains constant as illustrated in Figure 5.8c. Therefore, the delay time before branch 760 (forward predicted signal at observed location 17 downstream of branch 742 on the return airway), reaches a maximum concentration is 12 minutes (33 minutes minus 21 minutes) in real-time. The computational overhead in forward-prediction simulation time is 2 minutes, negligible in this case. Therefore, 10 minutes is available for advance notice (12 minutes minus 2 minutes forward prediction time). Nevertheless, it is observed that the methane concentration remains below the threshold value of 1% for EWS alarm and no warning is necessary.

5.1.2 Three methane sources (Scenario 1B, coal mine example 1)

Gas in-burst is modeled by injecting three methane sources, adding an extra gas source, S1 (80% CH_4 at 0.2 m^3/s) at the upstream of the working face in addition to S2 and S3 with the same concentrations and flow rates as in Scenario 1A. The same sensor locations are used. The simulation results for selected locations with significant changes only are plotted. The time-dependent VAM results for methane concentration are demonstrated in Figure 5.9a. The emulated sensor signals used as monitored data input to trigger the EWS system is shown in Figure 5.9b. Figure 5.9c depicts the APPS model forward prediction results for observed locations 15 and 17 based on the 0.5% methane crossing at assumed sensor 15. There is a slight increase in methane concentrations in branch 760, which is a return airway downstream of the methane sources. The concentration crosses the threshold limit compared to that of the previous scenario 1A, where only two methane sources are used. This indicates that there is a possibility of threshold crossing from unknown methane source accumulation as the air flows downstream. A threshold limit value of 1% methane for stopping work is used in this analysis. The air parameters (airflow, velocity, and absolute pressure) are unaffected by the increase in methane sources from the results. Using 0.5% methane for a safety assumption to start a forward prediction and using branch 742 (monitoring sensor 15), which is a sensor location just at the end of the active face as a reference, the delay time in methane front arrival can be estimated. Branch 742 reaches 0.5% in 21 minutes and branch 760 reaches 1% in 52 minutes as illustrated in Figure 5.9c. Therefore, the delay time before branch 760 (forward predicted signal at observed location 17 downstream of branch 742 on the return airway, not necessarily monitored), crosses the threshold is 31 minutes (52 minutes minus 21 minutes) which triggers an EWS alarm. Since threshold crossing occurs, the gain time for management to take action is 29 minutes (31 minutes minus 2 minutes forward prediction time).

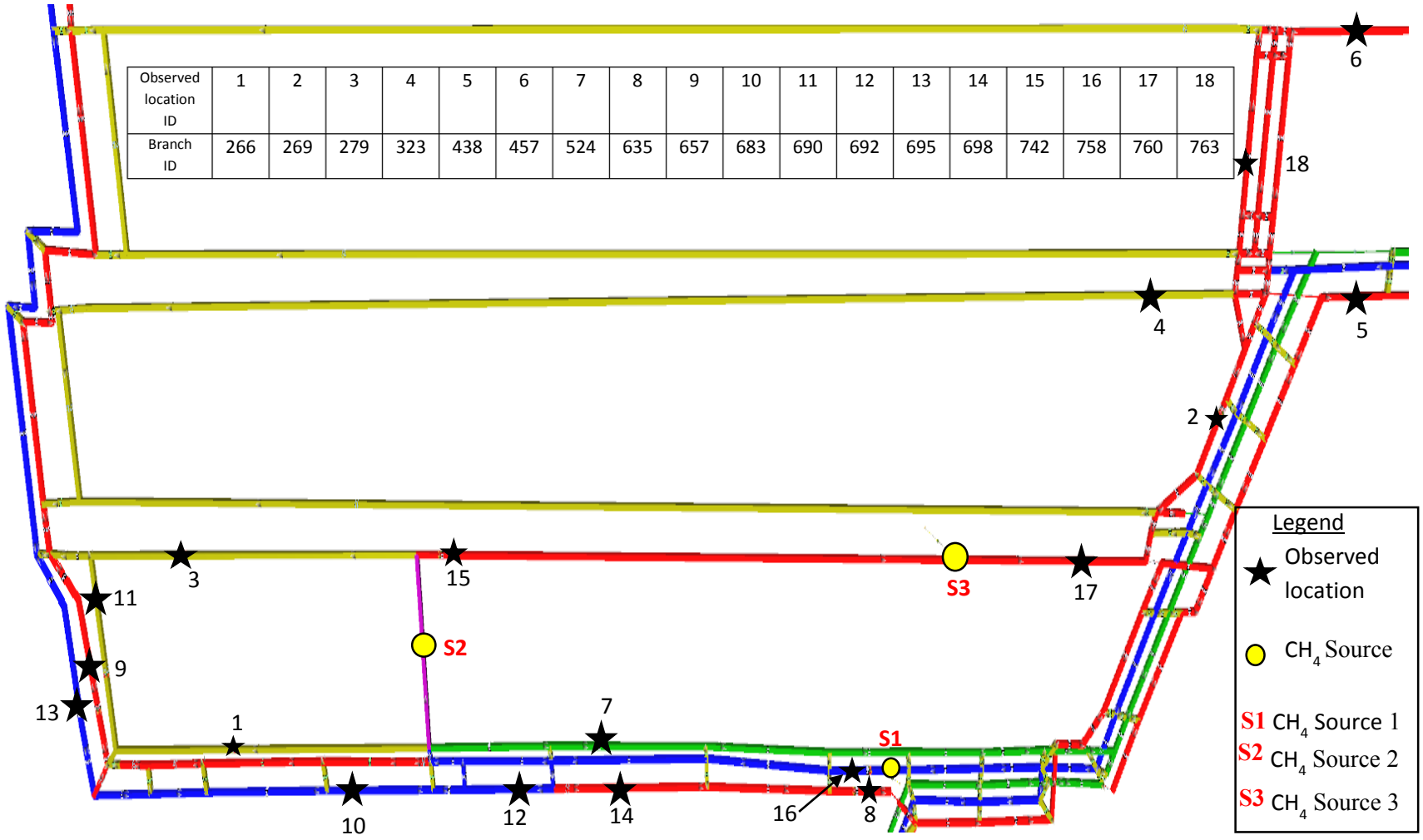

Figure 5.7. Layout of coal mine example 1 with methane sources and assumed monitored sensor locations in Ventsim.

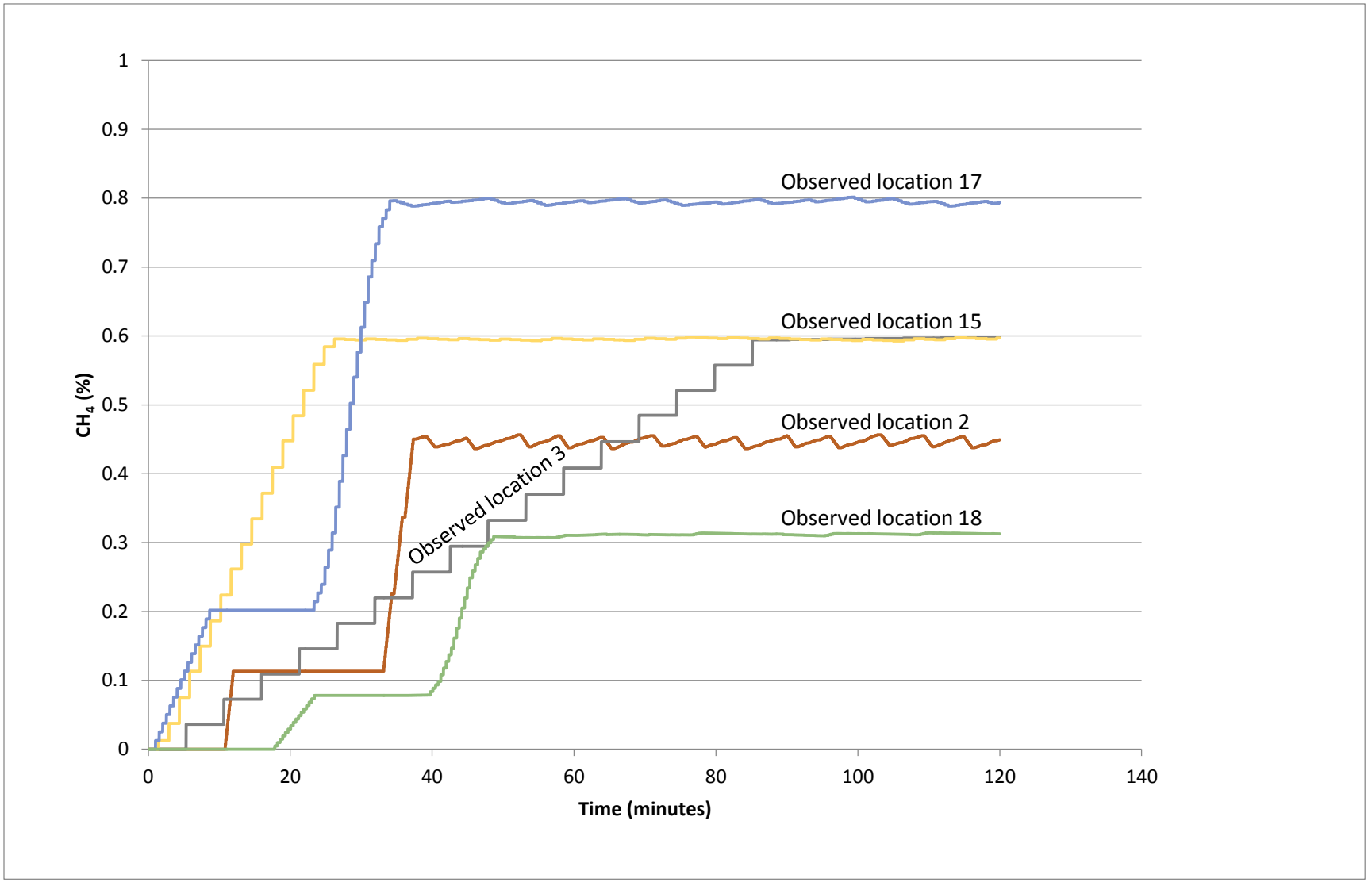

Figure 5.8a. Results of methane concentration at selected observed locations from native VAM simulation in Scenario 1A. Selected locations with significant changes only are plotted.

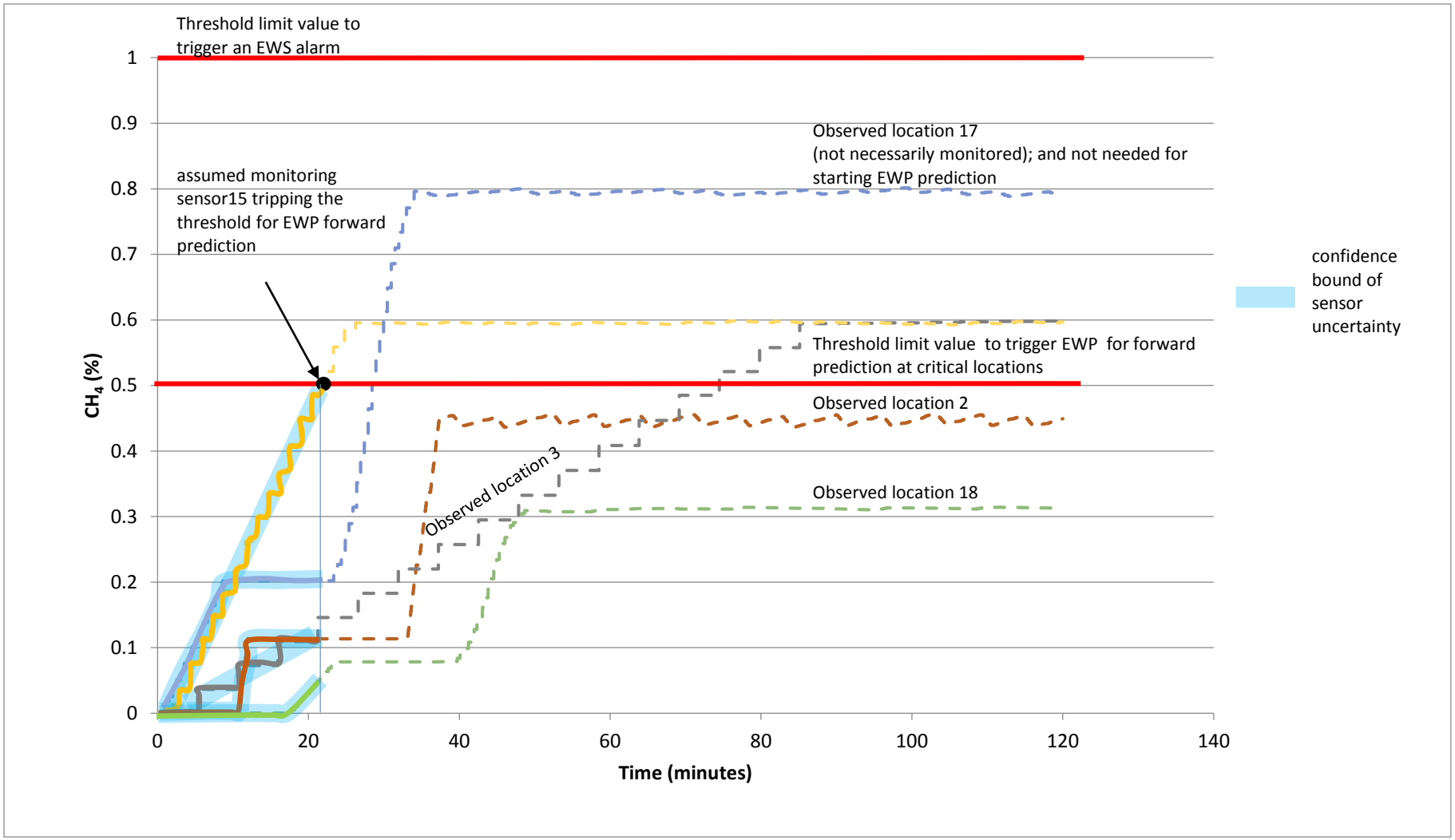

Figure 5.8b. Emulated sensor signals used as assumed monitored data input to trigger the APPS forward predictor in the EWS system in Scenario 1A (shown in thick lines with confidence bounds). Assumed sensor 15 (and 17 if installed) trip(s) threshold for EWP forward prediction. The curves show real-time changes in CH_4 concentration. Selected locations with significant changes only are plotted. Note that the sensor signals are also used for the APPS predictor continuously (shown in dashed lines).

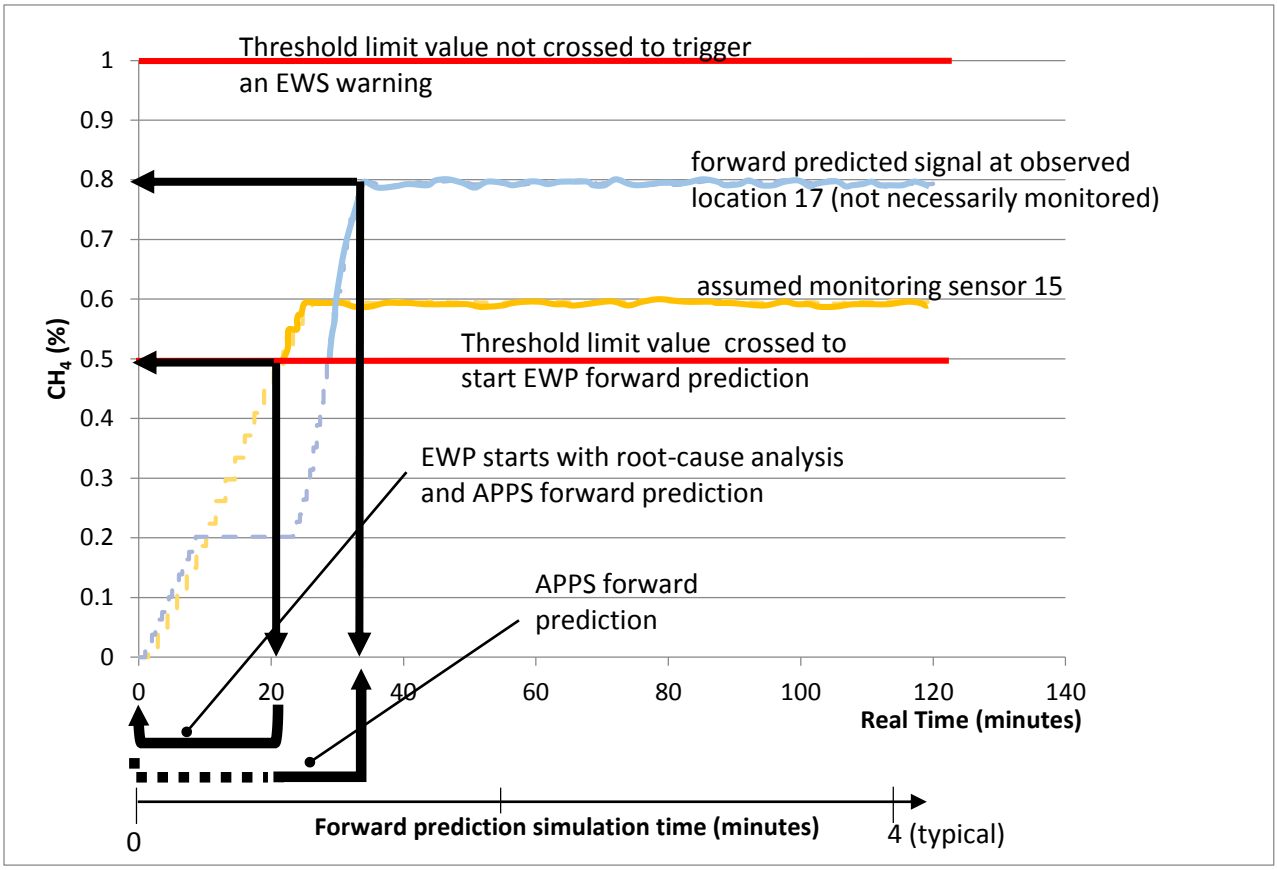

Figure 5.8c. APPS model forward prediction at selected observed locations in real-time and in fast simulation time scales for Scenario 1A. Only two selected locations are shown.

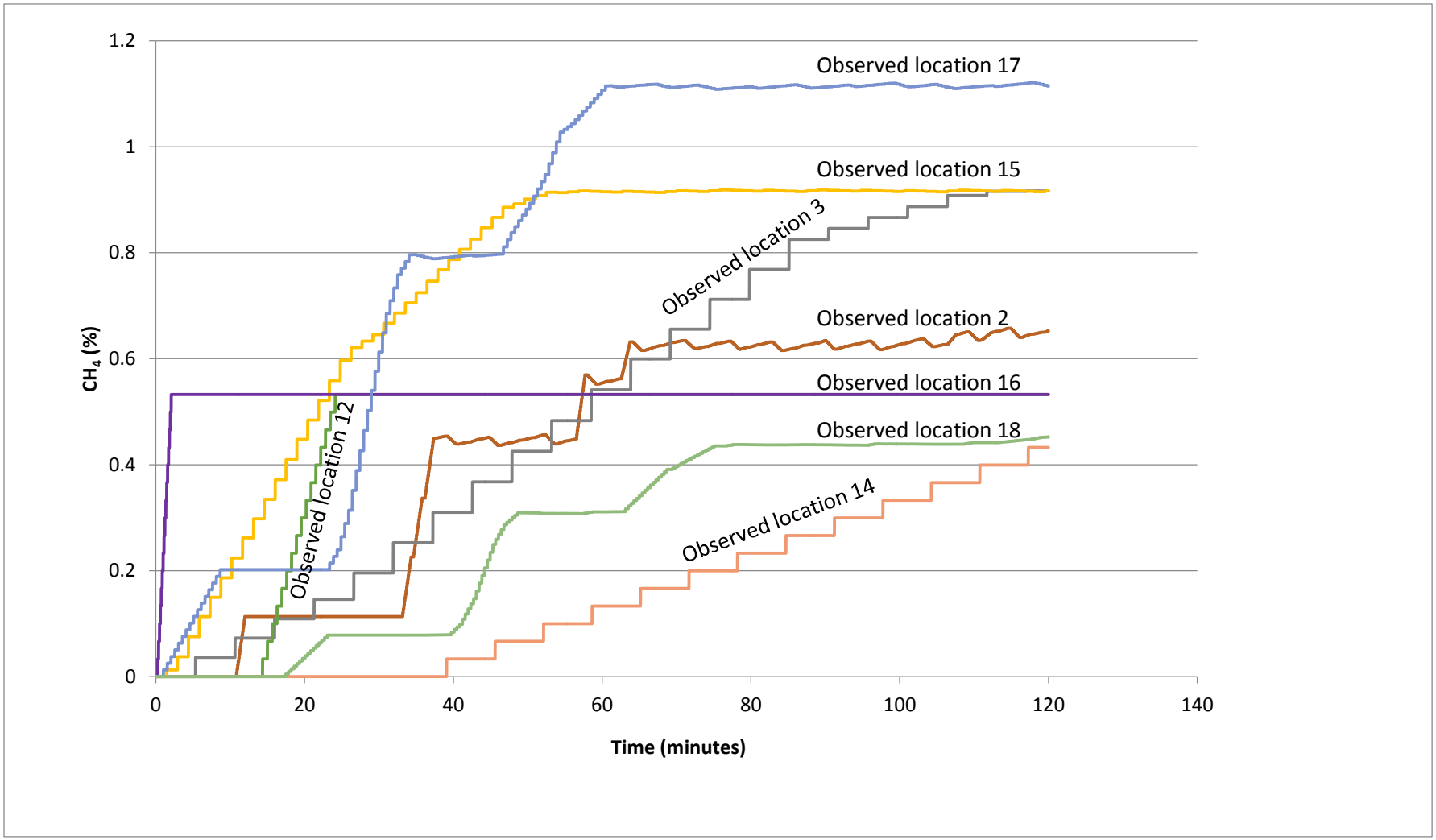

Figure 5.9a. Results of methane concentration at selected observed locations from native VAM simulation in Scenario 1B. Selected locations with significant changes only are plotted.

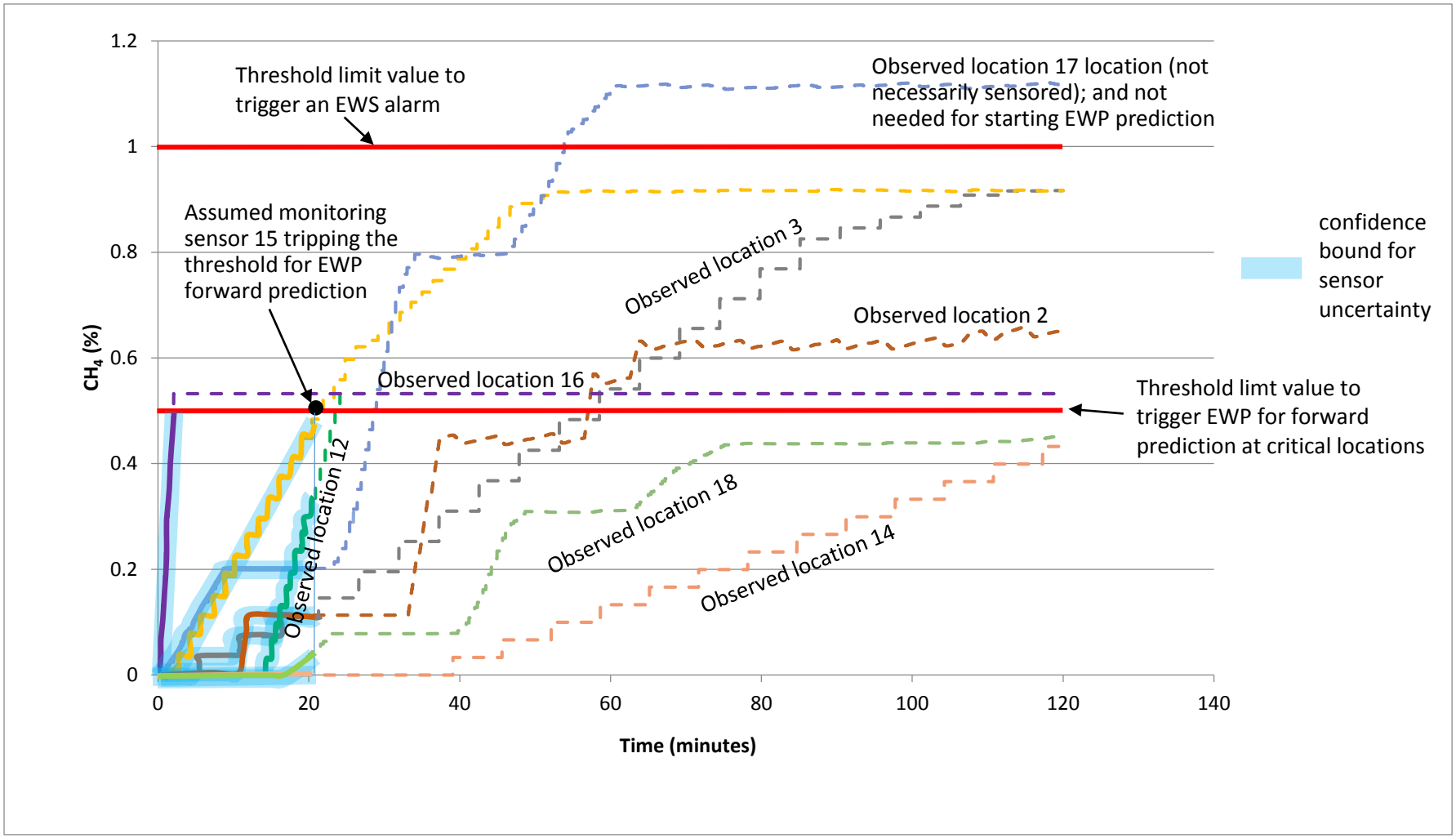

Figure 5.9b. Emulated sensor signals used as assumed monitored data input to trigger the EWS system in Scenario 1B (shown in thick lines with confidence bounds). Assumed sensors 15, 12, 16 (and 17 if installed) trip threshold for EWP forward prediction (sensor 16 is too close to threshold to trip). The curves show real-time changes in CH_4 concentration. Selected locations (with significant changes only) are plotted. Note that the sensor signals are also used for the APPS corrector continuously (shown in dashed lines).

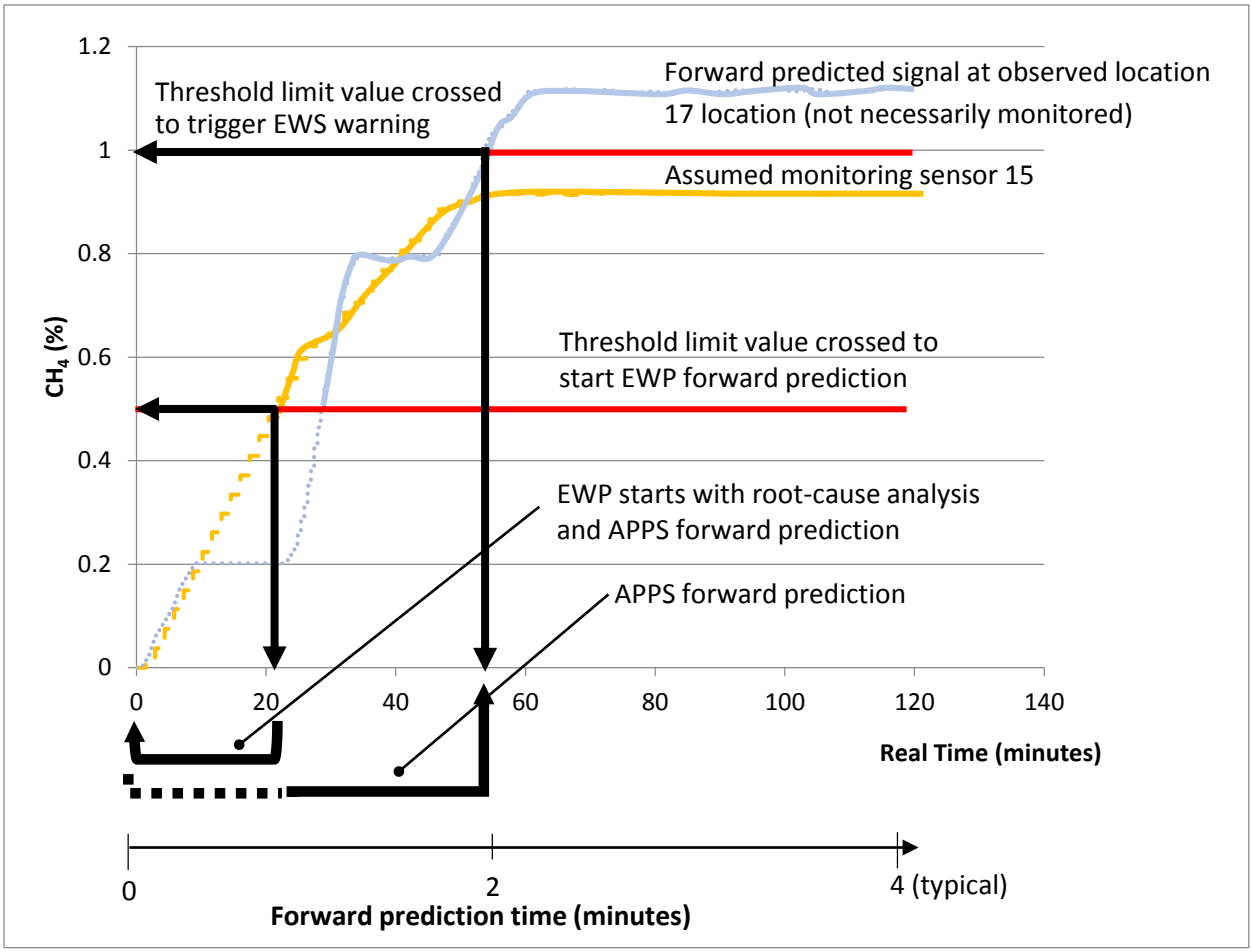

Figure 5.9c. APPS model forward prediction at selected observed locations in real-time and in fast simulation time scales for Scenario 1B. Only two selected locations are shown.

5.1.3 Three methane sources (Scenario 1C, coal mine example 2)

Coal mine 2 is used to model three methane sources. This coal mine example is converted from a native VnetPC model with 253 branches and 2 fans. The panel in this coal mine is ventilated by delivering fresh air through three entries, two from the headgate and one from the tailgate. The contaminated air is exhausted through back bleeder return airways. Three methane gas sources S1, S2, and S3 are injected into the mine at three different locations shown in Figure 5.10 with S1 in one of the longwall intake airways (branch 249), S2 at the working face (branch 100), and S3 in the longwall return airway (branch 251). Figure 5.11 illustrates the layout of the mine model with 18 observed locations of interest.

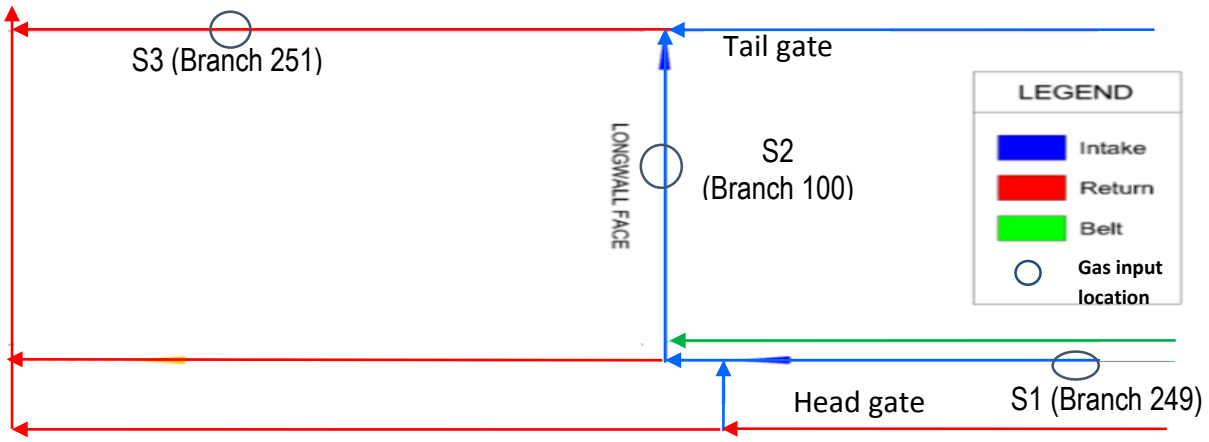

Figure 5.10. Schematic of modeled section showing areas of perturbation with source locations for coal mine example 2.

Scenario 1C is studied in mine example 2 as a base scenario to demonstrate fan malfunction and fire heat load. Gas in-burst into the mine airway is modeled by injecting three methane sources at S1 (80% CH_4 at 0.2 m^3/s), S2 (line load, 55 liters/second/100m of CH_4) and S3 (point source, 50% CH_4 at 0.1m^3/s). The simulation results for selected locations with significant changes only are plotted. The time-dependent VAM results for methane concentration are demonstrated in Figure 5.12a. The emulated sensor signals used as monitored data input to trigger the EWS system is shown in Figure 5.12b. Figure 5.12c depicts the APPS model forward prediction results for observed locations 13 and 18 based on the 0.5% methane crossing at assumed sensor 13. The results for airflow, velocity, and absolute pressure are not shown since there are no changes at the 18 observed locations. A threshold limit value of 1% methane for stopping work is used in this analysis and from the results. It is observed that the methane concentration is below the threshold limit for all the 18 assumed monitored locations. Using 0.5% methane for a safety assumption to start a forward prediction and using branch 219 (monitoring sensor 13), which is a sensor location just at the end of the active face as a reference, the delay time in methane front arrival can be estimated. Branch 219 reaches 0.5% in 7 minutes and branch 251 reaches 0.8% in 17 minutes and remains constant as illustrated in Figure 5.8c. Therefore, the delay time before branch 251 (forward predicted signal at observed location 18 downstream of branch 219 on the return airway, not necessarily monitored), reaches a maximum concentration in 10 minutes (17 minutes minus 7 minutes). Hence, 8 minutes are available for advance notice (10 minutes minus 2 minutes forward prediction time). However, it is observed that the methane concentration remains below the threshold value for the observed location 18 and no warning is necessary.

The typical signal trends for methane in-burst are depicted in Figures 5.8a, 5.9b, and 5.12c. In order to identify gas in-burst as a root cause, the signal trends must be analyzed. There is only the methane concentration signal from the results useful for detection. The future effect of scenario 1 that can lead to a hazard is the increase in methane as a result of gas accumulation. Therefore, the gas accumulation model is a necessary and useful APPS forward predictor to evaluate the effect of methane in-burst at the face and the allowable delay time for concentration threshold crossing.

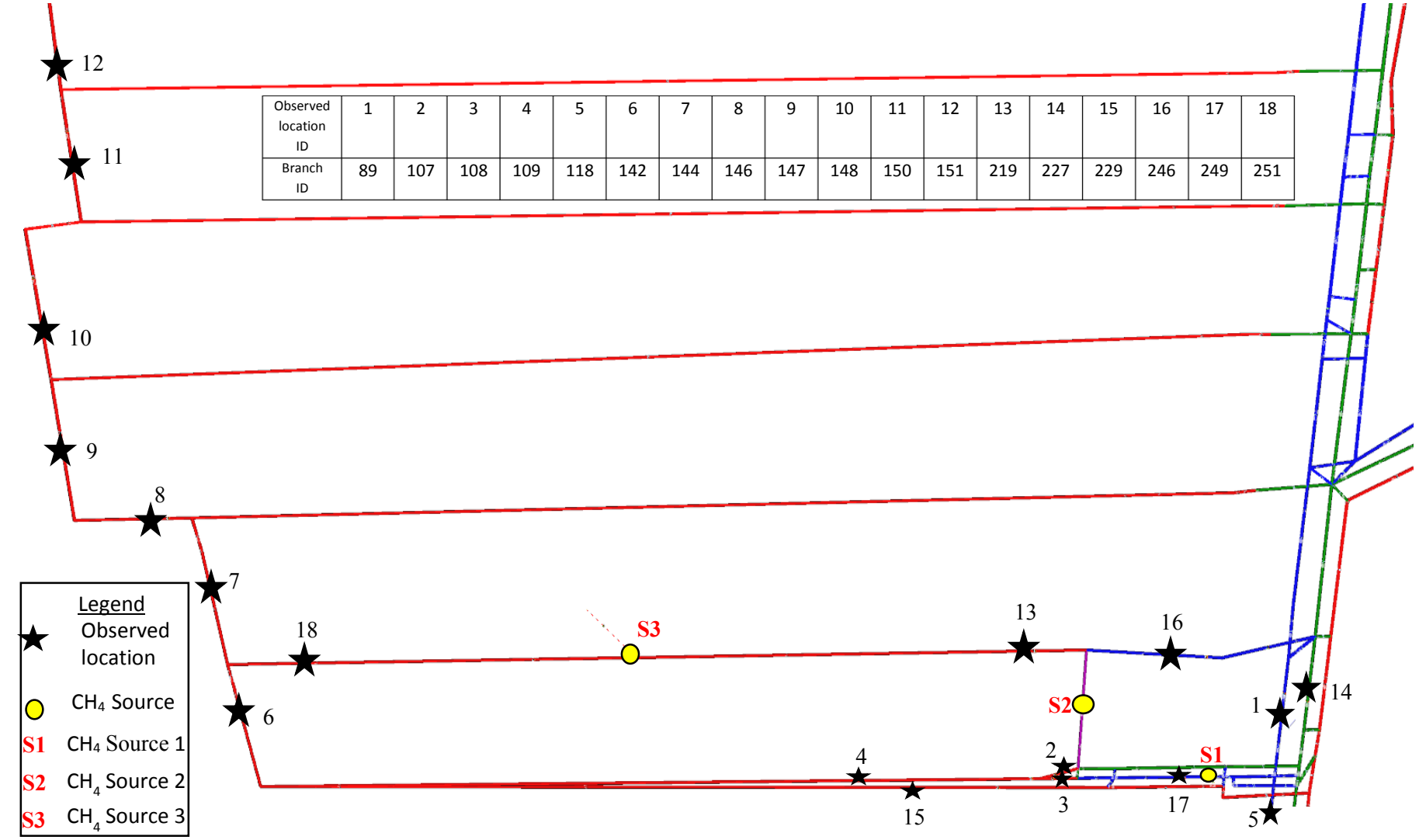

Figure 5.11. Layout of coal mine example 2 with methane sources and assumed monitored sensor locations in Ventsim.

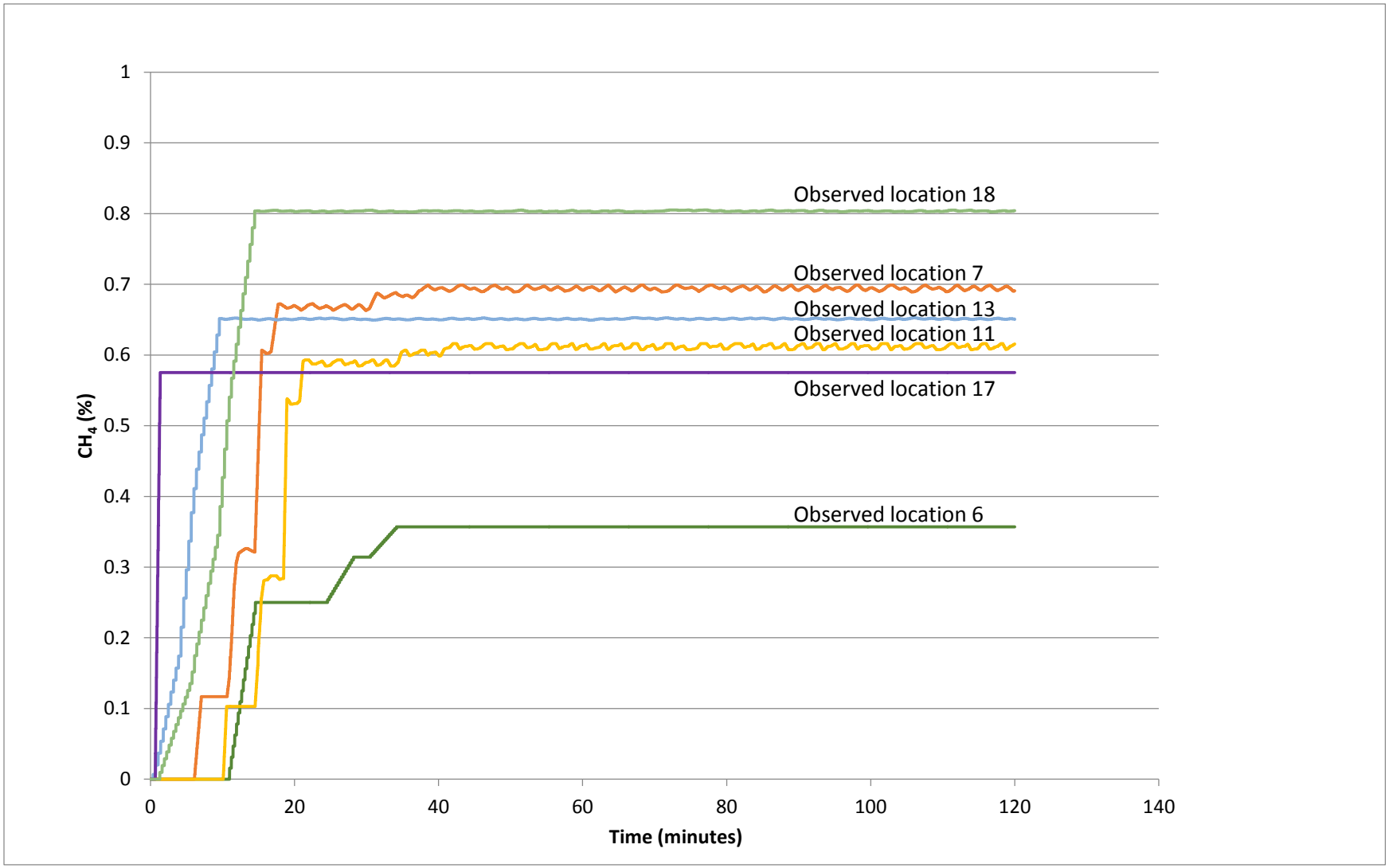

Figure 5.12a. Results of methane concentration at selected observed locations from native VAM simulation in Scenario 1C. Selected locations with significant changes only are plotted.

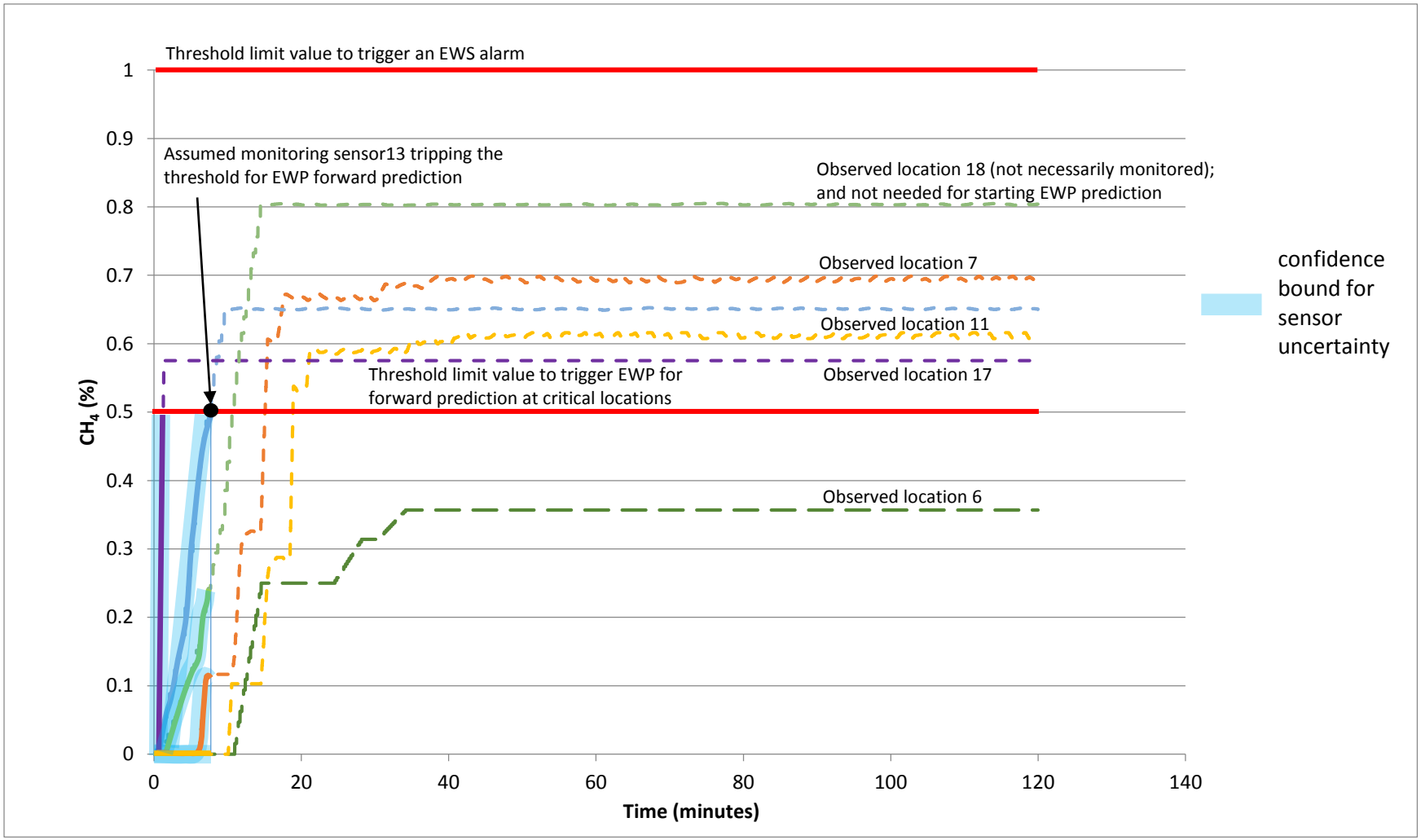

Figure 5.12b. Emulated sensor signal used as assumed monitored data input to trigger the EWS system in Scenario 1C (shown in thick lines with confidence bounds). Assumed sensors 13, 17 (and 18 if installed) trip(s) threshold for EWP forward prediction. The curves show real-time changes in CH_4 concentration. Selected locations with significant changes only are plotted. Note that the sensor signals are also used for the APPS predictor continuously (shown in dashed lines).

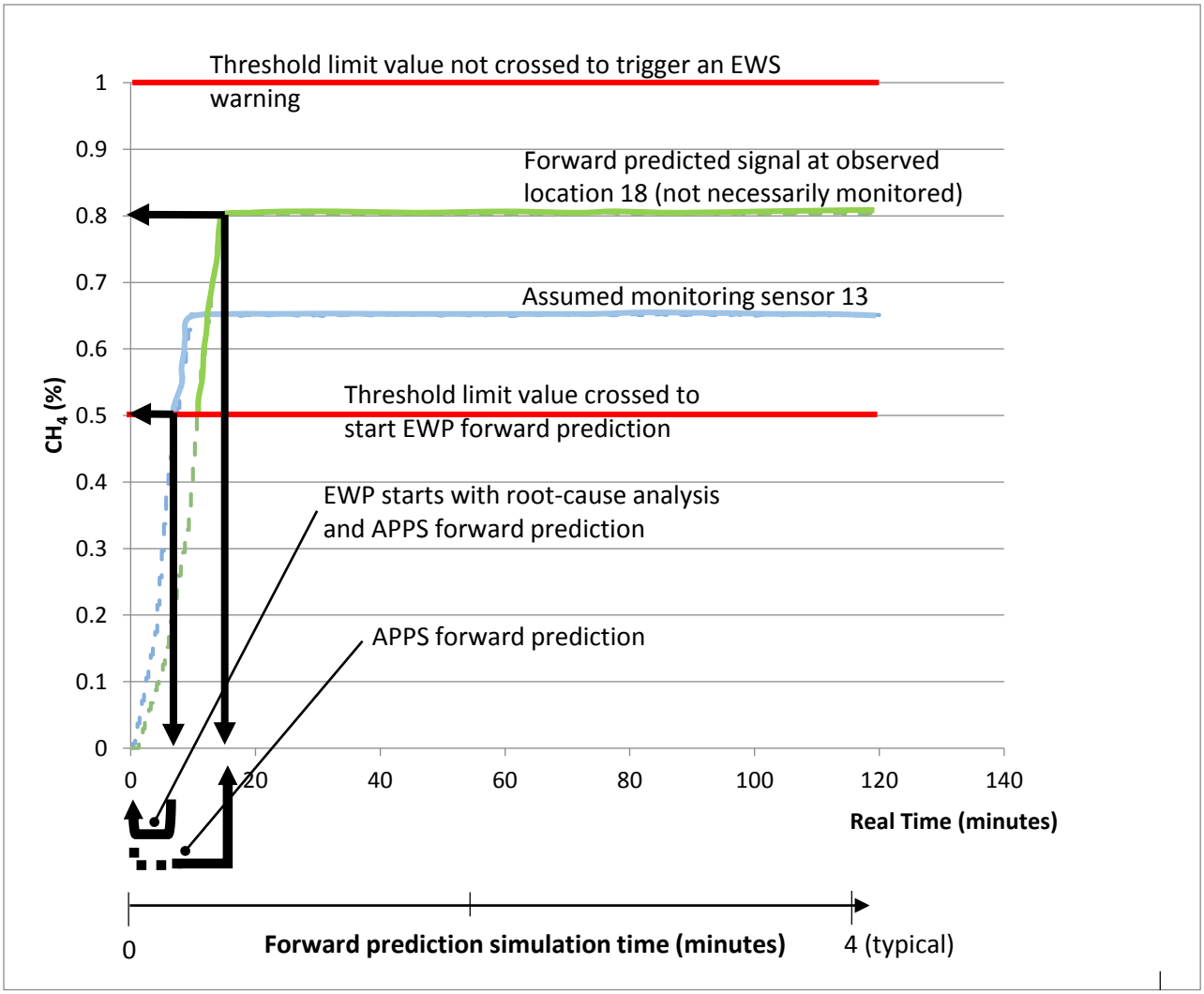

Figure 5.12c. APPS model forward prediction at selected observed locations in real-time and in fast simulation time scales for Scenario 1C. Only two selected locations are shown.

5.2 Airway blockage as a result of partial collapse of a hazardous roof section in the mine (Scenario 2, mine example 1)

Airway blockage may occur from a roof collapse, equipment and other malfunctions. The roof collapse is caused by ground failure. This is a dangerous but very rare type of event that could occur in mines. Airway blockage causes a decrease in airflow that results in methane concentration increase. There are two ways in which this scenario can be detected. Firstly, the primary detection is used which comprises of ground control and roof stability sensory signals; and secondly, detection of the change in airflow, as well as in barometric pressure, and temperature. These signals must be analyzed together to collaborate in the recognition of airway blockage. Airway blockage is modeled as Scenario 2 in mine example 1. Figure 5.7 shows the layout of the mine model with 18 observed locations of interest, which is used to access the time dependent behavior of the performance elements.

The signature of the primary detection parameters is a step change which directly gives the root cause and therefore there is no need for modeling. However, the secondary changes are simulated to determine the forms of signatures expected in such a scenario.

This scenario is modeled by blocking one of the intake airways (branch 758) upstream of S2 and S3 sources, after 10 minutes into a 2-hour simulation**.**

Two methane gas sources S2 and S3 are modeled. In order to mimic an airway blockage, the resistance in branch 758, which is about 3500 ft away from the longwall face is increased from 0.00170 Ns^2/m^8 to 8000 Ns^2/m^8. The area of perturbation for airway blockage is shown Figure 5.13. Blockage reduced the airflow in this branch from $30m^3/s$ to $0.1m^3/s$ depicting a total blockage with little amount of leakage.

The simulation results for selected locations with significant changes only are plotted. The time-dependent VAM results for methane concentration are demonstrated in Figure 5.14a. The emulated sensor signals used as monitored data input to trigger the EWS system is shown in Figure 5.14b. Figure 5.14c depicts the APPS model forward prediction results for observed locations 15 and 17 based on the 0.5% methane crossing at assumed sensor 15. The results for airflow, velocity, and absolute pressure are demonstrated in Figures 5.15, 5.16, and 5.17, respectively. There is an increase in airflow in some branches as well as decrease in other branches. The results indicate that methane concentration increases with reduction in airflow that leads to threshold crossing in one branch (branch 760). A threshold limit value of 1% methane for stopping work is used in this analysis. Therefore, using 0.5% methane as a safety concentration value to start a forward prediction and using branch 742 (monitoring sensor 15), which is a sensor location just at the end of the active face as a reference and using a safety factor of 0.5% methane, the delay time can be estimated. Branch 742 reaches 0.5% in 23 minutes and branch 760 (forward predicted signal at observed location 17 downstream of branch 742 on the return airway, not necessarily monitored), reaches 1% in 46 minutes as illustrated in Figure 5.14c. Therefore, the delay time before branch 760 crosses the threshold is 23 minutes (46 minutes minus 23 minutes), which triggers an EWS

alarm. Since there is a threshold crossing, the gain time for management to take action is 21 minutes (23 minutes minus 2 minutes forward prediction time).

Figure 5.14a through 5.17 depict typical trends due to an airway blockage for air parameters and concentrations. These signals are step changes. Therefore, these signal trends have to be searched for in order to determine airway blockage as a root cause. The future effect of scenario 2 is methane increase due to reduced airflow required for proper dilution. A gas accumulation model, in the form of a fast-running APPS is an adequate EWP method for this example.

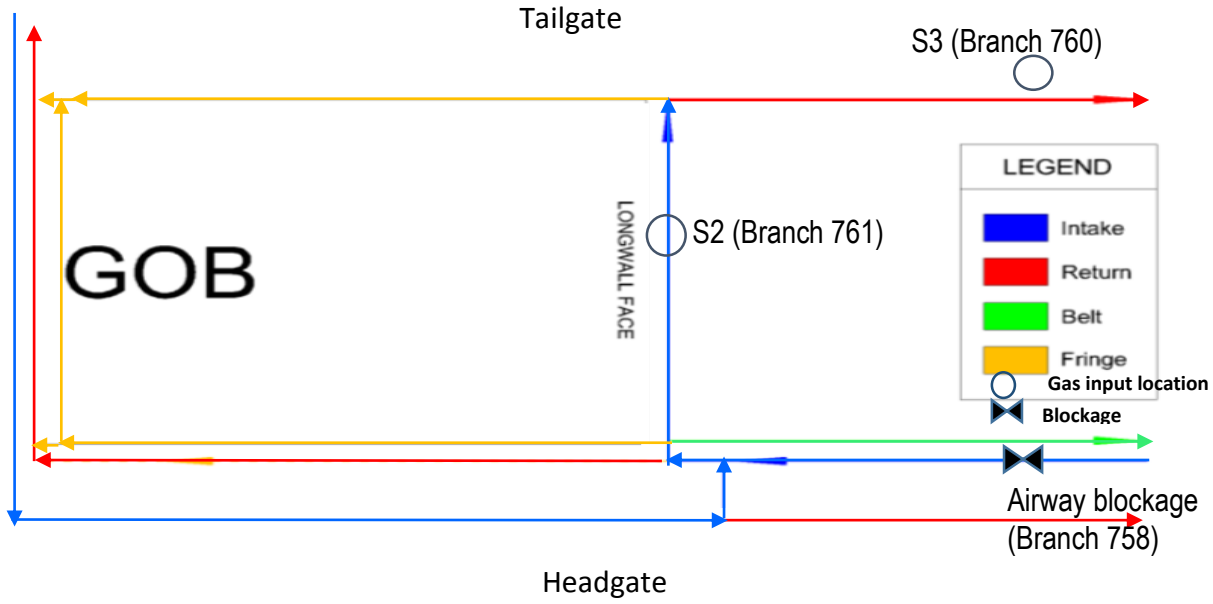

Figure 5.13. Schematic of area of perturbation for airway blockage for coal mine example 1.

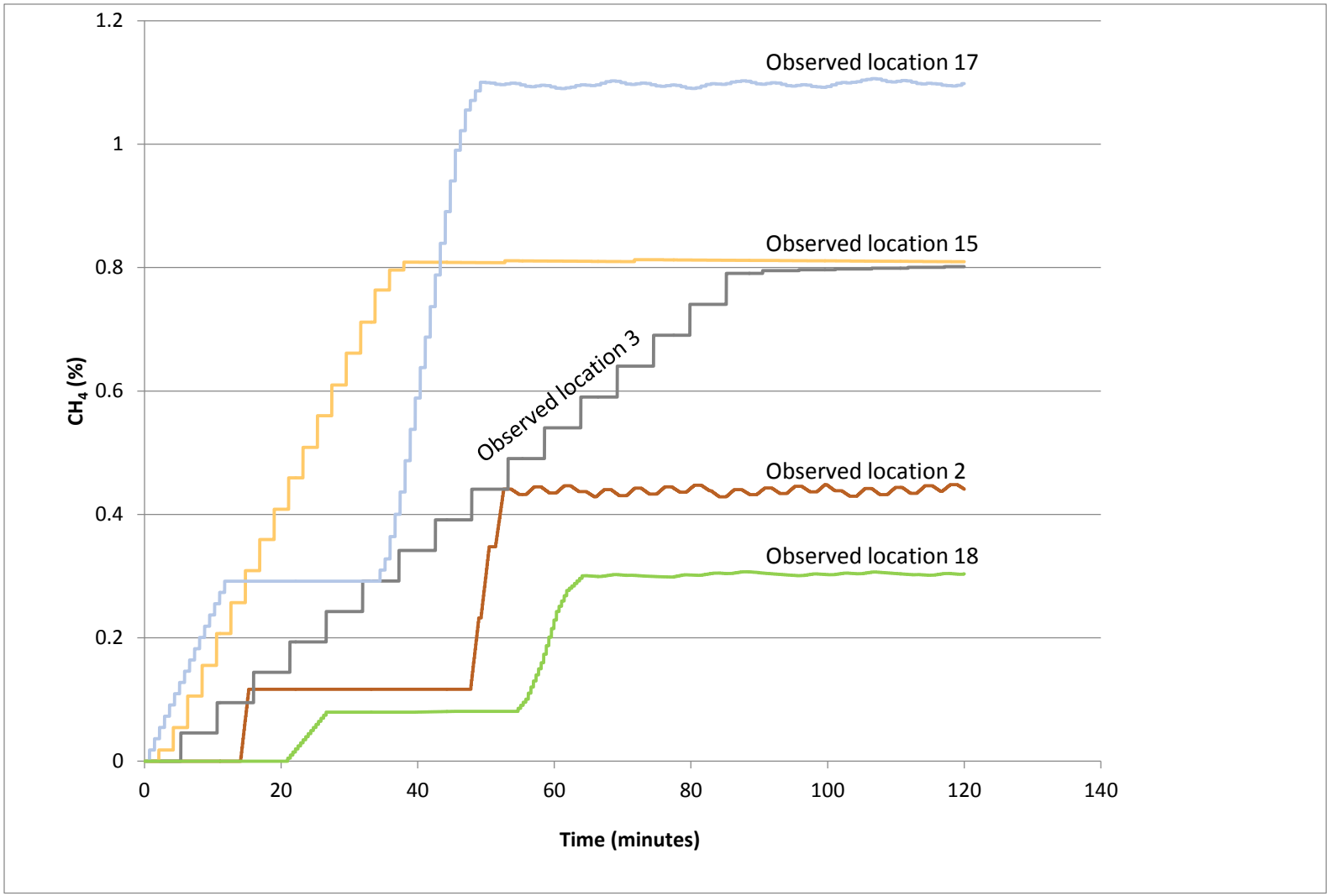

Figure 5.14a. Results of methane concentration at selected observed locations from native VAM simulation in Scenario 2. Selected locations with significant changes only are plotted.

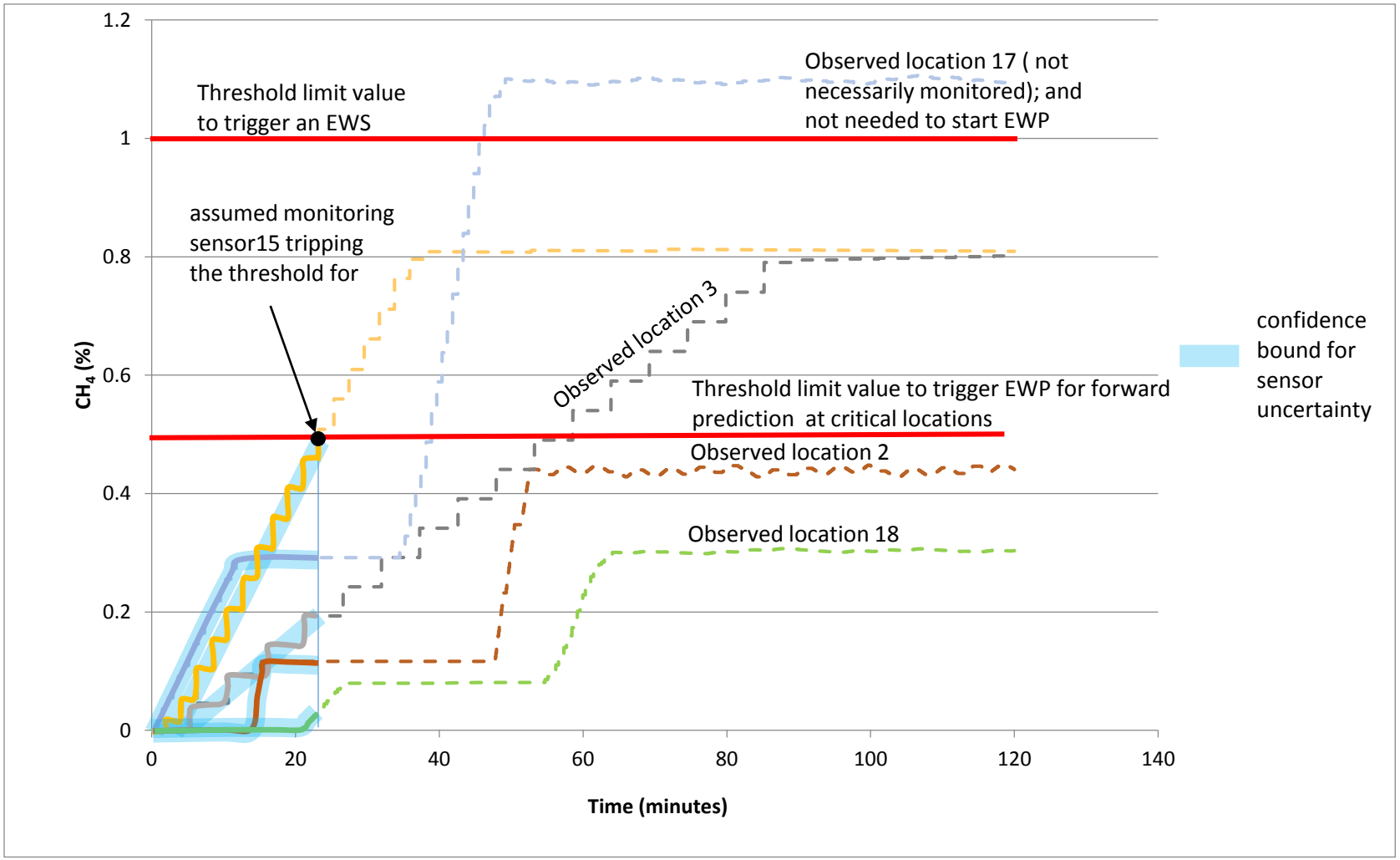

Figure 5.14b. Emulated sensor signal used as assumed monitored data input to trigger the EWS system in Scenario 2 (shown in thick lines with confidence bounds). Assumed sensors 15 (and 17 if installed) trip threshold for EWP forward prediction. The curves show real-time changes in CH_4 concentration. Selected locations with significant changes only are plotted. Note that the sensor signals are also used for the APPS predictor continuously (shown in dashed lines).

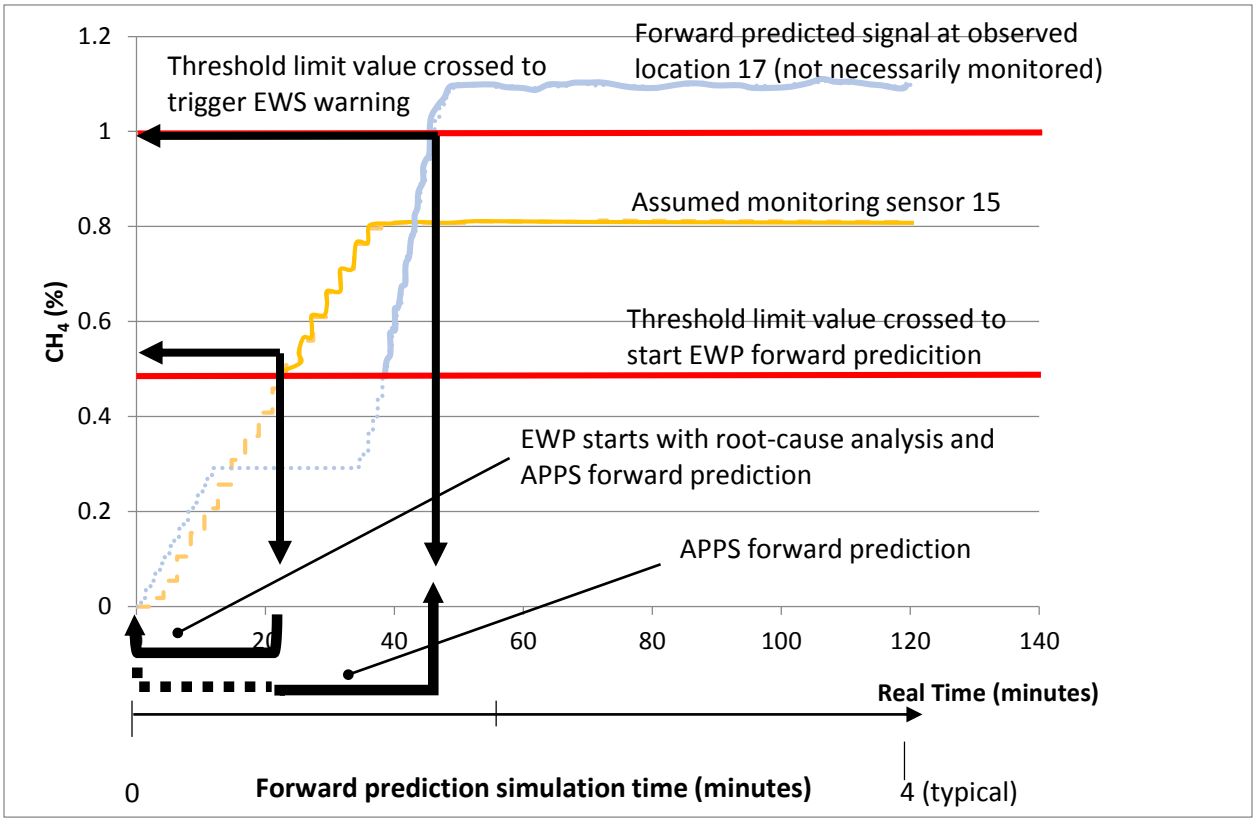

Figure 5.14c. APPS model forward prediction at selected observed locations in real-time and in fast simulation time scales for Scenario 2. Only two selected locations are shown.

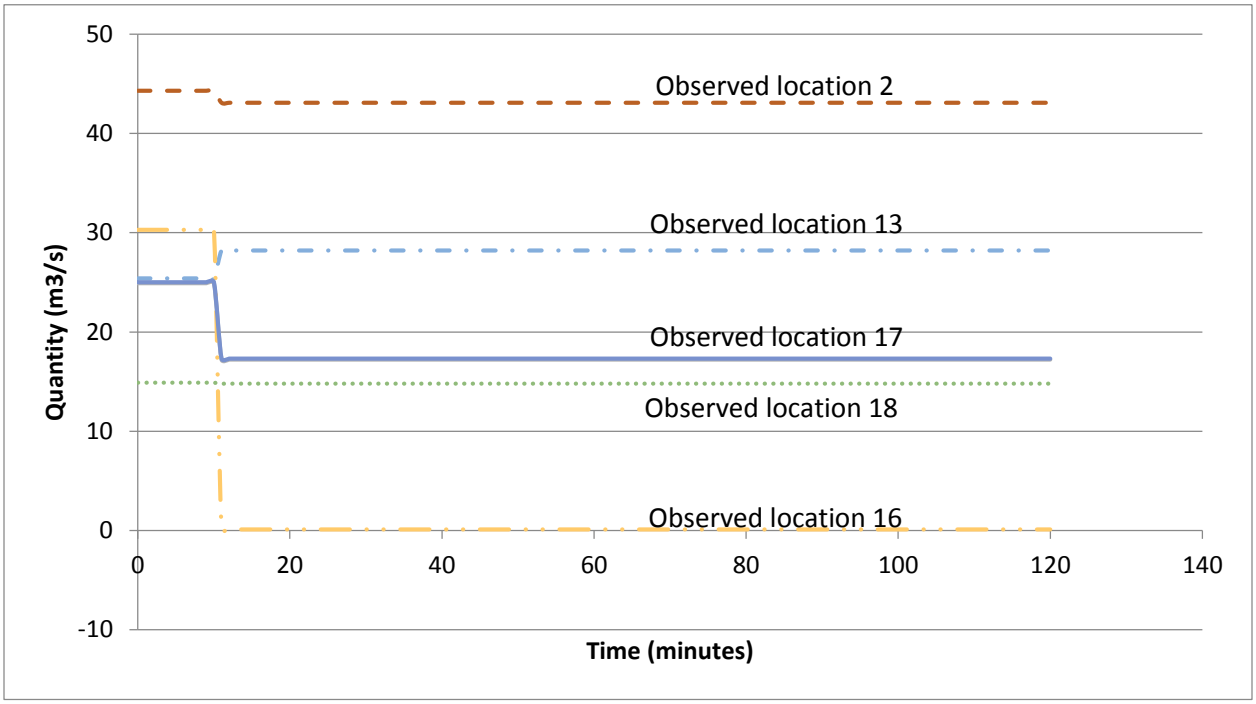

Figure 5.15. Results of airflow at assumed monitored locations due to airway blockage in coal mine example 1.

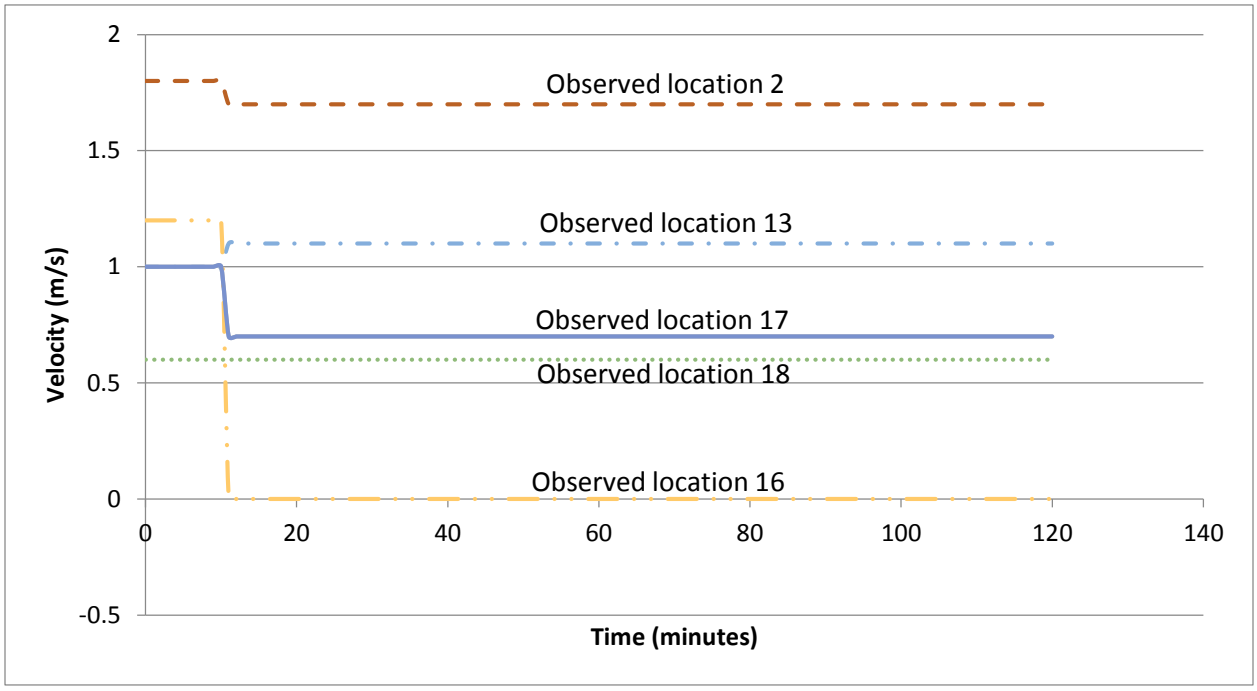

Figure 5.16. Results of velocity at assumed monitored locations due to airway blockage in coal mine example 1.

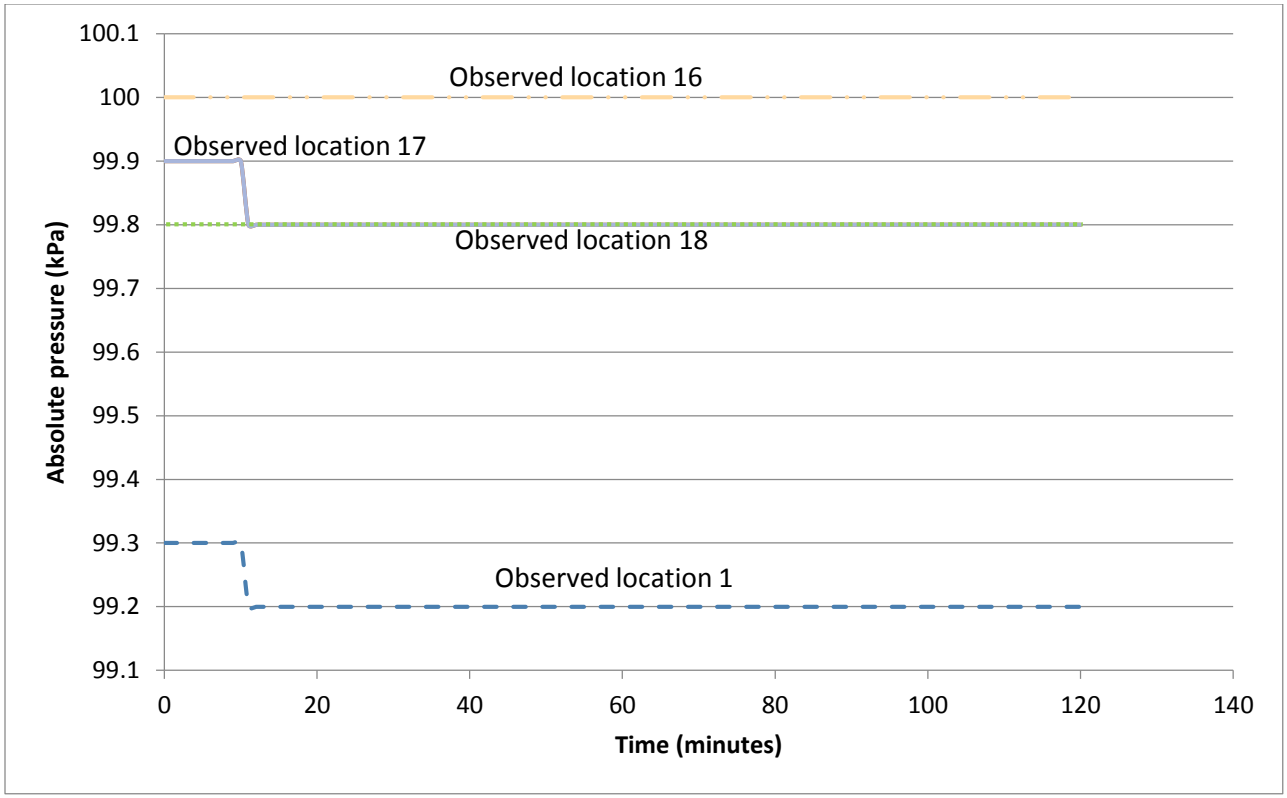

Figure 5.17. Results of absolute pressure at assumed monitored locations due to airway blockage in coal mine example 1.

5.3 Atmospheric barometric pressure variations causing methane inflow from the gob (Scenario 3, mine example 1)

A large volume of porous and fractured methane coal seam under pressure variations, described in Appendices A4 and A12, may release a large amount of methane by Darcy flow. Gob, strata, and partially sealed off dead zones are examples of such a volume.

One methane gas source S2 is modeled in mine example 1, illustrated in Figure 5.7. The effect of barometric pressure change upon methane inflow from the gob is modeled assuming a 2000 Pa drop from a previously high value in 20 minutes and keeping it low for an hour. Although no problem may be caused by CH_4 release due to slow barometric pressure changes under normal weather conditions, sudden change may induce CH_4 from the gob into the airway as demonstrated in Figure 5.18. The data is for 60 minutes, 20 minutes of drop and 40 minutes of no change in pressure. Pressure variation of large amplitude is seen in Figure A4.4 from real weather data, showing pressure drops of the same magnitude in about 10 days intervals, therefore, the sudden-drop scenario may happen during a fast-moving storm or a weather front.

The methane source is modeled using a gob model in MULTIFLUX. The details of the gob model is depicted in Appendix 12. The results from MULTIFLUX are entered into Ventsim and modeled to determine its effects on methane concentrations and airflow parameters. The simulation results for selected locations with significant changes only are plotted. The time-dependent VAM results for methane concentration are demonstrated in Figure 5.19a. The emulated sensor signals used as monitored data input to trigger the EWS system is shown in Figure 5.19b. Figure 5.19c depicts the APPS model forward prediction results for observed locations 15 and 17 based on the 0.5% methane crossing at assumed sensor 15. There are slight changes in airflow and velocity illustrated in Appendix A12.7 and A12.8, respectively and significant drop in absolute pressure depicted in Figure 5.20. A threshold limit value of 1% methane for stopping work is used in this analysis. Using branch 742, which is a sensor location just at the end of the active face as a reference and using a safety level of 0.5% methane, the delay time can be estimated. Branch 742 reaches 0.5% in 19 minutes and branch 760 (forward predicted signal at observed location 17 downstream of branch 742 on the return airway, not necessarily monitored), reaches 1% in 42 minutes as illustrated in Figure 5.19c. Therefore, the delay time before branch 760 crosses the threshold is 23 minutes (42 minutes minus19 minutes), which triggers an EWS alarm. Since, there is a threshold crossing, the gain time for management to take action is 21 minutes (23 minutes minus 2 minutes forward prediction time).

The type of methane increase is a dynamic delayed signal trend shown in Figure 5.19a, from too complex of a process to be described by a simple model. Therefore, an NTCF predictive model as a dynamic Jacobian gob model is used to simulate such a scenario.

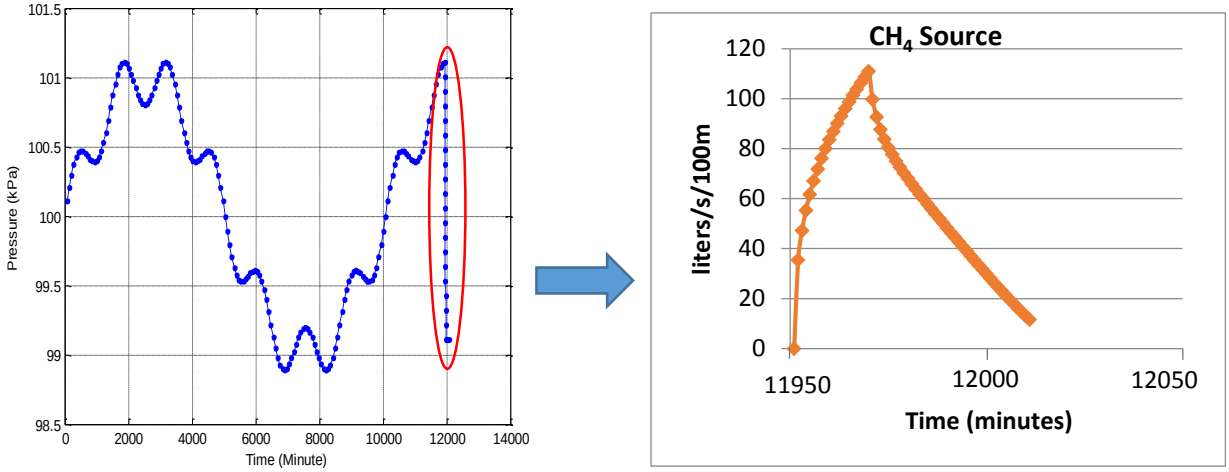

Figure 5.18: Barometric pressure drop inducing CH_4 flow.

5.4. Fan malfunctioning (Scenario 4, mine example 2)

Fans are very important equipment in underground mines to provide fresh air to dilute gases in the mine. However, interruptions in fan power supply or fan malfunctioning may result in sudden fan stoppage. Reduction in airflow prevents proper dilution of gases in the working areas. Fluctuations may be caused by mechanical failure or electrical interruptions. The root cause for this scenario may be detected from the fan power and electrical equipment power usage. Changes of the airflow rate and pressure are other indications. This event is rarely observed regarding surface fans, nonetheless, it may happen frequently to booster fans.

Simulation of scenario 4:

A partial fan malfunction is modelled in mine example 2, by reducing one of the fans' static pressure by 30% (fan #4 in branch 230) on the surface connected to the return shaft after 10 minutes into a 2-hour simulation. All three methane sources, S1, S2, and S3 are kept unchanged. Table A13.1 in Appendix 13 demonstrates both the original and reduced fan points. Figure A13.1 illustrates the fan curves for the original (a) and reduced (b) fan points. The areas of perturbation are shown in Figure 5.21 with S1 in the longwall intake airways (branch 249), S2 at the working face (branch 100), and S3 in the longwall return airway (branch 251). The area of investigation for methane in-burst in the two coal mines is working face.

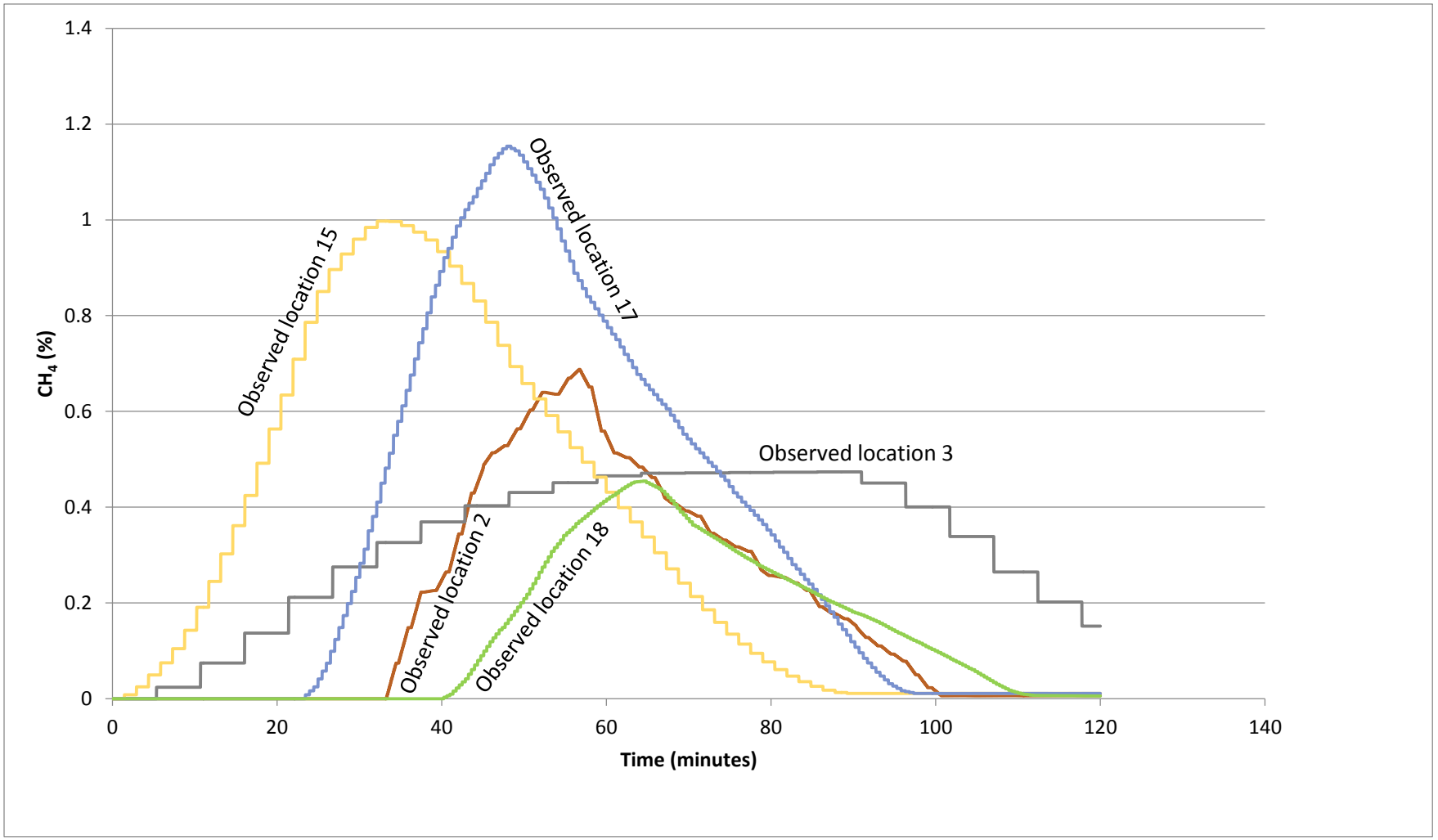

Figure 5.19a. Results of methane concentration at selected observed locations from native VAM simulation in Scenario 3. Selected locations with significant changes only are plotted.

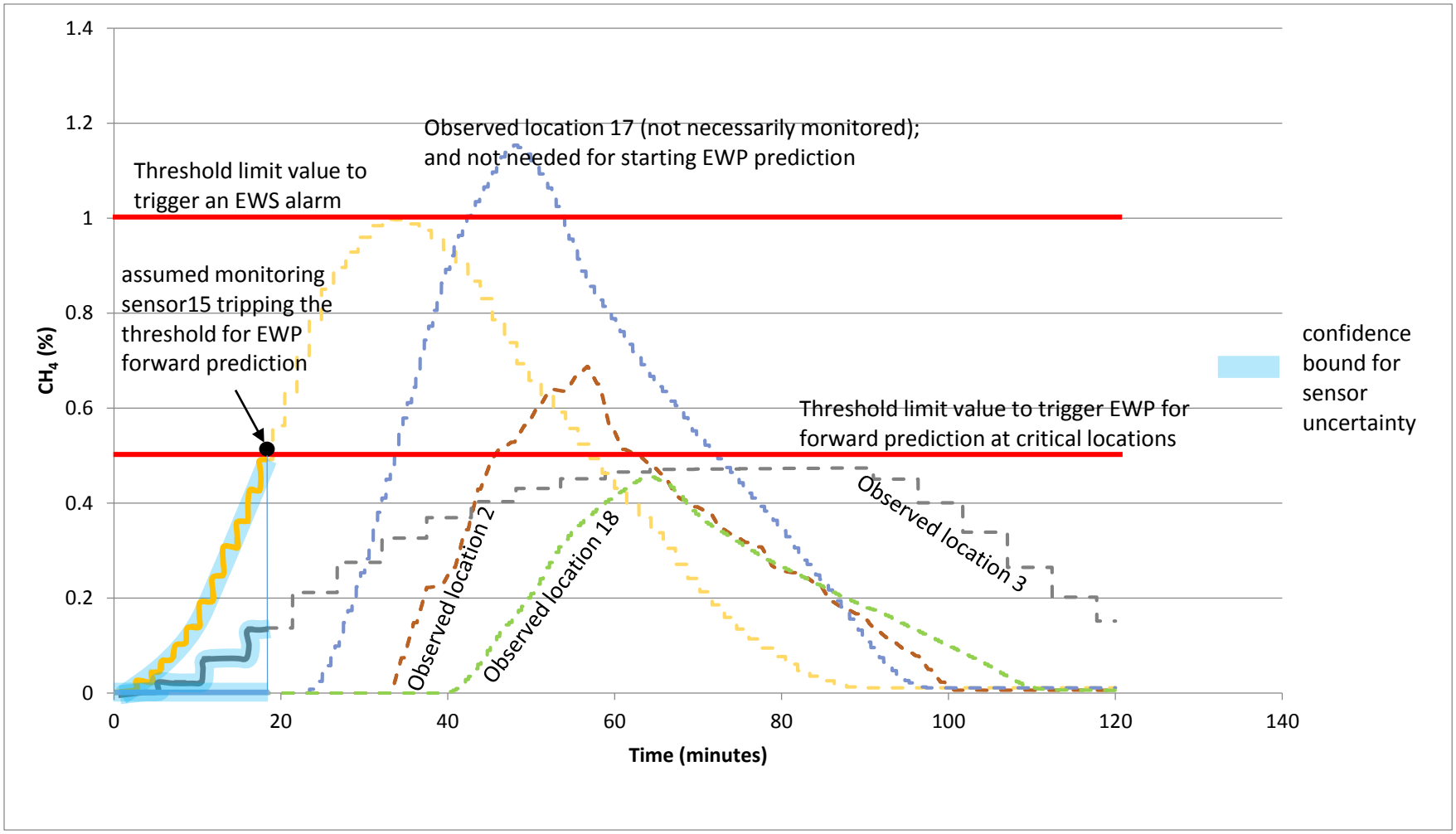

Figure 5.19b. Emulated sensor signal used as assumed monitored data input to trigger the EWS system Scenario 3 (shown in thick lines with confidence bounds). Assumed sensors 15 (and 17 if installed) trip threshold for EWP forward prediction. The curves show real-time changes in CH_4 concentration. Selected locations with significant changes only are plotted. Note that the sensor signals are also used for the APPS corrector continuously (shown in dashed lines).

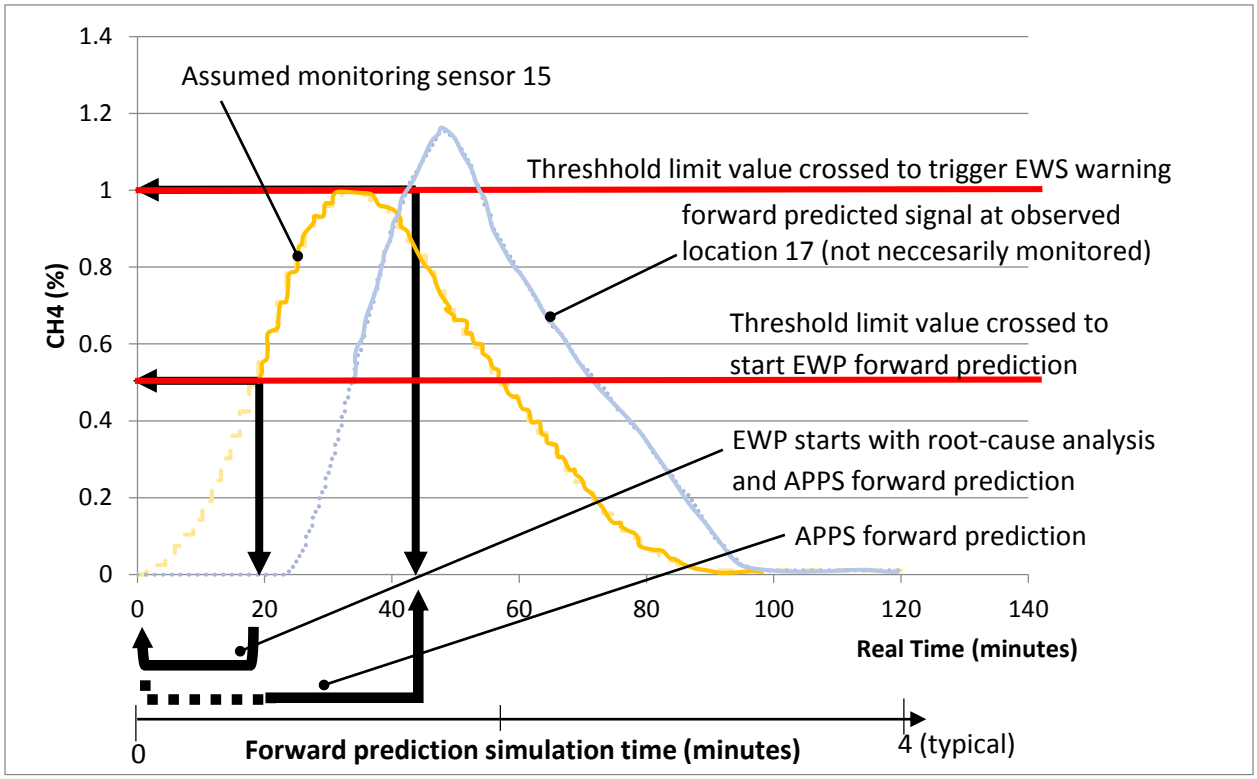

Figure 5.19c. APPS model forward prediction at selected observed locations in real-time and in fast simulation time scales for Scenario 3. Only two selected locations are shown.

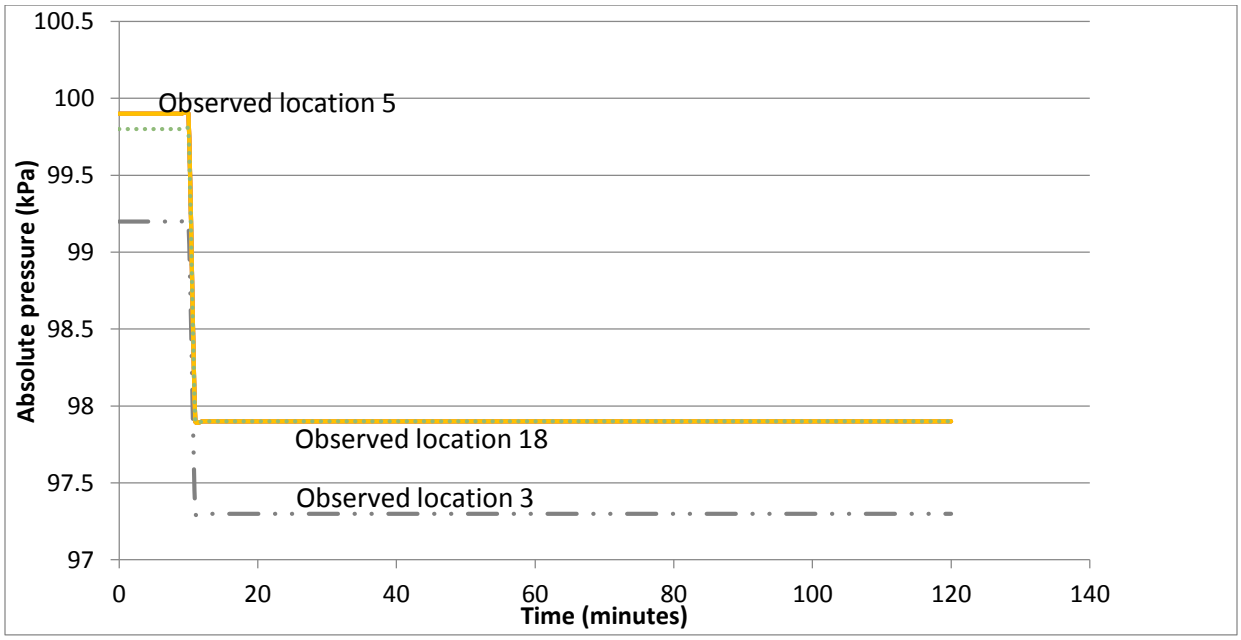

Figure 5.20. Results of absolute pressure at assumed monitored locations due to barometric pressure drop in coal mine example 1.

The simulation results for selected locations with significant changes only are plotted. The time-dependent VAM results for methane concentration are demonstrated in Figure 5.22a. The emulated sensor signals used as monitored data input to trigger the EWS system is shown in Figure 5.22b. Figure 5.22c depicts the APPS model forward prediction results for observed locations 13 and 18 based on the 0.5% methane crossing at assumed sensor 13. The airflow, velocity and absolute pressure simulation results are depicted in Figures 5.23, 5.24, and 5.25, respectively. Comparing this scenario to the base scenario 1C for mine example 2, it is seen that the airflow reduced significantly resulting in increased methane concentration and absolute pressure at some locations. Therefore, using branch 219 (monitoring sensor 13), which is a sensor location just at the end of the active face as a reference and using a safety concentration of 0.5% methane, the delay time can be estimated. Branch 219 reaches 0.5% in 9 minutes and branch 251 (forward predicted signal at observed location 18 downstream of branch 219 on the return airway, not necessarily monitored), reaches a maximum of 0.91% in 19 minutes and remains constant as illustrated in Figure 5.22c. Hence, the delay time before branch 219 reaches 0.91% is 10 minutes (19 minutes minus 9 minutes). Therefore, 8 minutes is available for advance notice (10 minutes minus 2 minutes forward prediction time). However, there is no 1% methane threshold crossing at this time.

The results indicate that a delayed mixing process decreased dilution and increased methane concentration. The signature trends for a fan malfunction is a step change as shown in Figure 5.22a through 5.25 which is similar to scenario 2. For forward prediction, a gas accumulation model is required in APPS for this scenario.

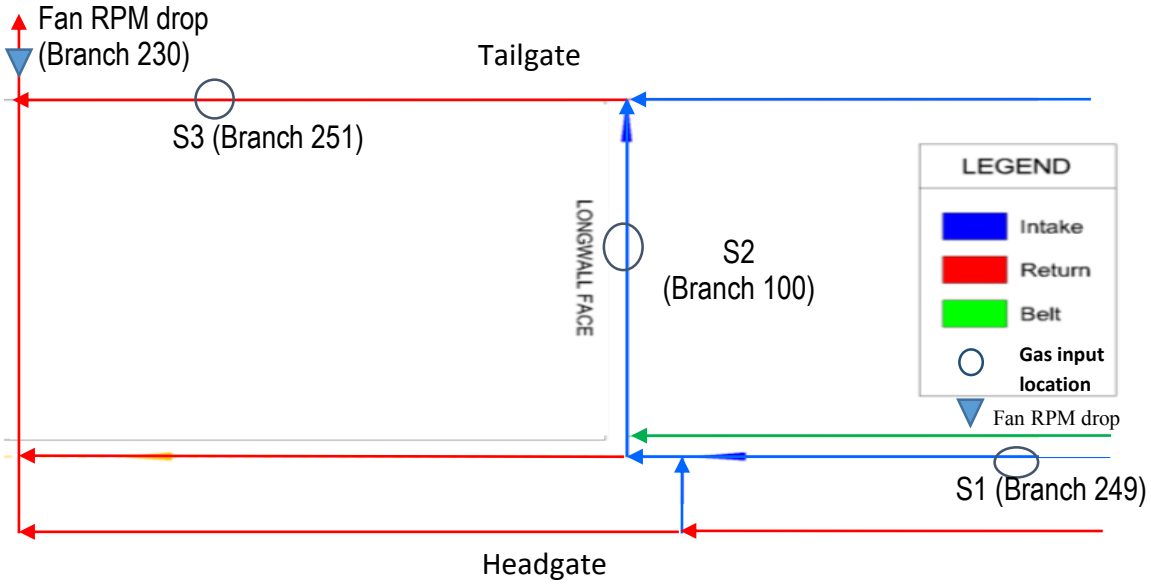

Figure 5.21. Schematic of modeled section showing areas of perturbation with source locations and fan RPM drop location for coal mine example 2.

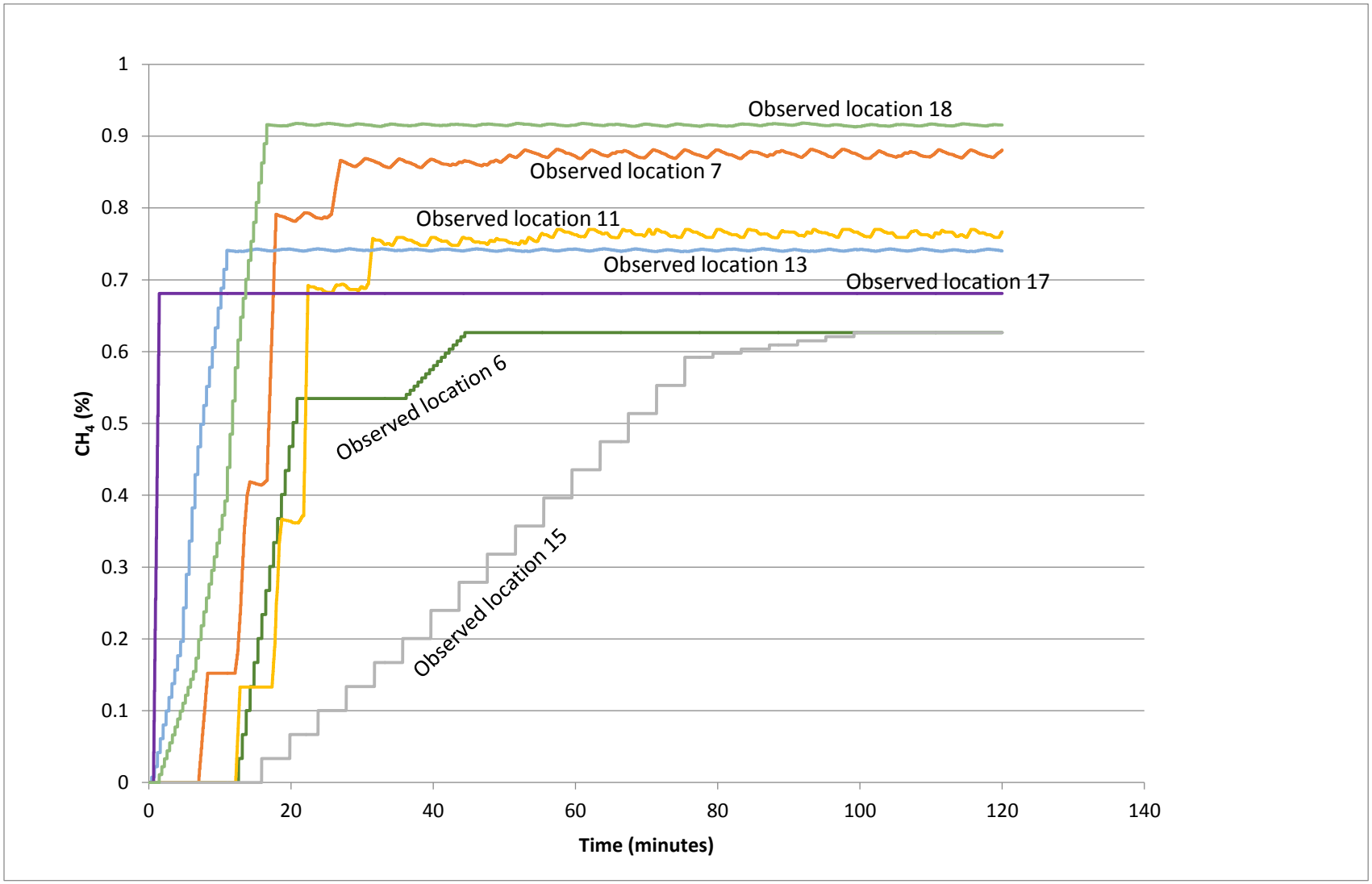

Figure 5.22a. Results of methane concentration at selected observed locations from native VAM simulation in Scenario 4. Selected locations with significant changes only are plotted.

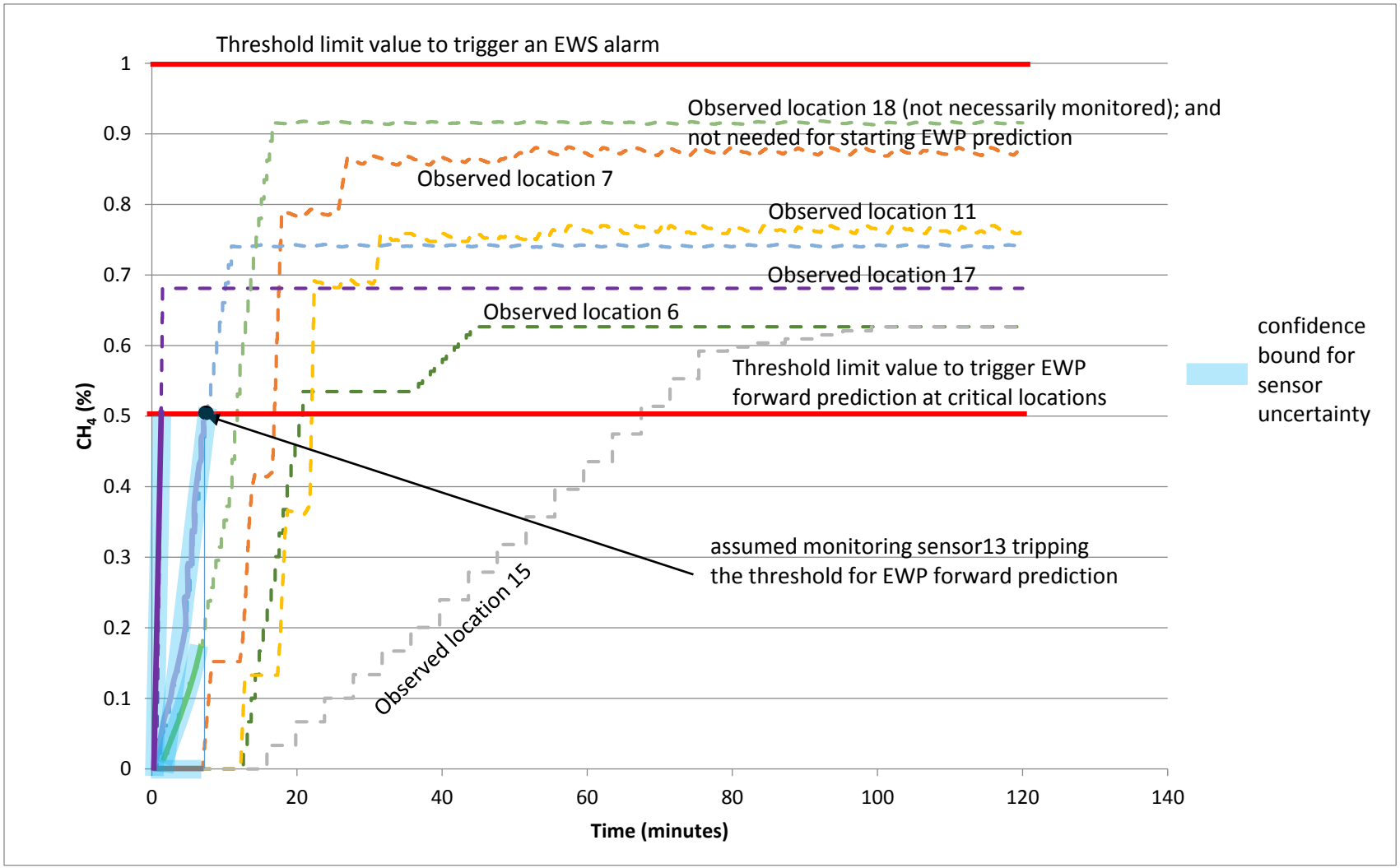

Figure 5.22b. Emulated sensor signal used as assumed monitored data input to trigger the EWS system in Scenario 4 (shown in thick lines with confidence bounds). Assumed sensors 13, 17 (and 18 if installed) trip(s) threshold for EWP forward prediction. The curves show real-time changes in CH_4 concentration. Selected locations with significant changes only are plotted. Note that the sensor signals are also used for the APPS predictor continuously (shown in dashed lines).

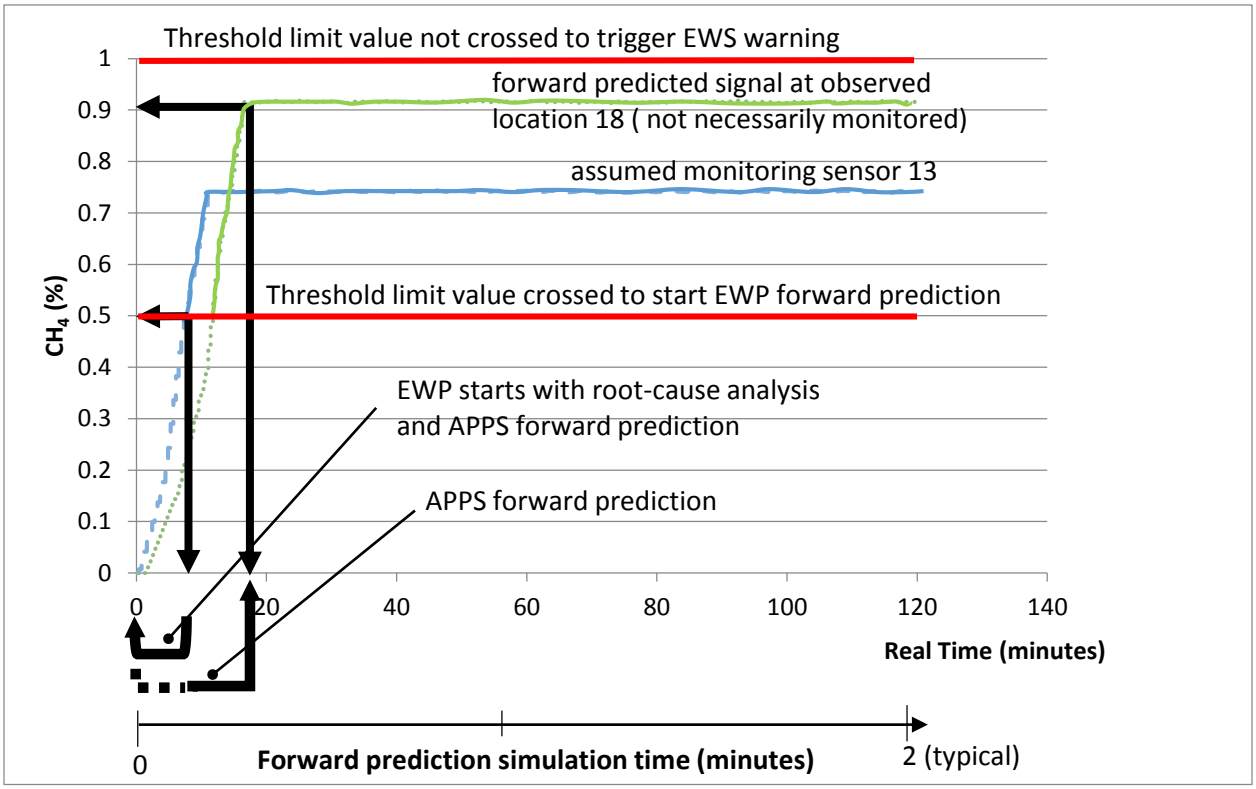

Figure 5.22c. APPS model forward prediction at selected observed locations in real-time and in fast simulation time scales for Scenario 4. Only two selected locations are shown.

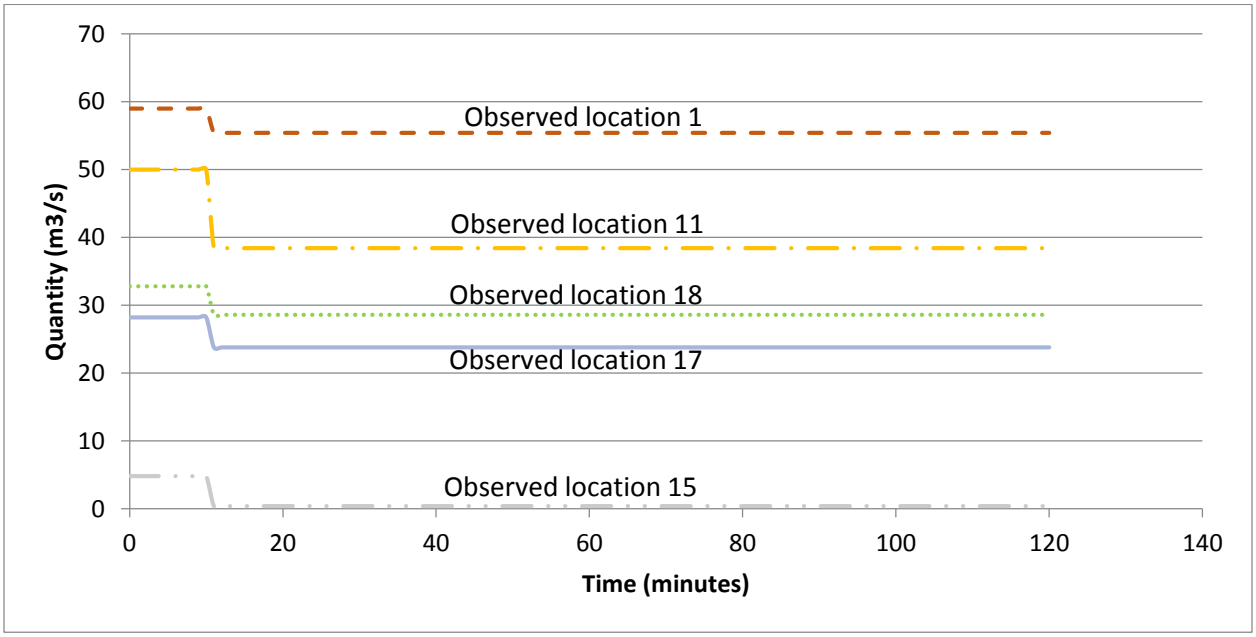

Figure 5.23. Results of airflow at assumed monitored locations due to fan malfunction in coal mine example 2.

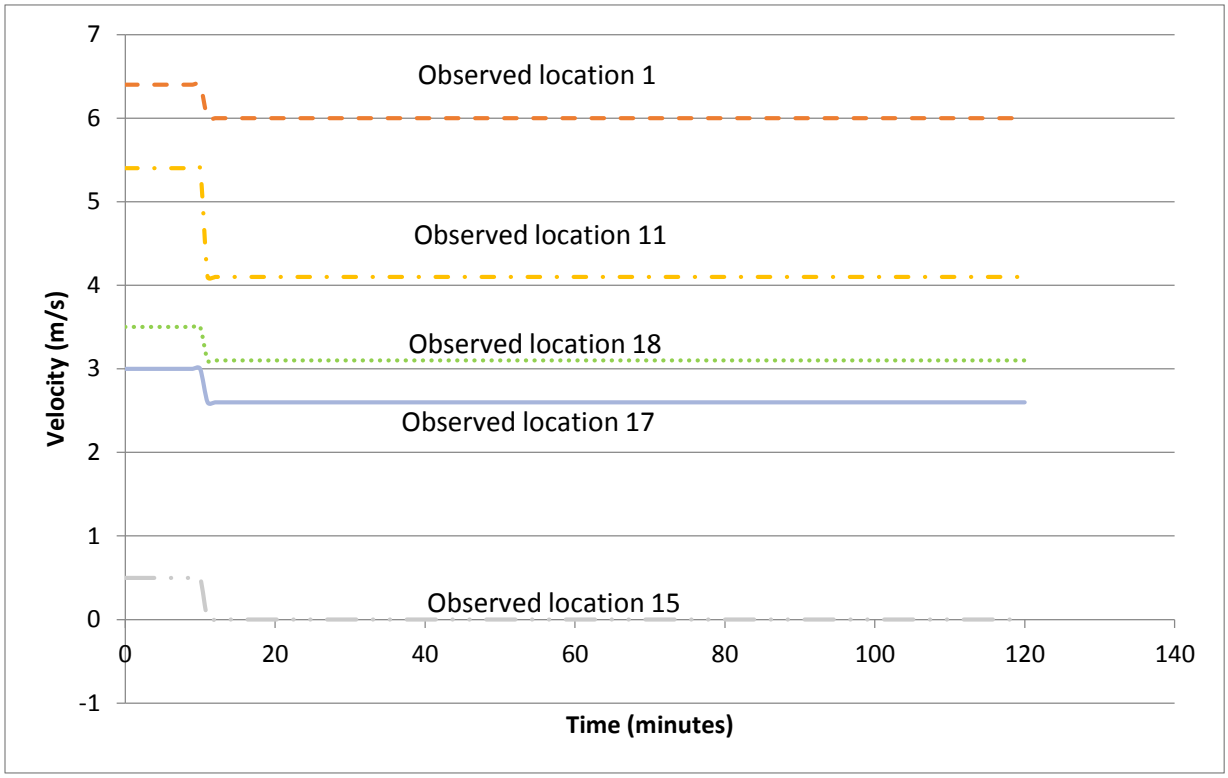

Figure 5.24. Results of velocity at assumed monitored locations due to fan malfunction in coal mine example 2.

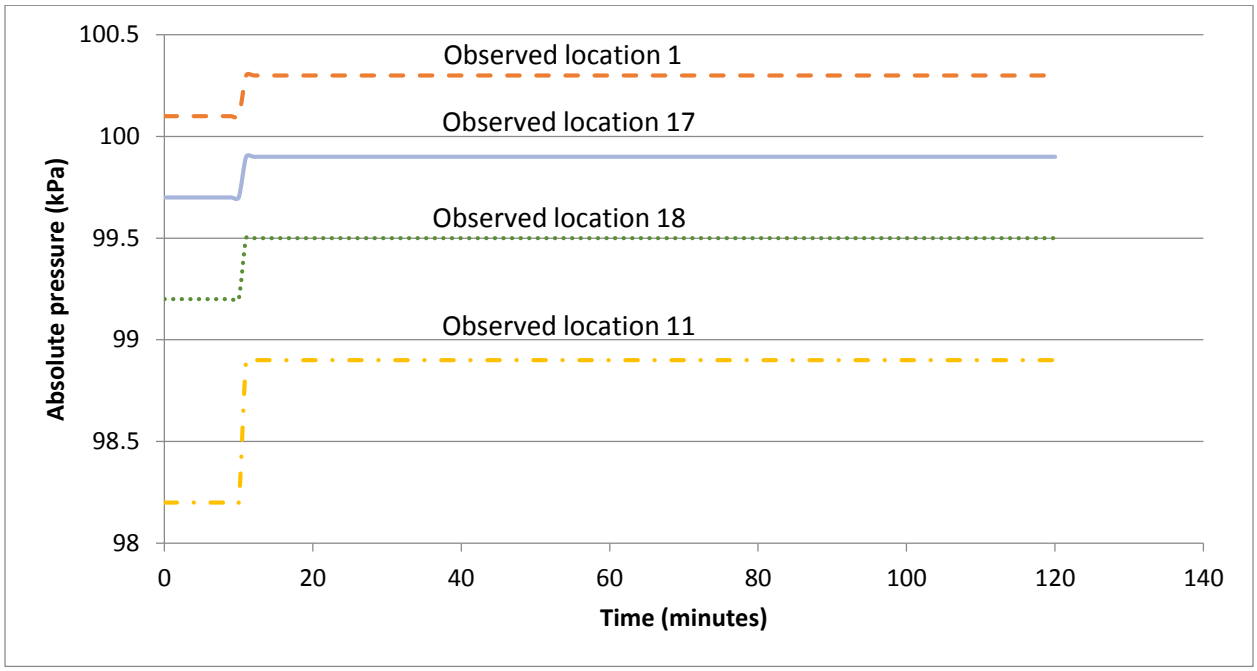

Figure 5.25. Results of absolute pressure at assumed monitored locations due to fan malfunction in coal mine example 2.

5. 5. Fire heat load (Scenario 5, mine example 2)

Fire of coal dust, belt, truck, fuel and lube bays are serious hazard scenarios. Truck fires may be due to an overload. Overheating of the longwall cutter heads as a result of overload might lead to fire which could ignite the coal dust. Although, this event is not frequent, it is highly dangerous once it occurs in a mine.

Simulation of scenario 5:

Fire load is modeled using conveyor belt fire with S1, S2 and S3 in mine example 2 illustrated in Figure 5.11. A conveyor belt fire with an assumed burning rate of 1000 kg/hr to 3000 kg/hr is modeled in branch 96 approximately 350 ft away from the longwall face in order to examine its effect on gas concentrations and airflow parameters. The fire is set up to start from 600 seconds through 3600 seconds during the simulation period of 2 hours. The areas of perturbation are shown in Figure 5.26 with S1 in one of the longwall intake airways (branch 249), S2 at the working face (branch 100), and S3 in the longwall return airway (branch 251).

The area of investigation is methane concentration variation due to changes carried by the fire at the working face. The simulation results for selected locations with significant changes only are plotted. The time-dependent VAM results for methane concentration are demonstrated in Figure 5.27a. The emulated sensor signals used as monitored data input to trigger the EWS system is shown in Figure 5.27b. Figure 5.27c depicts the APPS model forward prediction results for observed locations 13 and 18 based on the 0.5% methane crossing at assumed sensor 13. However, there are slight variations in the airflow and velocity results illustrated in Figures 5.28 and 5.29, respectively. The absolute pressure does not change. No significant methane concentration change is seen from the face due to fire at a different location. However, immediate action must be taken as soon as a signal indicates there is fire in the mine and it is confirmed. There is no need for further forward prediction for the other gas concentrations since the mine is placed in an alarm state in a real mine fire.

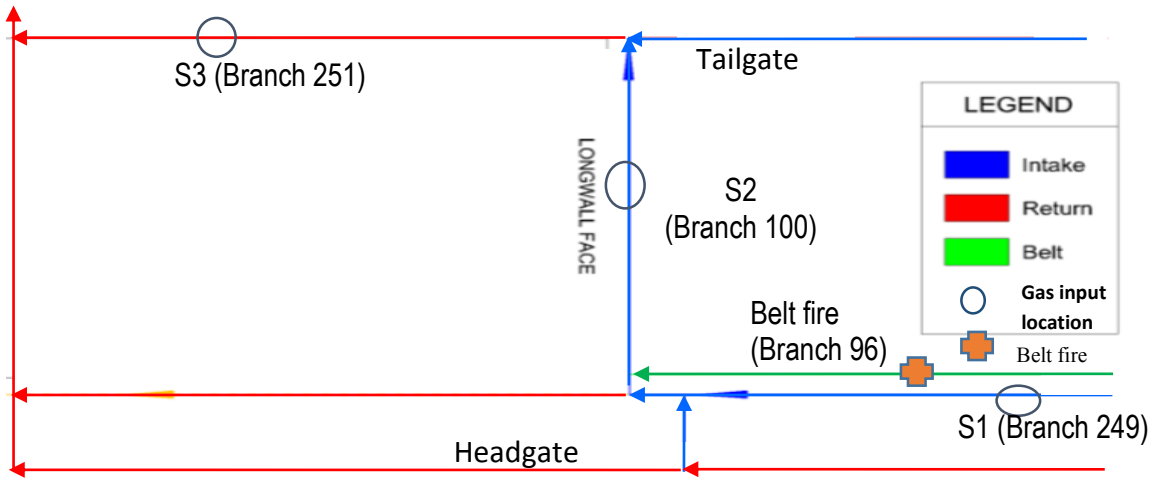

Figure 5.26. Schematic of modeled section illustrating areas of perturbation with source locations and belt fire location for coal mine example 2.

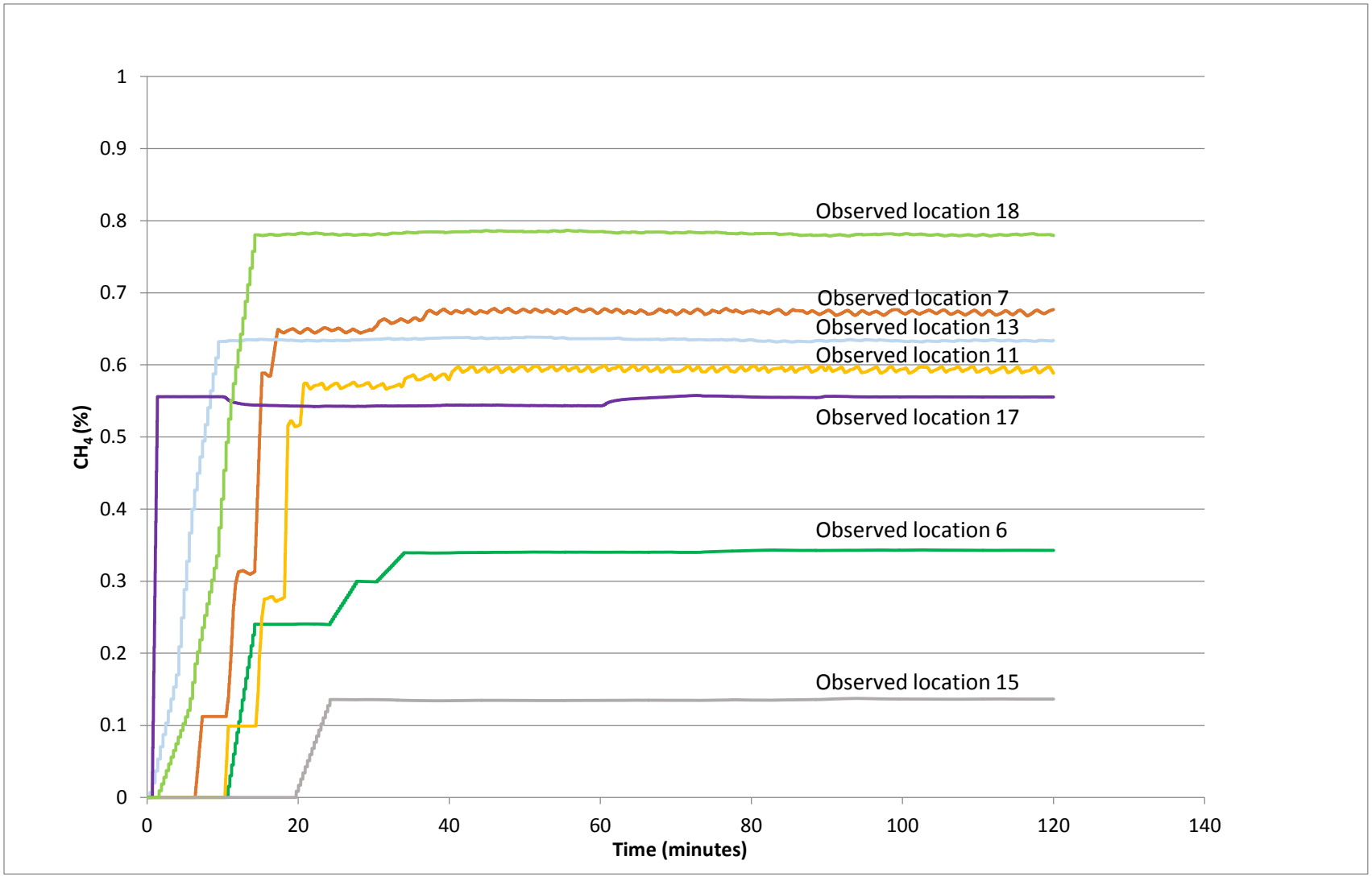

Figure 5.27a. Results of methane concentration at selected observed locations from native VAM simulation in Scenario 5. Selected locations with significant changes only are plotted.

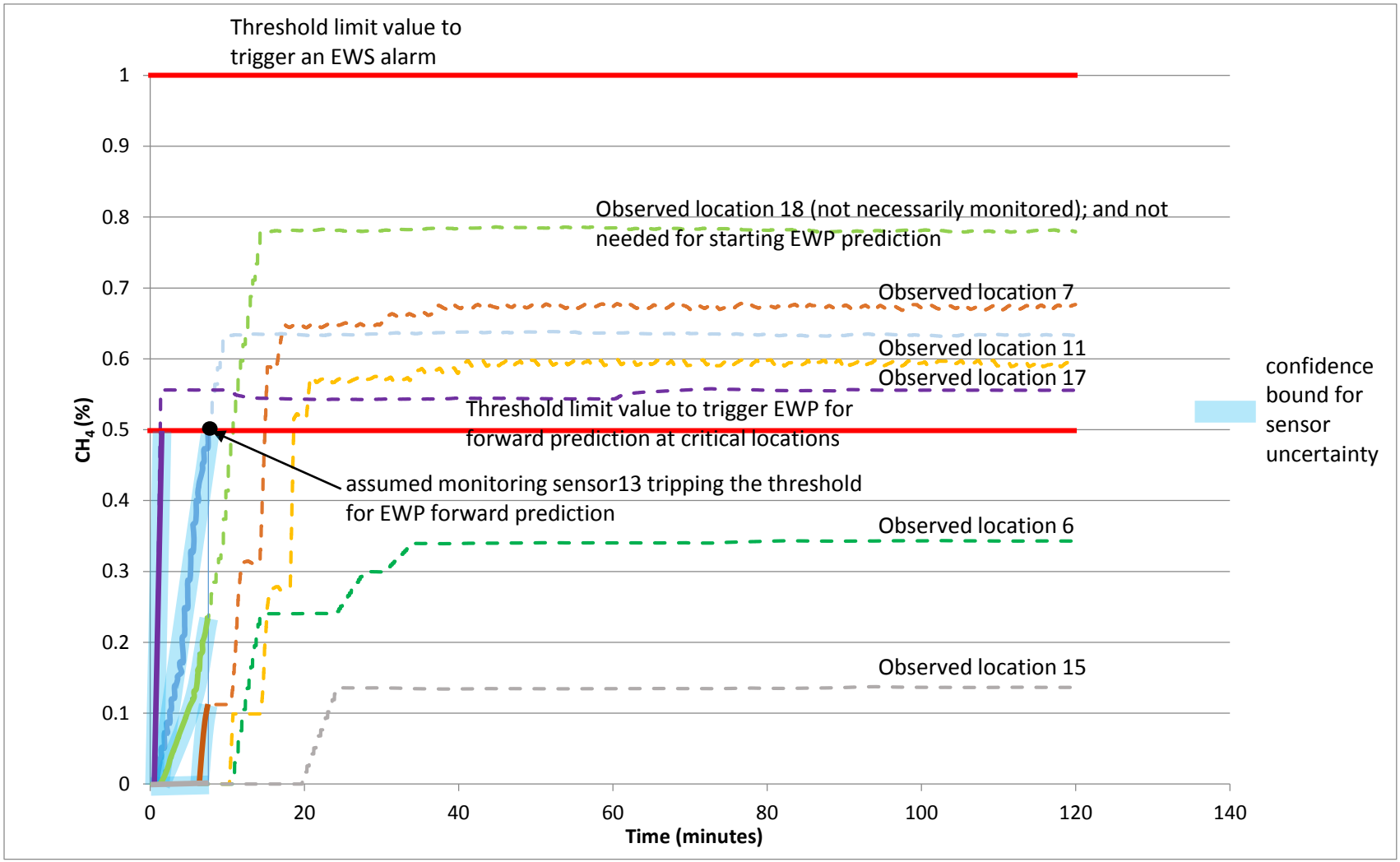

Figure 5.27b. Emulated sensor signal used as assumed monitored data input to trigger the EWS system in Scenario 5 (shown in thick lines with confidence bounds). Assumed sensors 13, 17 (and 18 if installed) trip(s) threshold for EWP forward prediction. The curves show real-time changes in CH_4 concentration. Selected locations with significant changes only are plotted. Note that the sensor signals are also used for the APPS predictor continuously (shown in dashed lines).

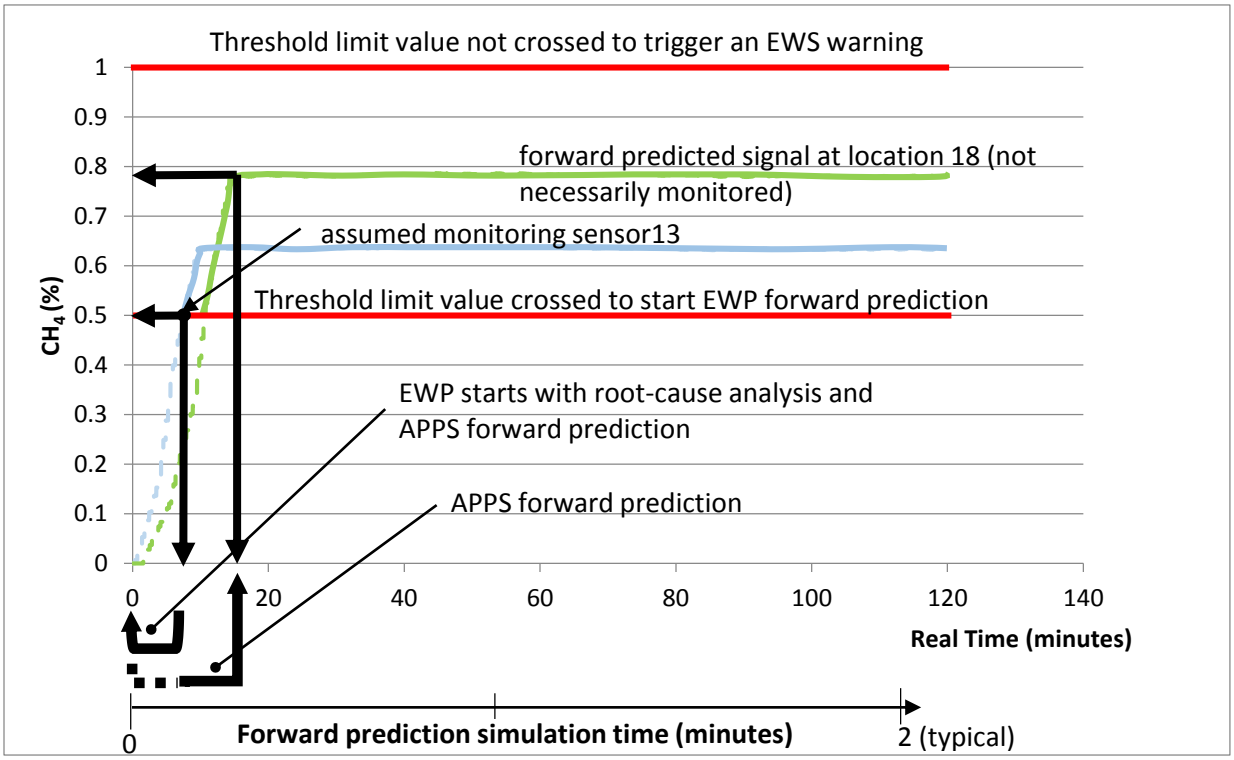

Figure 5.27c. APPS model forward prediction at selected observed locations in real-time and in fast simulation time scales for Scenario 5. Only two selected locations are shown.

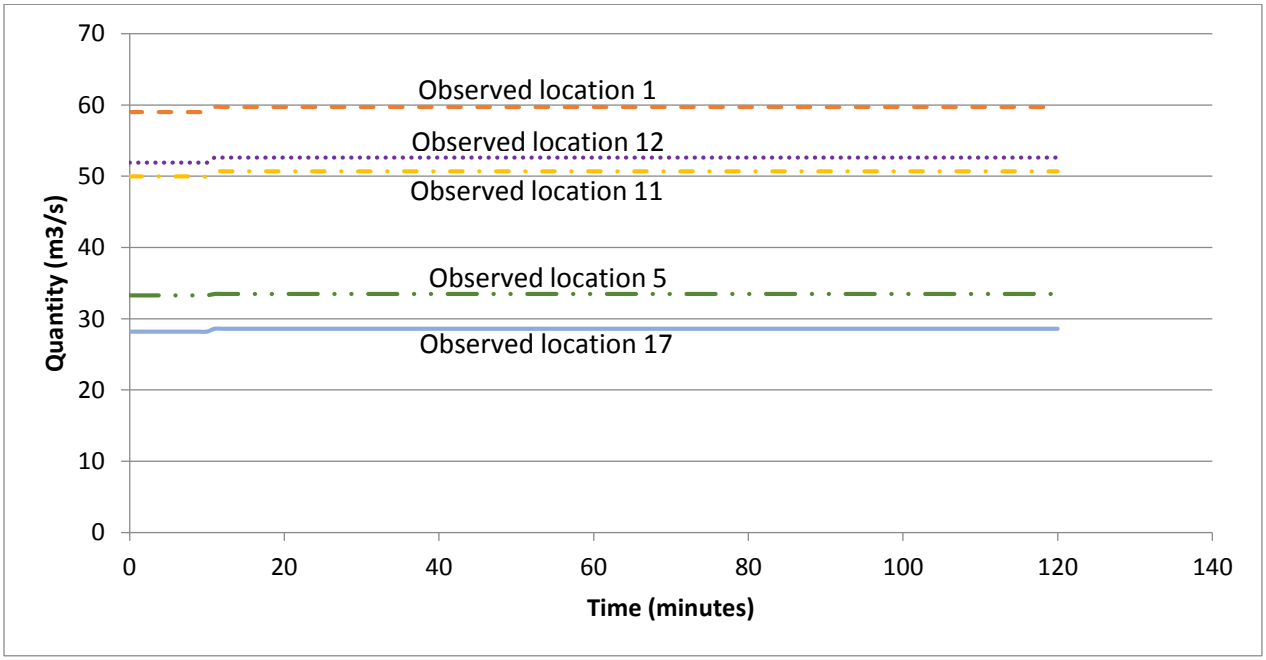

Figure 5.28. Results of airflow at assumed monitored locations due to belt fire in coal mine example 2.

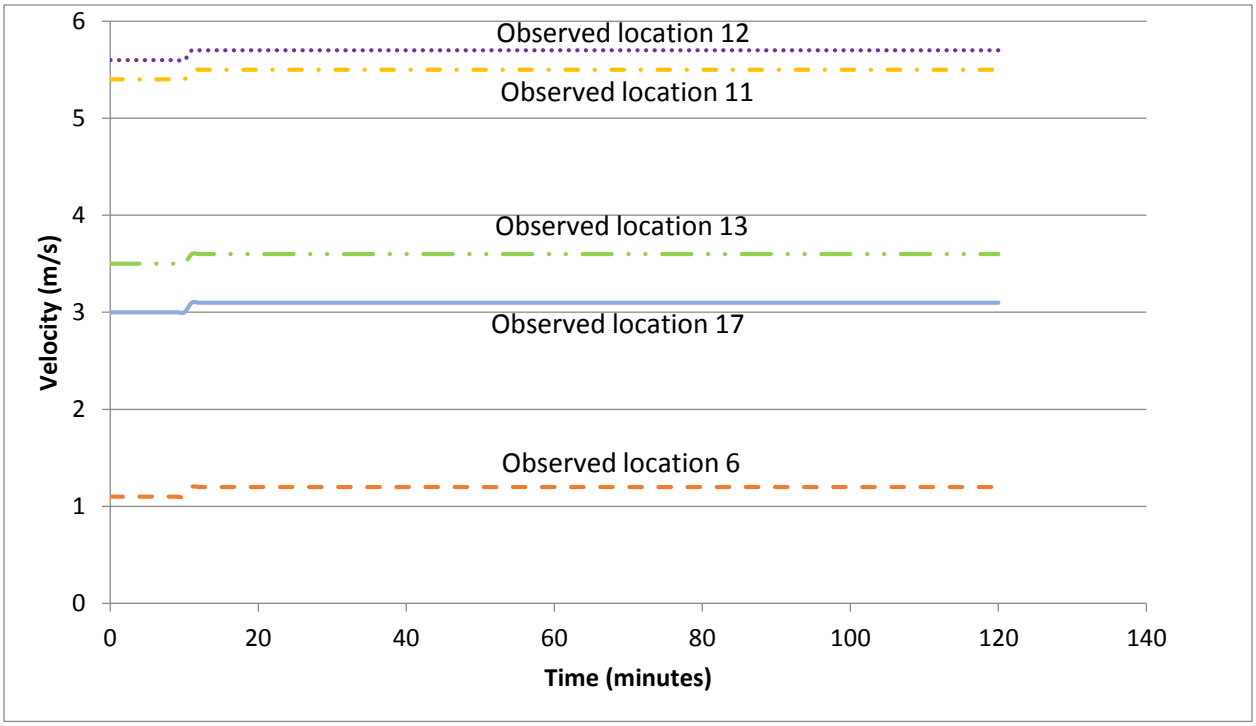

Figure 5.29. Results of velocity at assumed monitored locations due to belt fire in coal mine example 2.

The comparison of fan power for scenarios 1A, 1B, 2, and 3 modeled in example 2 is shown in Appendix A14.1. Also, the comparison of fan power for scenarios 1B, 4, and 5 modeled in example 2 is demonstrated in Appendix A14.2. The signal type and the model type for each scenario is given in Table 14.3 in Appendix 14.

5.6 Prepare reports, publications and plan for follow-up phase

- Two written interim reports of the research findings were submitted on a semi-annual basis.
- An abstract was submitted for publication and a presentation given of the research findings at the SME Annual Meeting & Exhibit, February 15 - 18, 2015, in Denver CO (Asante et al., 2015).
- An abstract is submitted for publication at the upcoming 2016 SME Annual Meeting & Exhibit to be held in Arizona entitled "Early-warning safety hazard predictor for preventive ventilation management."
- A Ph.D. dissertation is in development in the topic of root-cause analysis of atmospheric sensor data, an important element of EWS.
- A manuscript is being prepared for submission to an international journal.

6.0 Conclusions and Innovation Assessment

The exploratory work shows promising results of the Early-Warning System in identifying hazard-causing atmospheric conditions in their evolution toward an accident in the mine ventilating air based on analyzing monitored data against a calibrated mine ventilation, heat and contaminant transport model.

Numerical simulations indicate that even if the individual gas concentration signals from sensors at fixed monitoring locations all stay below the threshold for safety, there may be dangerous concentrations due to accumulation from gas sources along the airway in other locations. Such critical points with likely safety threshold crossings can be forward-predicted by the Early-Warning Predictor of the Early-Warning System. The system can notify mine management of the nature of the hazard scenario for preventive action. Since high concentration fronts travel with the air velocity in the mine, precious time may be available to prevent the disaster from happening by timely intervention.

It is demonstrated that accident-prone atmospheric conditions, such as caused by barometric pressure variations that may be difficult to notice, can be recognized using a ventilation and contaminant model in forward-predicting mode to foresee the outcome of real-time dynamic changes at future times. An innovative, forward-predicting model-element is demonstrated using the Numerical Transport Code Functionalization (NTCF) technique for strata and gob gas source simulation as a root-cause of gas inflow to the ventilating air. The NTCF modeling method, an efficient, patented, numerical modeling technique, is a built-in component of MULTIFLUX.

An even more powerful application of the NTCF method is discovered during the project in the form of the Continuous Dynamic Correlator application. Such a modeling method is can be used in all gassy mines for all sealed but leaky areas as well as for pillars, floors, ribs and roofs in contact of ventilating air using the NTCF method. The dynamic storage and discharge of gases from the porous and fractured rock in a coal mine can be modeled with the NTCF method similarly to heat and humidity transport simulations in hot underground mines in which the NTCF model element is a standard component.

A powerful forward-predicting simulator in the MULTIFLUX software is demonstrated as an Early-Warning Predictor with unprecedented speed and mine-size capacity. Computational speed tests, requested by Ventsim for commercialization evaluations revealed that the air flow distribution in a mine with as many as 27,000 air branches can be solved in less than 2 seconds. The direct forward-predicting MULTIFLUX solver is completed, and is being tested by the Ventsim distributor for future commercialization. The speed and accuracy of MULTIFLUX together with its potential market accessibility through Ventsim, the most widely-used ventilation software, makes the Early-Warning System a potential reality for mining applications.

The early warning system is tested against typical simulated error signals for potential hazard scenarios under controlled conditions. The test results are conclusively positive. Significant time gain, in the order of 20 minutes is seen in the examples between the hazard detection time and the critical threshold crossing time at some critical locations.

Proposed steps for commercialization and broad applicability to improve mine safety

Launching a complex system to the mining industry needs a Champion. The Alpha Foundation is recommended to assume such a role in introducing the game-changing Early-Warning System to increase mine safety. Based on the promising results from the exploratory work, continuation to prototype phase for commercialization is suggested to the Alpha Foundation. The proposed, additional development steps are summarized as follows:

1. Support full integration of the MULTIFLUX solver into Ventsim by expanding it to the Ventfire component. Fast and accurate fire simulation is very important for both early fire detection as well as for mine rescue operations. The MULTIFLUX network-based solver engine outperforms the native Ventsim solver significantly both in time and accuracy, both critical elements for a successful Early-Warning System.
2. Support full integration and software validation of the Early-Warning System into Ventsim with its world-wide market that includes hundreds of coal mines.
3. Support the development of on-site ventilation model calibration tools automated with self-calibration for easing the burden on the mines to apply the Early-Warning System.

Justifications

The justification for supporting steps 1 through 3 is to integrate and market an easy-to-use Early-Warning System by the established Ventsim software distributor. The mining industry needs a unified mine ventilation and fire simulation software with all critical components, including the EWS, integrated for ease of use, accuracy, and simulation speed.

Steps 1 through 3 will enhance the incentive for the mines to invest into real-time sensor systems. Such sensor system, together with the runnable EWS included in Ventsim will in turn result in safer and healthier mines.

Therefore, with the role of a Champion, the days will be moved closer when metal and coal mines use their mandated ventilation model not only for ventilations survey reports but as a real-time risk assessment tool to avoid the likelihood of an accident due to inadequate atmospheric conditions.

7. References

Asante, W., Bahrami, D., and Danko, G., (2015), "Early warning system design for accident prevention with ventilation monitoring and evaluation," SME Annual Meeting & Exhibit, February 15 - 18, 2015, Denver, CO.

Code of Federal Regulations, 30 CFR §7.504, (2012), Washington, DC: U.S. Government Printing Office, Office of the Federal Register.

Danko, G., (2006), "Functional or Operator Representation of Numerical Heat and Mass

Transport Models," ASME J. of Heat Transfer, Vol. 128, p. 162-175.

Danko, G., (2012), "Ventilation and climate control of deep mines," McGraw-Hill 2012 Yearbook of Science and Technology, p. 296-299.

Danko G., (2014), "Safety, Health, and Ventilation Cost Optimization with Simulation and Control," Report submitted to NIOSH, Grant Number: 200-2009-30157, p. 1-228.

Danko, G., and Bahrami, D., (2014a), "Contaminant Species Modeling With Advection, Dispersion, and Stratification in Ventilation Networks," 10th Int. Mine Ventilation Congress, August 2-8, 2014, Sun City, South Africa, p. 379-387.

Danko, G., and Bahrami, D., (2014b), "Safety, Health and Ventilation Cost Benefit Optimization with Simulation and Control," Workshop, 10th Int. Mine Ventilation Congress, August 2-8, 2014, Sun City, South Africa.

Jianqing F., and Qiwei, Y., (2003), "Nonlinear Time Series-Nonparametric and Parametric Methods," Springer-Verlag, New York, Berlin, Heidelberg. ISBN 0-387-95170-9, page 1-88.

Jong E. C., Luxbacher, K. D., Karmis, M. E., and Westman, E. C., (2013), "Field test of a perfluoromethylcyclohexane (PMCH) permeation plug release vessel (PPRV) using a dual tracer deployment in an underground longwall mine," Department of Mining and Minerals Engineering Holden Hall, Virginia Tech, personal communications.

Schatzel, S. J., Karacan, C, Ö, Krog, R. B., Esterhuizen, G. S., and Goodman, G. V., (2008), "Guidelines for the Prediction and Control of Methane Emissions on Longwalls," National Institute for Occupational Safety and Health, DHHS (NIOSH) Publication No. 2008-114, Information Circular 9502, page 1-83.

Shumway, R. H., and Stoffer, D. S., (2010), "Time Series Analysis with Applications," 3nd edition, Springer, New York, Dordrecht, Heidelberg, London, DOI 10.1007/978-1-4419-7865-3, ISBN 978-1-4419-7864-6.

Time Series, http://en.wikipedia.org/wiki/Time_series, Accessed April, 2015

U.S. Patent No. 7610183B2, (2008), U.S. Patent No. Patent 8396693 B2 (2013), "Multiphase physical transport modeling method and modeling system."

8.0 Appendices

APPENDIX 1. Declaration of interest in MULTIFLUX

CHASM Consulting Pty Ltd
(Incorporating Ventsim Software™)
ABN 52 129 440 866
PO Box 1457,
Capalaba 4157

Telephone +61 7 3390 2663
Facsimile +61 7 3390 3612
admin@chasm.com.au
www.chasm.com.au

10 Feb 2015

To Whom It May Concern:

Chasm Consulting is interested in further enhancing its popular Ventsim Visual mine ventilation, heat, moisture and contaminant simulation software with the solution techniques used in MULTIFLUX. We have been testing the MULTIFLUX model for speed and accuracy under a tryout license agreement signed by President Johnson of the University of Nevada, Reno (UNR).

During this time, we have been investing considerable time at Chasm developing the conversion importer functions in Ventsim in order to incorporate the innovative MULTIFLUX solver software in the latest 3D graphical user interface environment in Ventsim Visual. Upon successful completion of the tests, we intend to market our Ventsim model with an incorporated "Powered with MULTIFLUX" option under a separate commercial license agreement with UNR.

Craig Stewart
Managing Director
Chasm Consulting

APPENDIX 2. Testing of direct connection between Ventsim and MULTIFLUX

MULTIFLUX (MF) button in Ventsim Visual's toolbar illustrated in Figure A2.1. Comparison between the native VAM model in Ventsim and the results from APPS in MULTIFLUX at two sections of a coal mine are shown in Figure A2.2 and Figure A2.3. The coal mine example with 5206 airways is simulated by the APPS in 1.7 seconds.

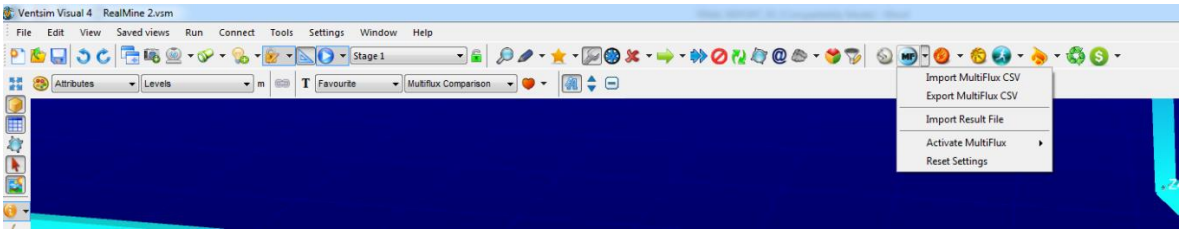

Figure A2.1. MULTIFLUX (MF) button in Ventsim Visual's toolbar.

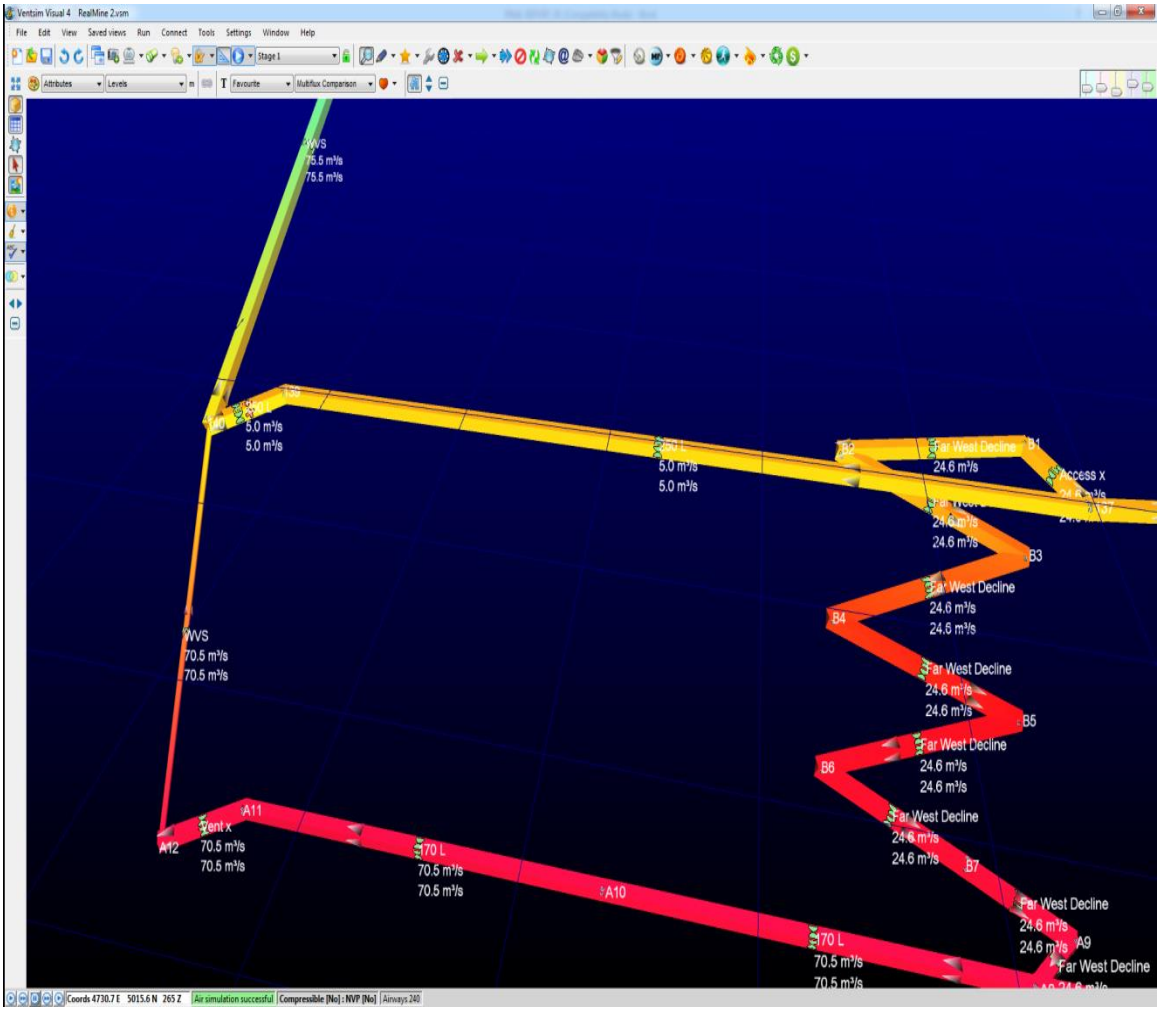

Figure A2.2. Comparison between the native VAM model in Ventsim and the results from APPS in MULTIFLUX.

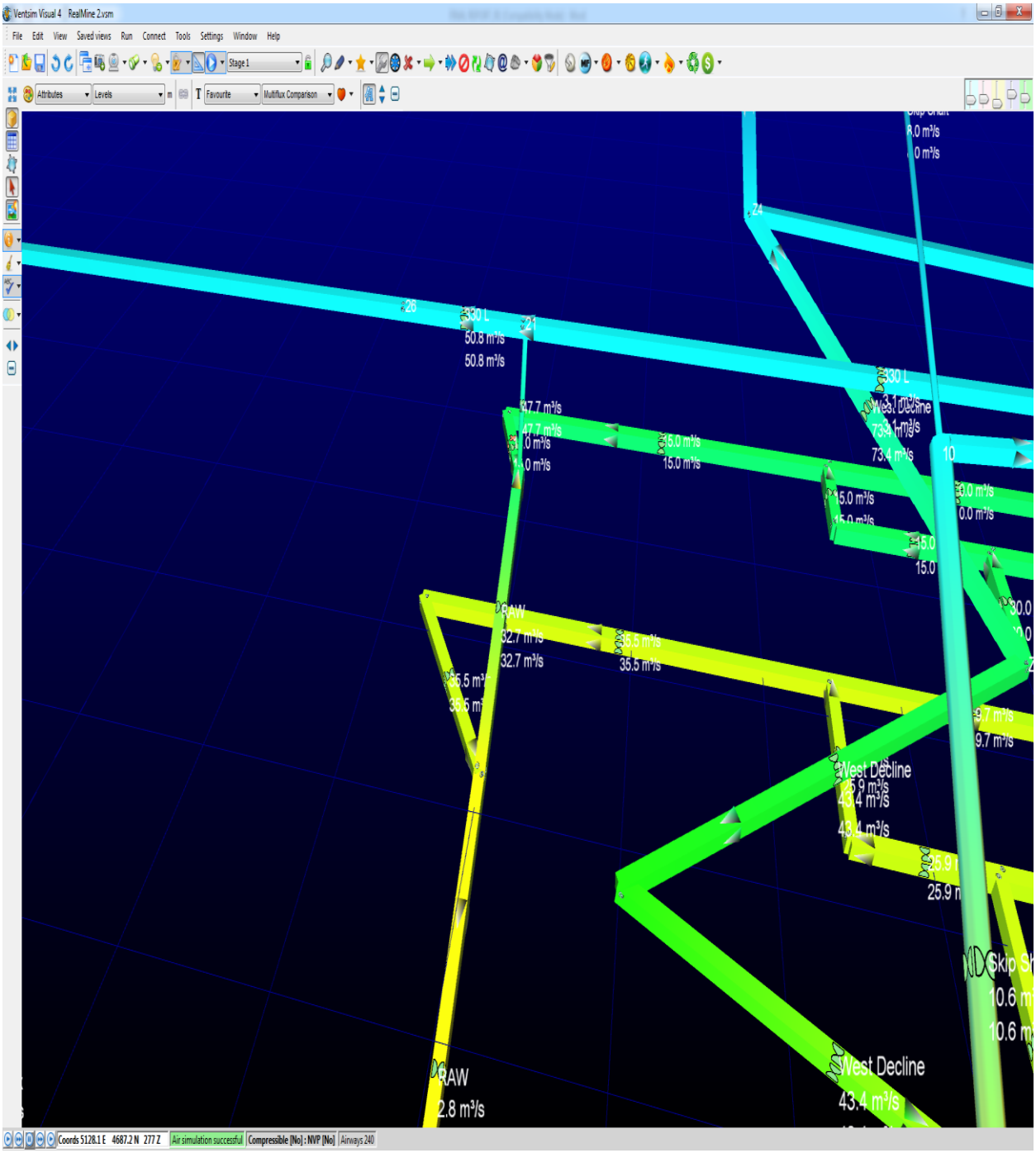

Figure A2.3. Comparison between the native VAM model in Ventsim and the results from APPS in MULTIFLUX at another mine section.

APPENDIX 3. Software macro to configure the APPS model from the native VAM data files.

A software macro has been written to convert models form VnetPC and Ventsim successfully. Model configuration for partner mine examples are converted and modeled in MULTIFLUX. Figure A3.1 shows the activity chart for converting the native VAM and running the converted model in MULTIFLUX.

VnetPC Model conversion

1. Save branch and fan input data as an excel csv file.
2. The VnetPC model is read and converted to MULTIFLUX csv file using the software macro.
3. The MULTIFLUX csv is then imported into the MULTIFLUX graphic user interface.

Ventsim Model conversion

1. Save the model as a text file from Ventsim.
2. The branch and fan input data in the text file are read and converted to MULTIFLUX csv file using the software macro.
3. The MULTIFLUX csv is then imported into the MULTIFLUX graphic user interface.

MineVent Model conversion

1. Save the model as a text file from MineVent using the "Setup Menu" and "Export All" to export as much data as possible. The fan data exists in a text file with "FAN" as the extension.
2. The branch and fan input data in the text files are read and converted to MULTIFLUX csv file using the software macro.
3. The MULTIFLUX csv is then imported into the MULTIFLUX graphic user interface.

The model configuration from the native VAMs models are converted exactly as they are defined in native VAM.

Figures A3.2, A3.3, and A3.4 illustrate three of the mine examples that are converted from VnetPC, and Ventsim into MULTILFUX using the written software macro. Figure A3.5 depicts a converted geometry of the MineVent example (Bingham Canyon Coal Mine) to MULTIFLUX using a written software macro. The MineVent conversion is kept in manual mode as it is deemed unnecessary in the numerical tests of the EWS.

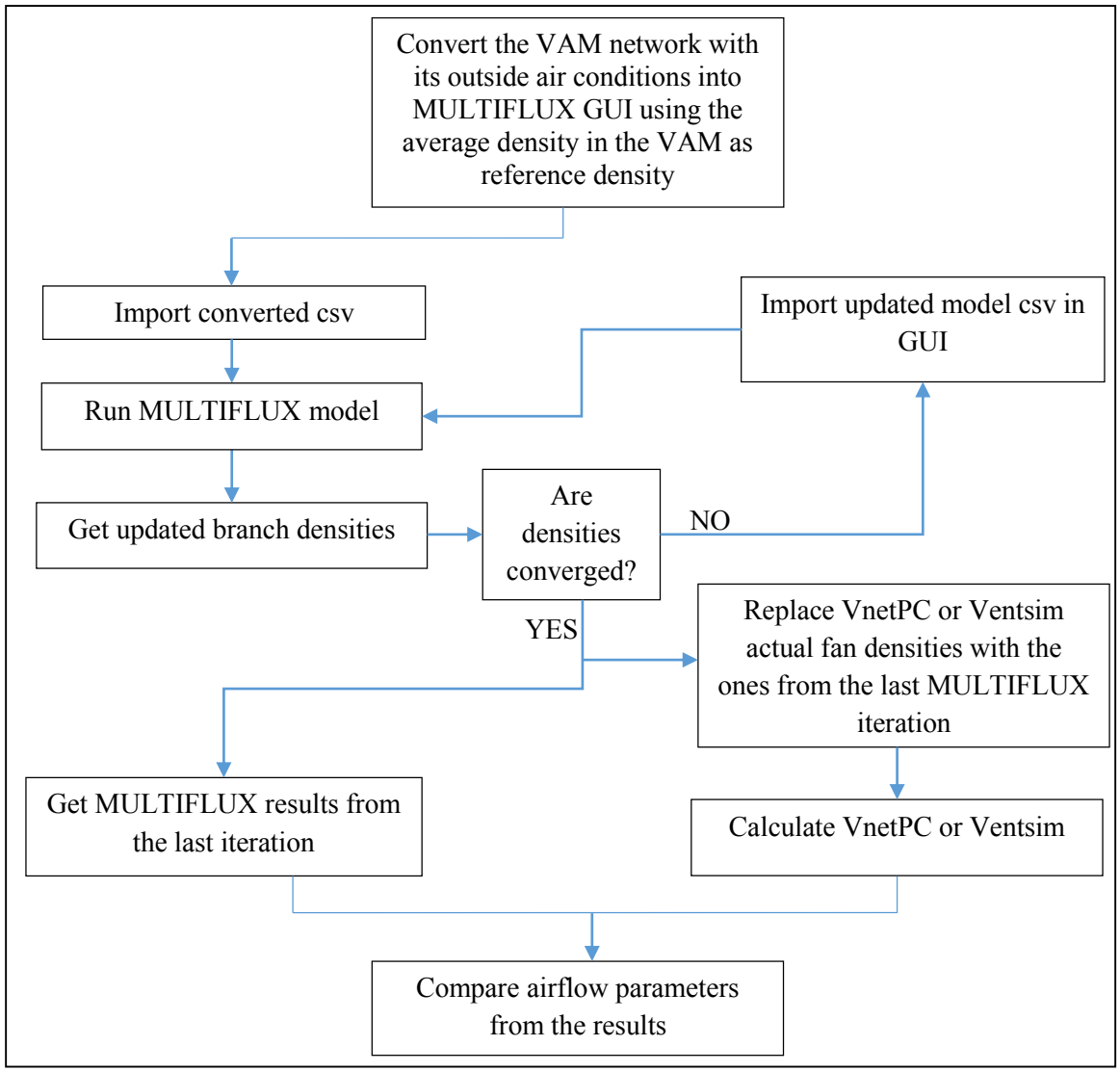

Figure A3.1. Activity chart for running MULTIFLUX.

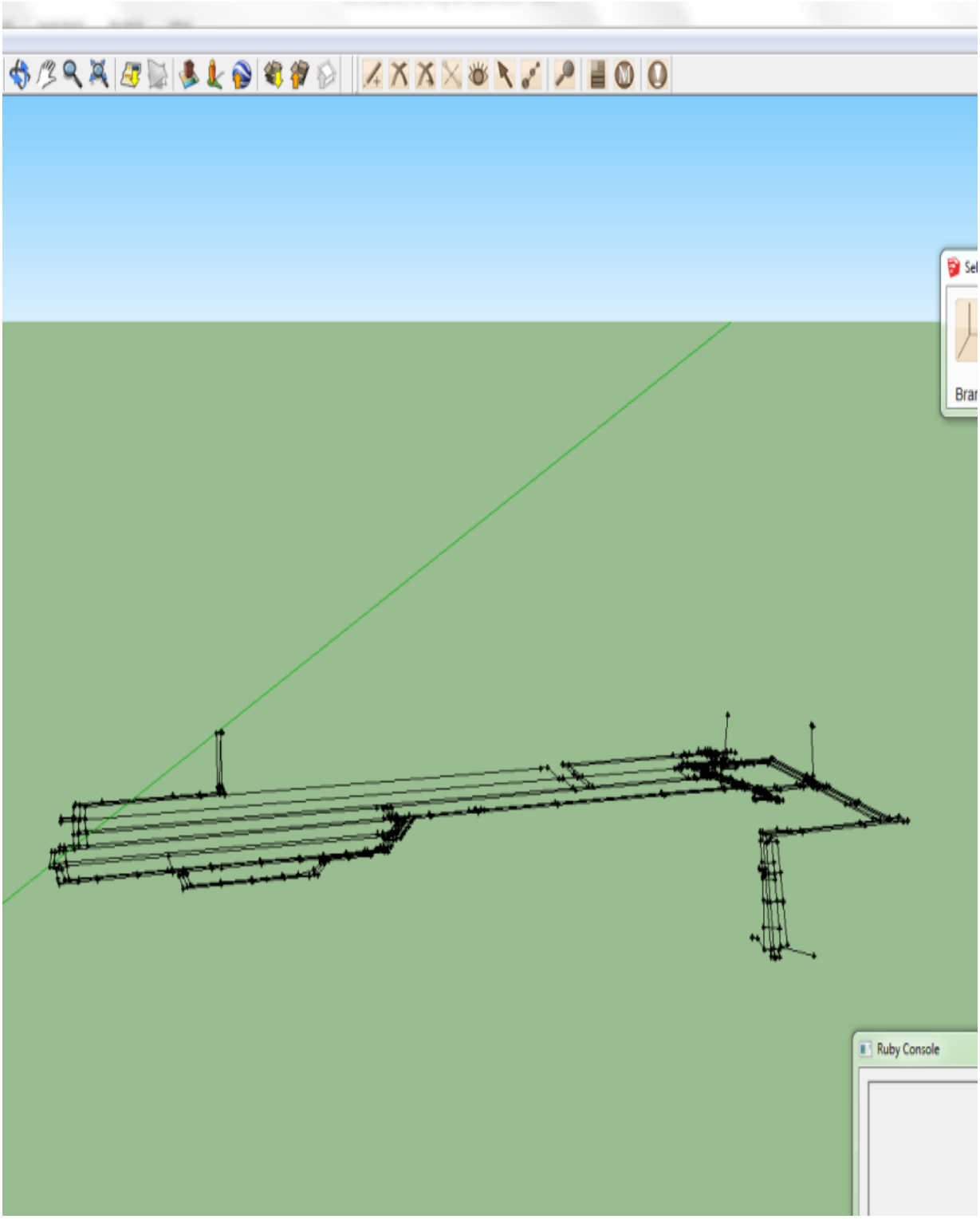

Figure A3.2. APPS model example 1in MULTIFLUX (coal mine) converted from VnetPC.

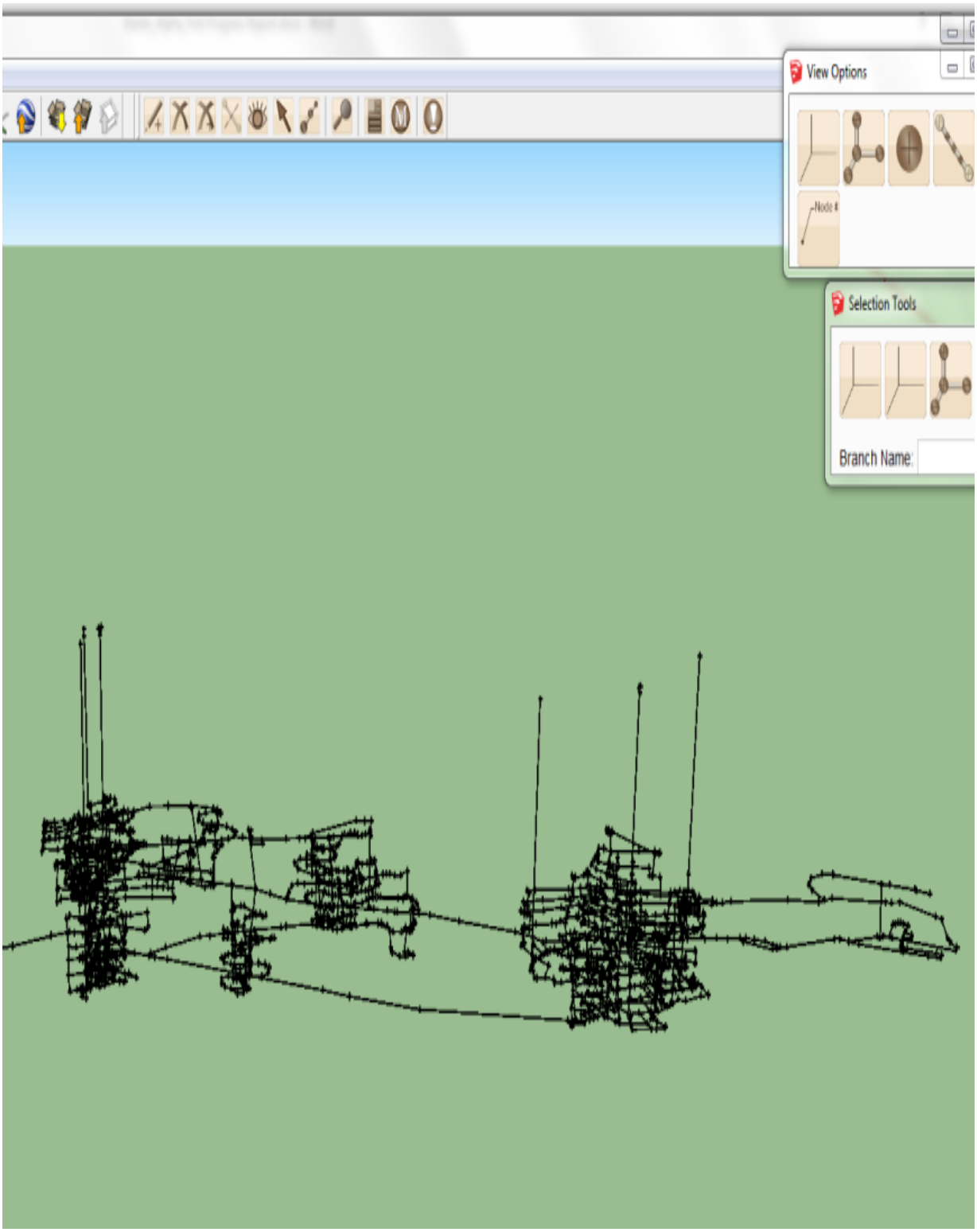

Figure A3.3. APPS model example 2 in MULTIFLUX (metal mine) converted from VnetPC.

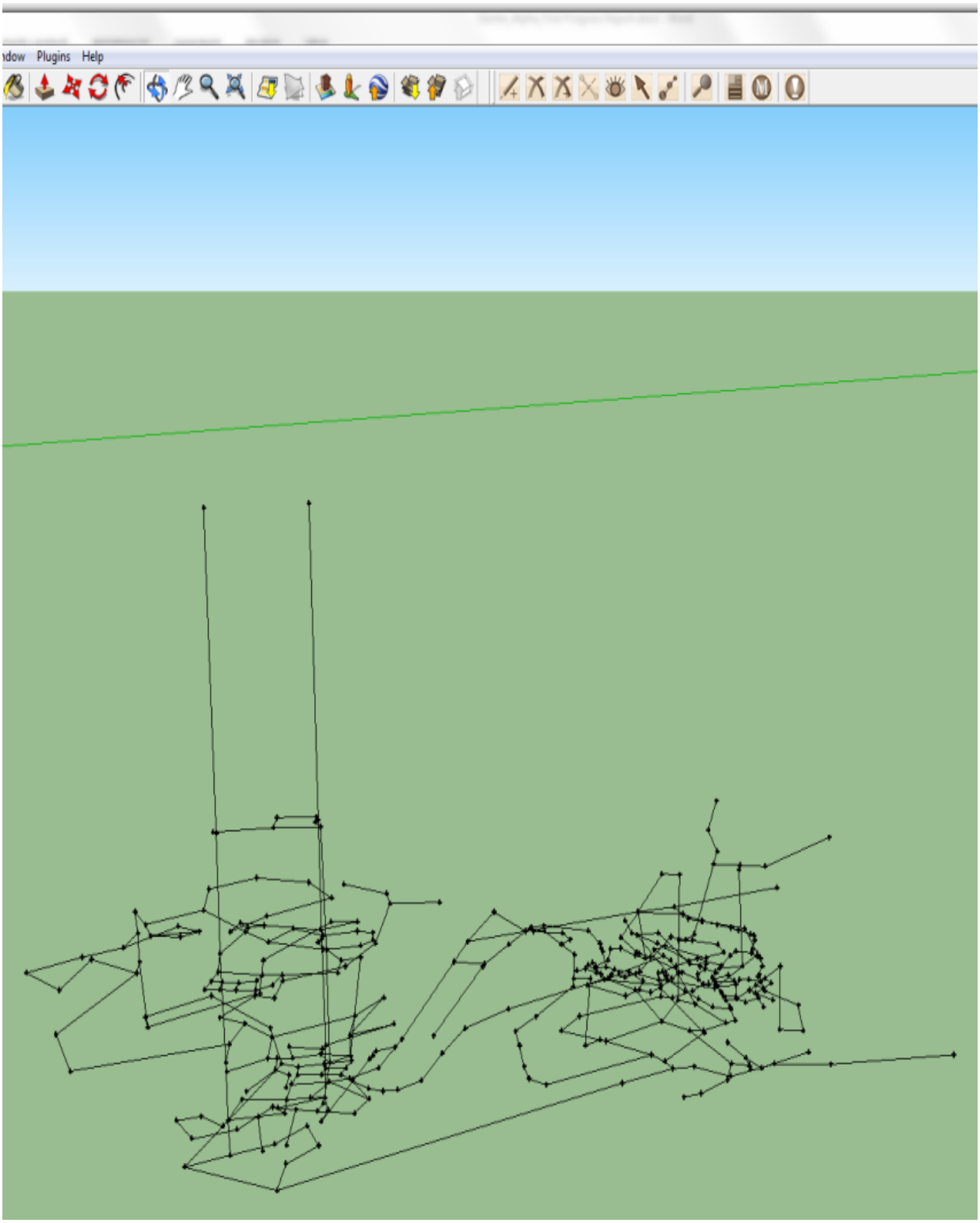

Figure A3.4. APPS model example 5 (metal mine) in MULTIFLUX converted from Ventsim.

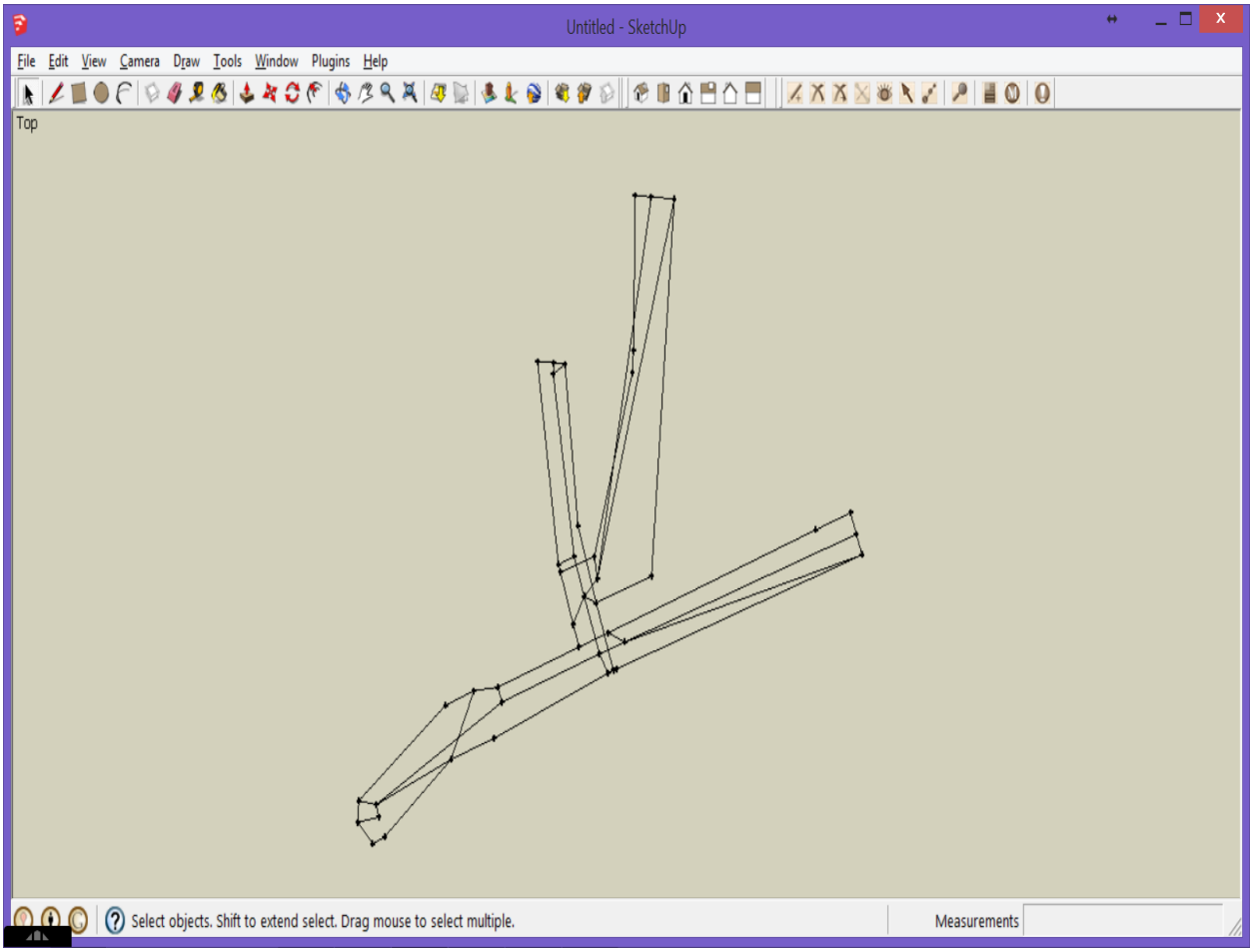

Figure A3.5. APPS model example of the Bingham Canyon Coal Mine in MULTIFLUX converted from MineVent.

APPENDIX 4. Gob model and analysis of expected gas inflow

A typical gob layout and its connection to the ventilation network for a coal mine obtained from one of our partners are demonstrated in Figure A4.1. Figure A4.2 depicts the ventilation schematic with the gob. A fringe ventilation system is shown to remove gas accumulation. Table A4.1 defines the mining parameters for modeling purposes (Schatzel et al, 2008).

Numerical modeling of the gob areas and sealed-off zones under variable input conditions is performed. The effect of barometric pressure changes on gas inflow into the airway from the strata is predicted by a coal seam model as follows. A drop of 1000 Pa barometric pressure change is used in the numerical model to predict gas inflow. The cause and results are illustrated together in Figures A4.3 (a) and (b).

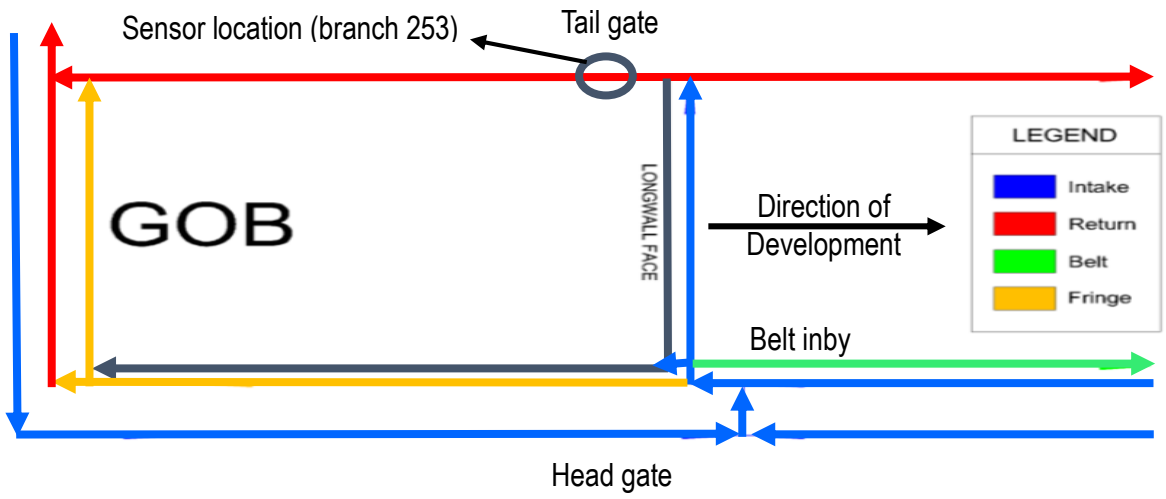

Figure A4.1. Schematic diagram of the longwall panel ventilation system (Jong et al, 2013).

Table A4.1. Development mining parameters and their range of values used for modeling purposes (Schatzel et al, 2008).

Mining parameter	Range of values
Mining height, ft	5.0–7.0
Entry development length, ft	1,000–12,000
Mining rate, ft/day	25–175
Methane concentration in mine air, %	0.5–1.5
Distance of shielding wells to entries, ft	19–87
Duration of degasification before mining, days	0–180

Shielding wells are wells drilled to gate road entries to reduce methane inflow rate into the development entries (Schatzel et al, 2008).

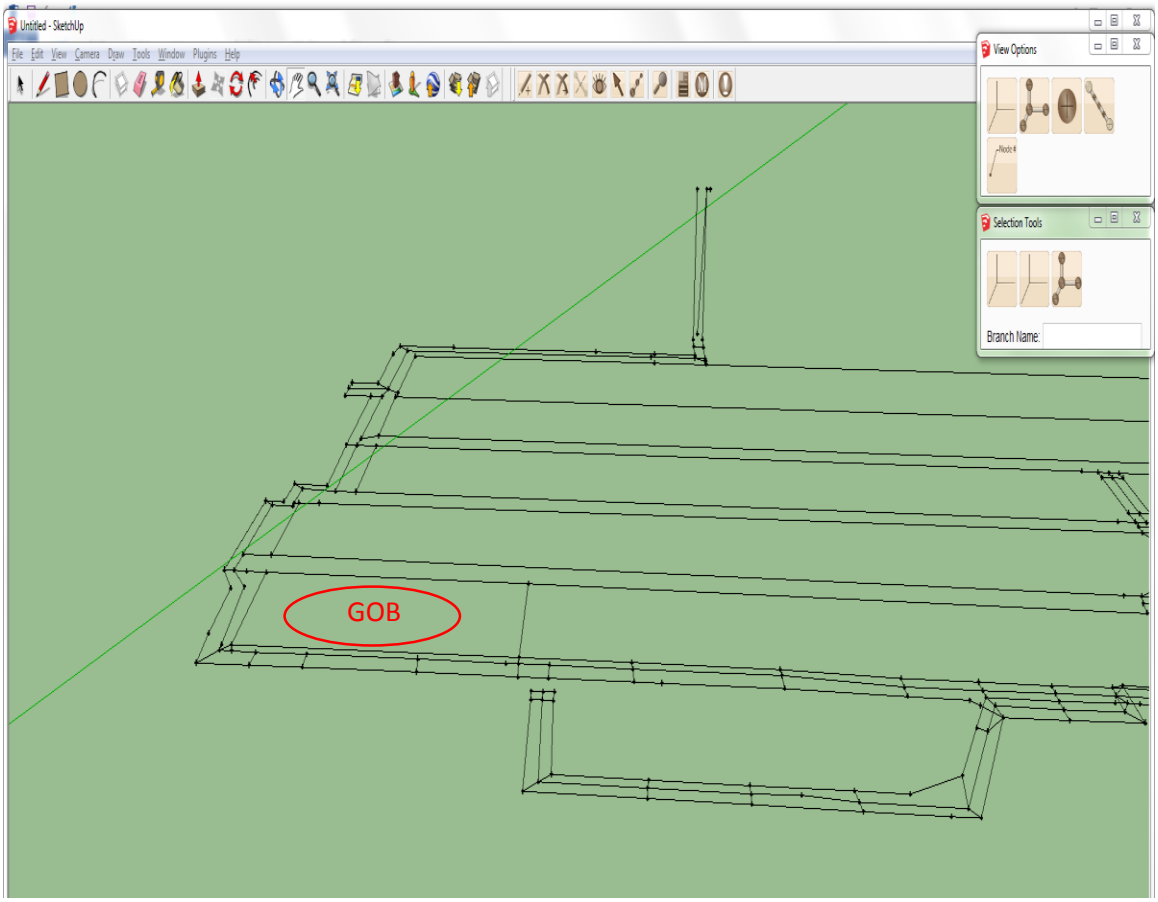

Figure A4.2. Ventilation schematic demonstrating the gob in MULTIFLUX.

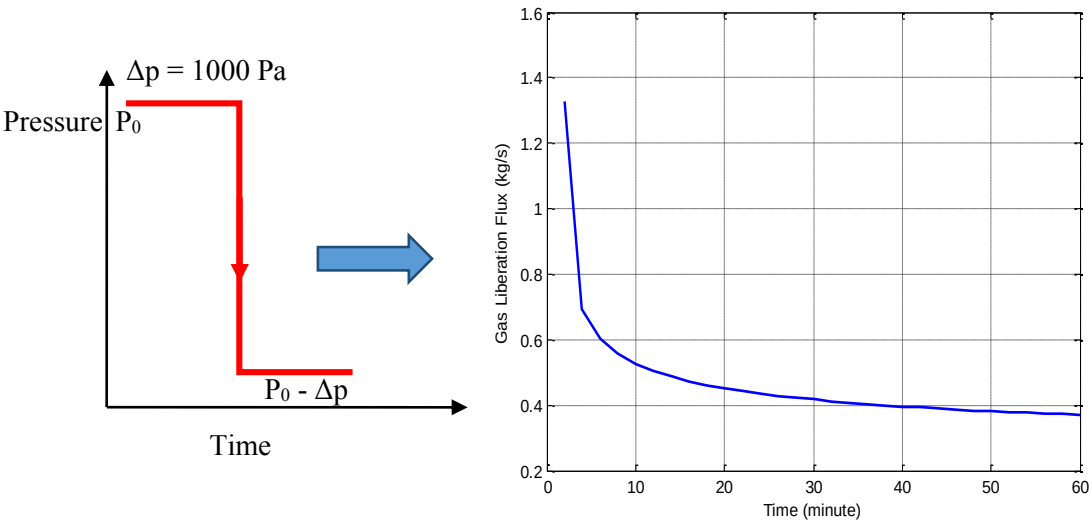

(a) (b)

Figure A4.3. Flux increase (b) due to pressure drop (a) per 1000 m airway section (Danko et al, 2013).

Such a gas liberation source is initially modeled with the APPS model and checked for criticality. However, no time delay is seen in the response inflow giving no time period for early-warning forward predictions in this case.

Another type of gas inflow from the gob is predicted with a simplified, conceptual model due to Darcy flow from the gob into the return airway. It is assumed that periodic barometric pressure pumping establishes low methane concentrations in the preferential pathways from the gob to the airway which has to be cleared by Darcy flow before high methane concentration arrives at the airway surface.

Barometric pressure pumping is caused by the continuous and periodic variation of pressure as shown from meteorological data. Pulsating pressure and flow mixes methane with air and is assumed to establish a low average concentration near the wall in the advection channels between the gob and the airway ± 2000 Pa variations as illustrated in Figure A4.4.

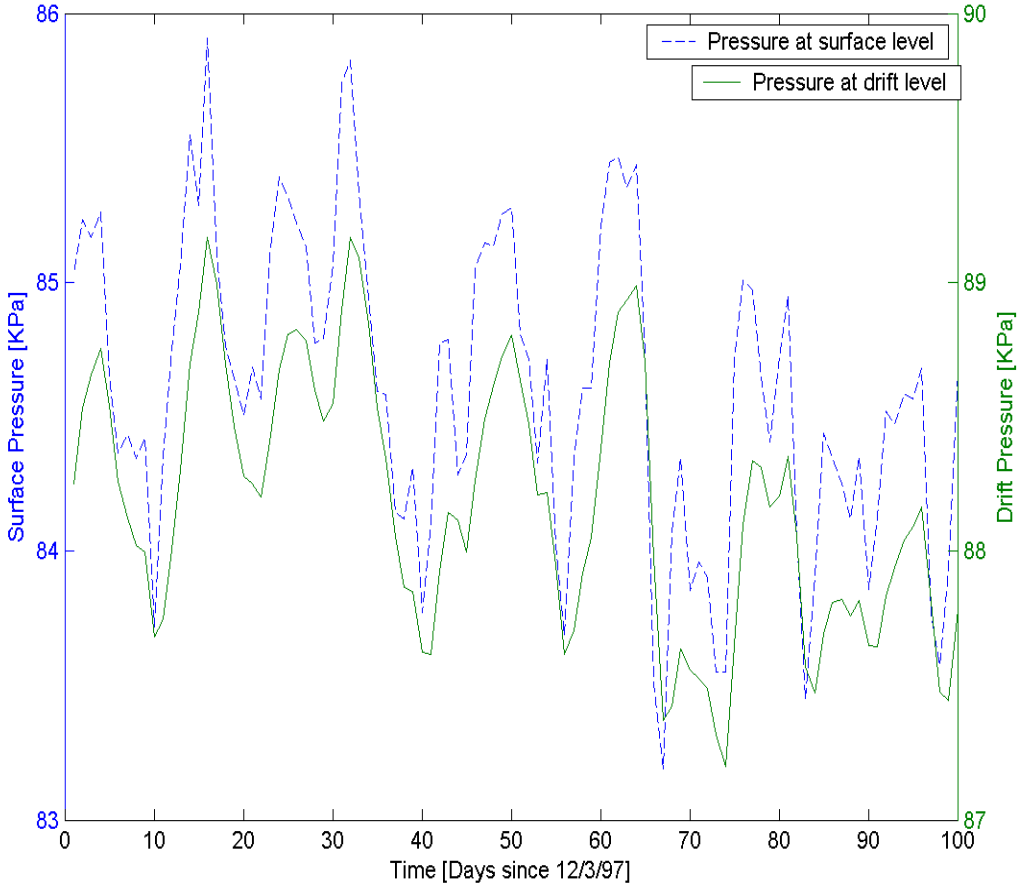

Figure A4.4. Typical Barometric Pressure, Pb, variation in Nevada (Danko et al, 2013).

Disturbances in pressure after a 2-day high barometric pressure event followed by Δp decrease causes Darcy flow. Calculating Darcy flow from the gob through a gap of aperture, b,

throughout the length, L, of the longwall return airway (branch 280) into the middle of the gob of width, W, is as follows:

$$Q = -\frac{k}{\mu} * \Delta p * b \frac{L}{0.5W}$$

Where the following data are substituted:

b= 0.0065, [m]
k= $b^2/12$, permeability, [m^2]
Δp= 300, pressure change from simulation, [Pa]
L= 840, [m]
W= 300, [m]
μ= 1.73×10^{-5}, Viscosity of air-methane mixture, [Pas]

The methane flow rate from the Darcy equation gives 1.48 m^3/s. A delay time, Δt is calculated assuming that half of the gob width has to be cleared by Darcy flow before high methane concentration arrives at the airway surface.

Velocity:

$$\vartheta = \frac{Q}{bL} = \frac{1.48}{0.0065 * 840} = 0.27\ [m/s]$$

Delay time:

$$\Delta t = \frac{W/2}{\vartheta} = \frac{150}{0.27} = 555\ [s]$$

The time variation of the methane inflow is depicted in Figure A4.6. Methane concentration is calculated from the ventilation airflow rate and Q as follows:

$$\frac{(3.7 * 0\%\ CH_4) + (1.48 * 50\% CH_4)}{5.18} = 14.28\%\ methane$$

Figure A4.5 demonstrates methane inflow concentration as a function of time.

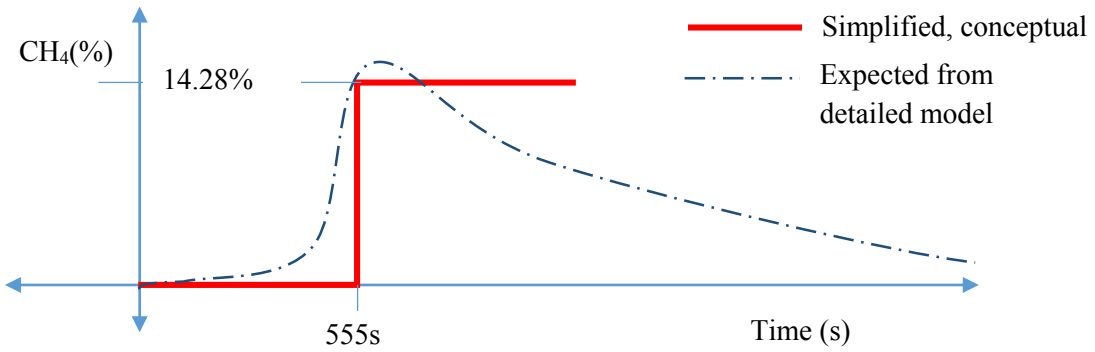

Figure A4.5. Methane concentration change from gob with time due to airway blockage.

Therefore, it takes 555 seconds to sound early warning due to 200 Pa pressure drop. Figures A4.5 and A4.6 illustrate the methane concentration and flow rate curves for the concept model in red solid line but a more realistic release curve is expected and modeled numerically shown in blue dashed line.

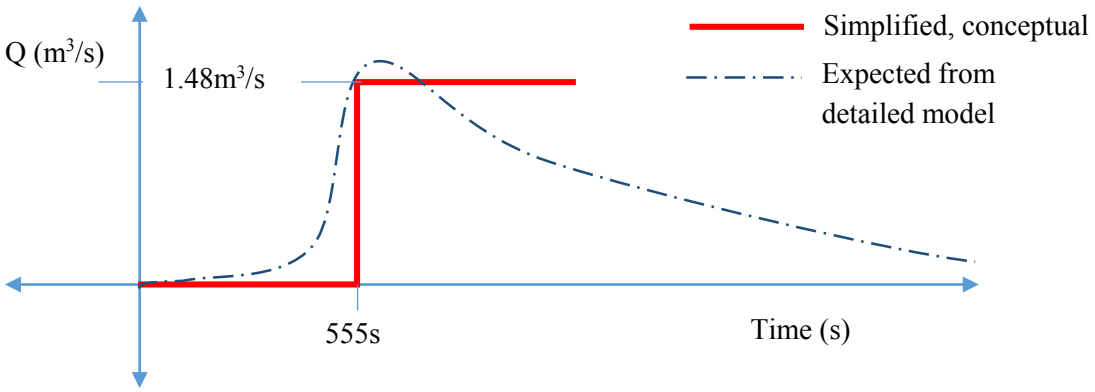

Figure A4.6. Methane inflow rate from gob due to barometric pressure change.

A second type of disturbance of airway blockage is also modeled for the longwall return airway (branch 280). The blockage caused Δp of 200 Pa and the airflow also dropped from 3.8 m^3/s to 3.7 m^3/s. The methane inflow response to this disturbance is similar to that illustrated in Figure 5.1-10, causing a delayed methane concentration increase in the ventilating air.

As shown in Figures A4.5 and A4.6, it takes about 10 minutes for the incoming methane to reach peak values, giving a chance to trigger an alarm for caution before the condition become critical.

The solution of the detailed model is described in section 5.3 under Scenario 3 studies.

APPENDIX 5. Emergency Rescue Chambers (ERC) in the APPS model

A set of macros have been developed to process user input data for a given ERC and produce the airflow and thermal transport connections in MULTIFLUX. The import/export functions for the MULTIFLUX model are added to the Ventsim GUI, depicted in Figure A5.1.

The RA model imported into the Ventsim GUI is demonstrated in Figure A5.2. The thickness of the tent wall is exaggerated in Figure A5.2. Natural ventilation air loops are also shown in Figure A5.2 that allow to model air circulation in the closed tent due to temperature differences.

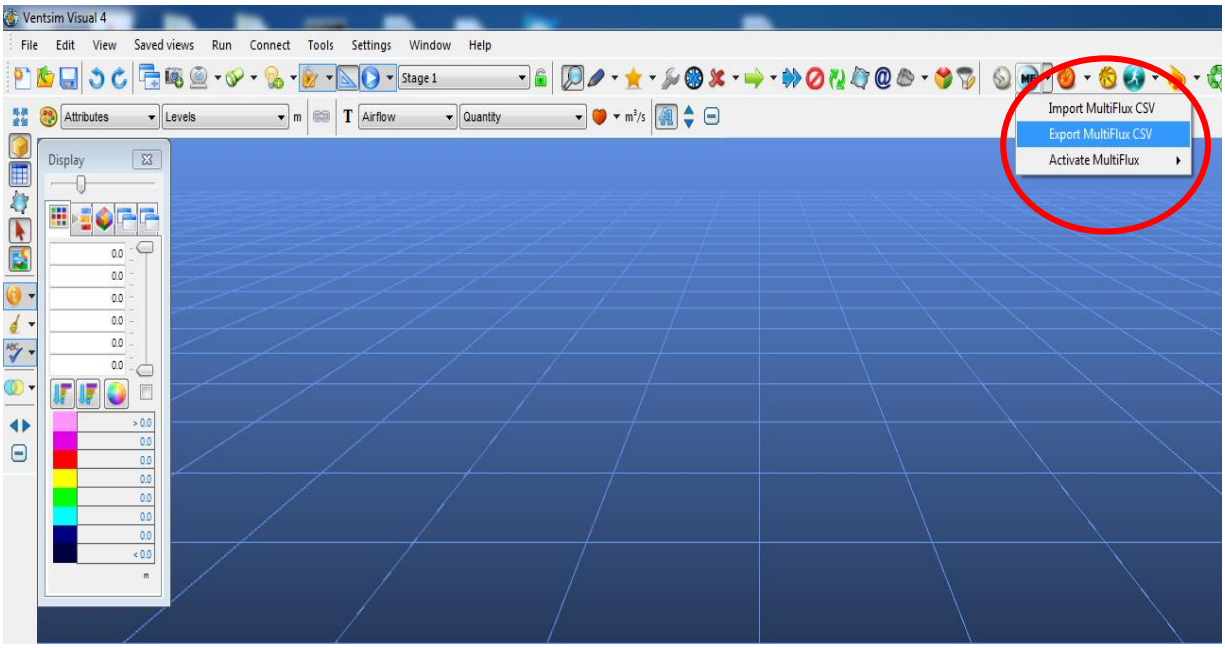

Figure A5.1. MULTIFLUX import/export module added to the Ventsim GUI.

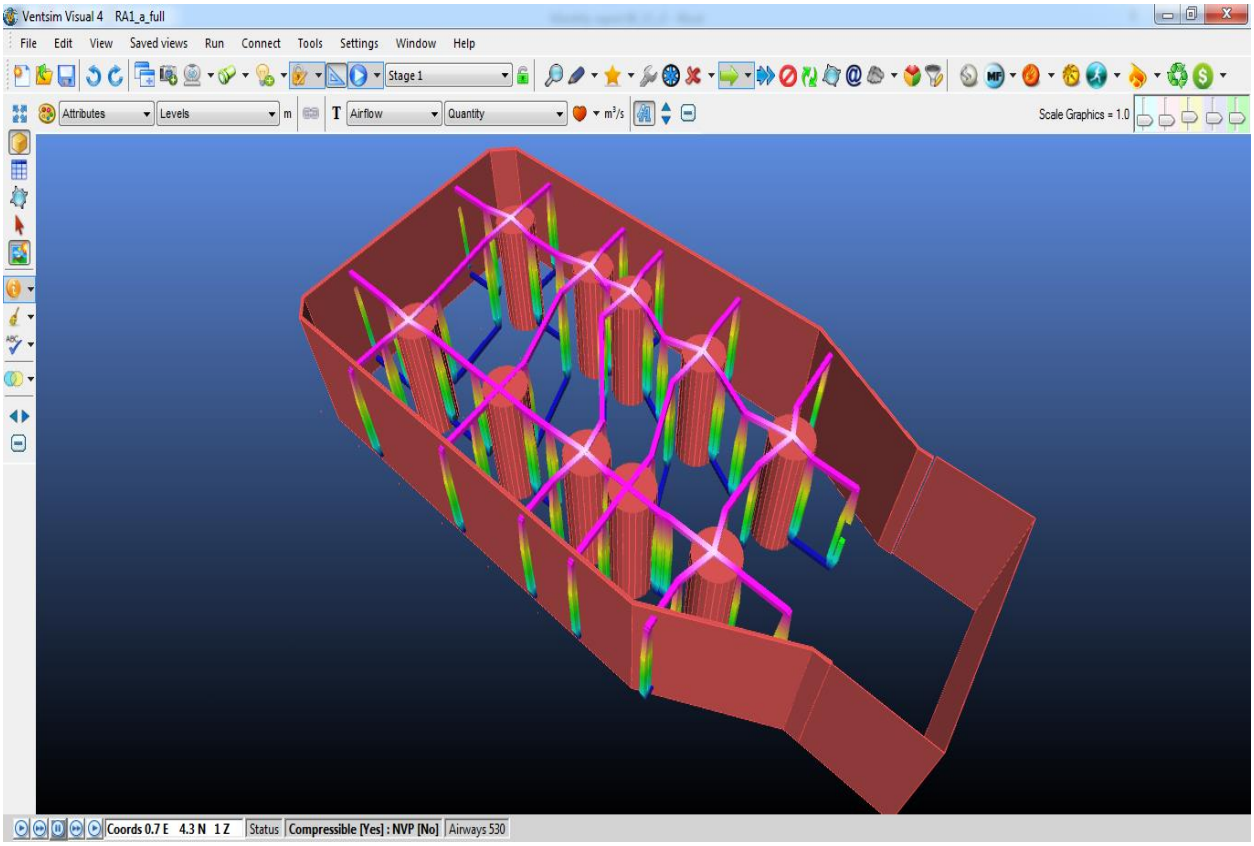

Figure A5.2. MULTIFLUX model of the example RA imported into the Ventsim GUI.

APPENDIX 6. Model comparison and validation of the APPS model

The software macro is tested using five examples from the partner mines for acceptable match between the APPS model and the native VAM model in air flow predictions.

Test example 1 for matching APPS model and VAM model for airflow predictions

This model is a longwall coal mine which has 762 branches and 3 fans. Figure A6.1 shows the for airflow differences between VnetPC and MULTIFLUX models for mine example 1 (coal mine). The difference between the models in the average airflow is 0.42m^3/s. The difference between the models in average pressure is 5.6Pa. Figure A6.2 illustrates fan working point's comparison between VnetPC and MULTIFLUX models for the three fans. The maximum difference in pressure and airflow are 72.8Pa and 5.6m^3/s, respectively, as depicted in Figure A6.3.

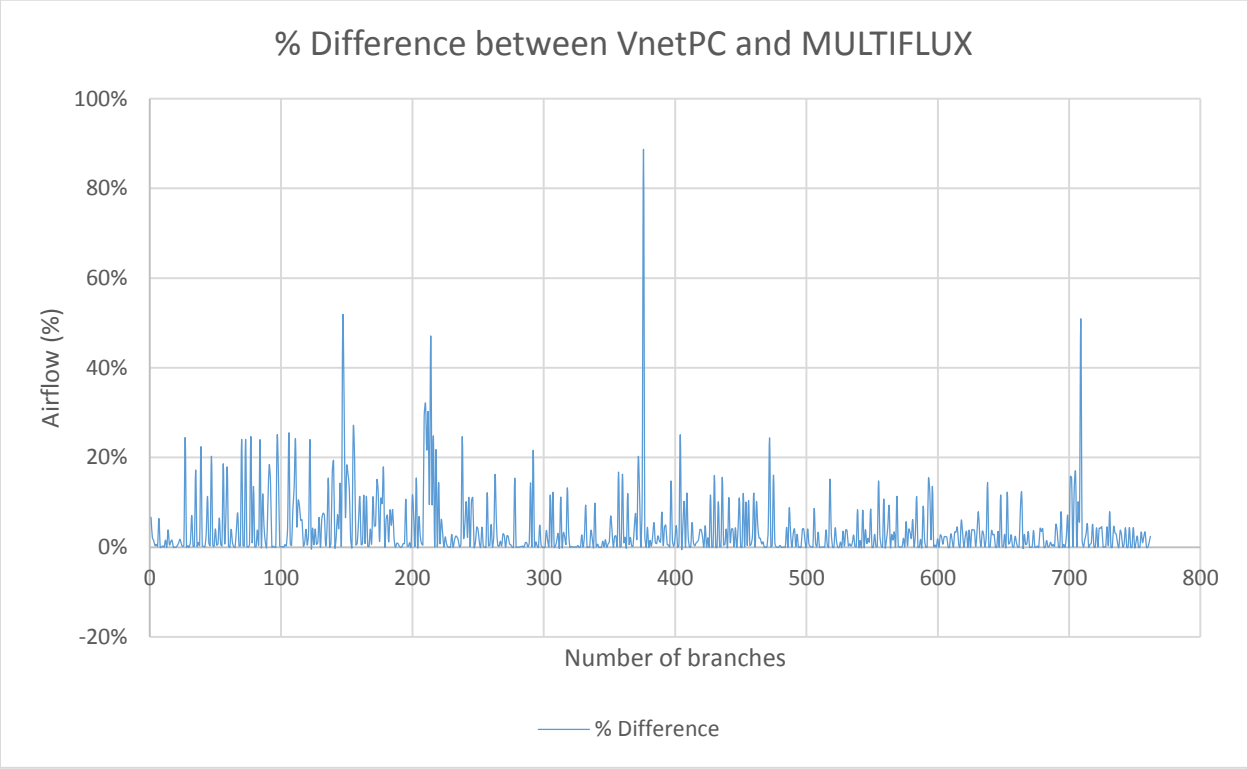

Figure A6.1. Airflow % difference between VnetPC and MULTIFLUX models for mine example 1 (coal mine).

The differences in branch flow rate and pressure averages are insignificant, however, the percentage differences may be significant in airways with low pressure loss and/or air flow rate. The same observation may be made from comparing the fan working points in the VnetPC and MULTIFLUX models.

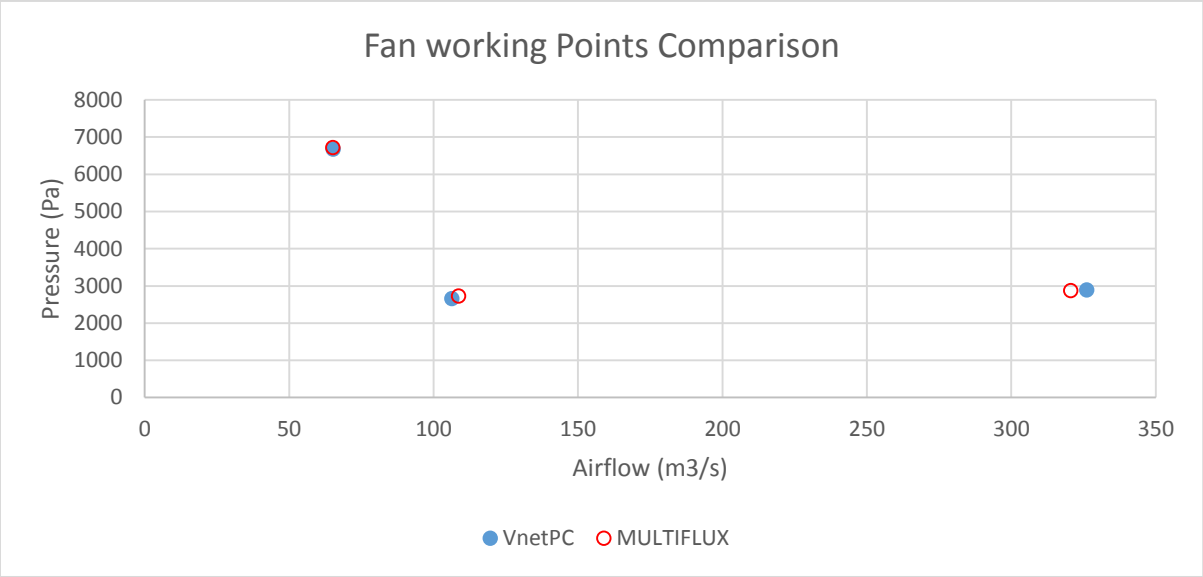

Figure A6.2. Fan working points comparison between VnetPC and MULTIFLUX models for mine example 1 (coal mine).

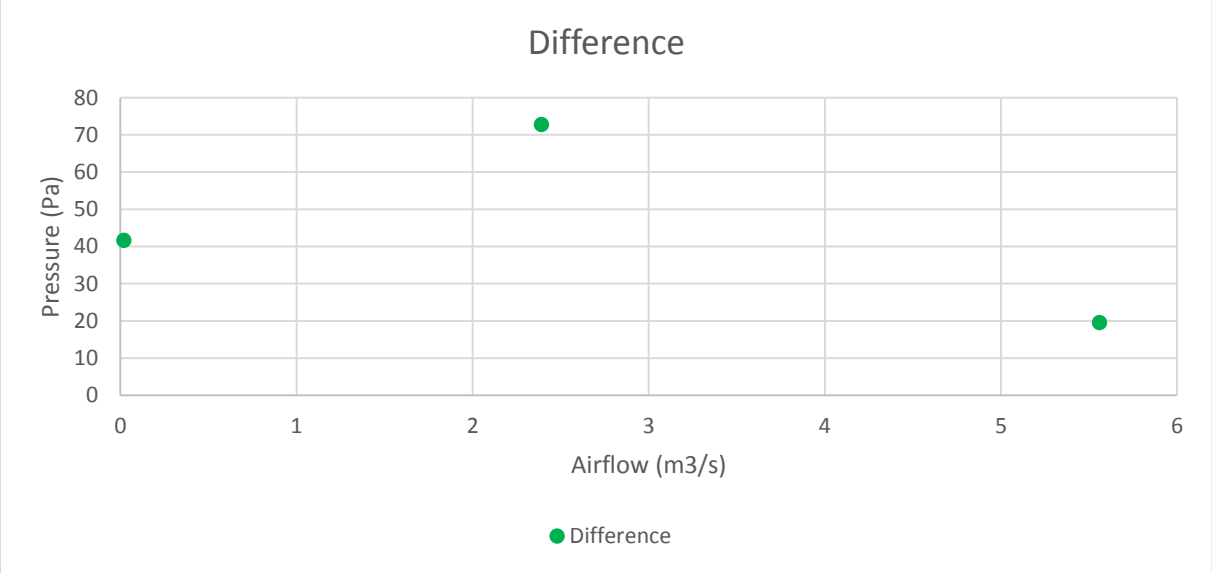

Figure A6.3. Difference for fan working points between VnetPC and MULTIFLUX models for mine example 1 (coal mine).

Test example 2 for matching APPS model and VAM model for airflow predictions

This is a large model of a metal mine which has 2272 branches with 62 fans. Figure A6.4 shows airflow differences between the VnetPC and the MULTIFLUX models for mine example 2. The difference in average airflow between the models is 0.02m^3/s. The difference in average pressures between the models is 7.65Pa. Figures A6.5 and A6.6, respectively, illustrate the fan

pressures and fan airflow rates comparison between VnetPC and MULTIFLUX for the working points of all the fans in the model. The differences in the fan pressures and airflow rates between the two models are, respectively depicted in Figures A6.7 and A6.8.

The fan working points (WP) for most critical two fans where differences are the highest between the VnetPC and MULTIFLUX are shown in Figures A6.9 and A6.10. As depicted, these fans are not in their proper working range, a problem with the VAM model, which must be accepted.

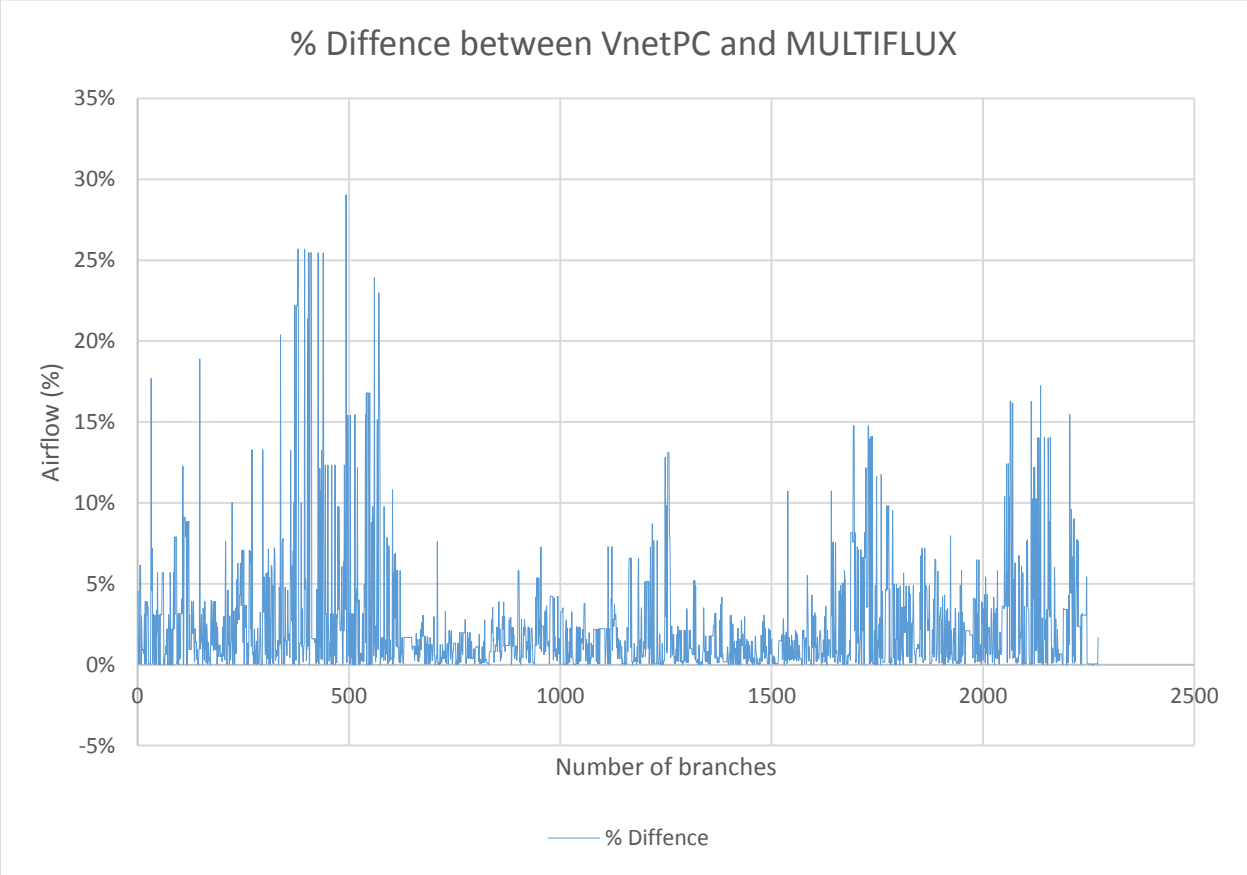

Figure A6.4. Airflow % difference between VnetPC and MULTIFLUX models for mine example 2 (metal mine).

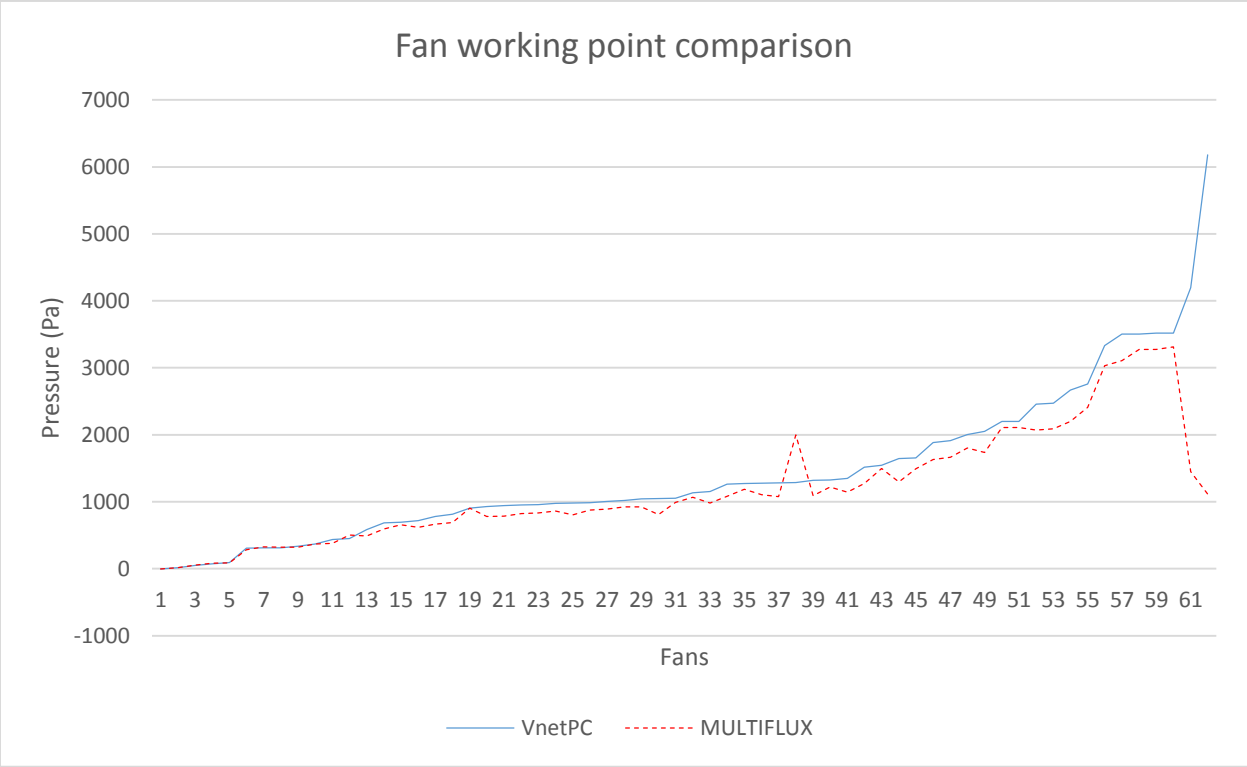

Figure A6.5. Fan pressure comparison between VnetPC and MULTIFLUX.

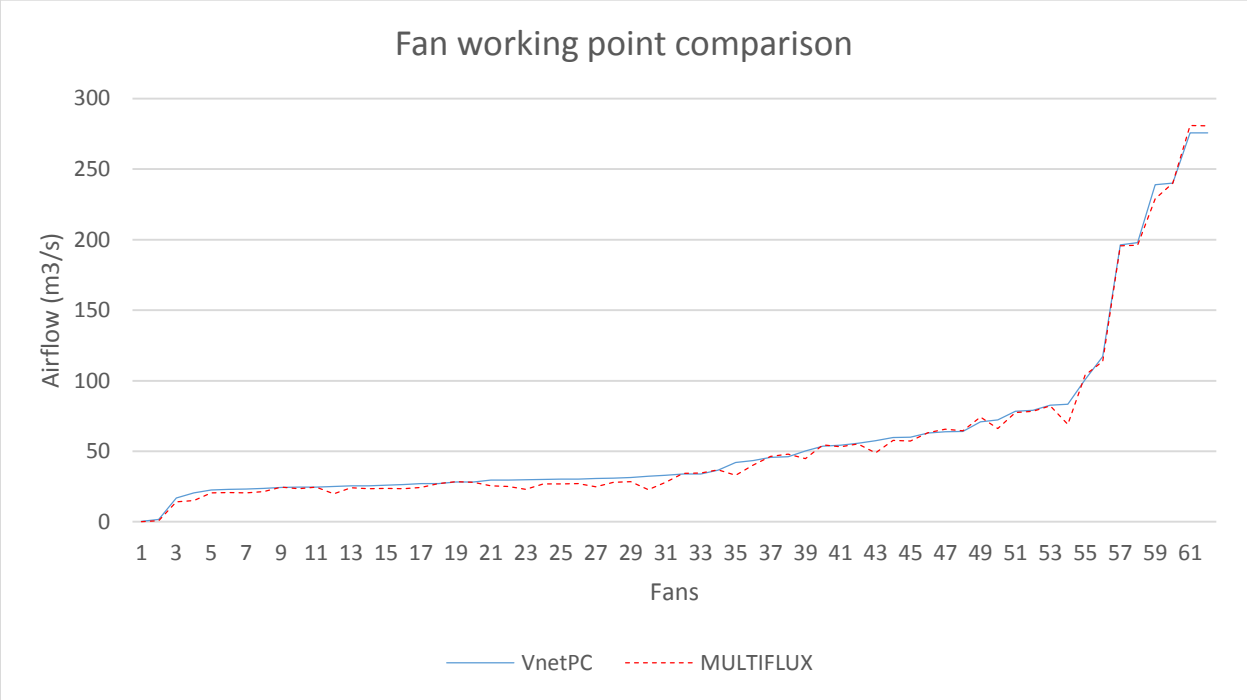

Figure A6.6. Fan airflow rate comparison between VnetPC and MULTIFLUX.

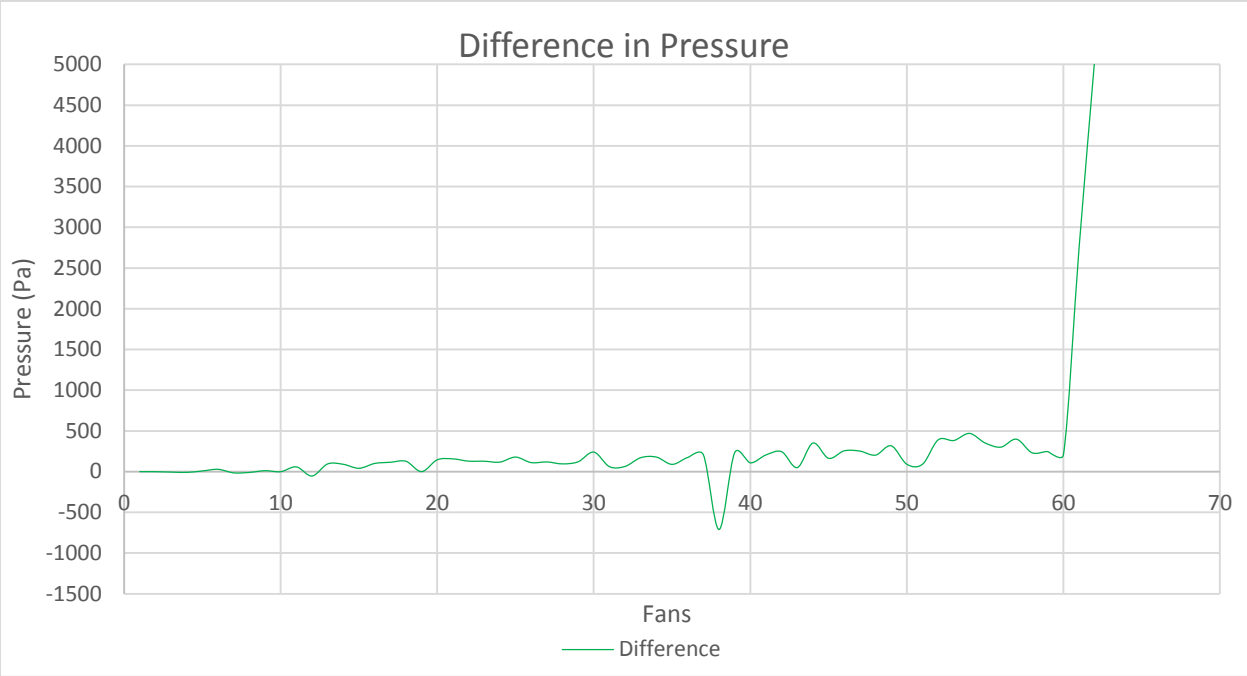

Figure A6.7. Fan pressure difference between VnetPC and MULTIFLUX.

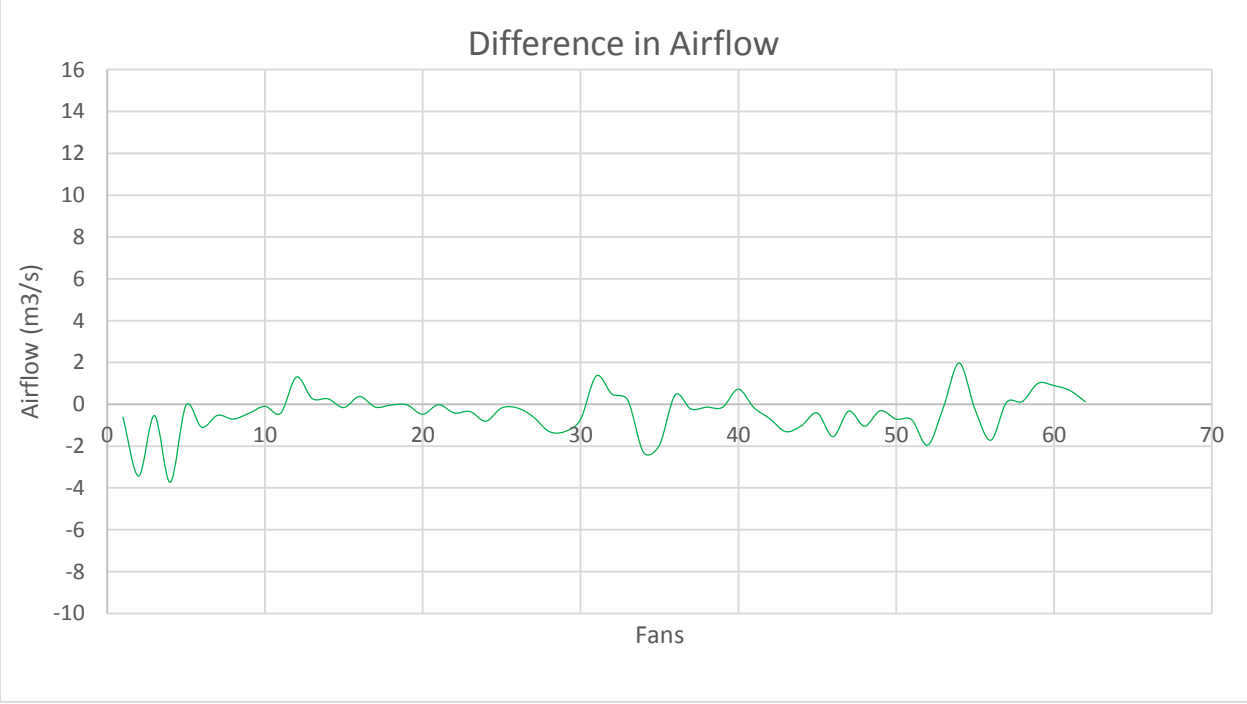

Figure A6.8. Fan airflow rate difference between VnetPC and MULTIFLUX.

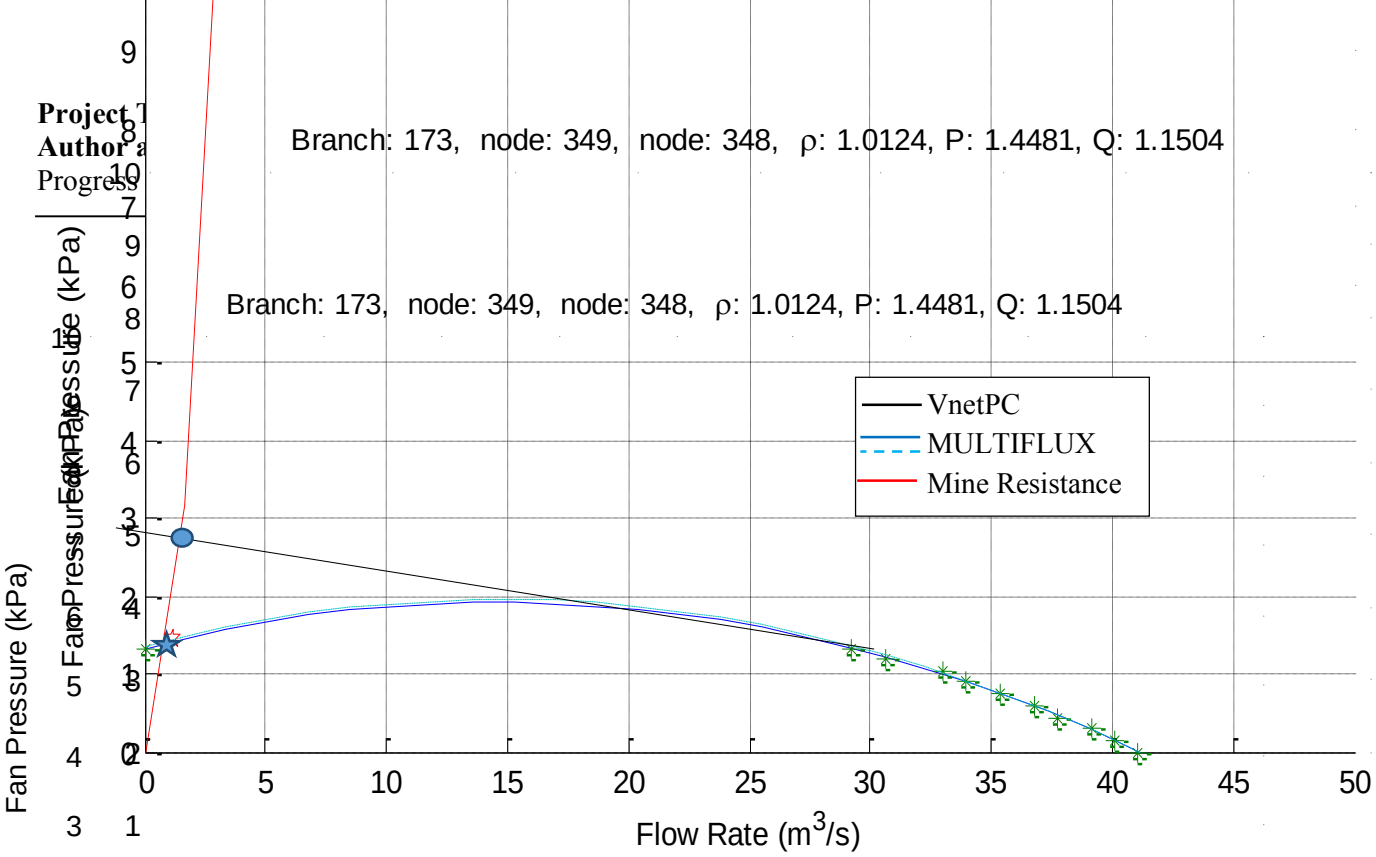

Figure A6.9. Fan curve comparison difference between VnetPC and MULTIFLUX for fan number 61.

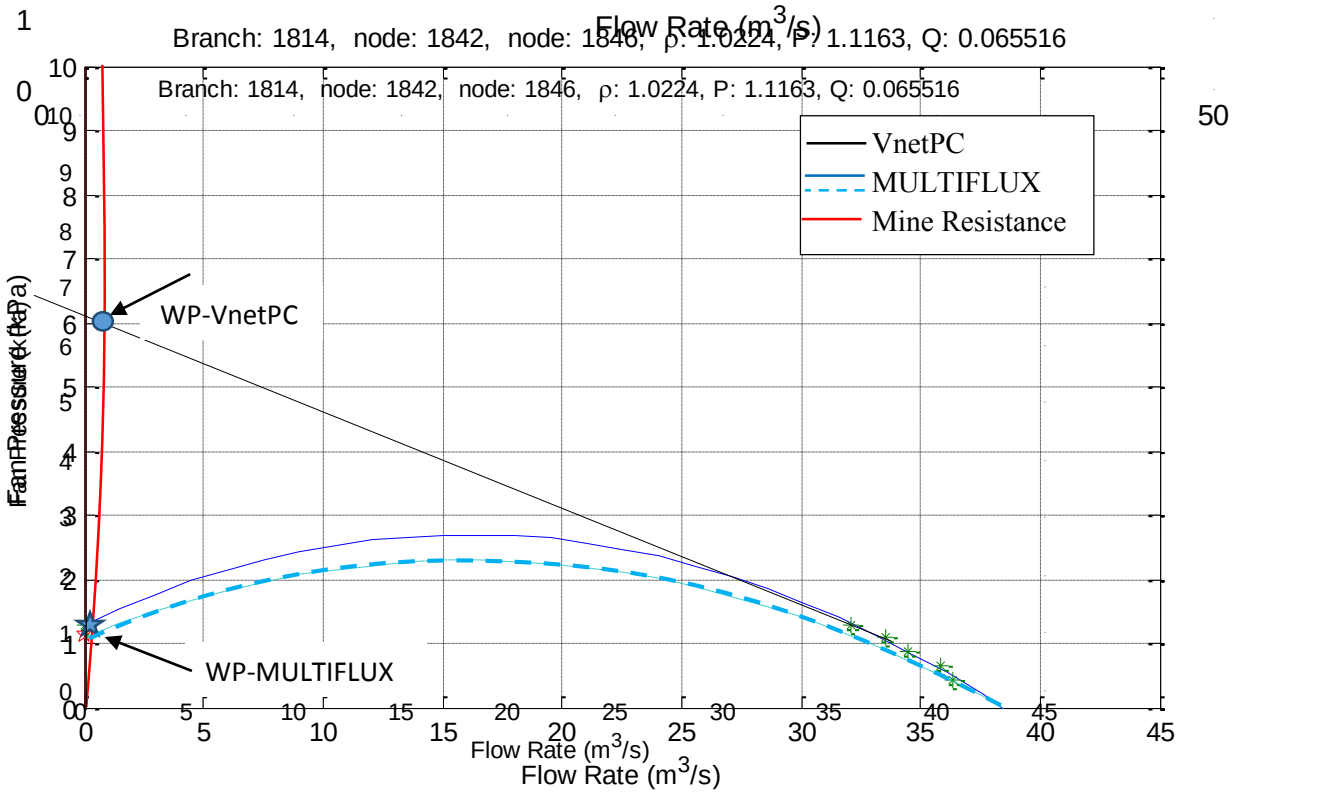

Figure A6.10. Fan curve comparison difference between VnetPC and MULTIFLUX for fan number 62.

Test example 3 for matching APPS model and VAM model for airflow predictions

This model is a metal mine example from VnetPC which has 60 branches and one working fan. Figure A6.11 depicts the airflow differences between the VnetPC and MULTIFLUX models for mine example 3 (metal mine example from VnetPC). The difference in the average airflow between the models is 1.29m^3/s. Figure A6.12 demonstrates the fan working point's comparison between VnetPC and MULTIFLUX models. The difference in pressure and airflow are 6Pa and 2.99m^3/s, respectively, as illustrated in Figure A6.13.

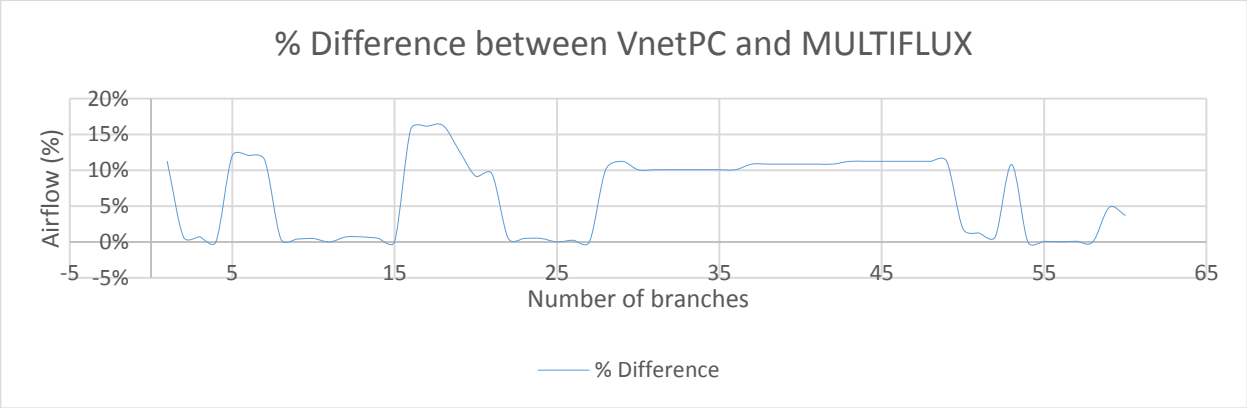

Figure A6.11. Airflow difference comparison between VnetPC and MULTIFLUX models for mine example 3 (metal mine example from VnetPC).

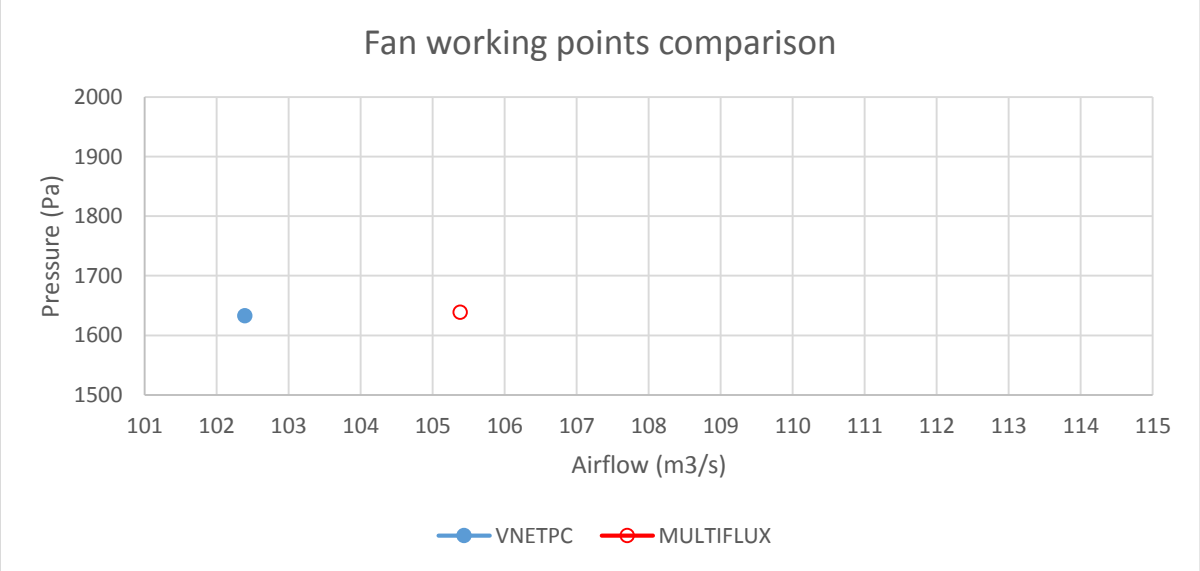

Figure A6.12. Fan working points comparison between VnetPC and MULTIFLUX models for mine example 3 (metal mine example from VnetPC).

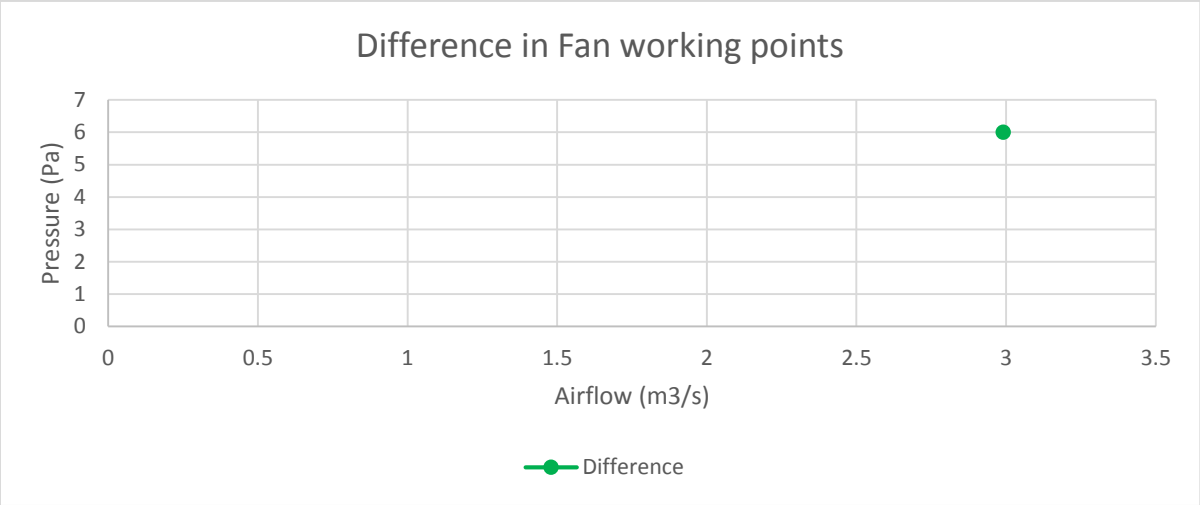

Figure A6.13. Difference in fan working points between VnetPC and MULTIFLUX models for mine example 3 (metal mine example from VnetPC).

Test example 4 for matching APPS model and VAM model for airflow predictions

This model is a longwall coal mine from VnetPC which has 247 branches and 1 fan. Figure A6.14 shows the airflow differences between VnetPC and MULTIFLUX models. The difference in the average airflow between the models is 0.17m^3/s. The difference in the average pressures between the models is 4.8Pa. Figure A6.15 illustrates the fan working point's comparison between VnetPC and MULTIFLUX. The difference in pressure and airflow are 12.5Pa and 0.41m^3/s, respectively, as depicted in Figure A6.16.

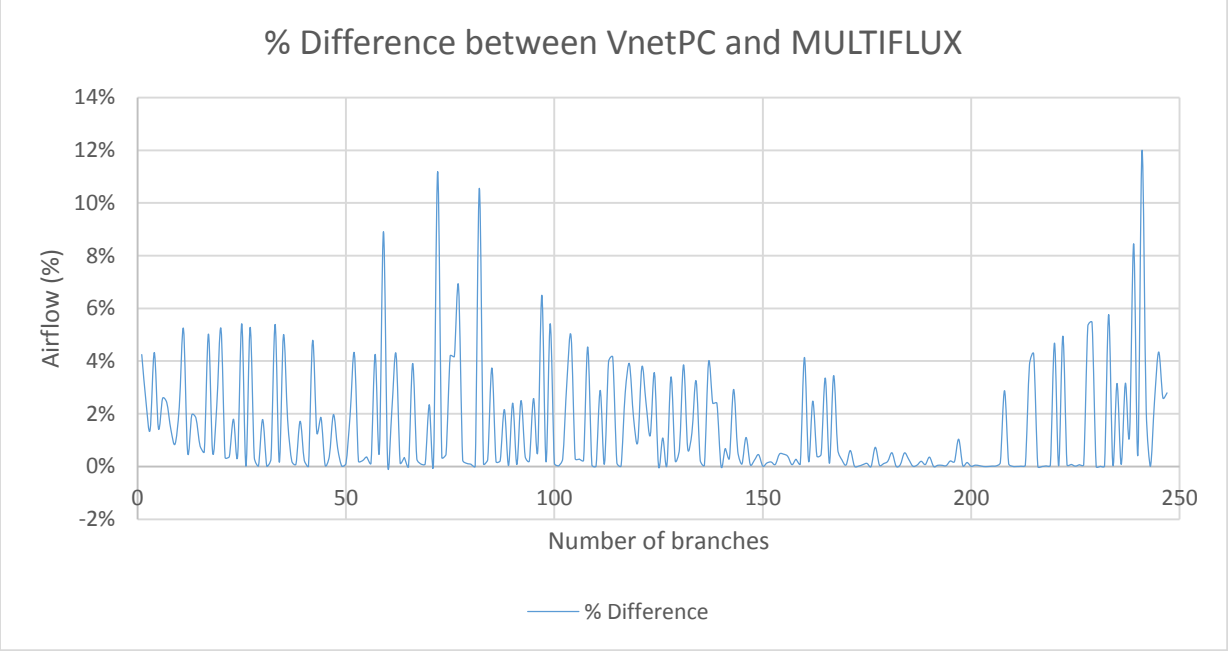

Figure A6.14. Airflow % difference comparison between VnetPC and MULTIFLUX models for mine example 4 (coal mine example from VnetPC).

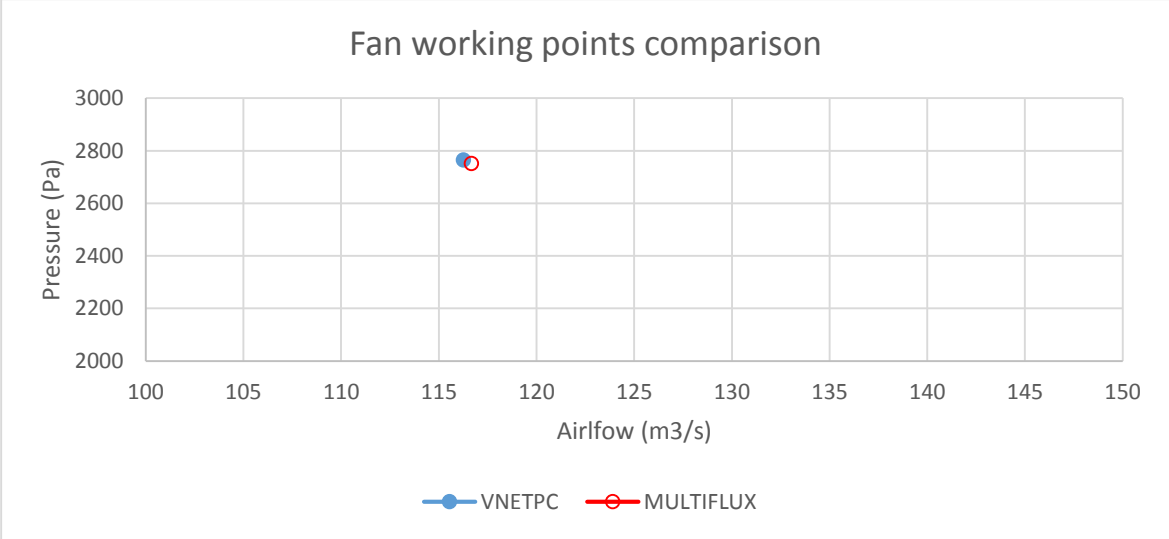

Figure A6.15. Fan working points comparison between VnetPC and MULTIFLUX for mine example 4 (coal mine example from VnetPC).

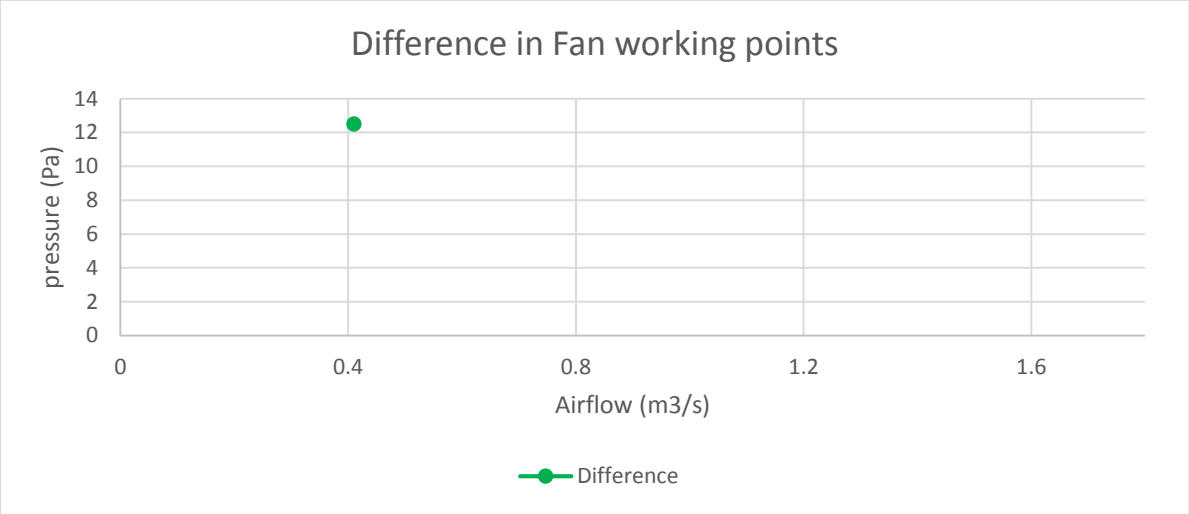

Figure A6.16. Difference for fan working points between VnetPC and MULTIFLUX for mine example 4 (coal mine example from VnetPC).

Test example 5 for matching APPS model and VAM model for airflow predictions

This model is a metal mine which has 447 branches. It has two shafts, one for intake and one for exhaust with 3 working fans located underground. Figure A6.17 depicts the airflow differences between the Ventsim and MULTIFLUX models for mine example 5. The difference in the average airflow rate between the models is 0.17m^3/s. The difference in the average pressures between the models is 12.1Pa. Figure A6.18 shows the fan working point's comparison between Ventsim and MULTIFLUX for the three fans. The maximum difference in pressure and airflow

are 13.4Pa and 3.02m^3/s as illustrated in Figure A6.19. The difference can be attributed to the Ventsim fans being off-curve for small airflow rates.

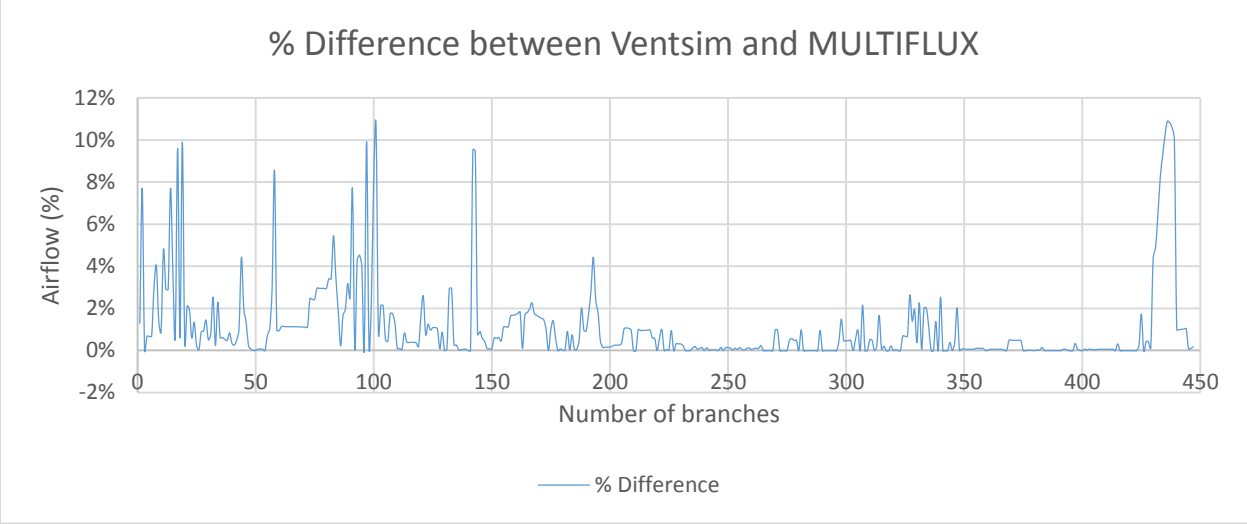

Figure A6.17. Airflow % difference comparison between Ventsim and MULTIFLUX models for mine example 5 (metal mine).

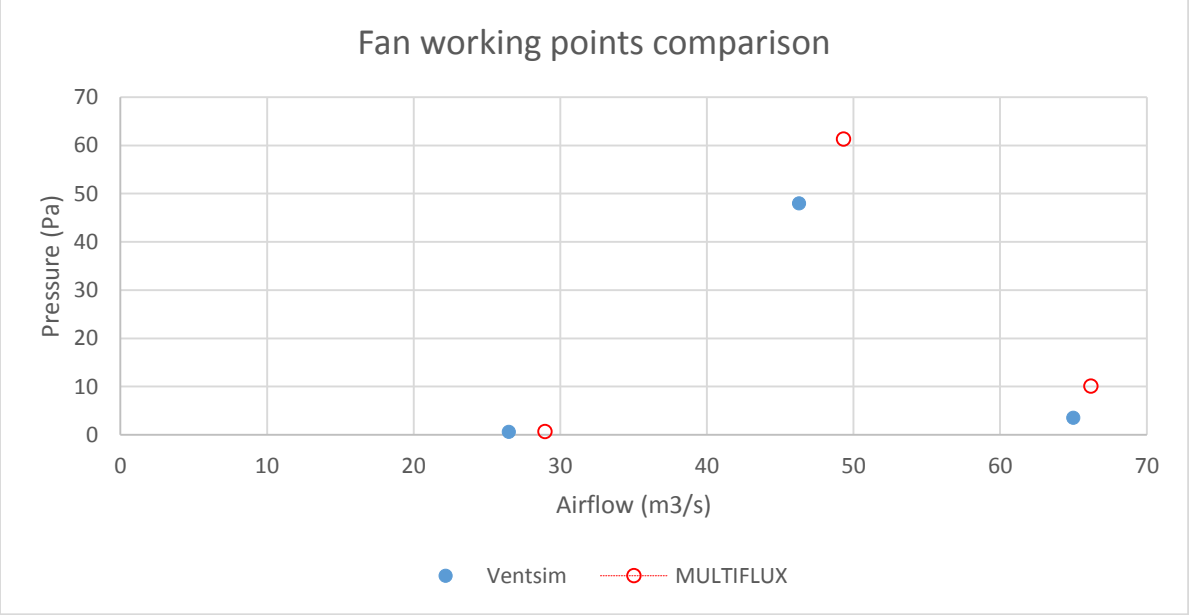

Figure A6.18. Fan working points comparison between Ventsim and MULTIFLUX models for mine example 5 (metal mine).

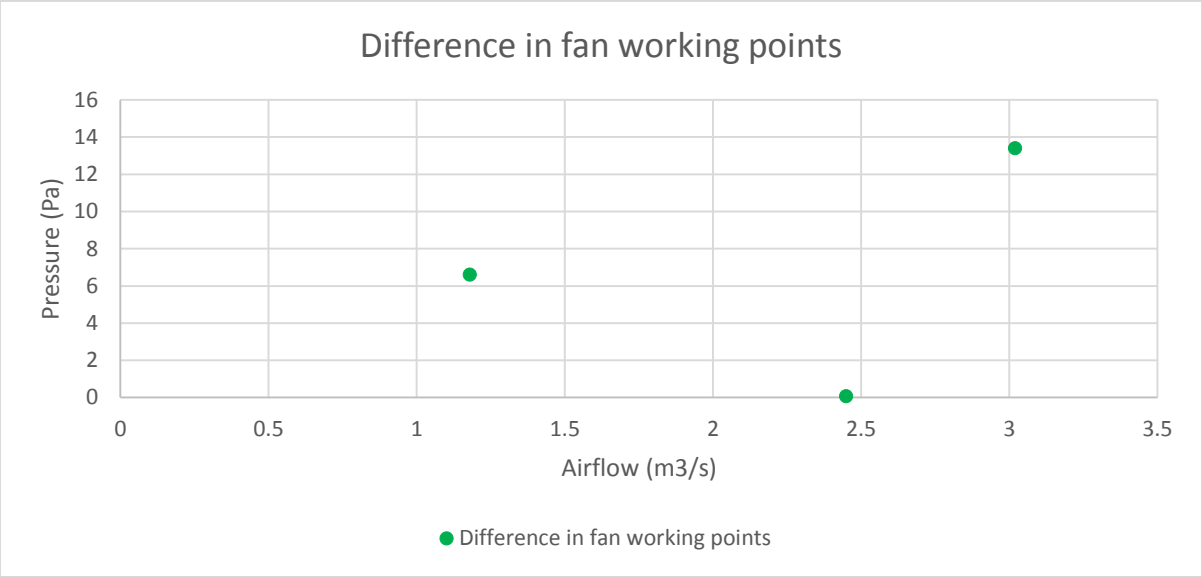

Figure A6.19. Difference for fan working points between Ventsim and MULTIFLUX models for mine example 5 (metal mine).

APPENDIX 7. Definition of measurement locations in Ventsim Live GUI

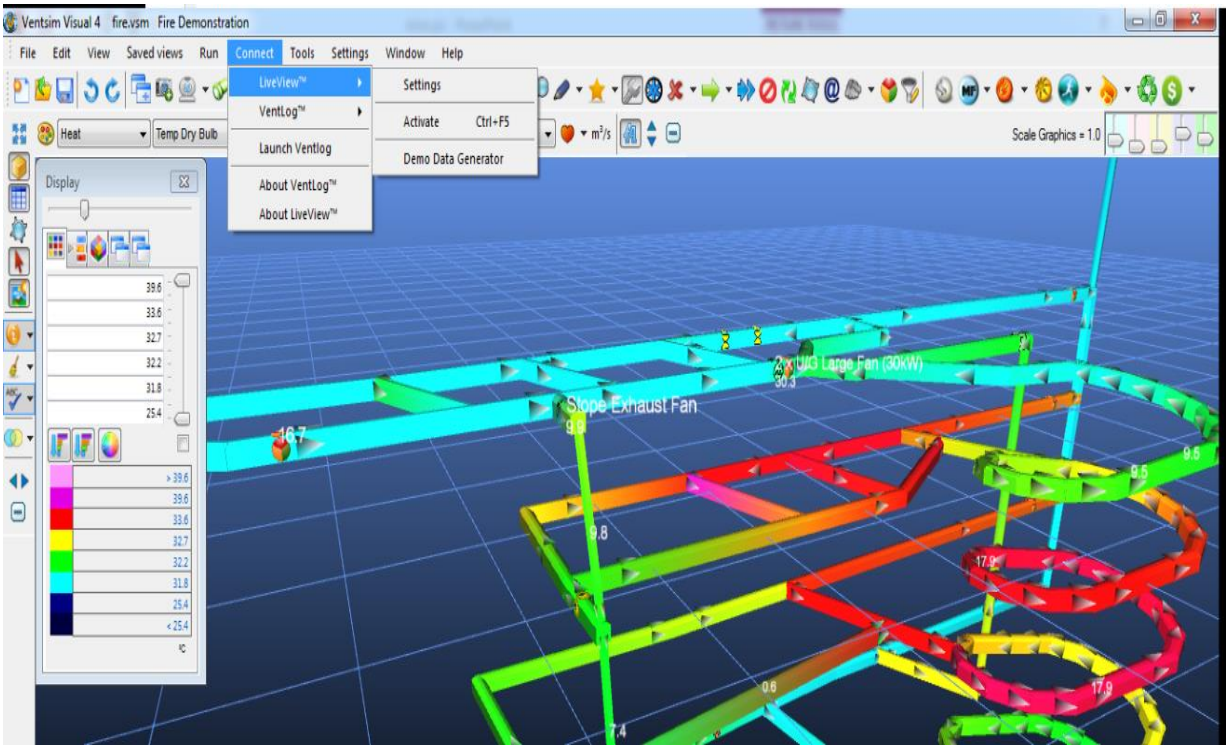

Figure A7.1. Ventsim LiveView feature to connect to real-time monitoring data.

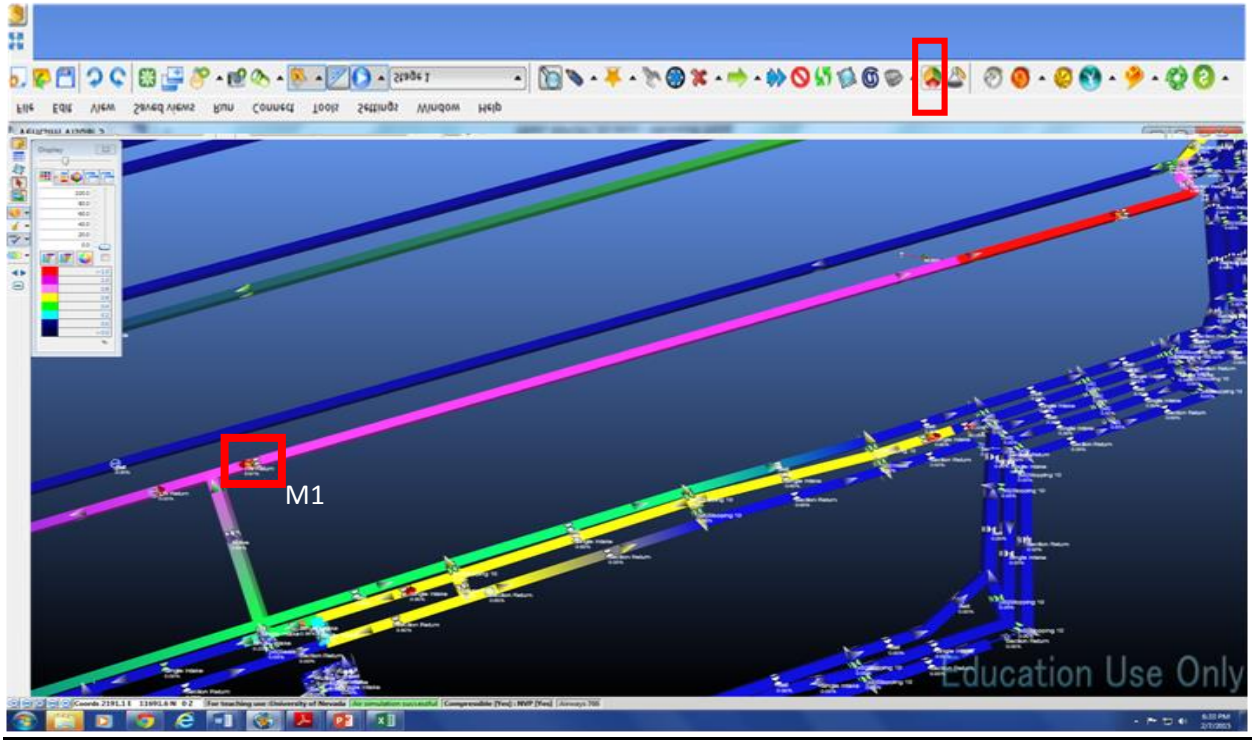

Figure A7.2. Example of monitoring station mapping using dynamic monitor icon in Ventsim.

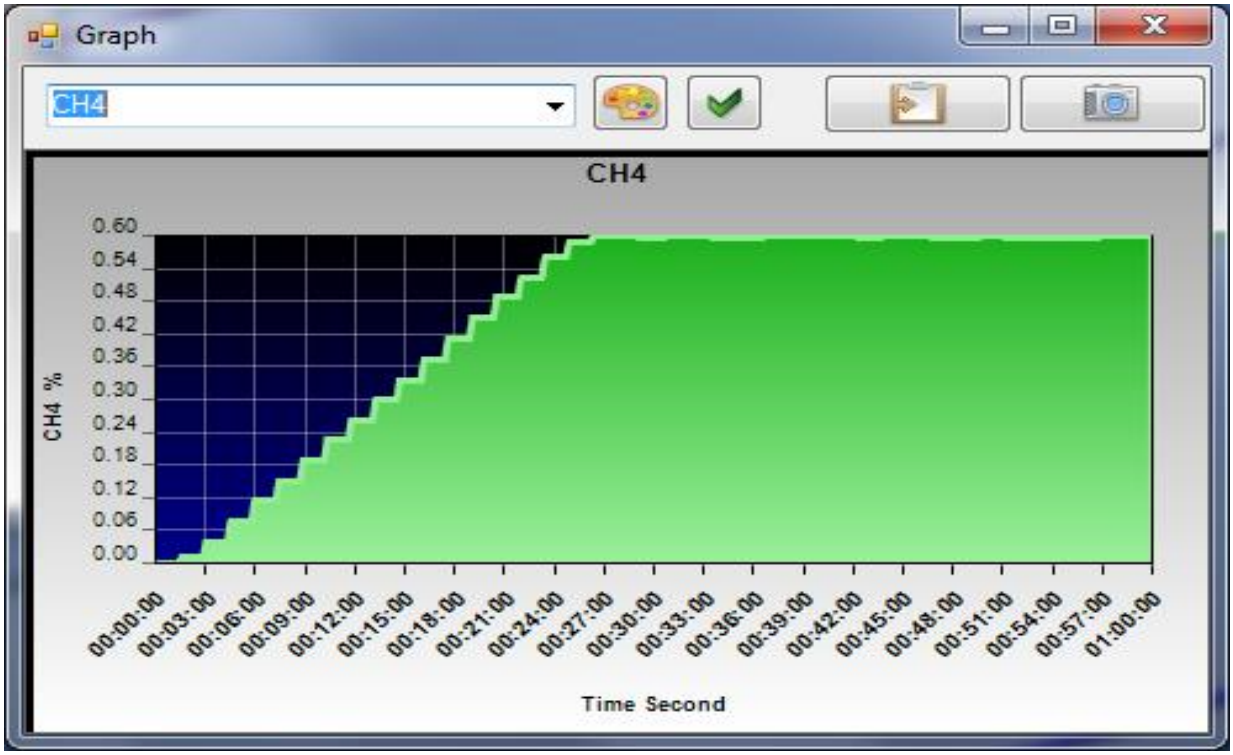

Figure A7.3. Example of plotted data from a monitoring station, M1 in Ventsim.

APPENDIX 8. Testing and evaluation of the EWP system with random and perturbed data

There are different typical error limits for various air parameters that must be taken into consideration for signal processing. Some typical error limits are ±3% for velocity, ±0.3°C for temperature, ±3% for relative humidity, and ±2% for barometric pressure. Agreement and measurement uncertainty in an operating mine is evaluated by comparing measured data from an operating mine and the predicted results from MULTIFLUX and Ventsim. The measured data are imported from a previous NIOSH-funded research project (Danko et al, 2014). Figures A8.1 and A8.2 illustrate the comparison between in-situ measurement results for air velocity and barometric pressure distributions with MULTIFLUX model results for a partner metal mine in Nevada. The confidence bound for velocity and pressure measurement is ± 2.2 m/s and ± 650 Pa are used based on measurement uncertainty of a given location in a metal mine as a result of mining operations and ventilation changes from traffic. The velocity unit has an accuracy of ± 3% and that of the pressure unit is ± 2.0%. It can be seen that the model results are not matching the measurement results due to some factors such as unknown source terms, ventilation changes from mining operations which are not entered in the model. However, all these factors are incorporated in the early warning system in order not to sound unwarranted alarms. For un-wanted spikes, moving average low pass filter is used to smoothen out the fluctuations. On-site model adjustment relative to measurement data at sensor locations are recommended as part of the EWS initialization. In addition, tolerable bounds with upper and lower limits from various mining activities are to be defined in the EWP.

A real weather data for Elko, Nevada are used in Ventsim to demonstrate the effects of atmospheric temperature variations in the mine. The objective is to correlate the outside and the inside conditions for the early warning system. The weather data used as an input are depicted in Figure A8.3. A monitoring sensor location close to the active face is set in branch 253 (40 ft perimeter and 3938.1 ft length) of the selected mine for this study is shown in Figure A8.4. The model results for this branch are depicted in Figure A8.5 with a measurement error of ±3◦C from a typical measurement unit. Since the temperature variations affect the mine ventilation air in a similar manner as the outside condition changes but which a smaller amplitude and some level of delay, variations in the outside conditions are taken into account in the EWP system to ensure accurate predictions.

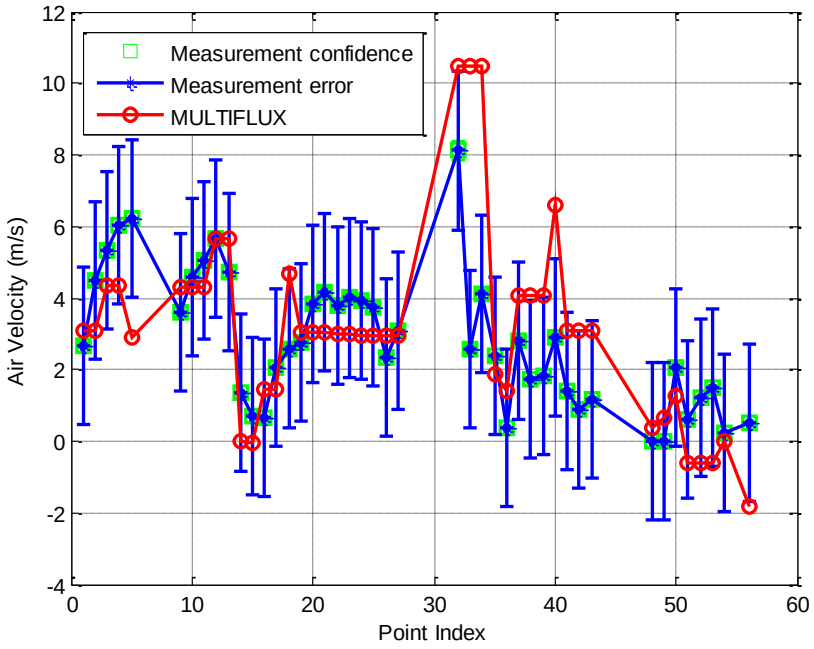

Figure A8.1. Comparison between measured velocities and the results from the MULTIFLUX model with confidence bound.

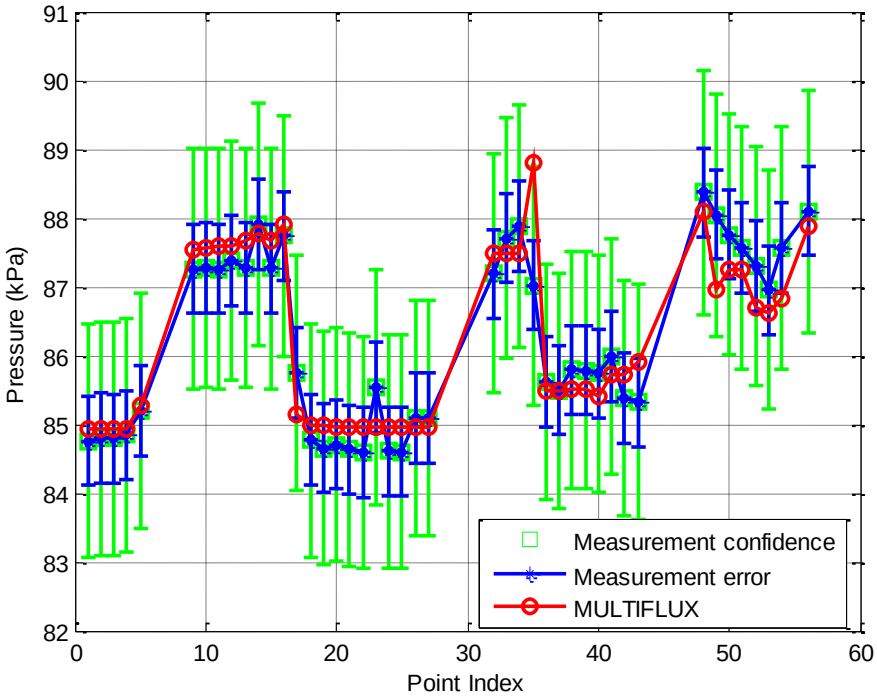

Figure A8.2. Comparison between measured barometric pressure and the results from the MULTIFLUX model with confidence bound.

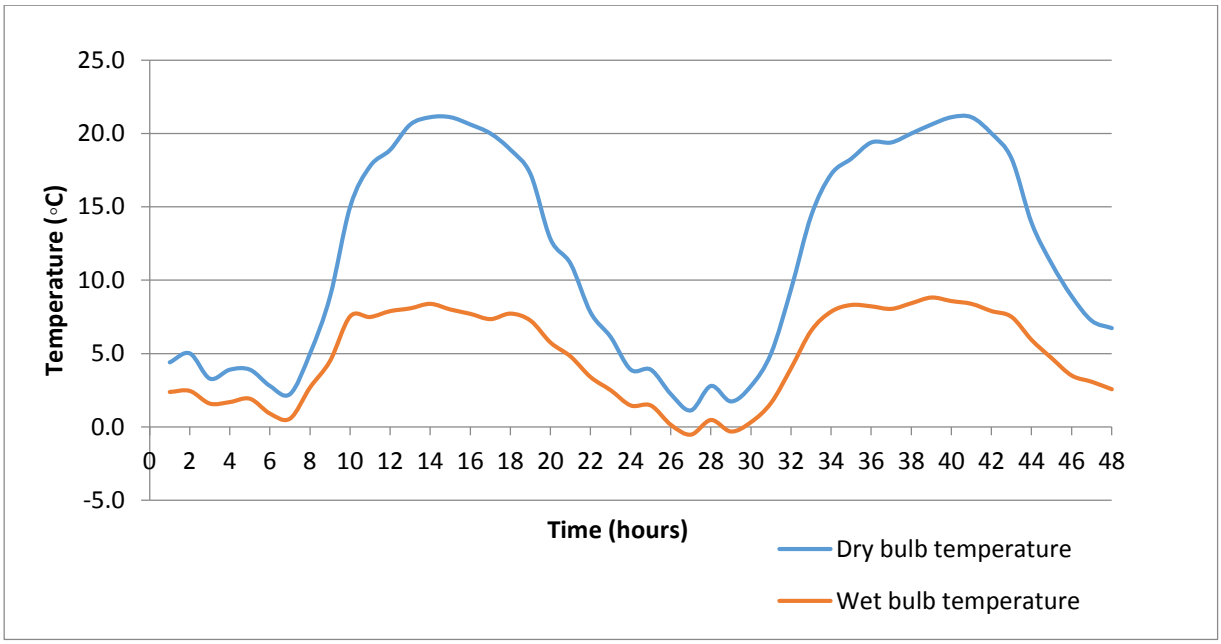

Figure A8.3. Weather data, Elko, NV. April 9-10, 2014 http://www.wunderground.com/history).

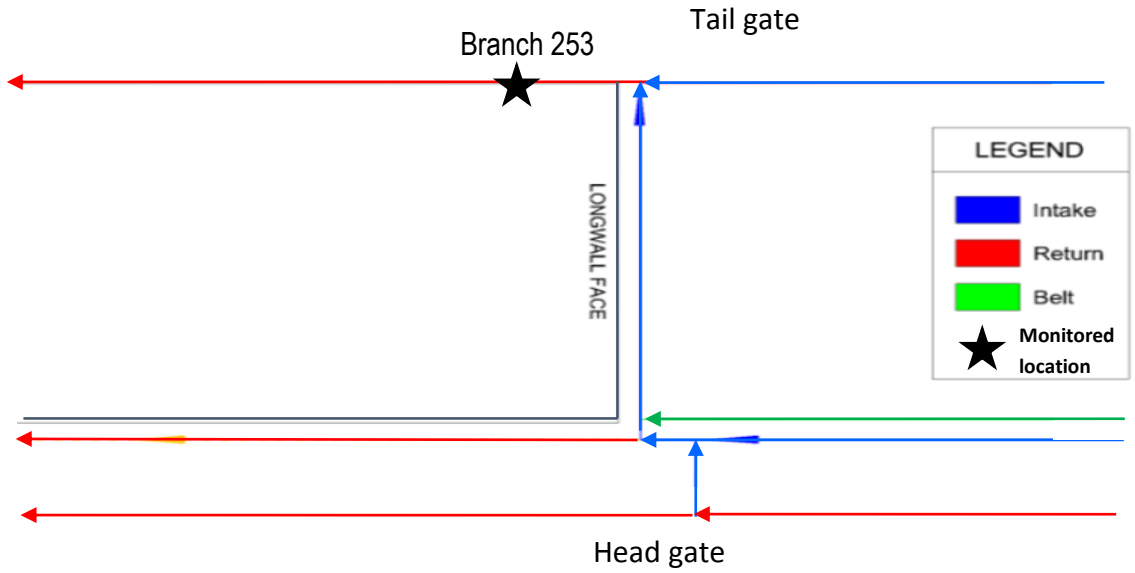

Figure A8.4. Branch 253 monitored location for mine temperature.

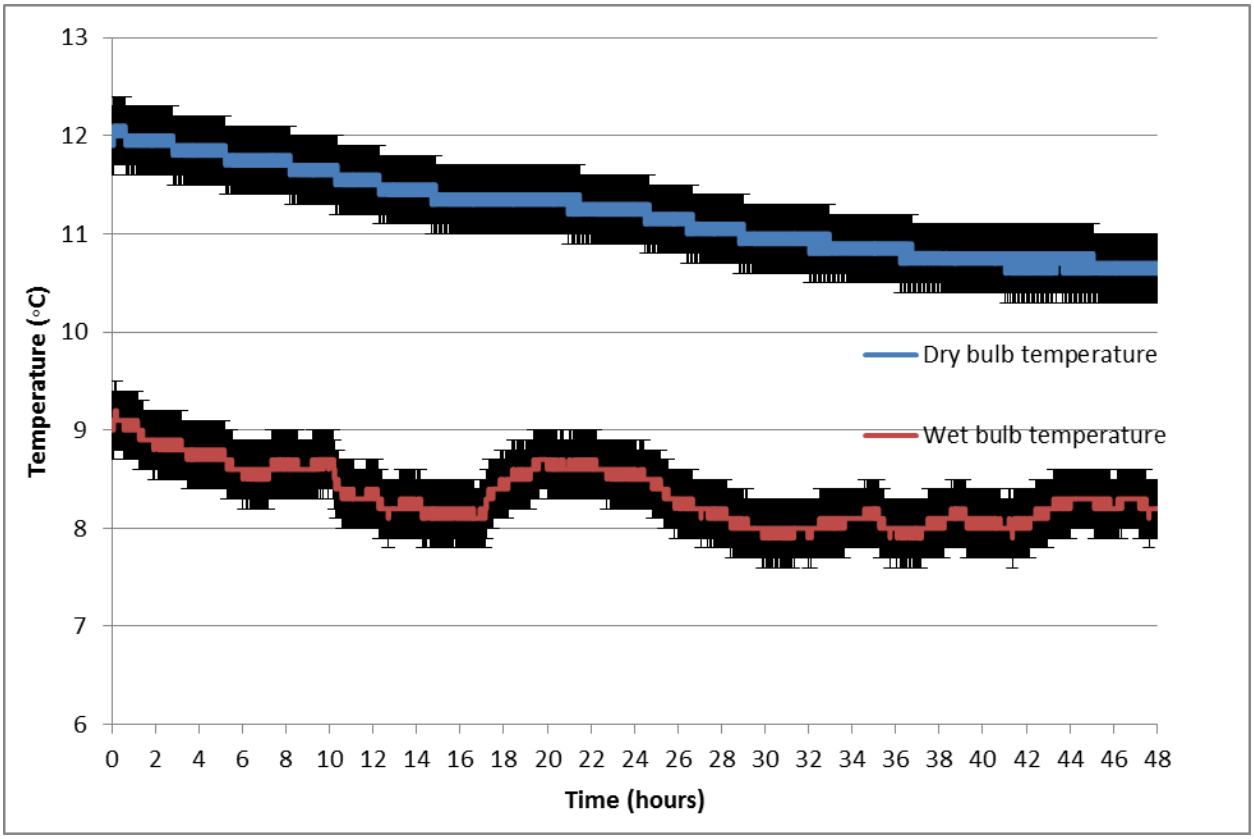

Figure A8.5. Model results for wet bulb and dry bulb temperatures for branch 253 with error.

APPENDIX 9. Forward-prediction algorithms

A9.1 NTCF dynamic correlator

Figure A9.1 illustrates the methane flux from the gob model used for SME presentation (Asante et al, 2015). A pressure drop of 2000 Pa from 100000 Pa ambient airway pressure is considered in building a surrogate gob model using the Numerical Transport Code Functionalization (NTCF) method (Danko, 2006). The gob volume is assumed to be generating a 0.01 kg/s ambient methane flow rate. The gob model response in terms of mass flow rate to the 2000 Pa pressure drop is shown in Figure A9.2. The NTCF model performance in predicting this response is also demonstrated in Figure A9.5 verifying the base input response using the NTCF model. Figure A9.3 illustrates a variable in-drift pressure variation or +/-2000 Pa around the ambient pressure for the undisrupted state. Figure A9.4 depicts the comparison between the gob model for the variable pressure of Figure A9.3 and the NTCF prediction with excellent agreement.

Figure A9.5 depicts the ambient air pressure change as a sudden drop by 2000 Pa. Figure A9.6 shows the comparison between the gob model response to a 2000 Pa drop in a variable periodic pressure and the NTCF prediction with the same NTCF surrogate model. The excellent agreement observed from these various pressure variations in the airway air proves that the surrogate NTCF model can replace the gob CFD model. The NTCF-based CDC model is an important new element of the innovative procedure in this research project.

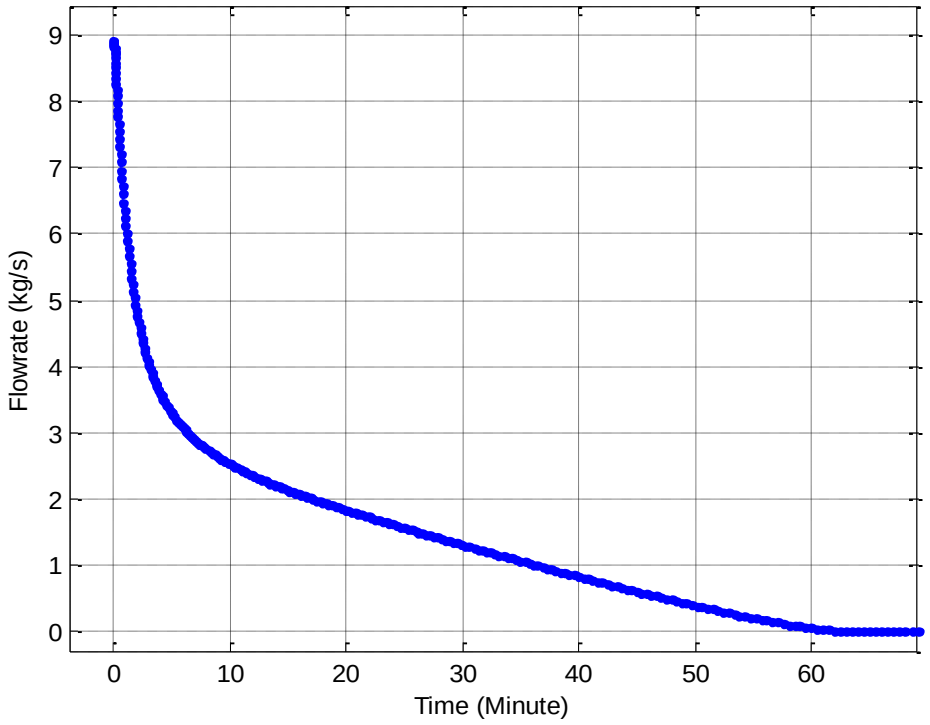

Figure A9.1. Methane flow rate from gob model for 2000 Pa pressure drop.

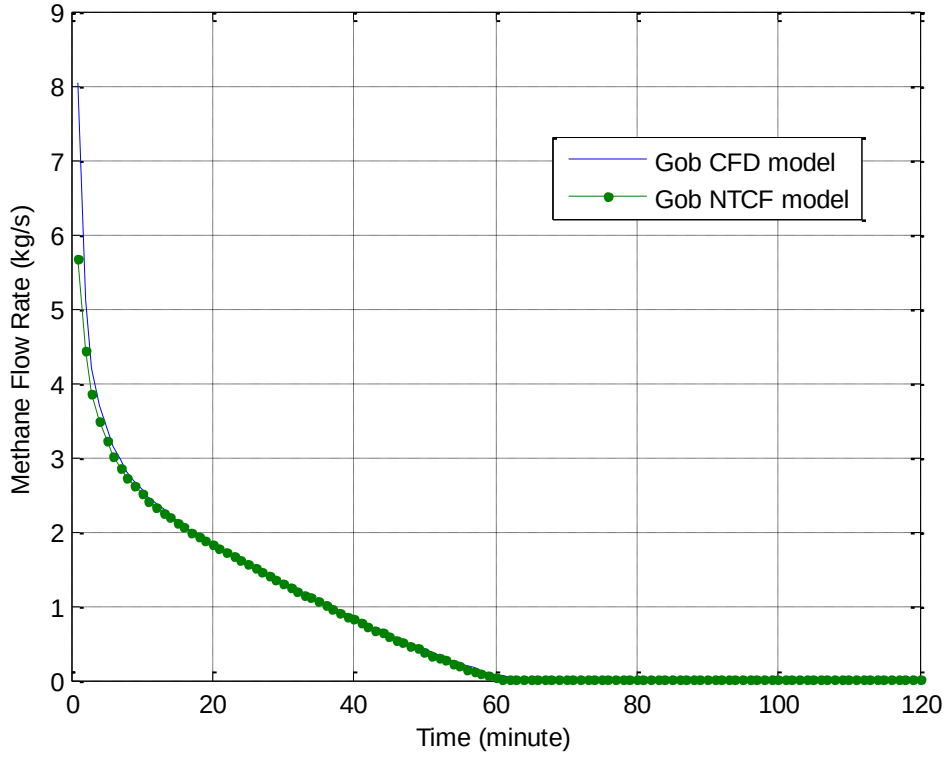

Figure A9.2. NTCF surrogate model compared with the CFD gob model for -2000 Pa drop.

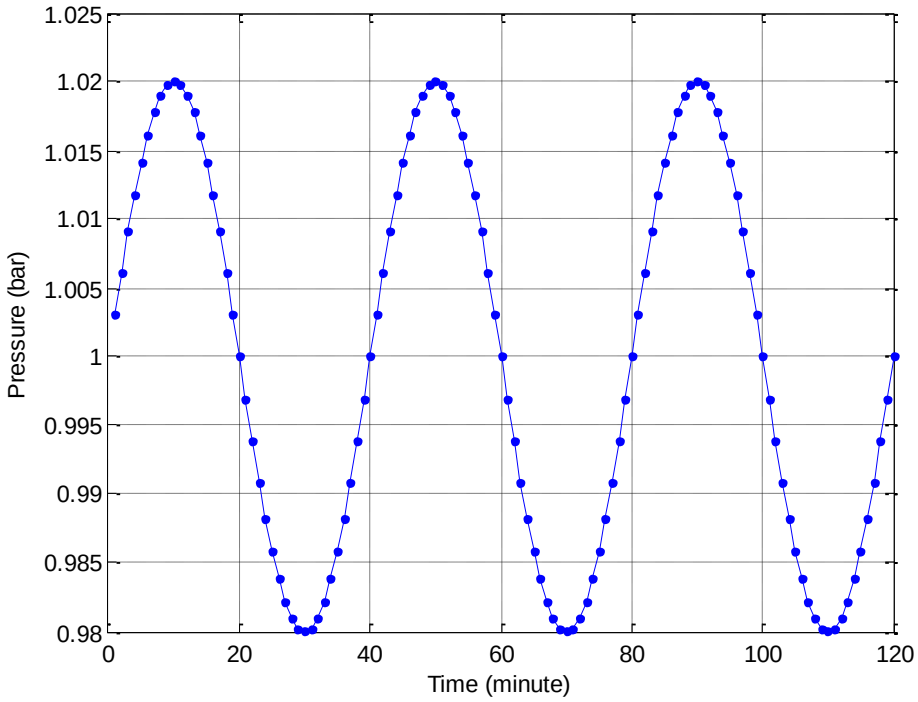

Figure A9.3. Airway pressure variation for the +/-2000 Pa variable pressure.

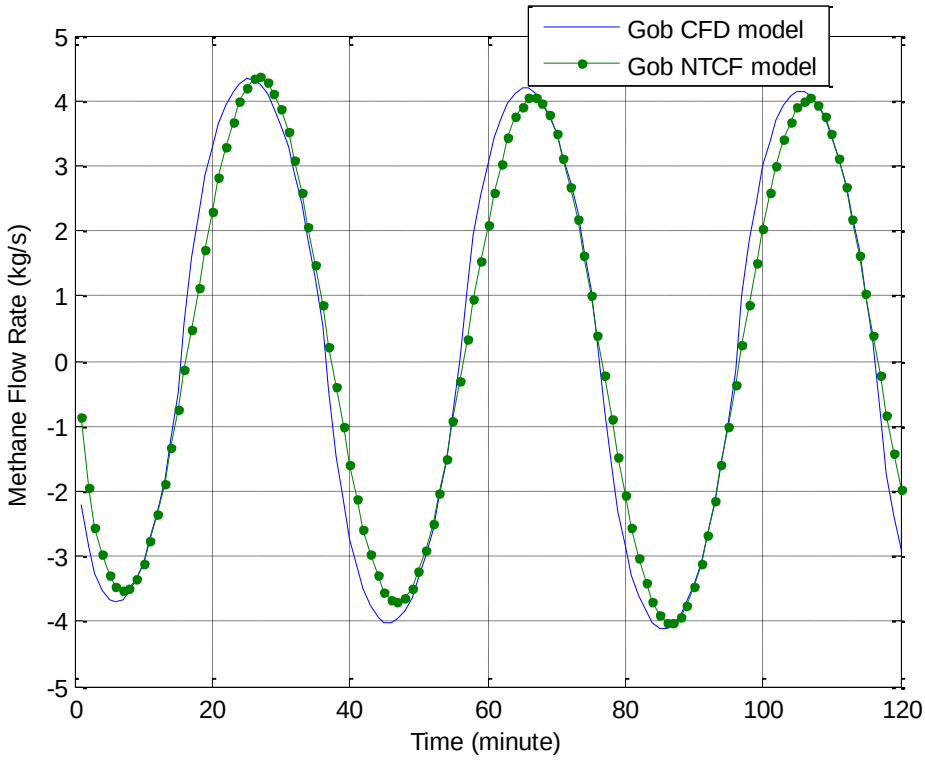

Figure A9.4. NTCF surrogate model comparison with the CFD gob model for the +/-2000 Pa variable pressure.

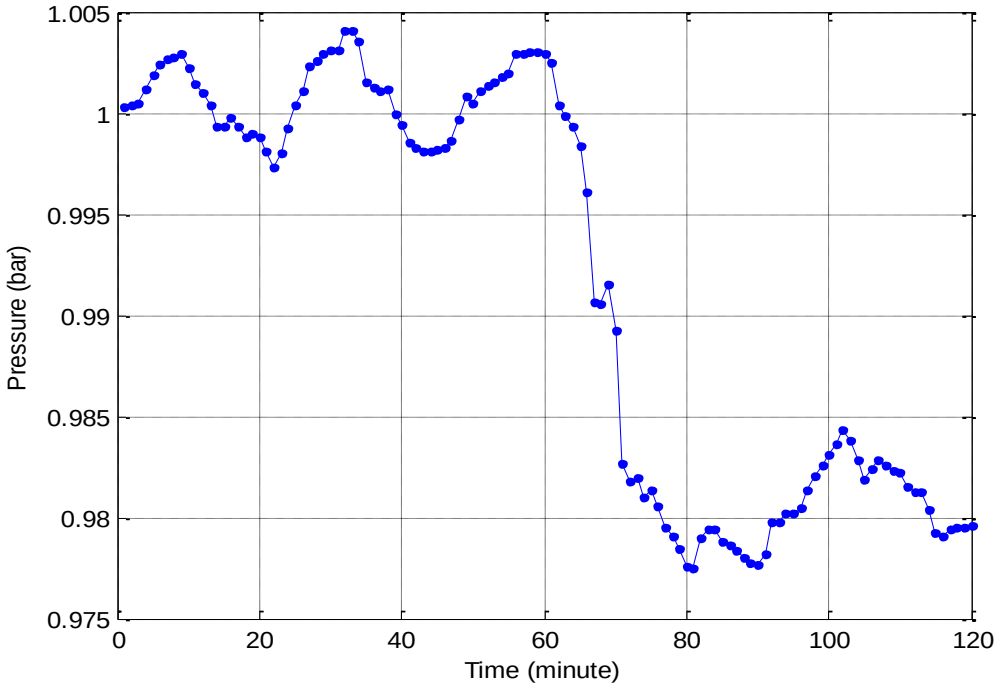

Figure A9.5. Airway pressure variation including a sudden change.

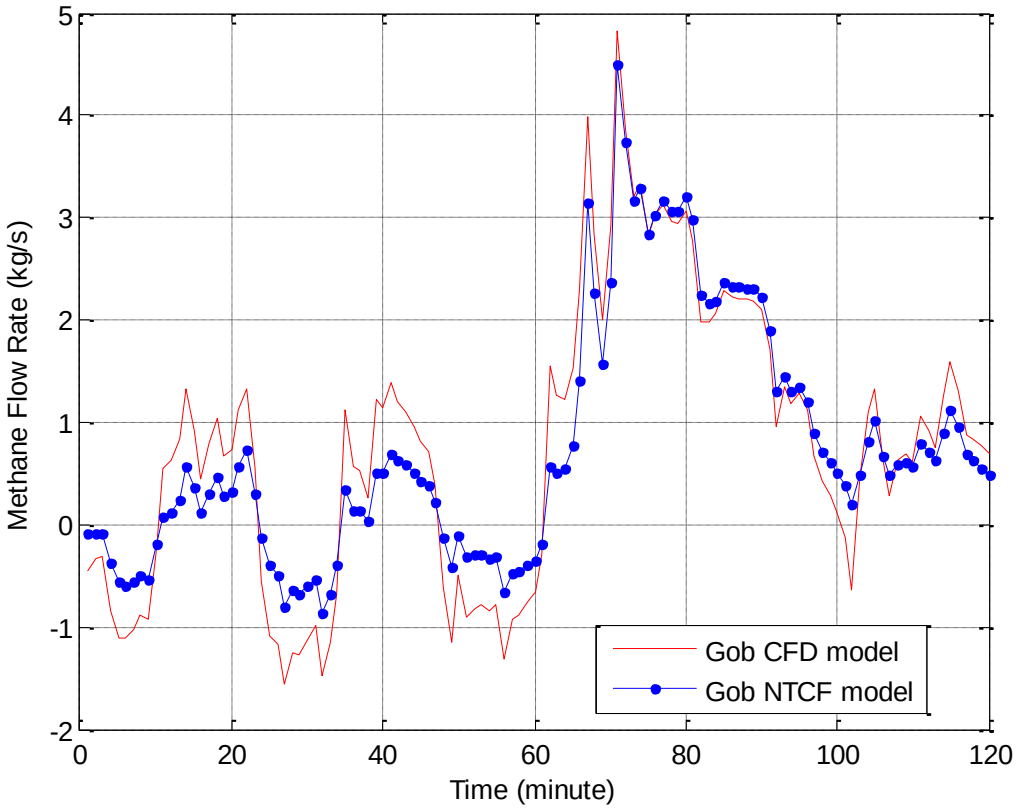

Figure A9.6. NTCF surrogate model comparison with the CFD gob model.

A9.2 Example of signal processing

Figure A9.7 illustrates a typical pressure sensor data, measured at every second, with some fluctuation and some noise together with the same data filtered through a 1000- second moving average window. The data also includes a rapid drop in pressure by about 2000 Pa. The filtered data is used for trend analysis example. The first derivative shows a significant change around 4000 second time, depicted in Figure A9.8. The first derivative demonstrates the slope variation where it maximizes and how the filtered data indicates this change. Similar trend is seen from the second derivative, illustrated in Figure A9.9, with more noise suppression. The second derivative also shows the two inflection points clearly. These signal properties can be used to identify the sharp drop in pressure. However, these signal properties cannot characterize duration and may not give conclusive indication for hazardous changes.

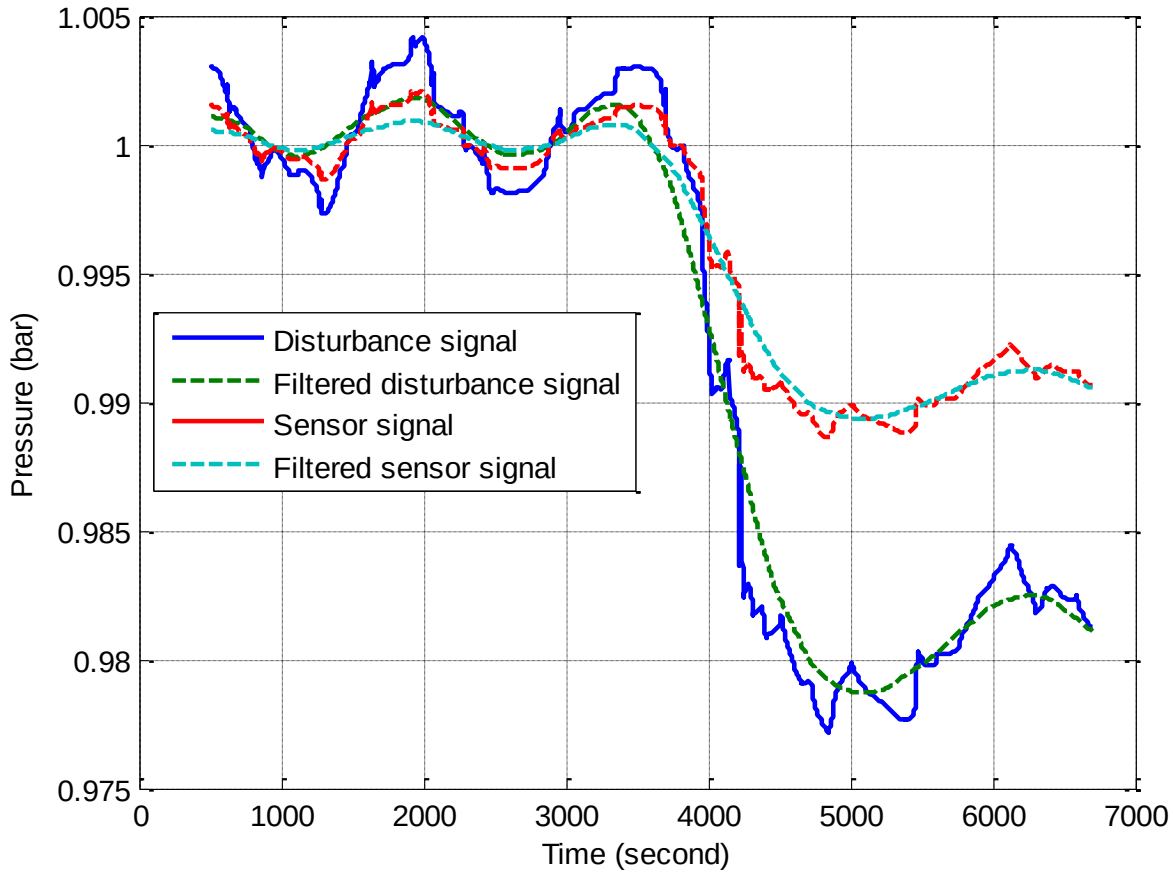

Figure A9.7. Pressure sensor data together with the filtered data.

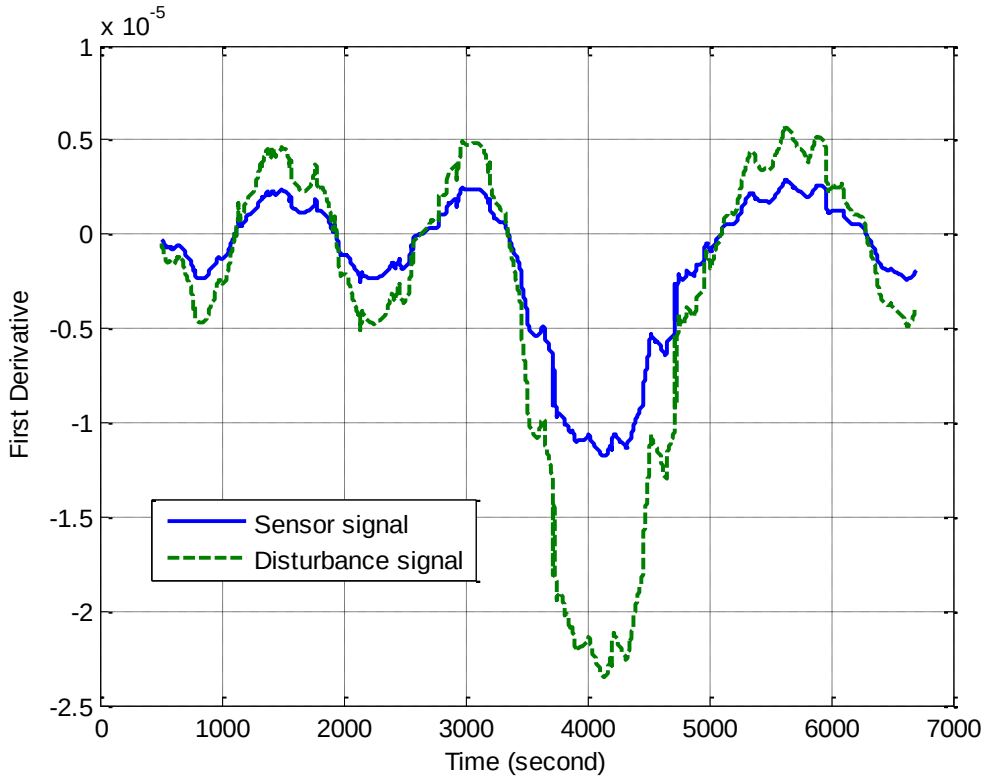

Figure A9.8. Pressure first derivative.

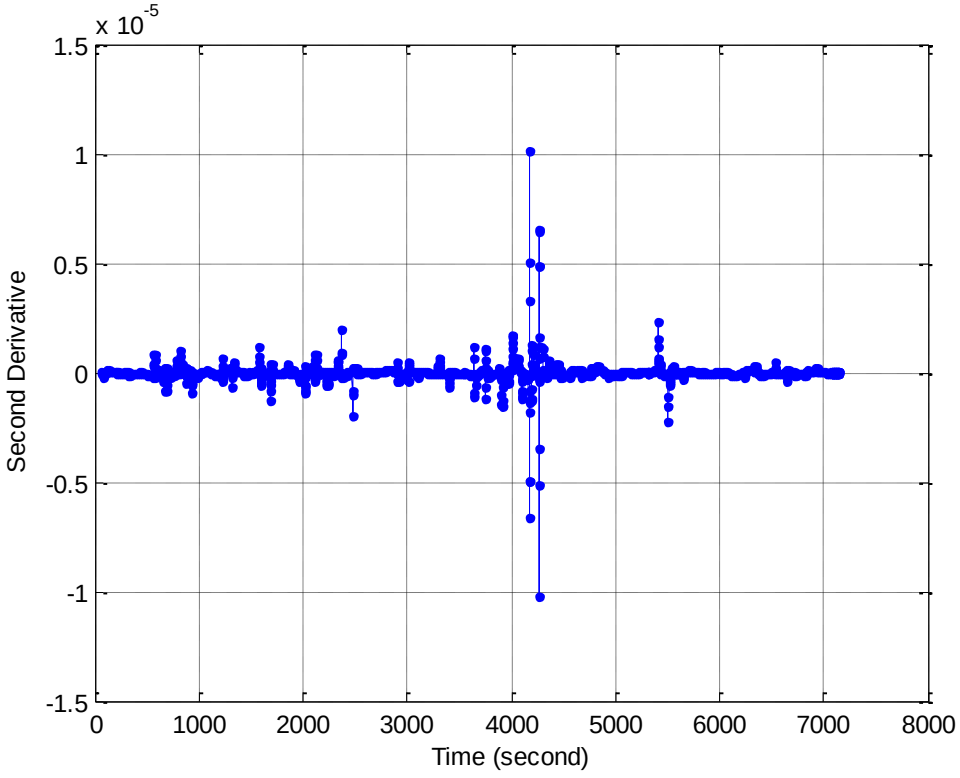

Figure A9.9. Pressure second derivative.

APPENDIX 10. Signal-based trend analysis for EWP evaluation

Each signal for the various air parameters, fan powers, concentrations and the production disturbances is analyzed and processed into properties by a trend analyzer. Examples of a trend analyzer are as follows:

a) Sliding average value of sensor signal
b) First derivative of sliding average
c) Second derivative of sliding average
d) Root Mean Square (RMS) spread over sliding average (significance check)
e) Sliding average value of disturbance
f) First derivative sliding average value of disturbance

First, signal signatures are searched for and identified by mathematical properties, i.e., signal and system properties. Most important are the average value, the RMS value, and the upper and lower limits as shown in Figure A10.1a. In addition, the first and the second derivatives are also very informative as depicted in Figure A10.1b and A10.1c, respectively.

a. Signal properties

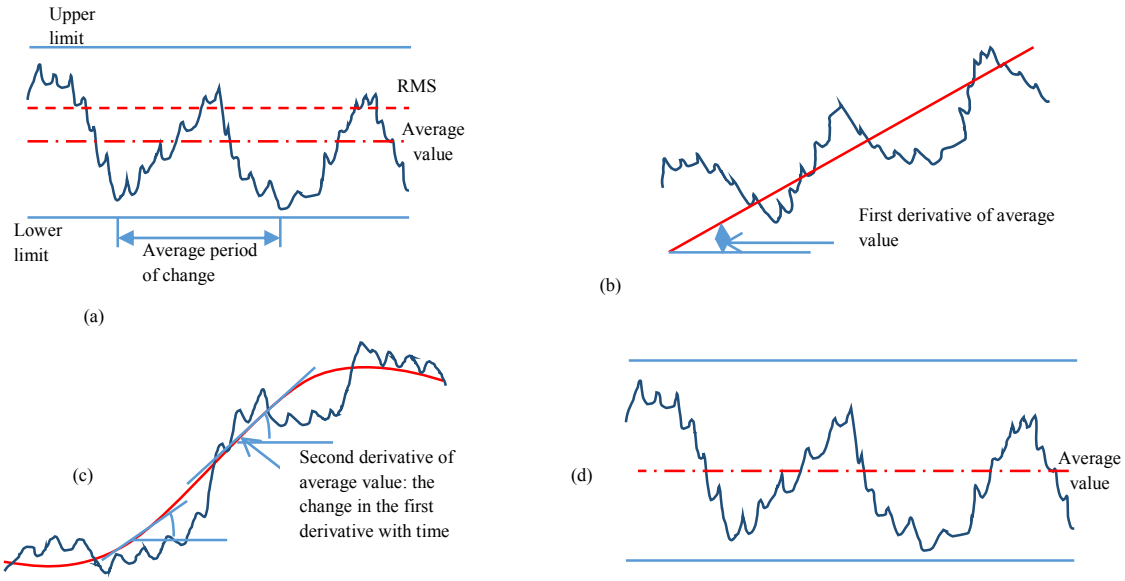

Figure A10.1. (a) Primary signal (b) first derivative (c) second derivative and (d) trend of system constants.

b. System properties

Each measurement signal of an air parameter is an outcome of a mass transport system. There are system characteristics imprinted in the signal trend. The system characteristics should not change if the system is not disturbed. System characteristics and their trends are identified. An n-order system can be characterized by an n-order differential model.

$$A_n \frac{dX^n}{d^n t} + A_{n-1} \frac{dX^{n-1}}{d^{n-1} t} + \cdots + A_o X = B$$

After normalization, an n-order system is described by n constants. The EWS identifies the system constants as system properties behind the signal itself. Next, the trends of each system constant is analyzed the same way the signals are analyzed. For example, A_n may look like Figure A10.1d. Examples of system properties identification are shown in Figures A10.4 through A10.15.

Second, the EWP self-calibrates and defines the allowable a) signal changes and b) system constant change characteristics to the operation of the mine. These parameters are mine specific and even location-specific to a mine.

Third, the EWS flags any threshold crossing of the signals at any location. Any crossing triggers a warning message. Any warning from ground control and power system monitoring also triggers a warning message as a kind of threshold crossing.

Fourth, the EWS looks for changes in the system constants. These parameters are assumed to be in-site calibrated with limits and trends, all site and mine specific. If the changes are outside the average trends, a warning message is sent.

Firth, a root-cause analysis is conducted on the signals if the changes are significant and out of the ordinary if a warning message is already sent.

Five cases from (a) to (e) are identified for specific attention to EWP.

a) Gas in-burst is detected from sudden, unusual gas concentration increase from the measurement of one or more sensors. This event is analyzed with the forward predictor APPS model using a changed boundary condition at the sensed location. The expected time for direct simulation is 15 seconds showing all concentrations at critical locations. If the mine has gas source that ads sources of gas to the upcoming air with elevated concentration, the accumulated effect may cause threshold crossing in the future time, delayed by travel time. A simulation exercise is described in Section 5.1 giving a threshold crossing 31 minutes in the example. This means that significant time is given with a warning signal for taking preventive measures.
b) Air flow change is identified is detected and accompanied by pressure change which indicates air flow blockage in an upstream drift section as illustrated in Figure A10.2.

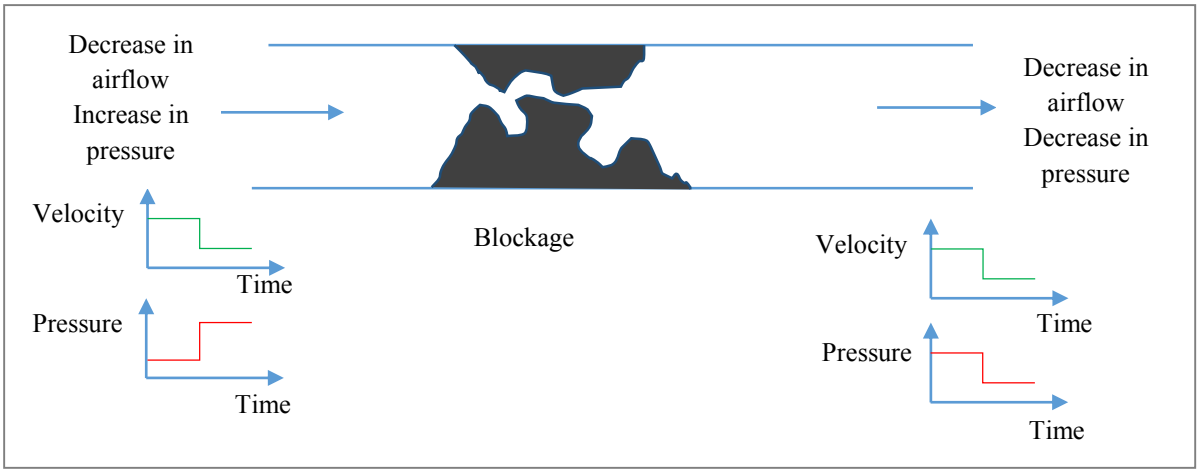

Figure A10.2. Schematic of an airflow blockage and its effect on pressure and airflow.

The signal evaluation algorithm first looks for ground control and roof stability sensory signals from the RSM. Second, mine-wide changes are analyzed in pressure and velocities before and after this detected event. If the changes are consistent with the signature in Figure A10.2, the likelihood of air flow blockage is identified. The APPS forward predictor algorithm is lunched calculating concentrations at critical locations due to this change in the entire mine's flow and gas concentration distributions. The root-cause signals of the sensed concentrations at given locations are used as deviated boundary conditions in the APPS predictor. The expected time for direct simulation is 15 seconds. If the simulation results indicate threshold crossing in any critical location, a warning message is sent. A simulation exercise is described in section 5.2 giving a threshold crossing in 23 minutes in the example. This means that significant time is given with a warning signal for taking preventive measures.

c) Barometric pressure variation is continuously detected that has an effect on the gas inflow to the mine from the porous gas bearing strata, sealed-off but leaky mine zones or the gob. The critical signals from the sensors are characterized by the amplitude and frequency of the pressure change. It is a particularly difficult signal to characterize for criticality. The ordinary range of change is +/_ 1000Pa, which is in the order of the magnitude of mine fans. An example demonstrating critical methane inflow due to sudden pressure change is in this range. A sudden decrease after an elongated time period with high barometric pressure is considered to be the most critical. However, it impossible to foresee the time period of continuous pressure deviation from a given value at any time instant. A truly continuous simulation is designed to predict this effect as a potentially critical source term from a continuously variable cause of gas inflow. The continuous signal processing flow chart is shown in Figure A10.3. A simulation example in 5.3 shows a 23 minutes delay time before critical crossing of threshold.

d) Fan malfunction is detected from the electrical signal of the power system. The MPD signal is checked, and the EWP signal is immediately generated for the management to check if the fan stoppage is not intentional. If it is an unscheduled event, the effect is analyzed by a direct run with the APPS model. The computational time is 15seconds. An example is illustrated with time delay of approximately 10 minutes to raise the gas concentration close to the threshold limit without crossing. Threshold crossing may happen with a higher methane inflow rate in the example in Section 5.4.

e) Belt fire is detected by the increased level of multiple gas components as well as of increased temperature. The signature of sensor signals is either step change-type in the average value or in the first derivative. The root cause of these signals is unmistakable, flagging criticality and sending a EWP warning for fire hazard. No forward prediction simulation is necessary in this case. An example of the simulation for signature identification is explained in Section 5.5.

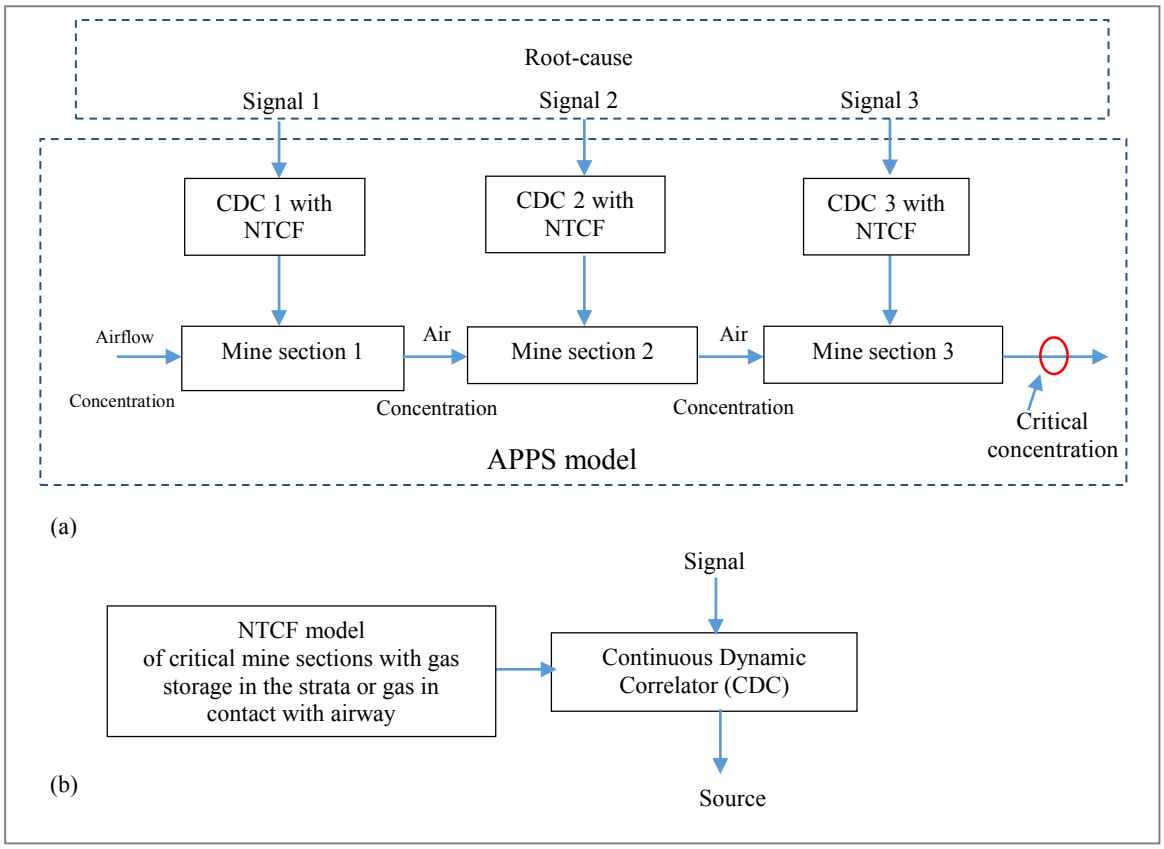

Figure A10.3.Continuous mine-wide APPS Simulator with root-cause source terms, (a); detail of CDC with NTCF, (b).

Examples of system properties identification

Figure A10.4 depicts a typical sensor data, X, over a period of 30 minutes, generated from a second order system, see Eq. (1), considered for proof of the concept and implemented as part of the EWP system to analyze the signal and system properties.

$$A_2^* \frac{\partial^2 X}{\partial t^2} + A_1^* \frac{\partial X}{\partial t} + A_0^* X = B \quad (1)$$

Where A_0^* , A_1^*, and A_2^* are system properties; X is sensor data; *t* is time, and B is the constant. The Eq. (1) can be normalized to eliminate the need for constant *B*.

$$A_2 \frac{\partial^2 X}{\partial t^2} + A_1 \frac{\partial X}{\partial t} + A_O X = 1 \quad (2)$$

Figures A10.5 and A10.6 demonstrate the first and second derivatives of the signal, respectively, revealing any linear and second order trends in the signal data. Figures A10.7 through A10.9 show the three system properties A_0, A_1, and A_2 of the system used in this example, respectively. The system constants are fairly unchanged until a disturbance causes a change in the system properties causing the system constants to be significantly different from the ordinary operating condition.

Figure A10.10 illustrates the signal used in the first exercise with a linear trend added. Figures A10.11 and A10.12 show the first and second derivatives of the signal, respectively, revealing any linear and second order trends in the signal data. The linear trend can be detected by the average first derivative curve being nearly constant positive indicating positive slope in the trend. Figures A10.13 through A10.15 depicts the three system constants A_0, A_1, and A_2 of the system used in this example. The system constants are fairly unchanged until a disturbance causes a change in system properties causing the system constants to be significantly different from the ordinary operating condition.

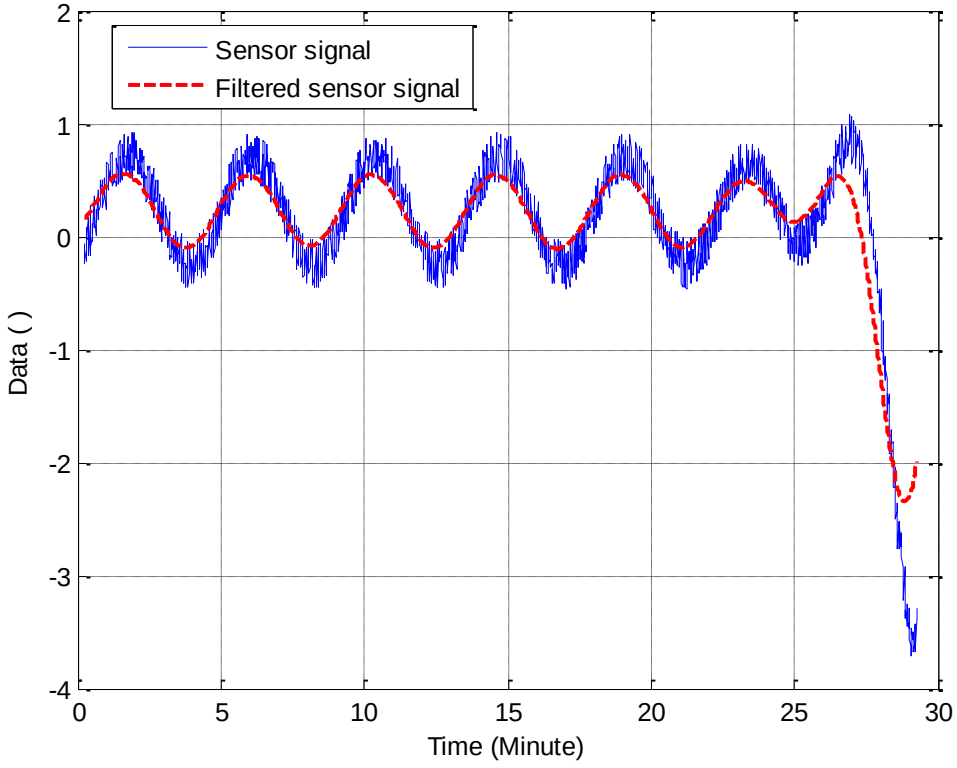

Figure A10.4. Signal data together with the filtered data.

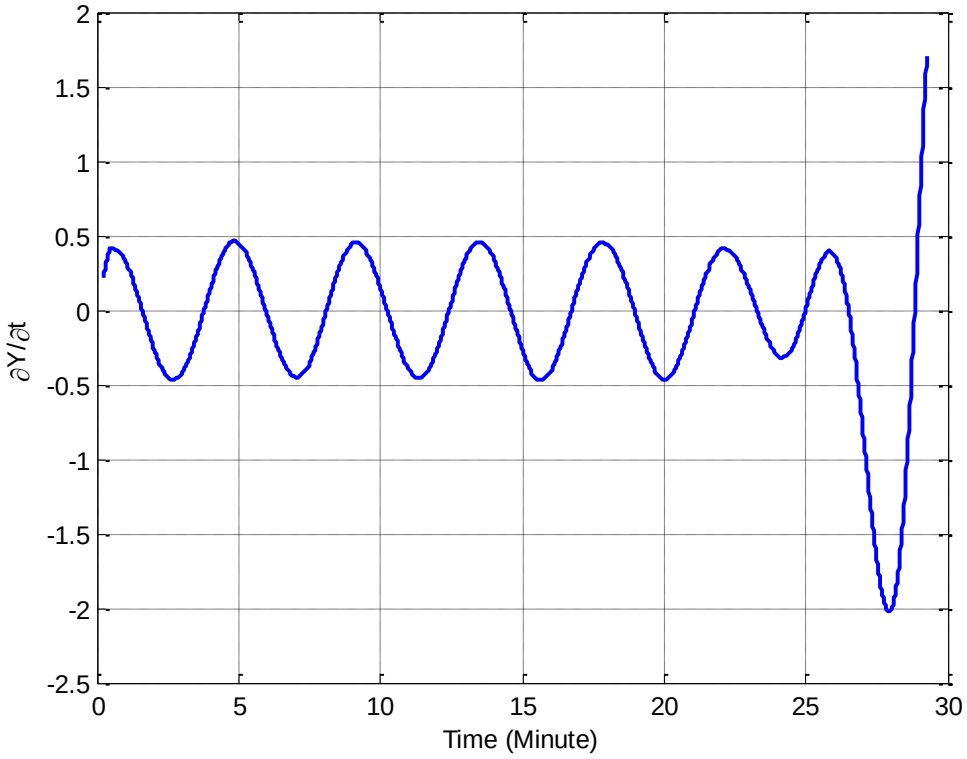

Figure A10.5. Signal data first derivative.

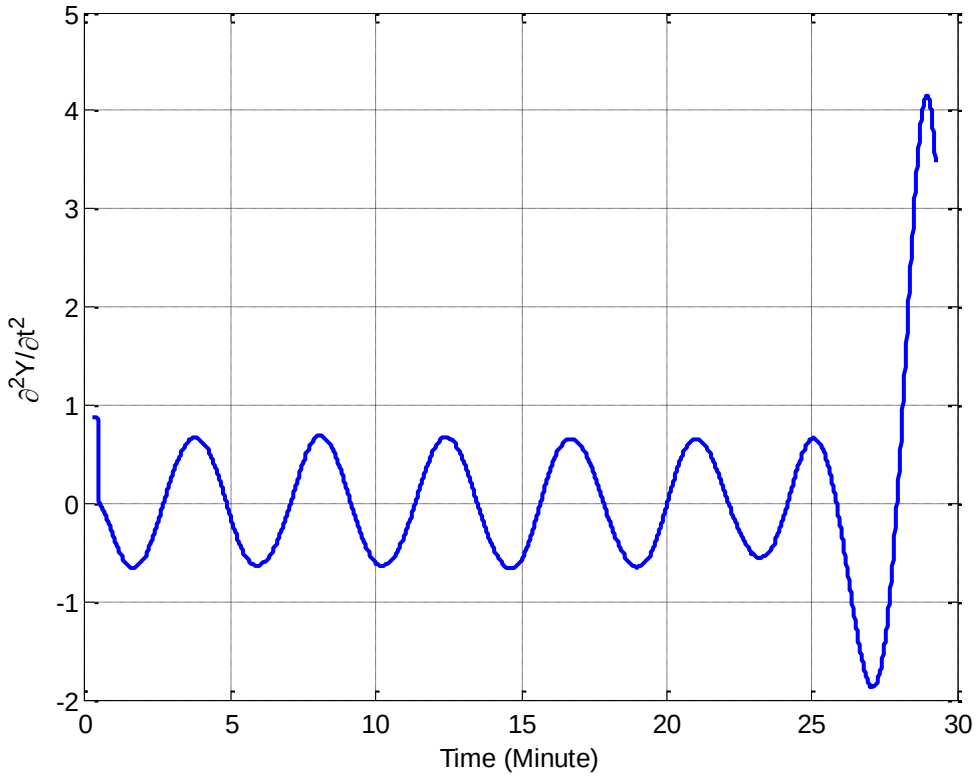

Figure A10.6. Signal data second derivative.

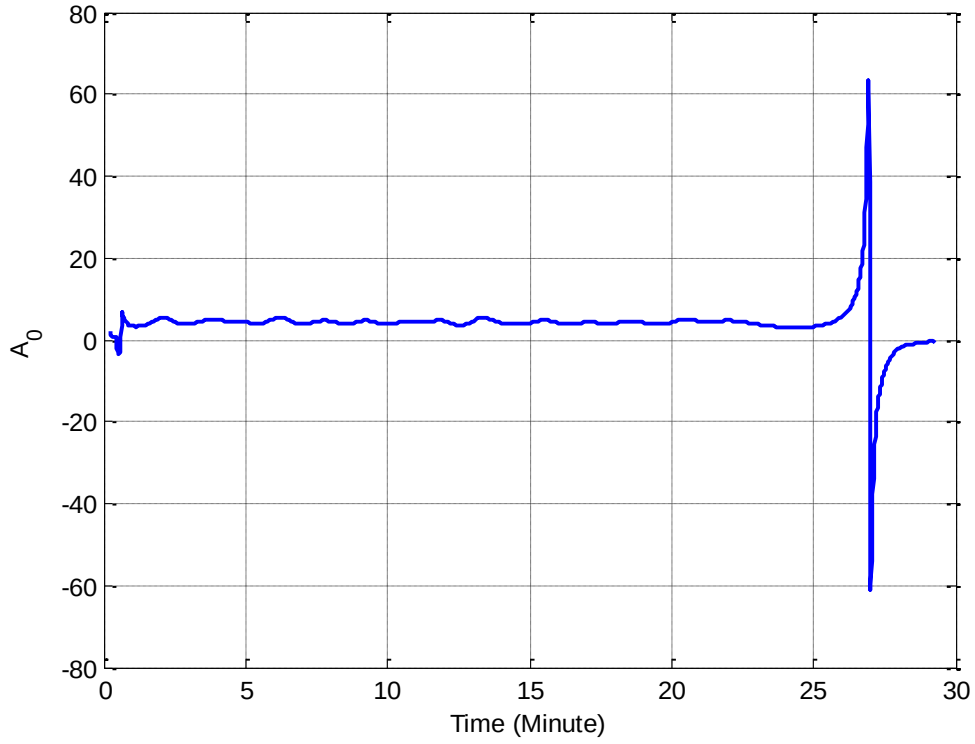

Figure A10.7. Signal system properties, A_0 constant.

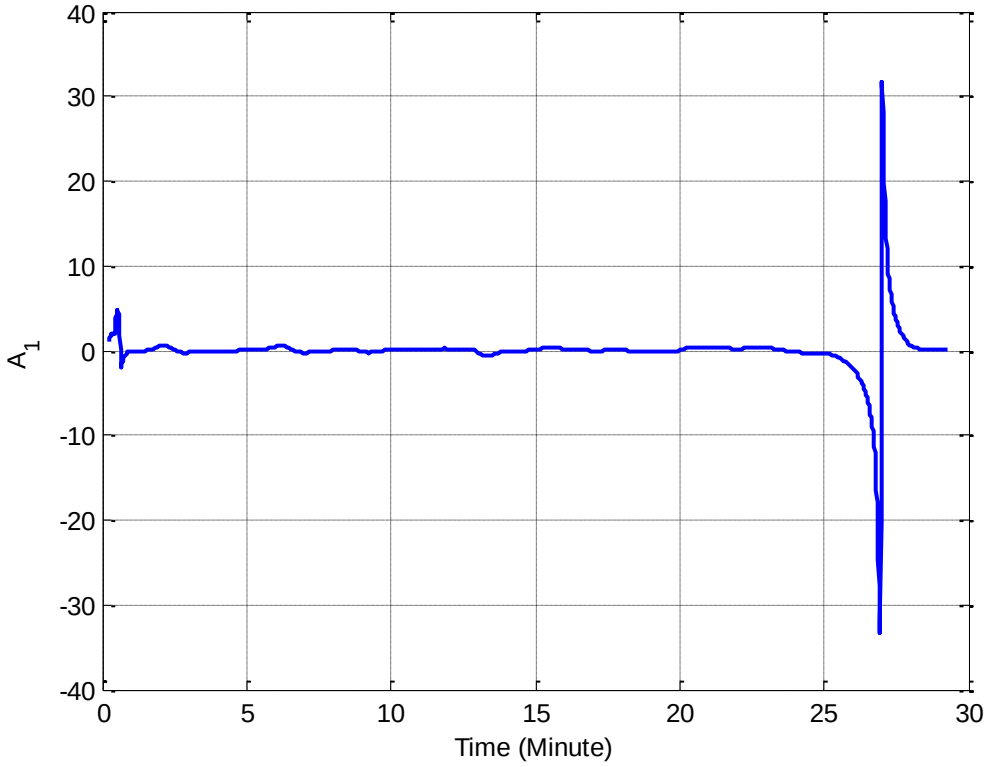

Figure A10.8. Signal system properties, A_1 constant.

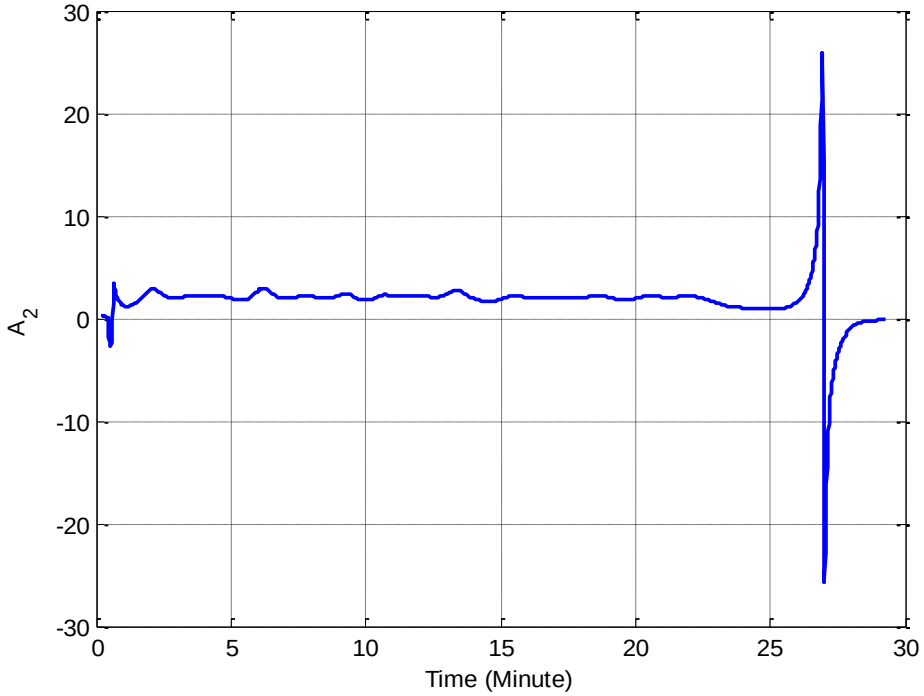

Figure A10.9. Signal system properties, A_2 constant

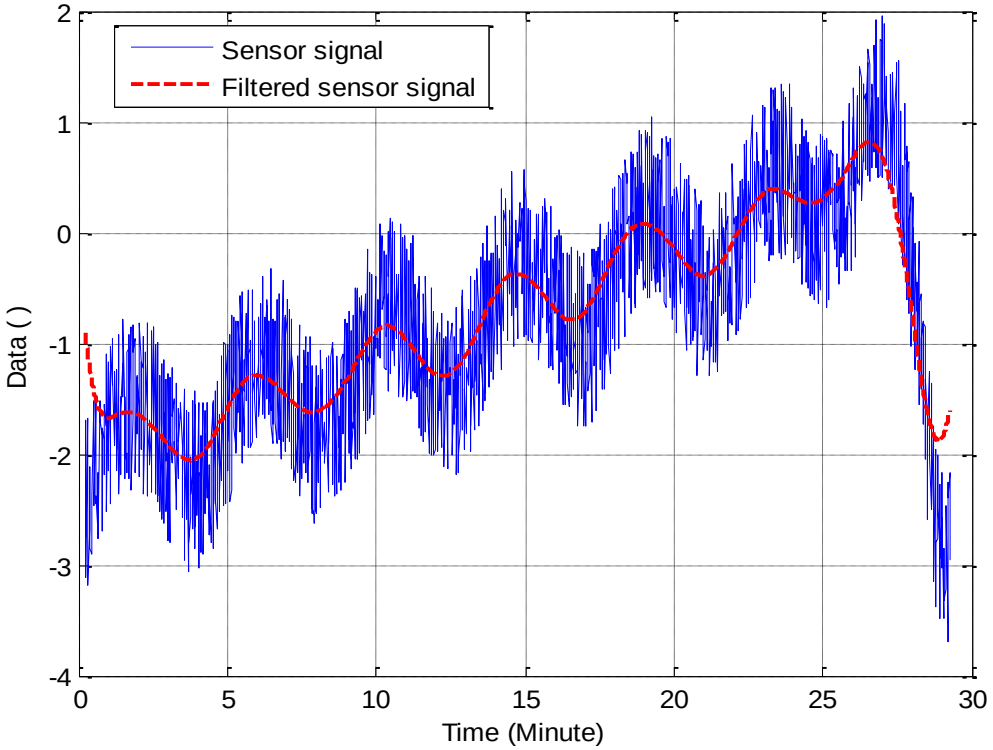

Figure A10.10. Signal data together with the filtered data.

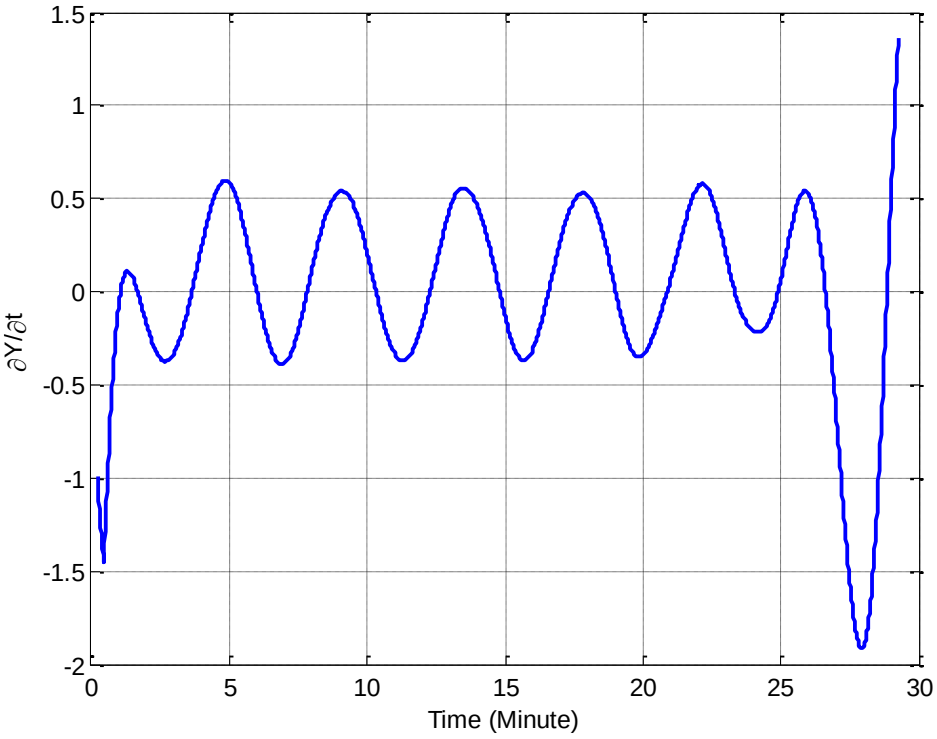

Figure A10.11. Signal data first derivative.

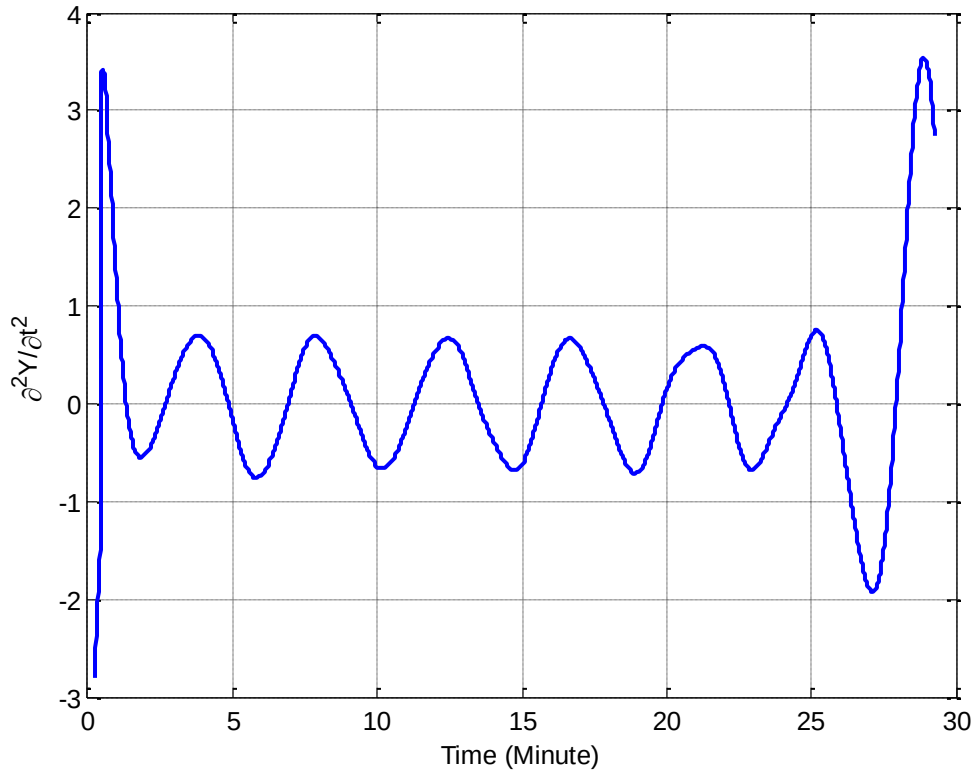

Figure A10.12. Signal data second derivative.

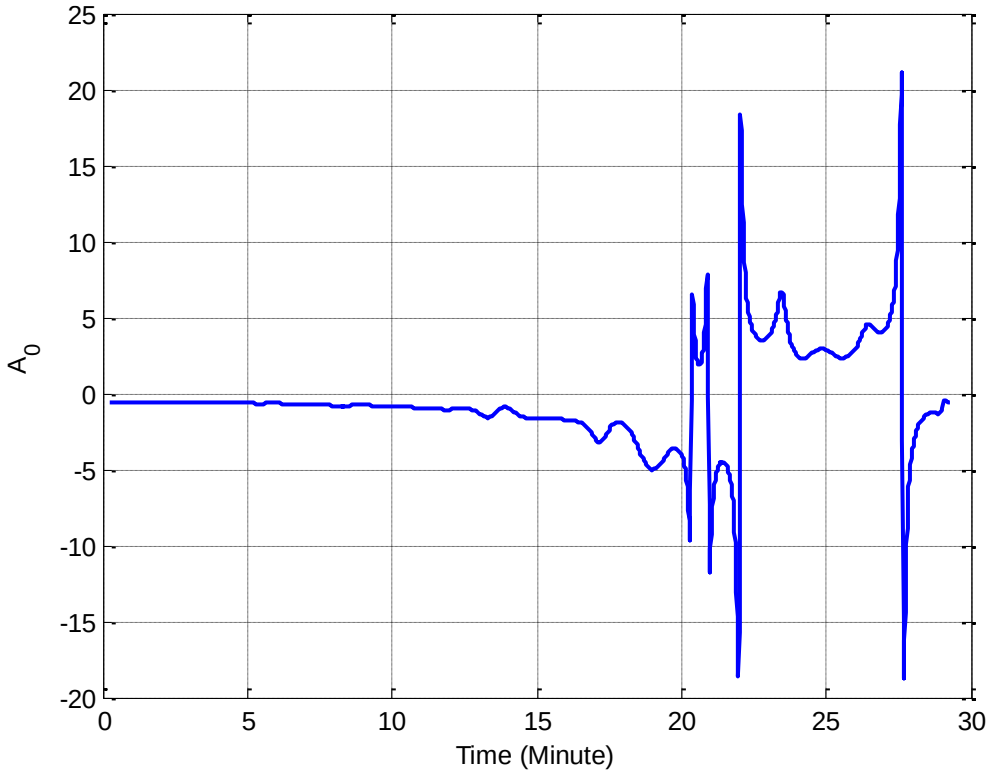

Figure A10.13. Signal system properties, A_0 constant.

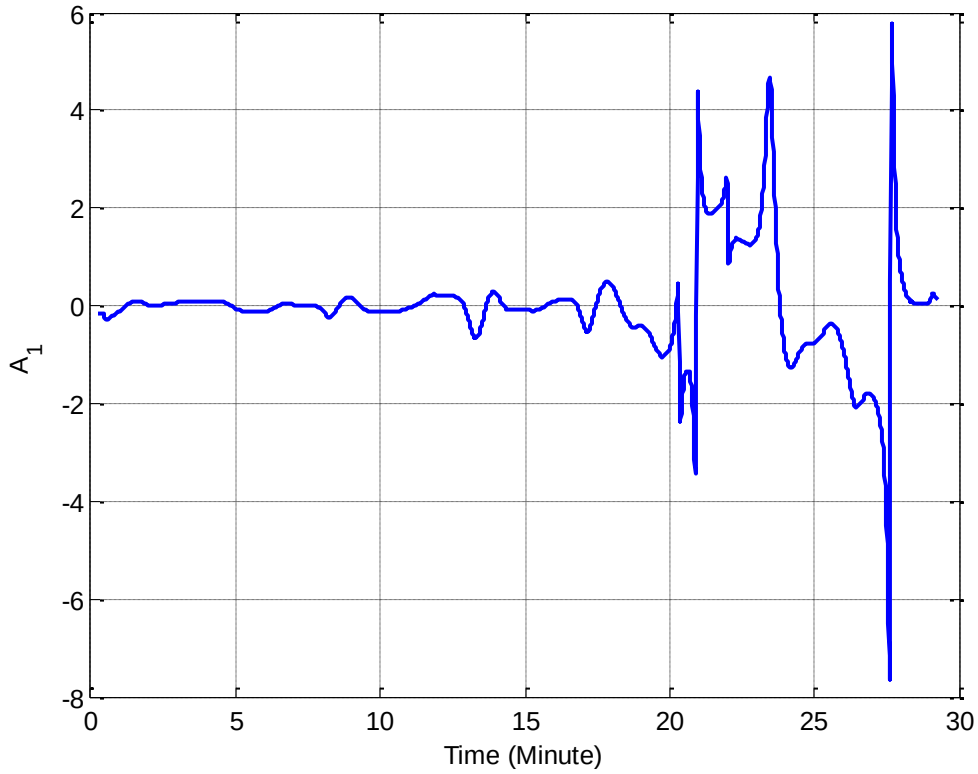

Figure A3. A10.14. Signal system properties, A_1 constant.

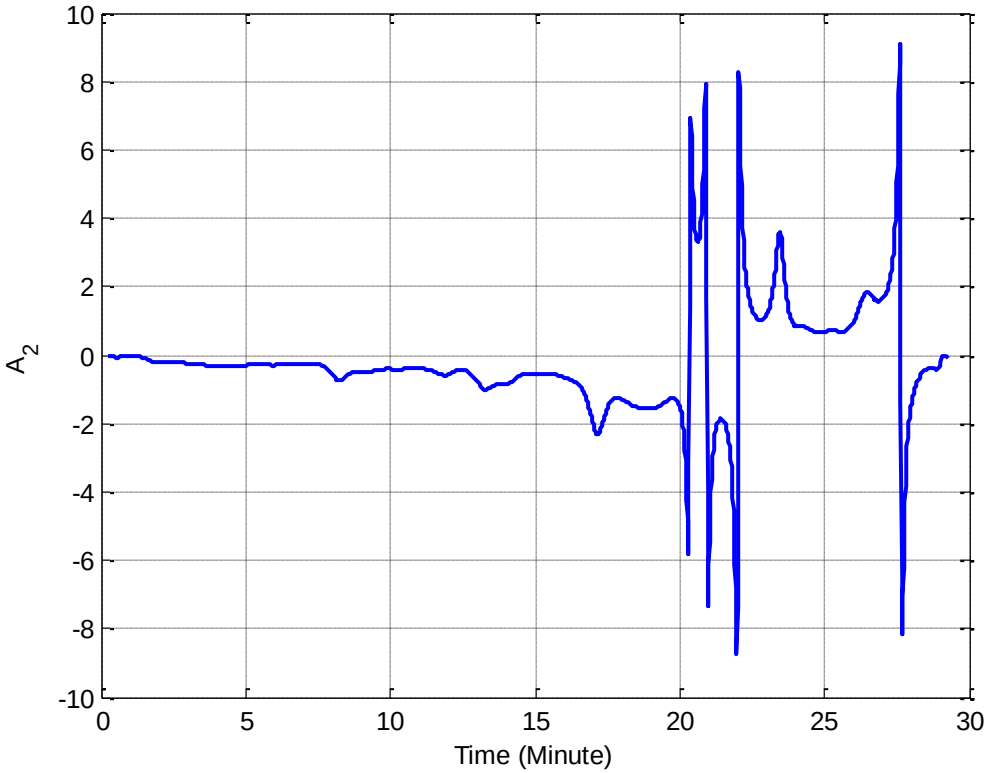

Figure A10.15. Signal system properties, A_2 constant.

APPENDIX 11. Signal analysis for flagging threshold crossing

Different signals from monitoring sensors are collected by any mine central data acquisition system. Different mine air parameters, concentrations, and disturbances may have different signals as demonstrated in Figure A11.1. The mine air parameters all have fluctuating signals with time due to disturbances from ambient conditions as well as from mining operations. "Moving window" evaluation of the signal flow is shown in Figure A11.2. Figure A11.3 outlines the "Moving window" filter processing schematic. It is necessary to use signal processing and trend analysis as illustrated in Figure A11.4.

Document simulated EWP examples and show critical needs for real-time MPD, RSM, and AMS data

Simulated examples are explained in section 5 for five selected examples for capacity demonstrations. The conclusion of the simulated, hazard scenarios is that the EWS is capable of identifying future threshold crossing in time to raise an alarm. The five examples are described in section 5 applied 18 sensors well-placed in locations that provided sufficient information for conclusive evaluations. The 18 sensors may not be always sufficient for the EWP evaluation.

It is necessary to evaluate the critical needs for MPD, RSM, and AMS data using sensitivity studies regarding the spatial density of the sensors in a mine ventilation network. This task is mine specific and no general recipe can be given at this point. However, based on the documented simulation examples, it is realistic to assume the need for few dozens of sensors or more at any given mine for hazardous gas concentration monitoring with a one minute response time placed close to the highest concentrations points. In addition, at the same or upstream points, sensors should be placed for airflow rate, barometric pressure, temperature and humidity monitoring with the same one minute acquisition time.

Integrated signals in the ventilation network can be used as a warning indicator for hazardous conditions. Such signals can be obtained from Continuous Dynamic Correlator (CDC) model elements as a combination of monitored signals (for example, concentration and barometric pressure as inputs) and simulated hazardous gas concentration (as output). Such integrated signals with models, if calibrated, can reduce the number of real, physical sensors since their outcome may be predictable. Therefore, if the operating mines are not willing to install, maintain, and use in real-time application dozens of sensors as recommended, then the only solution to increase safety is the innovative simulation combined with fewer sensors presented in this Final Report.

In conclusion, our recommendation is to invest, as Phase II, in the industrial prototype development of EWS real-time system with the goal of using it in operating mines.

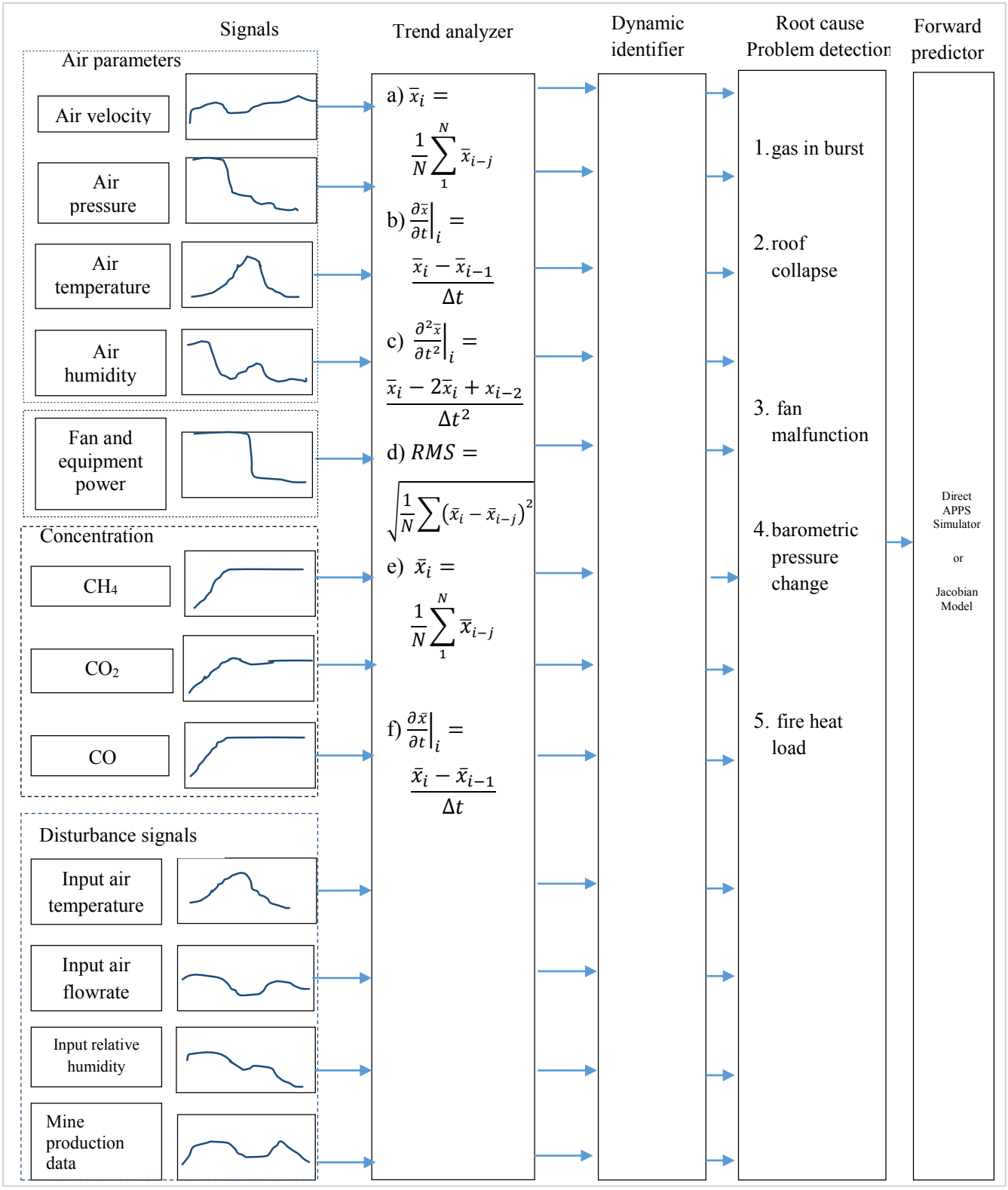

Figure A11.1. Flow chart for signal analysis problem identification

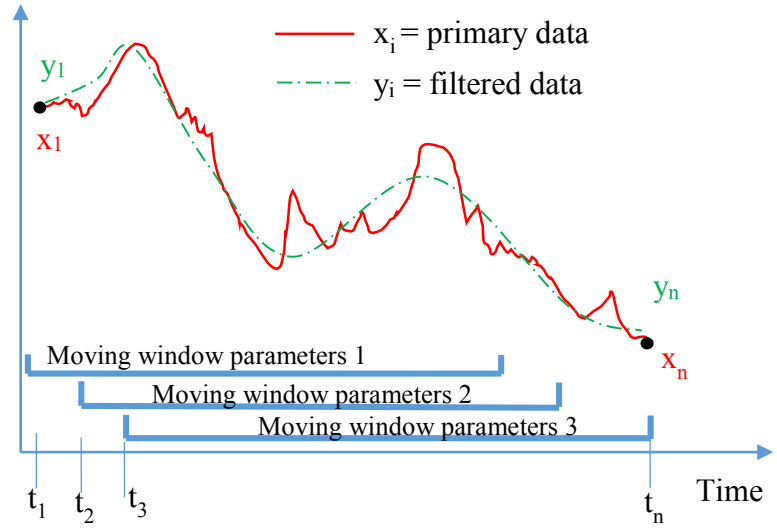

Figure A11.2. "Moving window" evaluation of the signal flow.

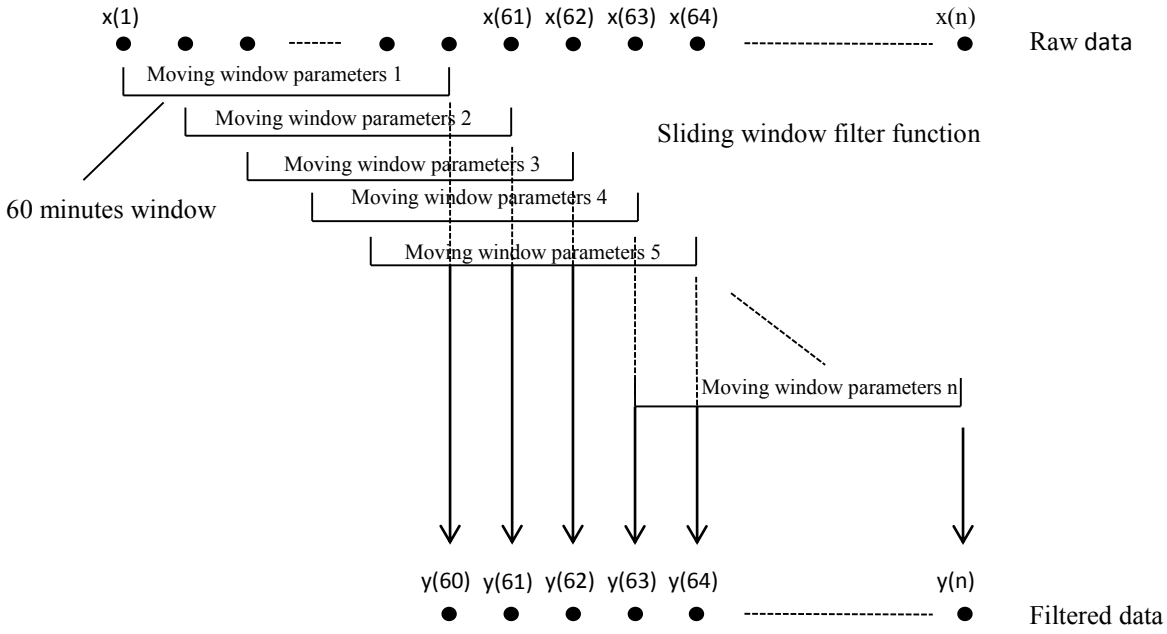

Figure A11.3: "Moving window" filter processing schematic.

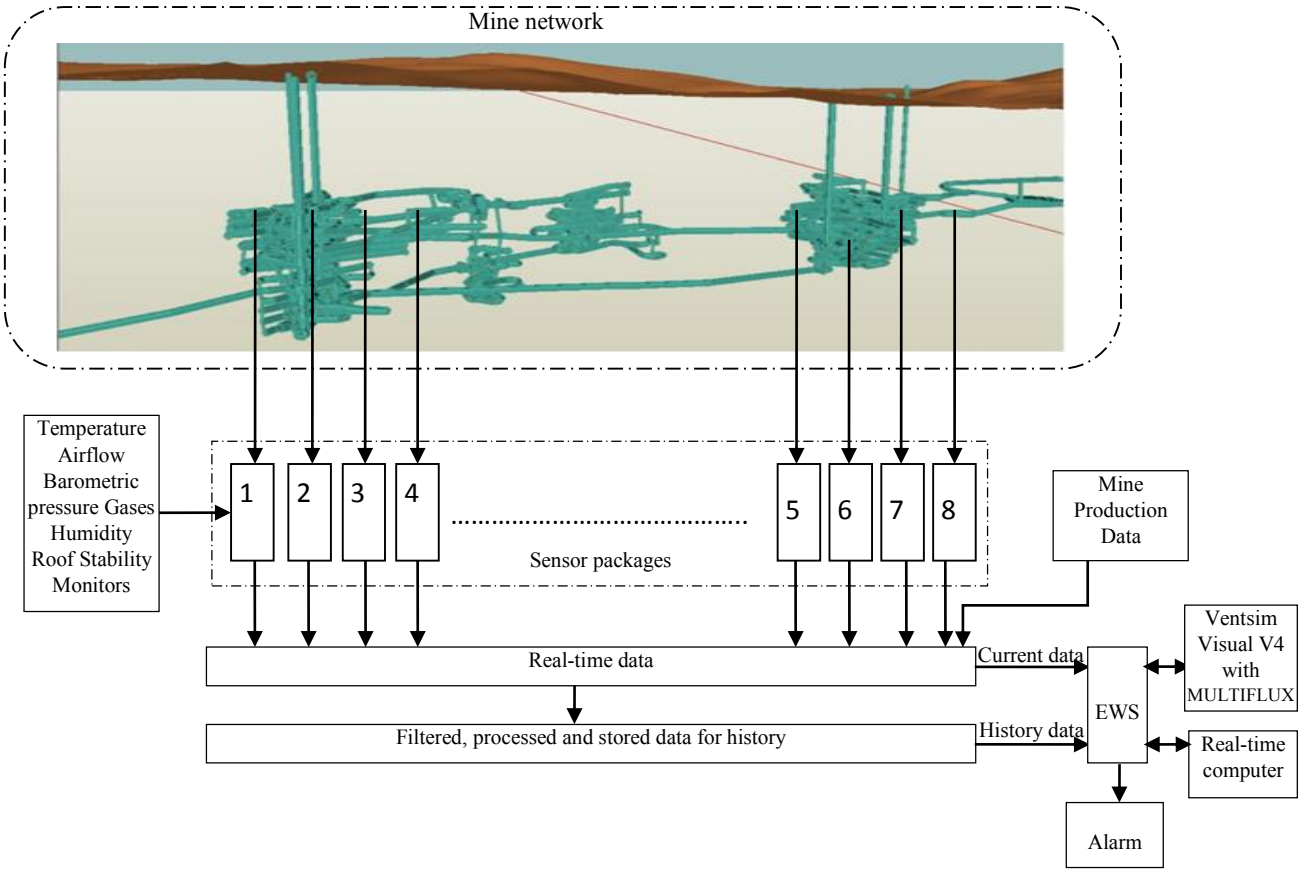

Figure A11.4. Signal processing and trend analysis chart.

APPENDIX 12. Atmospheric barometric pressure variations effects on methane inflow

A large volume of porous and fractured methane coal seam under pressure variations, shown in Figure A4.4, may release a large amount of methane by Darcy flow. Gob, strata, and partially sealed off dead zones, are examples of such a volume. Figures A12.1 and A12.2 illustrate the layout of longwall section and the 3D section of the gob as one of the example of such situation. Half of the gob size contains a volume of 240,000 m^3 methane. The barometric pressure changes induce flow of air in and out of the gob called barometric pressure pumping as depicted in Figure A12.3. This is modeled in the MULTIFLUX gob model and it establishes a methane concentration profile demonstrated in Figures A12.4 and A12.5. Darcy flow moves methane in and out of the gob and mixes air and methane inside the gob. The MULTIFLUX Air-CH_4 flow model shows that the mixing process results in a gradual methane profile close to linear and this is indicated in Figure A12.6. The effect of this scenario is the liberation of gas mixing into the air resulting in methane concentration increase which may cross threshold value. The root cause of pressure variations may be detected from outside barometric pressure decrease, pressure decrease in the airway or blockage of airway.

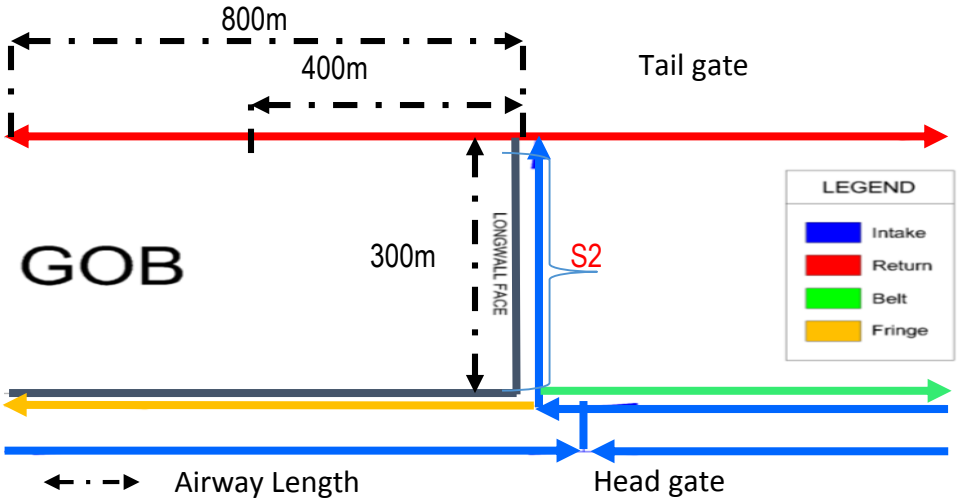

Figure A12.1. Layout of the longwall.

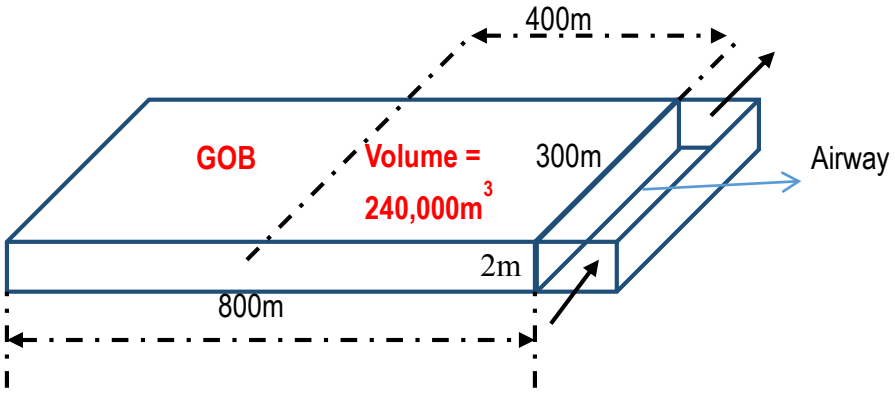

Figure A12.2. 3D section of the Gob.

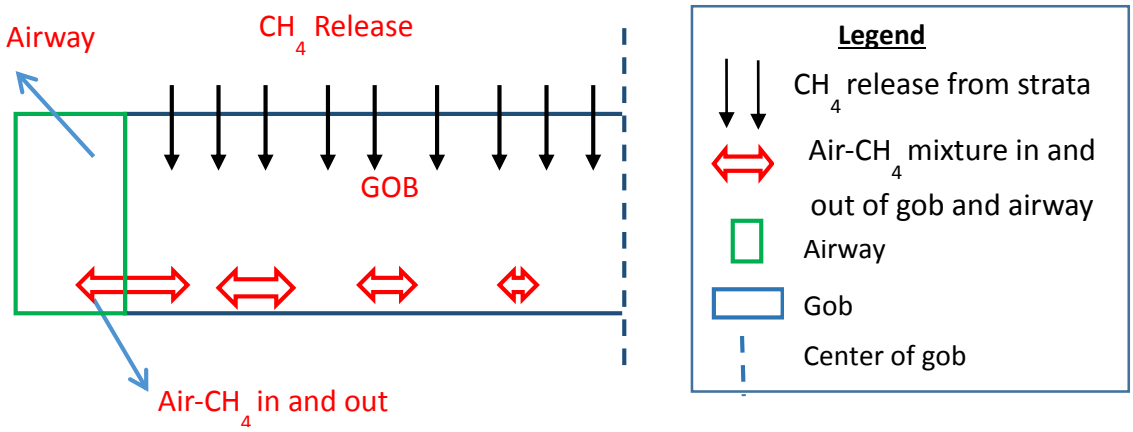

Figure A12.3. Layout of flow of Air-CH_4 mixture in and out of the airway due to barometric pressure drop.

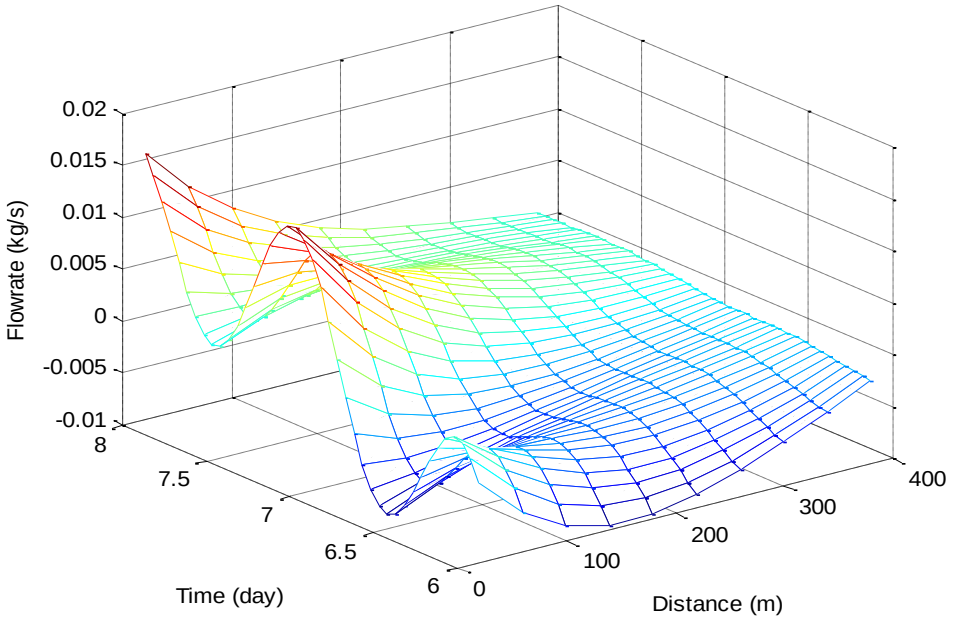

Figure A12.4. 3D Flow of Air- CH_4 mixture in and out of the airway.

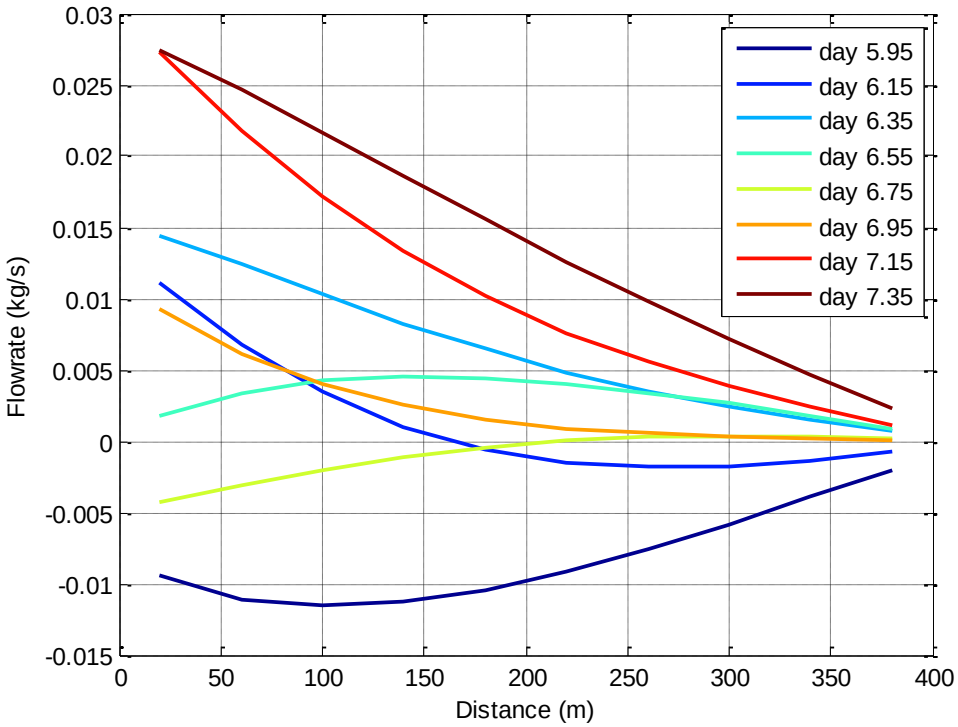

Figure A12.5. 2D Flow profile of Air- CH_4 mixture in and out of the airway for selected time divisions.

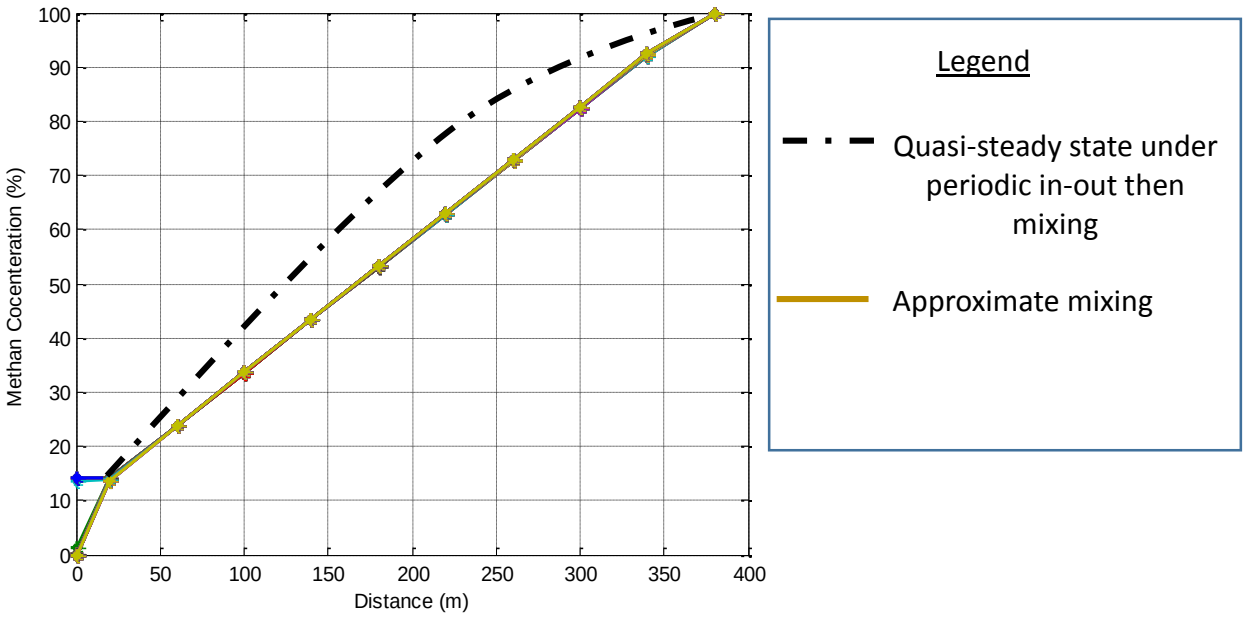

Figure A12.6. Methane concentration profile from Air-CH_4 mixing in the gob.

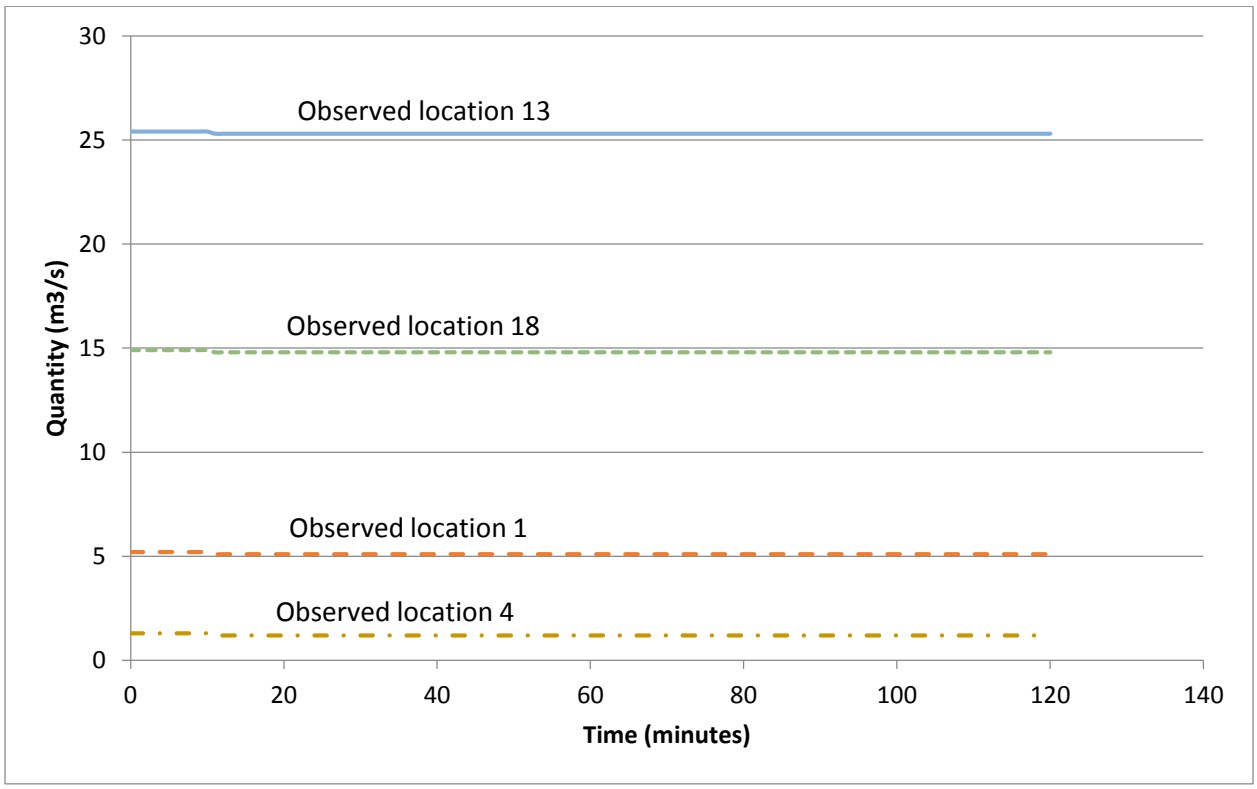

Figure A12.7. Results of airflow at monitored locations due to barometric pressure drop.

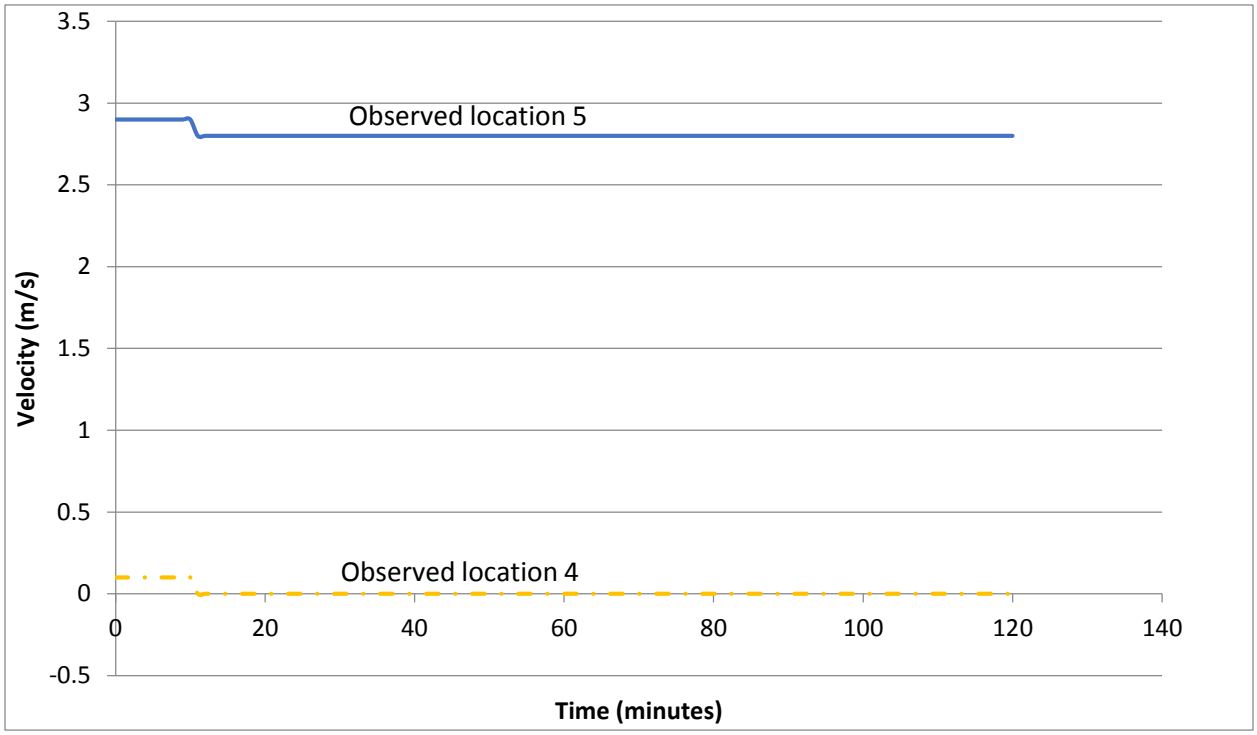

Figure A12.8. Results of velocity at monitored locations due to barometric pressure drop.

APPENDIX 13. Fan characteristics in fan malfunctioning scenario

The base points of the fan characteristics used in the scenario are given in table A13.1.

Table A13.1 Fan points.

ORIGINAL		REDUCED	
Quantity (m^3/s)	Fan static pressure (Pa)	Quantity (m^3/s)	Fan static pressure (Pa)
50	7500	50	3675
55	7000	55	3430
60	6500	60	3185
65	6000	65	2940
70	5500	70	2695
75	5000	75	2450
79.9	4484	79.9	2197.16
85	4000	85	1960
90	3500	90	1715
95	3000	95	1470

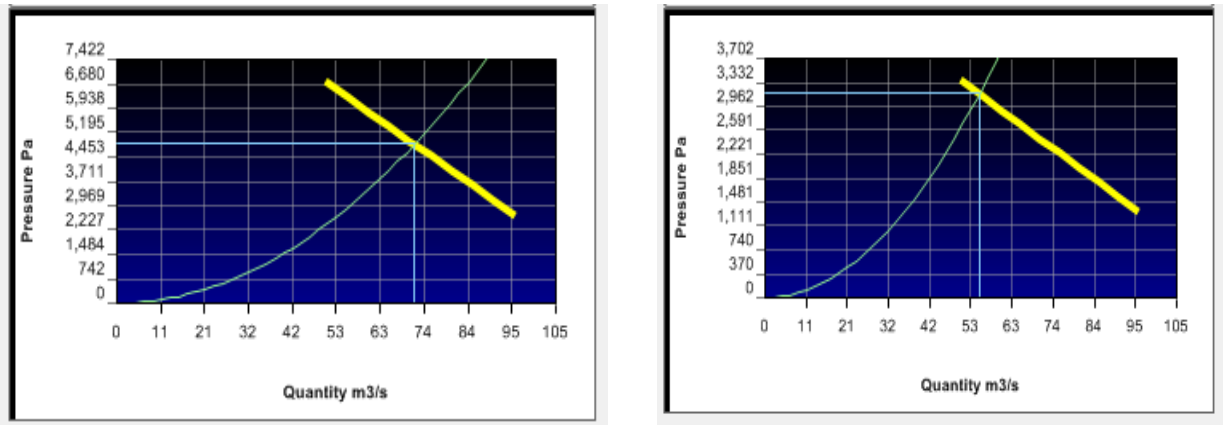

(a) (b)

Figure A13.1. Fan curves for original (a) and reduced (b) fan points.

APPENDIX 14. Fan power comparison

A14.1 Comparison of fan power for scenarios 1A, 1B, 2, and 3 modeled in example 1.

Table A14.1 shows the comparison between the fan powers for the various scenarios modeled in mine example 1. The table indicates that there is no difference between the fan power for scenarios 1A and 1B. There is a slight increase in the fan power for scenario 2 compared to the Base scenario 1A. The fan power of scenario 3 decreases slightly compared to the Base scenario 1A. Therefore, fan power measurements are conclusive only in the case of the fan malfunction.

Table A14.1. Fan power for various scenarios modeled in mine example 1.

Fan ID	Base Scenario 1A-2 sources		Scenario 1B-3 sources		Scenario 2-airway blockage		Scenario3-Pressure drop2000Pa	
	shaft Power (kW)	electrical Power (kW)	shaft Power (kW)	electrical Power (kW)	shaft Power (kW)	electrical Power (kW)	shaft Power (kW)	electrical Power (kW)
319	1864.5	1962.6	1864.5	1962.7	1867.2	1965.5	1836.8	1933.4
313	582.5	613.2	582.5	613.1	582.6	613.2	568.9	598.8
308	532.3	560.3	532.3	560.3	535.5	563.7	524.7	552.3

A14.2 Comparison of fan power for scenarios 1C, 4, and 5 modeled in example 2.

Table A14.2 shows the fan power for various scenarios modeled in mine example 2. There is a slight increase in the fan power for scenario 5 compared to the Base scenario 1C. The fan power of scenario 4 decreases significantly compared to the Base scenario 1B. Table A14.3 shows the signal type and the model type needed to simulate each scenario.

Table A14.2. Fan power for various scenarios modeled in mine example 2.

	Base Scenario 1C-3 sources		**Scenario 4-fan malfunction**		**Scenario 5- belt fire**	
Fan ID	**shaft Power**	**electrical Power**	**shaft Power**	**electrical Power**	**shaft Power**	**electrical Power**
	(kW)	**(kW)**	**(kW)**	**(kW)**	**(kW)**	**(kW)**
234	444.3	467.7	434.9	457.8	458.8	483
230	469.9	494.6	253.4	266.7	486.1	511.7

Table A14.3. Signal type and the model type for each scenario.

Scenario	**Type of signal**	**Type of model**
1	Step change	Gas accumulation model
2	Step change	Gas accumulation model
3	Dynamic delayed	Dynamic Jacobian NTCF predictive model
4	Step change	Gas accumulation model
5	Step change	Heat and concentration model

9.0 Acknowledgement/Disclaimer

This study was sponsored by the Alpha Foundation for the improvement of Mine Safety and Health, Inc. (ALPHA FOUNDATION). The views, opinions and recommendations expressed herein are solely those of the authors and do not imply any endorsement by the ALPHA FOUNDATION, its Directors and staff.